

**Inertially Stabilized Platforms for
SATCOM On-The-Move Applications:
A Hybrid Open/Closed-Loop Antenna Pointing
Strategy**

by
Eric Allen Marsh
B.S. Mechanical Engineering

United States Air Force Academy, 2006

Submitted to the Department of Aeronautics and Astronautics
in partial fulfillment of the requirements for the degree of
Master of Science in Aeronautics and Astronautics

at the
MASSACHUSETTS INSTITUTE OF TECHNOLOGY

June 2008

© Massachusetts Institute of Technology 2008. All rights reserved.

Author
Department of Aeronautics and Astronautics
June 6, 2008

Certified by
Dr. Dan Asta
Group Leader, MIT Lincoln Laboratory
Thesis Supervisor

Certified by
Dr. Timothy Gallagher
Technical Staff, MIT Lincoln Laboratory
Thesis Supervisor

Certified by
Prof. Jonathan P. How
Professor of Aeronautics & Astronautics
Thesis Supervisor

Accepted by
Prof. David L. Darmofal
Associate Department Head, Chair, Committee on Graduate Students

Report Documentation Page

Form Approved
OMB No. 0704-0188

Public reporting burden for the collection of information is estimated to average 1 hour per response, including the time for reviewing instructions, searching existing data sources, gathering and maintaining the data needed, and completing and reviewing the collection of information. Send comments regarding this burden estimate or any other aspect of this collection of information, including suggestions for reducing this burden, to Washington Headquarters Services, Directorate for Information Operations and Reports, 1215 Jefferson Davis Highway, Suite 1204, Arlington VA 22202-4302. Respondents should be aware that notwithstanding any other provision of law, no person shall be subject to a penalty for failing to comply with a collection of information if it does not display a currently valid OMB control number.

1. REPORT DATE 02 JUN 2008		2. REPORT TYPE N/A		3. DATES COVERED -	
4. TITLE AND SUBTITLE Inertially Stabilized Platforms for SATCOM On-The-Move Applications: A Hybrid Open/Closed-Loop Antenna Pointing Strategy				5a. CONTRACT NUMBER	
				5b. GRANT NUMBER	
				5c. PROGRAM ELEMENT NUMBER	
6. AUTHOR(S)				5d. PROJECT NUMBER	
				5e. TASK NUMBER	
				5f. WORK UNIT NUMBER	
7. PERFORMING ORGANIZATION NAME(S) AND ADDRESS(ES) Massachusetts Institute of Technology				8. PERFORMING ORGANIZATION REPORT NUMBER CI08-0015	
9. SPONSORING/MONITORING AGENCY NAME(S) AND ADDRESS(ES) The Department of the Air Force AFIT/ENEL, Bldg 16 2275 D Street WPAFB, OH 45433				10. SPONSOR/MONITOR'S ACRONYM(S)	
				11. SPONSOR/MONITOR'S REPORT NUMBER(S)	
12. DISTRIBUTION/AVAILABILITY STATEMENT Approved for public release, distribution unlimited					
13. SUPPLEMENTARY NOTES The original document contains color images.					
14. ABSTRACT					
15. SUBJECT TERMS					
16. SECURITY CLASSIFICATION OF:			17. LIMITATION OF ABSTRACT UU	18. NUMBER OF PAGES 216	19a. NAME OF RESPONSIBLE PERSON
a. REPORT unclassified	b. ABSTRACT unclassified	c. THIS PAGE unclassified			

**Inertially Stabilized Platforms for
SATCOM On-The-Move Applications:
A Hybrid Open/Closed-Loop Antenna Pointing Strategy**

by

Eric Allen Marsh

Submitted to the Department of Aeronautics and Astronautics
on June 6, 2008, in partial fulfillment of the
requirements for the degree of
Master of Science in Aeronautics and Astronautics

Abstract

The increasing need for timely information in any environment has led to the development of mobile SATCOM terminals. SATCOM terminals seeking to achieve high data-rate communications require inertial antenna pointing to within fractions of a degree. The base motion of the antenna platform complicates the pointing problem and must be accounted for in mobile SATCOM applications. Antenna Positioner Systems (APSs) provide Inertially Stabilized Platforms (ISPs) for accurate antenna pointing and may operate in either an open or closed-loop fashion. Closed-loop antenna pointing strategies provide greater inertial pointing accuracies but typically come at the expense of more complex and costly systems. This thesis defines a nominal two-axis APS used on an EHF SATCOM terminal on a 707 aircraft. The nominal APS seeks to accomplish mobile SATCOM using the simplest possible system; therefore, the system incorporates no hardware specific to closed-loop pointing. This thesis demonstrates that the nominal APS may achieve accurate antenna pointing for an airborne SATCOM application using a hybrid open/closed-loop pointing strategy.

The nominal APS implements the hybrid pointing strategy by employing an open-loop pedestal feedback controller in conjunction with a step-tracking procedure. The open-loop feedback controller is developed using optimal control techniques, and the pointing performance of the controller with the nominal APS is determined through simulation. This thesis develops closed-loop step-tracking algorithms to compensate for open-loop pointing errors. The pointing performance of several step-tracking algorithms is examined in both spatial pull-in and tracking simulations in order to determine the feasibility of employing hybrid pointing strategies on mobile SATCOM terminals.

Keywords: Mobile SATCOM, Antenna Pointing, Inertially Stabilized Platform, Two-axis Positioner, Linear Quadratic Gaussian Control, Nonlinear Optimization

Thesis Supervisor: Dr. Dan Asta
Title: Group Leader, MIT Lincoln Laboratory

Thesis Supervisor: Dr. Timothy Gallagher
Title: Technical Staff, MIT Lincoln Laboratory

Thesis Supervisor: Prof. Jonathan P. How
Title: Professor of Aeronautics & Astronautics

Acknowledgments

First off, I would like to thank Timothy Gallagher for his continued support, guidance, and encouragement in this research. I would also like to thank Dan Asta and Jonathon How for their contributions and support. A very special thanks is extended to John Kuconis for my sponsorship at MIT Lincoln Laboratory. The help I received from Mike Boulet and Anthony Hotz proved invaluable to this research, and their willingness to answer countless questions has been much appreciated. I would like to thank the following Lincoln Laboratory employees who have contributed in some way to this thesis or have at least given me a smile in the hallways: Kevin Kelly, Ed Bucher, Ross Conrad, Mark Deluca, Rajesh Viswanathan, Nagabushan Sivananjaiah, Mike Gridley, Ted O’Connell, Saunak Shah, John Sultana, John Choi, Misha Ivanov, Steve Targonski, David Savilonis, Dave Genovese, Peggy Speranza, and Rosa Figueroa. This list is by no means complete, and I would like to express my deepest gratitude toward all those who have made my tenure at MIT and Lincoln Laboratory most enjoyable. Last, but not least, I want to extend a warm thank you to my family and friends. Without you, none of this matters.

Disclaimer

The views expressed in this article are those of the author and do not reflect the official policy or position of the United States Air Force, Department of Defense, or the United States Government.

Contents

List of Figures	10
List of Tables	14
1 Introduction	17
1.1 Motivation for Work	17
1.2 Problem Statement	19
1.3 Contributions	20
1.4 Thesis Overview	21
2 Background and System Architecture	23
2.1 APS Hardware Configurations	24
2.1.1 APS Components	24
2.1.2 Antenna Payloads	24
2.1.3 Pedestals and Sensors	29
2.1.4 APS Design Requirements	32
2.2 Control Strategies	33
2.2.1 Open-loop Pointing and Sources of Error	34
2.2.2 Closed-Loop Antenna Pointing Methods	35
2.3 Nominal APS System Architecture	38
3 Open-Loop Controller Development	41
3.1 Equations of Motion	42
3.1.1 Response Side	42

3.1.2	Moment Side	43
3.1.3	Base Motion Disturbance Modeling	46
3.1.4	Linear Plant Model	49
3.2	Controller Development and Simulation	51
3.2.1	Linear-Quadratic Regulation Theory	52
3.2.2	Linear-Quadratic Estimation Theory	54
3.2.3	Linear-Quadratic Gaussian Theory	56
3.2.4	Reference Commands	56
3.2.5	Development of the LQG Pedestal Controller in MATLAB	57
3.2.6	Controlled Nonlinear Plant Simulation	63
3.3	Pointing Error Distributions	73
4	Closed-Loop Pointing Strategy	79
4.1	Defining the Cost Function	80
4.2	Facets of the Optimization Problem	83
4.3	Step-tracking Using Function Comparison Methods	84
4.3.1	Full-field Search	84
4.3.2	Spiral Search	85
4.4	Step-tracking Using Optimization Techniques	88
4.4.1	Modified Newton's Method	90
4.4.2	Quasi-Newton's Methods	93
4.4.3	Method of Steepest Descent	94
4.4.4	Step-tracking Algorithm Architecture	95
4.5	Spatial Pull-in Simulations	103
4.5.1	Observations	111
4.6	Spatial Pull-in Robustness Tests	113
4.6.1	Observations	114
4.7	A Look at Tracking	116
4.7.1	Observations	118

4.8	Simulation Processing Times	118
5	Conclusions	121
5.1	Open-loop Controller Simulation Results Summary	121
5.2	Closed-loop Step-tracking Simulation Results Summary	122
5.3	Overall Contributions	124
5.4	Suggestions for Future Work	125
A	Satellite Look Angle Calculations	127
A.1	Satellite Targeting Using Classical Orbital Element Sets	128
A.2	Targetting Using Known Inertial Look Angles	132
A.3	Keplar2RRR.m	134
A.4	basemotionlatlongalt2ECINAVDATA.m	136
B	Open-Loop Controller Simulations	139
B.1	controller.m	139
B.2	APS Simulink Model	143
C	Step-tracking Simulations	149
C.1	spiralsearch.m	149
C.2	modifiedNewton.m	154
C.3	BFGS.m	166
C.4	DFP.m	180
C.5	steepestdescent.m	194
C.6	getsignalpower.m (Subroutine)	205
D	List of Acronyms and Symbols	207

List of Figures

1-1	Photo examples of ISP Systems	18
2-1	APS Interconnect Block Diagram	24
2-2	Antenna Gain Pattern (24 in. dish)	26
2-3	Gain Pattern as a Function of Two Orthogonal Angles (24 in. dish)	26
2-4	HPBW as a Function of Antenna Size and Operating Frequency	27
2-5	Gimbal Structures	30
2-6	Two-axis Az/El positioner used in the “EHF SATCOM on the 707” project	30
2-7	Gyroscope (IMU) Accuracy Mapped to Applications	33
2-8	Monopulse Antenna System	36
3-1	Pedestal Coordinates	43
3-2	Aircraft Coordinate Frame	47
3-3	Disturbance Rate Input Power Spectral Density (Antenna Body z Axis)	48
3-4	Actual and Estimated Pitch Component of Antenna Inertial Pointing Error (Linear Plant)	61
3-5	Actual and Estimated Pitch Component of Antenna Inertial Velocity (Linear Plant)	61
3-6	Actual and Estimated Base Motion Disturbance Input to the Antenna Pitch Axis (Linear Plant)	62
3-7	Applied Motor Torque: Elevation Motor (Linear Plant)	62
3-8	Closed-Loop Frequency Response: Elevation Motor Controller (Linear Plant)	63

3-9	Yaw Component of Antenna Pointing Error at Different Elevations (Unmodified Controller)	64
3-10	Yaw Component of Antenna Pointing Error as Elevation Changes: Modified and Unmodified Controllers	65
3-11	Actual and Estimated Pitch Component of Antenna Inertial Pointing Error (Simulink Simulation)	67
3-12	Actual and Estimated Yaw Component of Antenna Inertial Pointing Error (Simulink Simulation)	67
3-13	Actual and Estimated Pitch Component of Antenna Inertial Velocity (Simulink Simulation)	68
3-14	Actual and Estimated Yaw Component of Antenna Inertial Velocity (Simulink Simulation)	68
3-15	Actual and Estimated Base Motion Disturbance Input to the Antenna Pitch Axis (Simulink Simulation)	69
3-16	Actual and Estimated Base Motion Disturbance Input to the Antenna Yaw Axis (Simulink Simulation)	69
3-17	Antenna Pitch Axis Inertial Angular Displacement Step Response (Simulink Simulation)	70
3-18	Antenna Yaw Axis Inertial Angular Displacement Step Response (Simulink Simulation)	70
3-19	Antenna Yaw Axis Commanded and Applied Torques for a Step Response	71
3-20	Pitch (q) and Yaw (r) Components of Antenna Pointing Error	74
3-21	q Auto-correlation Function	74
3-22	r Auto-correlation Function	75
3-23	q Histogram	75
3-24	r Histogram	76
4-1	X-El, El Coordinates with respect to Dish for Stationary, Level An- tenna Base	81
4-2	Antenna Gain Pattern Cost Function	81

4-3	Full-Field Search Example	86
4-4	Spiral Search Pattern	86
4-5	Cost Function as a Function of xel_i ($el_i = 0^\circ$)	87
4-6	Cost Function Finite Differencing Map	98
4-7	Strategy for Bracketing Minimum Along Descent Direction	102
4-8	Starting Coordinates for Spatial Pull-in Simulation	104
4-9	Magnitude of Satellite Inertial Angular Velocity	106
4-10	Number of Cost Function Evaluations per Trial Point vs. Spatial Pull-in Convergence Time	112
4-11	Starting Coordinates for Tracking Simulations	117
4-12	BFGS _{0.7} Spatial Pull-in Simulation Times vs. Number of Cost Function Evaluations per Trial Point (n) for Serial and Parallel Processing	119
A-1	Earth-Centered Inertial (ECI) Coordinate System	129
B-1	Nominal APS Pedestal Feedback Controller Simulink Model	143
B-2	Estimator Dynamics Subsystem	144
B-3	Aircraft Rate Disturbance Input and Measured Aircraft Position Subsystem	145
B-4	Antenna Roll Dynamics Subsystem	146
B-5	Linear Torque-Speed Curve Subsystem	147
B-6	KVH Gyro Sensor Subsystem	148
B-7	IMU Sensor Subsystem	148

List of Tables

3.1	Kolmogorov-Smirnoff Test for Pitch Error Component	76
4.1	Average Number of Trial Points Visited for Deterministic Gain Pattern Cost Function	108
4.2	Algorithm Comparison for Deterministic Cost Function	108
4.3	Average Number of Trial Points Visited when the Number of Cost Function Evaluations per Trial Point (n) equals 1	108
4.4	Algorithm Comparison when the Number of Cost Function Evaluations per Trial Point (n) equals 1	109
4.5	Average Number of Trial Points Visited when the Number of Cost Function Evaluations per Trial Point (n) equals 5	109
4.6	Algorithm Comparison when the Number of Cost Function Evaluations per Trial Point (n) equals 5	109
4.7	Average Number of Trial Points Visited when the Number of Cost Function Evaluations per Trial Point (n) equals 10	109
4.8	Algorithm Comparison when the Number of Cost Function Evaluations per Trial Point (n) equals 10	109
4.9	Average Number of Trial Points Visited when the Number of Cost Function Evaluations per Trial Point (n) equals 15	110
4.10	Algorithm Comparison when the Number of Cost Function Evaluations per Trial Point (n) equals 15	110
4.11	Average Number of Trial Points Visited when the Number of Cost Function Evaluations per Trial Point (n) equals 20	110

4.12	Algorithm Comparison when the Number of Cost Function Evaluations per Trial Point (n) equals 20	110
4.13	Spatial Pull-in Robustness Simulation (Number of Cost Function Evaluations per Trial Point (n) equals 1)	115
4.14	Spatial Pull-in Robustness Simulation (Number of Cost Function Evaluations per Trial Point (n) equals 5)	115
4.15	BFGS Tracking Simulation (Number of Cost Function Evaluations per Trial Point (n) equals 1)	117
4.16	BFGS Tracking Simulation (Number of Cost Function Evaluations per Trial Point (n) equals 5)	117
D.1	List of Acronyms and Abbreviations Used in This Work	207
D.2	List of Symbols Used in This Work	208

Chapter 1

Introduction

1.1 Motivation for Work

The demand for Inertially Stabilized Platforms (ISPs) stems from multiple applications that span a wide spectrum of engineering disciplines. Several engineering problems give rise to the need to either track a target or keep a payload device pointed at a fixed spot in inertial space while the given system operates in an environment which is itself moving in inertial space. Examples of applications requiring inertial pointing in dynamic environments include mobile Radio Frequency (RF) and optical communication systems, imaging and surveillance platforms, weapon targeting systems, and satellite to satellite communication links [1–4]. Figure 1-1 shows a few examples of systems that require ISPs. Many of these applications place strict requirements on the allowable inertial pointing error; a requirement complicated by the base motion of the given platform. ISPs minimize the effects of base motion disturbances enabling maximum performance of the attached payload.

Mobile RF Satellite Communication (SATCOM) systems provide an important arena for the application of ISP technology. The US military relies heavily on SATCOM terminal systems as key nodes in large information networks [5]. SATCOM often provides the only information medium capable of delivering required voice, imaging, and video information to military assets in deployed locations [6]. For dispersed military assets, SATCOM effectively spans distance, terrain, and hostile forces to



Figure 1-1: Photo examples of ISP Systems. Photos courtesy of Hilkert [4].

provide information to troops in need [7]. An increased expectation for instantaneous global communication also fuels a rapidly adapting commercial SATCOM market [5, 8]. Mobile SATCOM terminals fulfill both a military and a commercial need for global information availability, and the desire for instantaneous voice, picture, and video information requires that SATCOM systems achieve high data-rates.

RF SATCOM systems must maintain inertial pointing error to within tolerances specified by the components of the system in order to achieve the desired performance. Data transfer rates and Bit Error Rates (BER) provide the metrics for determining the performance of a SATCOM link, and these metrics may degrade substantially if the pointing error from the terminal to the satellite is increased by only fractions of a degree. An ISP in the form of a two-axis, servo-mechanical positioner with attached antenna payload provides a relatively simple and cheap solution to the inertial pointing problem for a mobile SATCOM terminal [9]. The two-axis positioner hardware requires the development of an adequate pointing strategy as well as an accompanying control software suite.

1.2 Problem Statement

High data-rate RF SATCOM terminals require accurate spatial pointing of the antenna payload. This thesis develops an inertial pointing strategy designed to meet the pointing requirements for an airborne, Extremely High Frequency (EHF) SATCOM terminal operating from a Boeing 707 aircraft owned and operated by MIT Lincoln Laboratory. The terminal uses a two-axis, servo-mechanical Antenna Positioner System (APS) with a dish antenna payload. The pointing strategy developed for this specific SATCOM application involves a hybrid open/closed loop approach. *Open-loop pointing* in the context of this paper is defined as the pointing of an antenna at a satellite without incorporating any RF signal strength measurements into the control scheme. By contrast, *closed-loop pointing* methods do incorporate RF signal strength feedback measurements in some fashion as a part of the pointing control strategy. It is the goal of this thesis to recommend a solution to the antenna pointing problem for the “EHF SATCOM on the 707” project, by:

1. Defining a nominal, two-axis APS and associated pointing requirements for accomplishing an airborne EHF SATCOM mission
2. Developing an open-loop controller for the nominal APS using state-space and optimal control techniques
3. Examining the performance of the open-loop pointing system through simulation
4. Obtaining a model for the open-loop pointing error distributions in two orthogonal inertial coordinates
5. Examining ways that optimization programming strategies for nonlinear functions may be applied to RF signal strength measurements to provide closed-loop feedback in the form of refinements to the APS’s open-loop pointing commands
6. Comparing the performance of several optimization step-tracking algorithms, in different configurations, on minimizing an antenna gain pattern cost function

7. Determining the overall feasibility of applying optimization methods to refine open-loop pointing commands to minimize inertial pointing error

1.3 Contributions

This thesis makes the following contributions while accomplishing the objectives outlined in Section 1.2:

1. The thesis develops an open-loop pedestal controller, using optimal control techniques, for a nominal two-axis, azimuth-elevation APS that mitigates the effects of 707 aircraft motion and tracks input reference commands. The techniques used to develop the open-loop controller for the nominal APS may be extended to projects wishing to use two-axis pedestals on other mobile or stationary SATCOM terminal systems.
2. A Simulink simulation is developed to test the performance of the open-loop controller. The same simulation may be used in a slightly modified form to test the open-loop pointing performance of similar APSs used on other SATCOM terminals.
3. This thesis demonstrates the feasibility of using step-tracking algorithms to accomplish closed-loop antenna pointing for a specific airborne SATCOM application. The performance of several step-tracking algorithms is tested through simulation, and the best performing algorithms are identified.
4. Simulations designed to test the robustness of the step-tracking algorithms are also implemented to show that step-tracking provides a viable closed-loop pointing strategy even under harsher operating conditions than what may be expected for the nominal APS's airborne EHF SATCOM mission. Although the thesis develops step-tracking algorithms for use on a particular airborne terminal system, the algorithms require only slight modifications to be used on other SATCOM terminals.

5. This thesis demonstrates that accurate antenna pointing may be accomplished by employing an open-loop pedestal controller in conjunction with a closed-loop step-tracking algorithm. The hybrid open/closed-loop pointing strategy presented in this thesis may be implemented on future stationary and mobile SATCOM terminals. Hybrid pointing systems utilizing step-tracking procedures require no additional hardware components to operate in a closed-loop fashion and may, therefore, lead to the proliferation of simpler, more cost-effective SATCOM terminal systems.

1.4 Thesis Overview

Chapter 2 of this thesis discusses the technologies available to accomplish a mobile SATCOM mission. These technologies vary in complexity and cost, and Chapter 2 defines a nominal APS that will meet the pointing requirements for an airborne EHF SATCOM mission with the simplest possible system. Thus, objective 1 from Section 1.2 is accomplished. Objectives 2 and 3 require the development of an open-loop feedback controller for the nominal APS. Chapter 3 follows the development of the feedback controller and develops linear and nonlinear open-loop pointing simulations. Chapter 3 also develops a model for the statistical distributions of the components of open-loop pointing error, satisfying objective number 4. The closed-loop pointing simulations implemented in Chapter 4 require an understanding of the behavior of the open-loop pointing error. Chapter 4 develops step-tracking algorithms that accomplish closed-loop antenna pointing. The step-tracking algorithms utilize nonlinear cost function optimization techniques, and several simulations are developed to test the pointing performance of these algorithms in different configurations, accomplishing objectives 5 and 6. Finally, objective 7 is satisfied as the results of both the open-loop pointing simulations and the closed-loop step-tracking simulations are discussed in Chapter 5 to determine the overall feasibility of a hybrid open/closed-loop pointing strategy.

Chapter 2

Background and System Architecture

Chapter Overview

Engineers may choose from multiple ISP configurations when determining the spatial pointing approach that will meet the requirements of a given system. In mobile RF SATCOM applications, the Antenna Positioner System (APS) serves as an ISP for pointing an antenna payload at a target satellite to establish a communications link. This chapter examines various configurations of APS hardware that could be used to solve the inertial pointing problem in an RF SATCOM application. The sources of error inherent in purely open-loop pointing strategies will be highlighted, and the closed-loop pointing methods that may be implemented to compensate for these shortcomings are discussed. Finally, this chapter identifies the hardware components and pointing requirements for a nominal two-axis Antenna Positioner System that closely models the actual APS used in the “EHF SATCOM on the 707 project.” The development of a pointing strategy for this nominal APS will be the topic of discussion in the following chapters.

2.1 APS Hardware Configurations

2.1.1 APS Components

An APS consists of all of the hardware components used to position an antenna in order to maintain an effective communications link with a satellite. APSs used in SATCOM On-The-Move applications share many common functional components regardless of differences in form. The building blocks of an APS include the antenna payload, servo-mechanical pedestal, gyroscopes and angular position sensors, Inertial Measurement Unit (IMU) with GPS hardware, pedestal control computer, and any necessary cabling and waveguide. The terminal's modem provides the pedestal control computer with signal strength measurements for use in closed-loop control schemes, but the modem is not considered part of the APS. Figure 2-1 shows an APS block diagram that may help the reader visualize the interconnect of APS hardware.

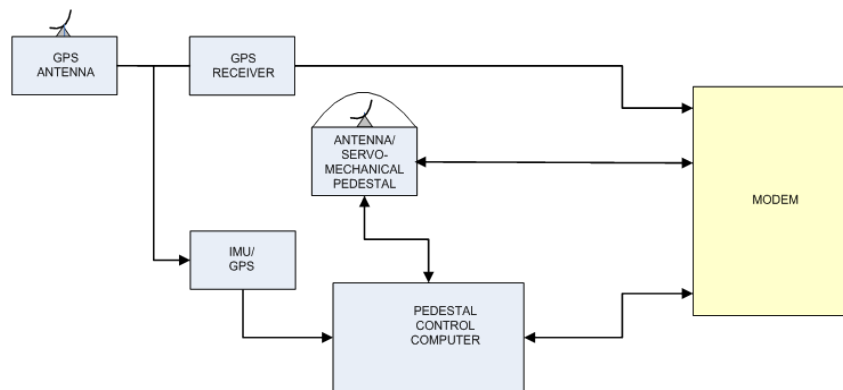


Figure 2-1: APS Interconnect Block Diagram. Figure courtesy of M. Gridley, MIT LL, Group 61

2.1.2 Antenna Payloads

ISP pointing requirements are dictated by the type of payload sensor being positioned and its role in the overall system architecture. In a mobile RF SATCOM application,

the ISP's payload is the antenna that the terminal uses to transmit to and receive data from the satellite. In high-bandwidth SATCOM applications, antennas must be directional and must exhibit high *gain* in accordance with the requirements of the terminal system [9]. Antenna gain, measured in dB, is a measure of how well a particular antenna directs electromagnetic energy relative to an isotropic antenna, which collects and emits electromagnetic energy equally in all directions. The gain of a directional antenna changes depending upon the incidence angle at which electromagnetic waves intersect the antenna's *boresight*, or direction of maximum gain. The variation of gain with respect to pointing angle away from boresight forms an antenna's *gain pattern* [9]. Figure 2-2 illustrates a nominal antenna gain pattern formed by varying the incidence angle across a single axis orthogonal to the antenna's boresight. Figure 2-3 shows the gain pattern formed when angular deviations from boresight occur in two axes that are orthogonal to both the boresight direction and to each other.

Figures 2-2 and 2-3 show that the maximum gain occurs when angular variations from boresight equal zero. The values of gain between the first *nulls*, or minimums, of the gain pattern constitute the antenna's *mainlobe*. As angular deviation from boresight increases and a null is crossed, the gain rises again forming secondary peaks known as *sidelobes*. Figure 2-2 also identifies the Half-Power Beamwidth (HPBW), or the distance between points on opposite sides of the mainlobe peak with gain values that are 3dB lower than the gain value at boresight. Directional antennas in SATCOM systems are usually designed to operate within the HPBW in order to achieve desired system performance; therefore, a directional antenna must be pointed at a target satellite with a maximum pointing error equivalent to half the HPBW of the antenna. Many systems require pointing accuracies better than half the HPBW, but the HPBW serves as a means of comparing pointing accuracy requirements across different terminal systems. In any system, the most desirable pointing scenario occurs when the antenna's boresight direction aligns perfectly with the terminal to satellite pointing vector and the antenna is said to be *on boresight*.

Two factors which directly impact the width of the HPBW are antenna aperture size and the transmit (TX)/receive (RX) frequencies at which the terminal operates.

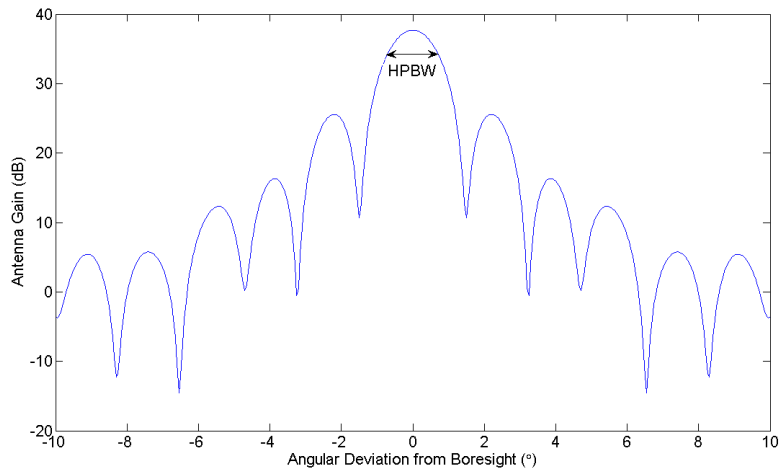


Figure 2-2: Antenna Gain Pattern (24 in. dish)

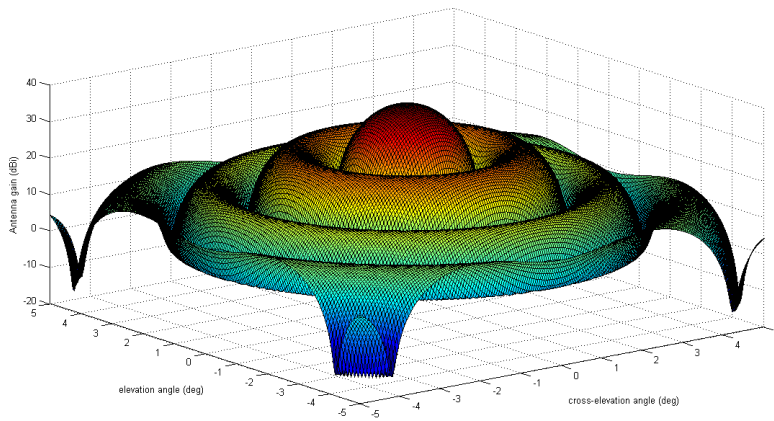


Figure 2-3: Gain Pattern as a Function of Two Orthogonal Angles (24 in. dish)

Figure 2-4 graphically shows the variation in HPBW with respect to changes in dish diameter and TX/RX frequencies for a dish antenna. Larger antennas produce higher gains but have narrower HPBWs and may be cumbersome when operating in a mobile environment. The size of the antenna also impacts the size, complexity, and cost of the pedestal used to point the antenna [2]. Government regulations determine the TX/RX frequencies for SATCOM systems, and the operating frequencies cannot be changed by the design engineer. Because TX frequencies are usually higher than RX frequencies, the terminal requires greater pointing accuracies when transmitting data across the SATCOM link.

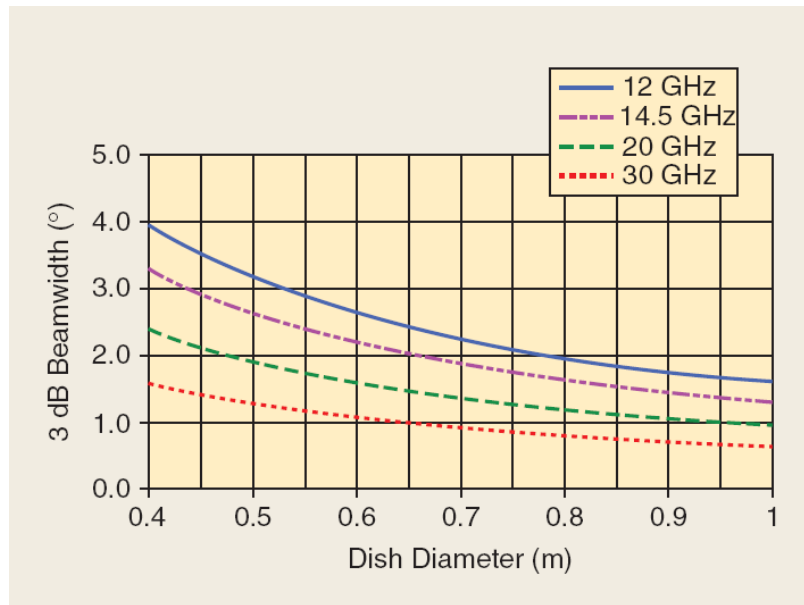


Figure 2-4: HPBW as a Function of Antenna Size and Operating Frequency. Figure courtesy of Debruin [9].

Antennas may be steered electronically, mechanically, or by a combination of electronic and mechanical means [9]. Dish antennas require mechanical steering; whereas, array antennas may be steered mechanically or electronically. The use of either type of antenna involves design trade-offs with implications on the pointing control strategy. Array antennas accomplish a great deal of the pointing problem by changing the phase of individual antenna elements on the array in order to change the direction of the antenna’s boresight [10]. Therefore, if required at all, the antenna positioner may need to only coarsely point the array in the general direction of a target

or control pointing in only one axis. Due to their small size and low profile, array antennas may integrate nicely with the structure of the given vehicle in a mobile application. However, array antennas are expensive relative to dish antennas, and they involve complex control algorithms for the electronic steering of the mainlobe [9]. As array antennas are electronically steered, the sidelobes in the gain pattern rise and fall resulting in required software algorithms to suppress them to acceptable levels [10]. Dish antennas are cheaper but necessitate a servo-mechanical pedestal to point the antenna in the desired direction. Integrating the RF waveguide with the particular pedestal-antenna combination may also be challenging. For instance, the APS may require a waveguide assembly to carry RF energy through the positioner by means of rotary joints. For multi-axis pedestals, this task becomes more difficult and poses additional design constraints. The use of simpler positioners or electronically steered array antennas alleviates some of the design challenges of the RF waveguide system.

Another consideration for selecting the appropriate antenna for a mobile SATCOM application is the method of antenna stabilization around the pointing vector. Dish antennas exhibit an advantageous property known as *mass stabilization* [9]. Mass stabilization is an extension of Newton's first law which affirms that objects at rest tend to remain at rest. Thus, although dish antennas require a servo-mechanical pedestal to steer the antenna to different points in the sky, the positioner system requires only relatively small amounts of motor torque to stabilize the antenna once it is pointed. Mass stabilization is most beneficial for SATCOM applications where target satellites are in geostationary orbits because the look angles from the terminal to the satellite change very little under these circumstances. Mass-stabilized systems still require motor control systems to provide motor torques to account for bearing friction and other disturbance torques as well as to slew the antenna to different positions in the sky.

Electronically steerable array antennas are, by nature, non-mass-stabilized [9]. If all pointing is done electronically, the lack of mass-stabilization does not pose a significant problem because there is no mass to move in order to steer the antenna; however, if some of the pointing is accomplished mechanically, torques proportional

to the size of the movable components are required from the pedestal motors. Inertial Pointing Applications utilize other forms of stabilization including momentum-wheel-stabilization, where rotating masses are used to provide inertially stable platforms for mounting sensors. Momentum-wheel-stabilization techniques pose problems for applications requiring sensors that change inertial pointing directions frequently, and the spinning momentum-wheels could interfere with vehicle motion. Therefore, momentum-wheel-stabilization techniques are not widely applied to terminals in SATCOM On-The-Move applications [4].

2.1.3 Pedestals and Sensors

The physical characteristics of servo-mechanical pedestals generally consist of a structural framework capable of rotational motion called a *gimbal* to which an assembly of motors, bearings, gyroscopes, and payload devices are attached [4]. Pedestals used in APSs may be classified as one-axis, two-axis, or multi-axis systems according to the number of controllable axes present. Figure 2-5(a) illustrates gimbal devices for typical two-axis pedestals. Multiple gimbals may sometimes be constructed to control a sensor payload in the same axis. This set-up typically takes the form of a *coarse* outer gimbal and accompanying motor configuration with an inner *fine* gimbal and motor configuration as seen in Figure 2-5(b). The capabilities needed to maintain adequate pointing of the payload in the region of inertial space relevant to the application determines the number of required controllable axes for a pedestal system.

In RF SATCOM applications, only the inertial axes orthogonal to the pointing vector from the antenna to the target satellite need to be controlled by the APS. Motion in the antenna's roll axis is not relevant to the pointing problem due to the symmetric nature of the gain pattern. Two-axis servo-mechanical pedestals using an azimuth-elevation gimbal configuration are commonplace in SATCOM applications because, together, the two axes provide a complete hemispherical field-of-regard [9]. Figure 2-6 shows the two-axis pedestal and antenna used on the "EHF SATCOM on the 707 Project." The azimuth-elevation positioner provides an adequate solution for

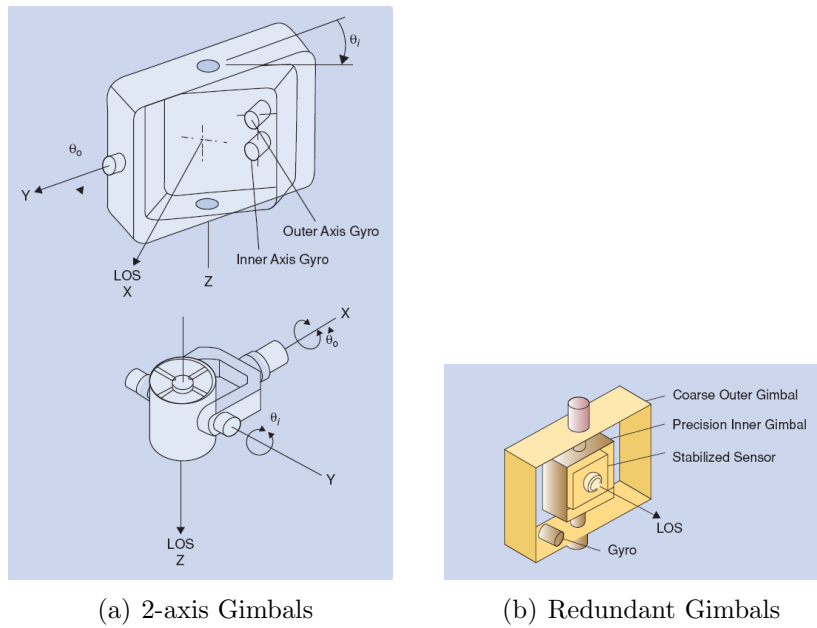


Figure 2-5: Gimbal Structures. Figures courtesy of Hilkert [4].

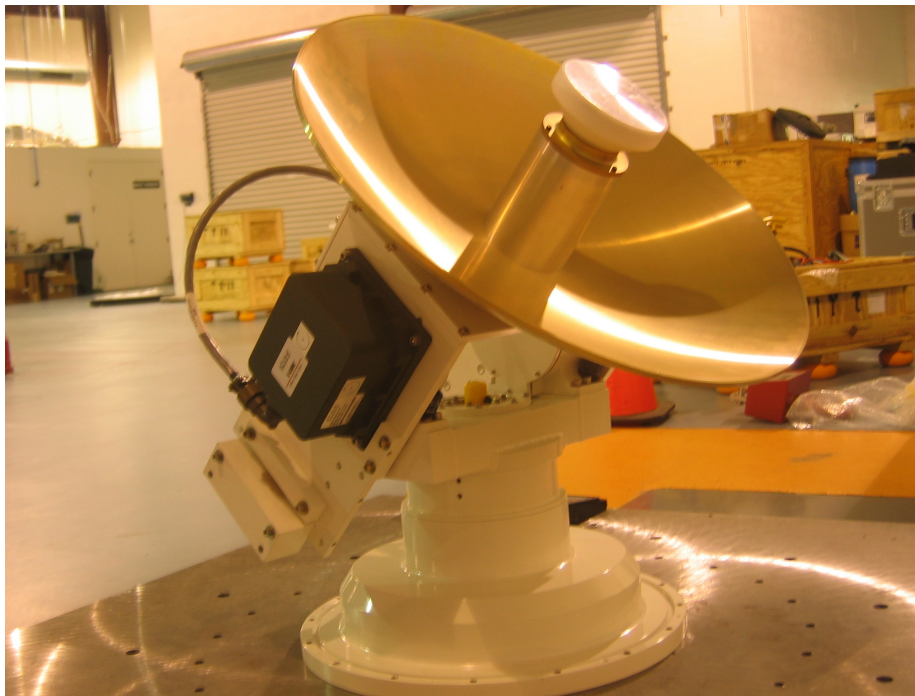


Figure 2-6: Two-axis Az/El positioner used in the “EHF SATCOM on the 707” project

antenna pointing under many conditions. Additional steerable axes may be added to the basic two-axis configuration to achieve added base motion disturbance rejection, increase the field-of-regard of the pedestal, and to eliminate singularities that can result from simple two-axis configurations [4].

The major concern with operating a two-axis, azimuth-elevation antenna positioner occurs when the application requires pointing in the *keyhole* region. The keyhole region is loosely defined as pedestal operation at local elevation angles greater than 80° [9]. During tracking, the azimuth motor attempts to correct for vehicle motions that occur in the roll axis of the pedestal's base. The pedestal base roll axis is the same as vehicle roll when the pedestal's azimuth gimbal is aligned with the front or back of the vehicle. Angular motion about the pedestal base roll axis corresponds to rotations in the vehicle's pitch direction when the pedestal's azimuth gimbal is pointed to either side of the vehicle. Vehicle motion in the roll axis of the pedestal's base becomes more difficult to account for with a two-axis pedestal as elevation angles approach the keyhole region and a singularity known as *gimbal lock* results [4]. The required azimuth motor velocity varies with elevation angle, el , according to

$$\dot{az}_d = -\tan(el)P'_{Base} - R'_{Base} \quad (2.1)$$

where \dot{az}_d is the azimuth motor velocity required to maintain fixed inertial pointing, P'_{Base} is the vehicle motion resolved in the roll axis of the pedestal's base, and R'_{Base} is the vehicle motion resolved in the yaw axis of the pedestal's base (Equations (A.17) and (A.18)). Equation (2.1) clearly shows how an infinite azimuth motor velocity is required at an elevation angle of 90° , and the azimuth motor eventually lacks the required torque to keep the antenna pointed correctly as elevation angles enter the keyhole region. Several different configurations for multi-axis pedestals exist, but most are designed explicitly to eliminate the gimbal lock singularity in the keyhole region. The reader is referred to the literature for more information on multi-axis pedestals [9,11]. Despite the advantages that multi-axis pedestals maintain over two-axis configurations in avoiding gimbal lock, all else being equal, two-axis pedestals

are generally stiffer, cheaper, more compact, and less complex than their multi-axis counterparts [9]. Therefore, the design engineer may find it beneficial to use a two-axis pedestal whenever possible.

Angular position and rate sensors are typically installed in locations of interest on the pedestal in order to facilitate feedback for the pedestal controller. Position sensors may take the form of encoders or resolvers and are installed in the movable axes of the pedestal. Angular position sensors exhibit different degrees of accuracy dependent upon their complexity and cost. Gyroscopic sensors measure angular rates about the axes of interest and vary greatly in terms of cost and performance. Figure 2-7 shows the relative accuracies, in terms of scale factor and bias stabilities, for a number of different types of gyroscopic sensors. Figure 2-7 also maps specific applications to the different types of gyroscopic sensors that may be used in the applications. This mapping provides a holistic comparison of the quality of gyroscopic sensors. Inertial Measurement Units contain gyroscopes and accelerometers and measure the inertial states of the vehicle upon which the pedestal is mounted. Because vehicles are not true rigid bodies, they exhibit varying degrees of flexure necessitating placement of the IMU in a location very near or on the base of the pedestal in order to obtain accurate measurements of the vehicle's motion. The accuracy and alignment of all sensors impacts the pointing performance of the APS.

2.1.4 APS Design Requirements

The specific SATCOM mission determines the requirements that an APS must fulfill. The design engineer must select the appropriate APS hardware such that all requirements of the system are met, and the desired inertial pointing accuracy is achieved. The APS must meet specified size and weight requirements which are particularly stringent for mobile terminal systems [2]. The mass and inertia of the antenna payload determines the size and weight of the servo-mechanical pedestal. When size and weight are limiting factors in design, the attainable pointing accuracy may become a design tradeoff. For mobile terminals using mechanically steered antennas, the dynamics of the operating environment determine velocity and acceleration requirements

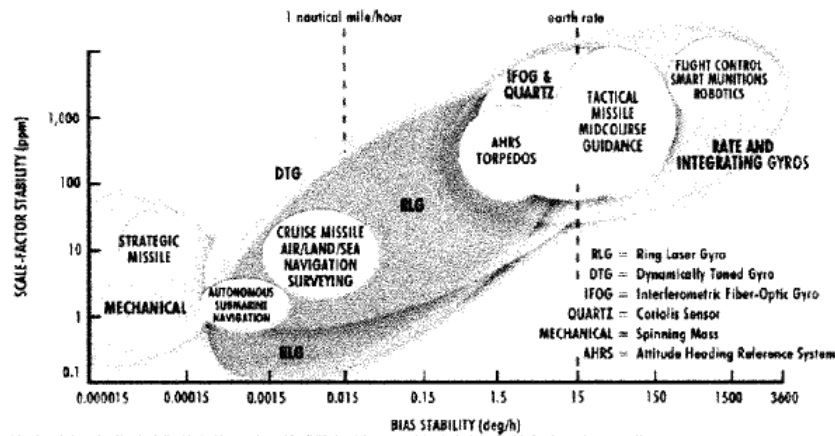


Figure 2-7: Gyroscope (IMU) Accuracy Mapped to Applications. Figure Courtesy of Barbour and Schmidt [12].

for antenna movement. More severe operating environments require larger pedestal accelerations and velocities, necessitating larger and more powerful actuators [2].

The operating environment dictates the required inertial pointing bandwidth of the positioner. The positioner must have a bandwidth greater than the highest notable frequency component of the base motion disturbances caused by vehicle motion. If the positioner lacks adequate bandwidth, then base motion disturbances at higher frequencies will cause mispointing. The first major resonance of the pedestal structure and attached antenna upper-bounds the positioner's bandwidth [2]. If the positioner is allowed to operate at frequencies near structural resonances, the pedestal structure could deform or break. APSs must also meet jitter and repeatability requirements which specify how well the pedestal controller can hold a particular look angle or return to a previously commanded look angle.

2.2 Control Strategies

The pedestal control computer governs the motion of the APS's servo-mechanical pedestal. Pedestal sensor data as well as vehicle inertial state data from the IMU are input to the pedestal controller which, in turn, outputs voltages that control

the DC motor circuits in the pedestal. The pedestal controller may also interface with the terminal's modem to receive RF signal strength measurements for use in closed-loop pointing control strategies. The voltage outputs to the pedestal motors are governed by feedback control loops that are implemented as a part of an overall pointing strategy which may be open or closed-loop.

2.2.1 Open-loop Pointing and Sources of Error

Open-loop pointing techniques implemented in mobile SATCOM systems involve similar pedestal control issues as those encountered in other applications such as fixed ground station SATCOM, aerial surveillance, and weapon systems targeting [9]. The goal of the controller in an open-loop configuration is to negate the effects of vehicle base motion disturbances while simultaneously following an input reference command. APSs used in mobile SATCOM applications continuously obtain measurements of the vehicle's inertial states and calculate desired look angles to the target satellite in the pedestal's local reference frame. These look angles are fed as reference commands to a feedback control loop which steers the pedestal to the desired location. The kinematic equations and coordinate transformations which govern the look angle calculations for a two-axis APS are presented in Appendix A. The open-loop controller accounts for base motion disturbances by quickly updating the look angle reference commands, by direct feedback of the antenna's inertial states to the feedback controller, or by a combination of the two approaches.

Open-loop pointing strategies involve sources of error which may lead to mispointing of the antenna in inertial space. Notable sources of error which may not be taken into account in open-loop pointing schemes include:

1. Aged satellite ephemeris data
2. Unmeasured IMU misalignment angles
3. Nonorthogonality of pedestal axes
4. Steady-state biases in pedestal position sensors and the IMU

5. Misalignment of gyroscopic rate sensors

Aged satellite ephemeris data causes inaccuracies in the pedestal look angle calculations that, in turn, cause steady-state inertial pointing errors. Unmeasured misalignment angles, with components in the roll, pitch, and yaw angles between the IMU and the pedestal base, cause pointing errors that are time-varying and become coupled with the vehicle's motion [13]. Nonorthogonality of the pedestal's axes also cause time-varying errors that are coupled with vehicle motion [14]. Sensor errors and biases impact pointing error similarly to misalignment errors. Steady state biases in the IMU and pedestal position sensors as well as gyro misalignments are sensor errors which are difficult to measure and may go unaccounted for in open-loop pointing strategies. Open-loop pointing strategies provide a viable means of conducting mobile SATCOM operations provided that the sources of error present are small relative to the allowable pointing error. If pointing error requirements are stringent and the possibility for sources of error likely, some form of closed-loop control strategy becomes needed.

2.2.2 Closed-Loop Antenna Pointing Methods

In many RF SATCOM systems with stringent pointing requirements, a closed-loop pointing strategy is needed to help mitigate the sources of error present in a purely open-loop pointing approach. Many of these errors are time-varying and become coupled with the dynamic motion of the vehicle in a mobile SATCOM application and are, therefore, difficult to compensate for with open-loop pointing. Closed-loop pointing strategies keep the antenna beam on boresight as deviations occur due to errors in open-loop pointing. At this point it is helpful to divide closed-loop pointing into two phases which occur in chronological order in a SATCOM terminal system; *spatial pull-in* and *tracking* [15]. The spatial pull-in process removes initial antenna pointing errors and terminates when the pointing error is reduced to some desirable amount such as the antenna's HPBW. Satellite tracking is any process which actively uses feedback in order to steer the antenna beam on boresight [15]. Three of the

most prevalent closed-loop pointing techniques are monopulse, conical scan, and step-tracking [16].

Monopulse tracking involves the use of additional hardware, in the form of one or more antennas in addition to the main antenna, which measure the signal strength of the communications link. By comparing the signal levels received in the monopulse antennas, the main antenna may be steered in the appropriate direction to eliminate pointing errors [17, 18]. Because the mispointing feedback is nearly continuous, controllers can be designed to close the loop around the pointing error feedback metric. Figure 2-8 shows a monopulse system design in which four separate monopulse antennas are mounted directly to the feed used with a dish antenna. Implementation of a monopulse system on a mobile SATCOM terminal could provide accurate and robust closed-loop satellite tracking at the expense of a more complex system.



Figure 2-8: Monopulse Antenna System. Photo courtesy of S. Targonski, MIT LL, Group 63

Conical scan (con-scan) systems harmonically raster the antenna beam to create signal strength power variations used to estimate the location of the satellite [19]. Antenna beam rastering is accomplished with a dish antenna either by physically steering the dish or by moving the feed assembly. The latter technique requires additional system hardware components, as the feed itself must be mechanically steered, but may be the more viable option for systems using larger dishes. Mobile SATCOM systems may accomplish beam scanning by steering the dish with the pedestal, as dishes used

in mobile terminals are typically small and additional moving hardware components are undesirable. Although conical scan methods pose a viable closed-loop pointing solution for mobile SATCOM applications, the strategy must be implemented with great care as the mobile pointing problem is greatly nuanced. Intentional antenna mispointing must be weighed against desired pointing performance. The pointing errors inherent in the open-loop control scheme also dictate how far the dish must be dithered off boresight and directly impact the con-scan signal measurements. Typically, a continuous, harmonic scan pattern is followed with a period between 30 and 120 seconds [19]. Pointing errors and terminal system noise may dictate longer con-scan periods because they necessitate longer integration times for obtaining accurate signal strength measurements. If the con-scan period is too long, time-varying pointing errors may go uncorrected.

Step-tracking methods are the simplest and least expensive to implement of the closed-loop pointing techniques and typically require no additional system hardware [11, 16]. The simplest step-tracking method compares signal strength measurements obtained by physically changing the antenna's angular position and then steers the antenna in the direction of the higher power measurement. More complicated step-tracking methods may be developed using nonlinear optimization techniques. Many closed-loop systems, such as monopulse and con-scan, cannot engage in tracking until the initial pointing error has been reduced to an acceptable amount in the spatial pull-in stage. Step-tracking methods are perhaps the only means available to perform the spatial pull-in task; thus, sound step-tracking techniques become more important because of their use with other forms of closed-loop tracking.

The goal of each of the closed-loop pointing strategies mentioned above is to improve the overall pointing performance of an APS, but all closed-loop methods add a degree of complexity to the pointing problem and many require additional hardware components which necessitate a more thoughtful APS design.

2.3 Nominal APS System Architecture

The APS used on the “EHF SATCOM on the 707” project incorporates each of the hardware components seen in Figure 2-1. Figure 2-6 shows the actual two-axis pedestal and dish assembly used on the project. The nominal APS, referenced throughout the remainder of the paper, models this real-life system and is intended to accomplish the same mission of airborne EHF SATCOM. The goal of the nominal APS is to achieve the greatest pointing accuracy possible with the simplest, most cost-effective system.

The nominal APS uses a parabolic dish antenna because it is more cost-effective than an array antenna. The nominal APS will incorporate the same 24 in. diameter dish design used in the “EHF SATCOM on the 707” project. The gain patterns for the 24 in. dish are shown in Figures 2-2 and 2-3. The use of a dish antenna necessitates a servo-mechanical pedestal in order to slew the antenna and correct for disturbance torques on the dish. A two-axis, azimuth-elevation pedestal is selected for the nominal APS because the operational tests for the “EHF SATCOM on the 707” project will be conducted at latitudes great enough to avoid pedestal operation in the keyhole region. Thus, a larger, heavier, and more complex three-axis pedestal is not required. The selection of a two-axis pedestal also simplifies the control system design due to a reduced gimbal order. Cleveland Motion Controls(CMC) 2100 series brush servo-motors with F windings are chosen as the steering motors in both the azimuth and elevation axes of the nominal pedestal [20]. The CMC 2100 F servo-motor is selected because the same motors were used with good results on a similar sized three-axis pedestal for a land-vehicle SATCOM On-The-Move project conducted at MIT Lincoln Laboratory in 2003. The operating environments for land-vehicles subject antenna positioners to much harsher base motion disturbance dynamics than those encountered in large aircraft. For this reason, the CMC 2100 F motors should be adequate for use in an APS conducting airborne SATCOM.

The nominal pedestal incorporates accurate angular resolvers in both the azimuth and elevation axes and includes a two-axis KVH Industries fiberoptic gyroscope pack-

age mounted to the elevation gimbal in order to measure the inertial rates of the dish antenna in the pitch and yaw axes [21]. The fiberoptic gyroscopes used are employed in munitions guidance systems and should provide adequate measurements in spatial tracking applications (Figure 2-7). The project uses a C-MIGITS IMU system to measure the inertial states of the 707 aircraft at the location where the pedestal is mounted. The C-MIGITS is a navigation-grade IMU that is also frequently used in munitions guidance applications [22].

The nominal APS must incorporate a pedestal feedback controller which will limit inertial pointing error to within 0.1° ($3\text{-}\sigma$) of boresight in an open-loop pointing simulation. The gain patterns for the 24 in. dish shown in Figures 2-2 and 2-3 illustrate that an inertial pointing error of 0.1° would have a negligible impact on the quality of the SATCOM link. Because of the sources of error identified in Section 2.2.1, the desired pointing requirement of 0.1° may not be achievable while operating in a purely open-loop fashion. For this reason, the nominal APS requires inertial pointing to within 0.25° of boresight or better in a closed-loop pointing simulation. Inertial pointing error of 0.25° corresponds to a 0.4 dB loss in signal strength and would have very little impact on the overall performance of the SATCOM link (Figure 2-2). With the hardware and pointing requirements for the nominal APS now defined, the open-loop portion of the hybrid pointing control strategy may be developed.

Chapter 3

Open-Loop Controller Development

Chapter Overview

Open-loop pointing strategies necessitate a feedback controller for the mechanical pedestal used to position the antenna payload. In this chapter, a Linear Quadratic Gaussian (LQG) controller will be developed, based on the nominal two-axis APS defined in the previous chapter, to effectively control the pedestal's azimuth and elevation DC servo-motors. For typical flight profiles, this controller will be able to reduce the effects of base motion disturbances caused by aircraft motion and keep the antenna dish inertially pointed at a target satellite. The controller will operate in a closed-loop fashion, obtaining feedback from the inertial states of the antenna, but because RF signal strength measurements are not introduced into the control scheme, the resulting controller is classified as open-loop in the context of the definitions from Section 1.2. After the feedback controller is developed, and the performance is simulated, the statistical distributions for the components of inertial pointing error will be modeled for use in closed-loop pointing simulations developed in the next chapter.

3.1 Equations of Motion

3.1.1 Response Side

In any control system design process, the first step is to determine the Equations of Motion (EOM) for the dynamics of the system *plant*. The plant constitutes the physical system that is to be controlled [23]. In the case of an APS, the servo-mechanical pedestal and attached antenna comprise the system plant. First, because the goal of the controller is to hold the *dish* inertially stable, an inertial coordinate frame with respect to the dish is defined and called the *Antenna Body Coordinate Frame*. The Antenna Body Coordinate Frame is represented by the solid axes lines in Figure 3-1. The equations of motion used to model the antenna positioner dynamics are derived from the standard rotating rigid body equations of motion [4, 24].

$$\dot{P}I_{xx} + QR(I_{zz} - I_{yy}) - (Q^2 - R^2)I_{yz} - (\dot{R} + PQ)I_{xz} + (PR - \dot{Q})I_{xy} = \sum_x T \quad (3.1)$$

$$\dot{Q}I_{yy} - PR(I_{zz} - I_{xx}) + (P^2 - R^2)I_{xz} - (RQ + \dot{P})I_{xy} + (PQ - \dot{R})I_{yz} = \sum_y T \quad (3.2)$$

$$\dot{R}I_{zz} + PQ(I_{yy} - I_{xx}) - (P^2 - Q^2)I_{xy} - (PR + \dot{Q})I_{yz} + (QR - \dot{P})I_{xz} = \sum_z T \quad (3.3)$$

In Equations (3.1)-(3.3), P , Q , and R represent inertial rotation rates in the antenna Body roll (x), pitch (y), and yaw (z) axes respectively, the I terms represent moments or cross products of inertia, and the T terms represent applied torques in the corresponding axes. Translational equations of motion are ignored in the development of antenna positioner equations of motion because they have negligible effects on satellite pointing accuracy due to the great distance from the terminal to the satellite [9]. Because of the symmetry of the antenna and the pedestal elevation axis gimbal, all of the cross products of inertia in (3.1)-(3.3) are assumed to be zero. The response sides (LHS) of Equations (3.1)-(3.3) are linearized about a stationary operating point (coinciding with the desired pointing vector), according to the technique described in [24], and no steady state antenna yaw, pitch, or roll velocities are incorporated into the linearized response side of the EOMs. The resulting linearized response side

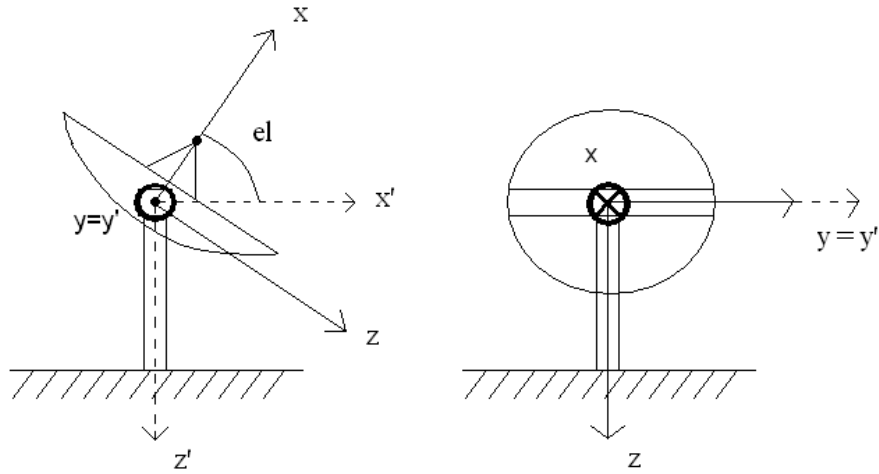


Figure 3-1: Pedestal Coordinates

of the Equations of Motion reduces to Equation (3.4) where \dot{P} , \dot{Q} , and \dot{R} represent inertial perturbation accelerations in each of the Body axes around the stationary operating point.

$$\begin{bmatrix} I_{xx} & 0 & 0 \\ 0 & I_{yy} & 0 \\ 0 & 0 & I_{zz} \end{bmatrix} \begin{bmatrix} \dot{P} \\ \dot{Q} \\ \dot{R} \end{bmatrix} = \begin{bmatrix} \sum_x T \\ \sum_y T \\ \sum_z T \end{bmatrix} \quad (3.4)$$

3.1.2 Moment Side

The right hand side of (3.4) consists of the applied moments which act on the dish. The two sources for applied moments are motor torques and base motion disturbance torques which will be discussed later. The two-axis nominal APS has two DC motors which effect changes in both the azimuth (z') and elevation ($y = y'$) axes which are represented in the *Antenna Base Coordinate Frame*. Figure 3-1 depicts the antenna Base Coordinate Frame with dashed axis lines. At this point it is convenient to completely specify local azimuth and elevation look angles. Local azimuth is specified as a rotation about the z' axis clockwise from the x' axis unit vector and may range from 0-360°. Elevation is specified as a rotation about the y' axis above the xy plane and may range from 0-90°. The relationship between the antenna's Body coordinates (x,y,z) and Base coordinates (x',y',z') involves a coordinate transformation through

a negative elevation angle (3.5).

$$\begin{bmatrix} x' \\ y' \\ z' \end{bmatrix}_{Base} = \begin{bmatrix} \cos(el) & 0 & \sin(el) \\ 0 & 1 & 0 \\ -\sin(el) & 0 & \cos(el) \end{bmatrix} \begin{bmatrix} x \\ y \\ z \end{bmatrix}_{Body} \quad (3.5)$$

Because the azimuth motor acts in the z' axis, its applied torque enters nonlinearly into the Body x and z axes due to a coordinate transformation; whereas, the elevation motor applies torque directly to the Body y axis (3.6).

$$\begin{bmatrix} \sum_x T_{motor} \\ \sum_y T_{motor} \\ \sum_z T_{motor} \end{bmatrix} = \begin{bmatrix} -\sin(el)T_{az} \\ T_{el} \\ \cos(el)T_{az} \end{bmatrix} \quad (3.6)$$

For a DC motor, applied torques (T) are proportional to the current in the armature circuit, i_a (3.7). In Equation (3.7), K_m is the motor constant for the particular DC motor. The armature current is governed by a differential equation that accounts for armature inductance (L_a) and resistance (R_a), back emf voltage (e_b), and applied armature voltage (e_a) (3.8). Back emf voltage results from the rotating armature and is proportional to the angular velocity ($\dot{\theta}_1$) of the motor shaft by a constant, (K_b), which is approximately the reciprocal of K_m (3.9). The applied armature voltage is the value eventually determined by the feedback controller to effect the desired motor torque [23].

$$T = K_m i_a \quad (3.7)$$

$$e_a = L_a \frac{di_a}{dt} + R_a i_a + e_b \quad (3.8)$$

$$e_b = K_b \dot{\theta}_1 \quad (3.9)$$

If armature inductance is neglected, which is often the case due to its small value, then the applied motor torques for the azimuth and elevation motors may be represented

as in (3.10) and (3.11).

$$T_{az} = \frac{K_{maz}}{R_{aaz}} e_{aaz} - \frac{K_{maz} K_{baz}}{R_{aaz}} [-\sin(el)\dot{\theta}_{roll} + \cos(el)\dot{\theta}_{yaw}] \quad (3.10)$$

$$T_{el} = \frac{K_{mel}}{R_{ael}} e_{ael} - \frac{K_{mel} K_{bel}}{R_{ael}} \dot{\theta}_{pitch} \quad (3.11)$$

In Equations (3.10)-(3.11) the angular velocities of the motor shafts, represented in the Base coordinate frame, are expressed in terms of the angular velocities of the dish with respect to the aircraft in the Body frame (3.12).

$$\begin{bmatrix} \dot{\theta}_{roll} \\ \dot{\theta}_{pitch} \\ \dot{\theta}_{yaw} \end{bmatrix}_{Base} = \begin{bmatrix} \cos(el) & 0 & -\sin(el) \\ 0 & 1 & 0 \\ \sin(el) & 0 & \cos(el) \end{bmatrix} \begin{bmatrix} 0 \\ \dot{\theta}_{el} \\ \dot{\theta}_{az} \end{bmatrix}_{Body} \quad (3.12)$$

The nominal APS incorporates a gear train to magnify the applied steering torques on the dish without using larger motors. The gear ratio (n_g) is defined as the ratio of the radius of the smaller gear (r_1), mounted to the motor shaft, to the radius of the larger gear (r_2) that is mounted to the output shaft [23]. The following relationship relating the angular velocities of the motor shaft and the output shaft may be determined [23]:

$$\frac{\dot{\theta}_2}{\dot{\theta}_1} = \frac{r_1}{r_2} = n_g \quad (3.13)$$

where $\dot{\theta}_1$ is the angular velocity of the motor shaft and $\dot{\theta}_2$ is the angular velocity of the output shaft. Using Equation (3.13) and the fact that the inertias of the motor shafts are very small compared to the inertias of the antenna and elevation gimbal assembly, Equations (3.4), (3.6), (3.10), and (3.11) may be combined, incorporating the gear train, to yield (3.14).

$$\begin{bmatrix} I_{xx} & 0 & 0 \\ 0 & I_{yy} & 0 \\ 0 & 0 & I_{zz} \end{bmatrix} \begin{bmatrix} \dot{P} \\ \dot{Q} \\ \dot{R} \end{bmatrix} = \begin{bmatrix} -\frac{K_{maz}}{n_g R_{aaz}} e_{aaz} \sin(el) - \frac{K_{maz} K_{baz}}{n_g^2 R_{aaz}} \sin^2(el) \dot{\theta}_{roll} \\ + \frac{K_{maz} K_{baz}}{n_g^2 R_{aaz}} \sin(el) \cos(el) \dot{\theta}_{yaw} + \sum_x T_{disturbance} \\ \frac{K_{mel}}{n_g R_{ael}} e_{ael} - \frac{K_{mel} K_{bel}}{n_g^2 R_{ael}} \dot{\theta}_{pitch} + \sum_y T_{disturbance} \\ \frac{K_{maz}}{n_g R_{aaz}} e_{aaz} \cos(el) + \frac{K_{maz} K_{baz}}{n_g^2 R_{aaz}} \sin(el) \cos(el) \dot{\theta}_{roll} \\ - \frac{K_{maz} K_{baz}}{n_g^2 R_{aaz}} \cos^2(el) \dot{\theta}_{yaw} + \sum_z T_{disturbance} \end{bmatrix} \quad (3.14)$$

The moment side of (3.14) has several trigonometric nonlinearities arising from coordinate transforms. Since the feedback controller that will be implemented acts on a linear plant model, (3.14) must be linearized. The system in (3.14) is linearized about a 0° elevation angle operating point in order to remove completely the trigonometric functions. The effects of this linearization and the resulting measures used to compensate for it in the simulation of the controller-system plant are discussed in 3.2.6. Once the disturbance torques in (3.14) are appropriately modeled, the linear plant model for the servo-mechanical pedestal will be complete.

3.1.3 Base Motion Disturbance Modeling

With a two-axis APS configuration, even if a mass-stabilized antenna is used, aircraft motion in the Base coordinate system x' axis causes antenna mispointing when elevation angles are greater than 0° and must be accounted for. For instance, when the elevation angle is 30° and the antenna is pointed at an azimuth angle of 0° (x' axis aligned with nose of aircraft), aircraft roll motion will cause the antenna to move off of boresight. Similarly, at an azimuth angle of 90° , aircraft pitch motion will cause the antenna to mispoint. The aircraft base motion also affects dish movement through friction with the bearings and motors in the azimuth and elevation axes. Because this friction is difficult to model, the aircraft's motion is assumed to always directly affect the antenna motion and a feedback controller must be used to compensate for the disturbances. Aircraft Euler angle (heading (Ψ), pitch (Θ), and roll (Φ)) rates were recorded for a representative 707 flight pattern and then translated into Aircraft

coordinates using Equation (3.15) [24]. Figure 3-2 shows the Aircraft Coordinate Frame.

$$\begin{bmatrix} P_{a/c} \\ Q_{a/c} \\ R_{a/c} \end{bmatrix}_{Aircraft} = \begin{bmatrix} -\sin \Theta \dot{\Psi} + \dot{\Phi} \\ \sin \Phi \cos \Theta \dot{\Psi} + \cos \Phi \dot{\Theta} \\ \cos \Phi \cos \Theta \dot{\Psi} - \sin \Phi \dot{\Theta} \end{bmatrix} \quad (3.15)$$

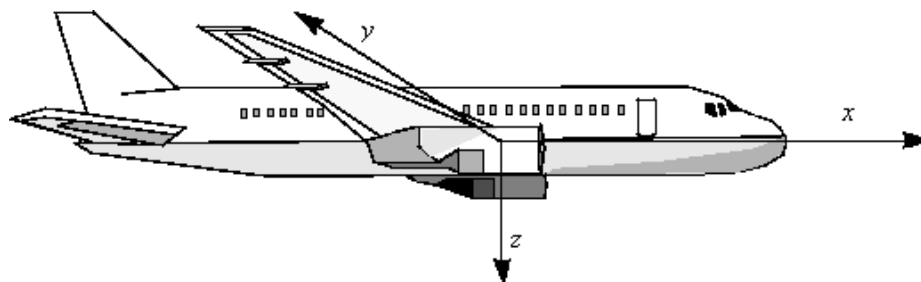


Figure 3-2: Aircraft Coordinate Frame. Photo courtesy of www.mathworks.com.

Next, Equation (3.16) translates the aircraft disturbance rates through the desired local azimuth and elevation look angles required to maintain tracking of the target satellite. The desired look angle calculations are presented for the reader in Appendix A. The resulting disturbance rates for the representative flight pattern are now resolved in the antenna Body coordinate frame.

$$\begin{bmatrix} D_P \\ D_Q \\ D_R \end{bmatrix}_{Body} = \begin{bmatrix} \cos(el_d) & 0 & -\sin(el_d) \\ 0 & 1 & 0 \\ \sin(el_d) & 0 & \cos(el_d) \end{bmatrix} \begin{bmatrix} \cos(az_d) & \sin(az_d) & 0 \\ -\sin(az_d) & \cos(az_d) & 0 \\ 0 & 0 & 1 \end{bmatrix} \begin{bmatrix} P_{a/c} \\ Q_{a/c} \\ R_{a/c} \end{bmatrix}_{Aircraft} \quad (3.16)$$

D_P , D_Q , and D_R represent the input disturbance rates in the antenna Body x, y, and z axes respectively. In order to model these disturbance rate inputs to the positioner control system, Power Spectral Density (PSD) plots were created using Welch's method for each of the antenna axes [25]. For simplification, the axis containing the harshest disturbance rates was selected as a model of the disturbance motion inputs to all three antenna axes. A second-order transfer function is used to over-bound the PSD of the harshest disturbance rate input and its frequency response is overlain on the PSD plot in Figure 3-3. The stable square root of the second-order transfer

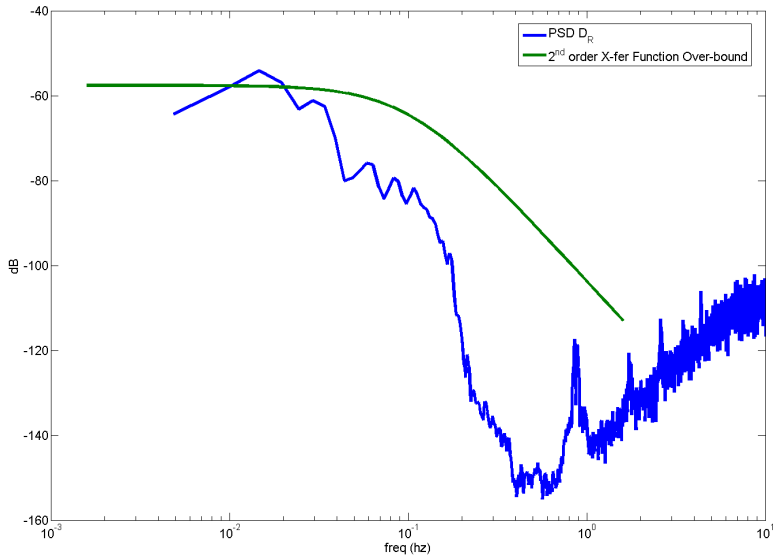


Figure 3-3: Disturbance Rate Input Power Spectral Density (Antenna Body z Axis)

function forms the model for a coloring filter through which white noise with unit density is passed and emerges as colored noise with approximately the same spectral content as the true disturbance rate [26]. The coloring filter may be represented in either transfer function or state-space form:

$$\frac{D_{P,Q,R}}{w_3} = \underbrace{\frac{0.03533}{s + 0.6283}}_{\text{Filter Transfer Function}} \quad \text{or} \quad \underbrace{\dot{D}_{P,Q,R} = \overbrace{-0.6283}^{\text{Afilt}} D_{P,Q,R} + \overbrace{0.03533 w_3}^{\text{Bfilt}}}_{\text{Filter State Equation}}$$

The filter state equation contains the term, $\dot{D}_{P,Q,R}$, which represents a disturbance *acceleration* in one of the three antenna axes. Further relationships between the response side inertial variables and moment side relative motion variables in Equation (3.14) may now be identified. The progression in Equations (3.17)-(3.19) uses the antenna's pitch axis as a representative example although the same relationships are defined in the other two Body axes as well:

$$I_{yy}\dot{Q} = I_{yy}(\ddot{\theta}_{pitch} + \dot{D}_Q) = \sum_y T_{motor} + \sum_y T_{disturbance} \quad (3.17)$$

$$Q = \dot{\theta}_{pitch} + D_Q \quad (3.18)$$

$$q = \theta_{pitch} + \int D_Q \quad (3.19)$$

where q is the inertial pointing error angle away from the stationary operating point (terminal to satellite pointing vector) about the y Body axis and $\int D_Q$ is the relative angular position of the aircraft from the pointing vector about the y Body axis. Similarly, p and r define inertial error angles away from the pointing vector in the x and z Body axes respectively while $\int D_P$ and $\int D_R$ represent relative aircraft angular positions away from the pointing vector in the x and z Body axes respectively. At this point a definition for total inertial pointing error may be defined as in (3.20) where Δ is the total inertial pointing error. Note that p does not affect the inertial pointing error as the antenna's roll motion cannot induce mispointing.

$$\Delta = \sqrt{q^2 + r^2} \quad (3.20)$$

3.1.4 Linear Plant Model

With the disturbance torques and state variables defined, Equation (3.14) is rewritten as Equation (3.21). If the moment side of Equation (3.21) is linearized about a 0° operating point, as alluded to in Section 3.1.2, the trigonometric functions vanish and the antenna roll and yaw equations decouple. The roll equation is left unmodeled in the development of the linear plant model because antenna roll motion does not affect pointing and is uncontrollable with a two-axis, azimuth-elevation pedestal configuration [4]. In the decoupled, linearized system, the EOMs for antenna pitch and yaw motion differ only in the motor and inertia parameters chosen. The linearized state equations for the pitch axis dynamics, and as an extension the yaw axis dynamics, are presented in Equation (3.22) augmented with the aircraft disturbance coloring filter state equation. Equations (3.22)-(3.23) constitute the linear, time invariant (constant coefficient matrices) state-space representation of the plant model that will be used

when developing the simulated, open-loop, pedestal feedback controller. The w and v variables in (3.22)-(3.23) represent white Gaussian process and sensor noises respectively that are added to the linear system dynamics. The modeling of these noise inputs is discussed in greater detail in the next section.

$$\begin{bmatrix} I_{xx} & 0 & 0 \\ 0 & I_{yy} & 0 \\ 0 & 0 & I_{zz} \end{bmatrix} \begin{bmatrix} P \\ Q \\ R \end{bmatrix} = \begin{bmatrix} -\frac{K_{maz}}{n_g R_{aaz}} e_{aaz} \sin(el) - \frac{K_{maz} K_{baz}}{n_g^2 R_{aaz}} \sin^2(el) [P - D_P] \\ + \frac{K_{maz} K_{baz}}{n_g^2 R_{aaz}} \sin(el) \cos(el) [R - D_R] + \sum_x T_{disturbance} \\ \frac{K_{mel}}{n_g R_{ael}} e_{ael} - \frac{K_{mel} K_{bel}}{n_g^2 R_{ael}} [Q - D_Q] + \sum_y T_{disturbance} \\ \frac{K_{maz}}{n_g R_{aaz}} e_{aaz} \cos(el) + \frac{K_{maz} K_{baz}}{n_g^2 R_{aaz}} \sin(el) \cos(el) [P - D_P] \\ - \frac{K_{maz} K_{baz}}{n_g^2 R_{aaz}} \cos^2(el) [R - D_R] + \sum_z T_{disturbance} \end{bmatrix} \quad (3.21)$$

$$\begin{bmatrix} I_{yy} & 0 & -I_{yy} \\ 0 & 1 & 0 \\ 0 & 0 & 1 \end{bmatrix} \begin{bmatrix} \dot{Q} \\ Q \\ \dot{D}_Q \end{bmatrix} = \begin{bmatrix} -\frac{K_{mel} K_{bel}}{n_g^2 R_{ael}} & 0 & \frac{K_{mel} K_{bel}}{n_g^2 R_{ael}} \\ 1 & 0 & 0 \\ 0 & 0 & \text{Afilt} \end{bmatrix} \begin{bmatrix} Q \\ q \\ D_Q \end{bmatrix} + \begin{bmatrix} \frac{K_{mel}}{n_g R_{ael}} \\ 0 \\ 0 \end{bmatrix} e_{ael} \\ + \begin{bmatrix} 1 & 0 & 0 \\ 0 & 1 & 0 \\ 0 & 0 & \text{Bfilt} \end{bmatrix} \begin{bmatrix} w_1 \\ w_2 \\ w_3 \end{bmatrix} \quad (3.22)$$

$$\mathbf{y} = \begin{bmatrix} 1 & 0 & 0 \\ 0 & 1 & 0 \end{bmatrix} \begin{bmatrix} Q \\ q \\ D_Q \end{bmatrix} + \begin{bmatrix} v_1 \\ v_2 \end{bmatrix} \quad (3.23)$$

3.2 Controller Development and Simulation

Several approaches to developing feedback controllers for the pedestal motors are available to the engineer. Classical control methods using Proportional Integral Derivative (PID) tools and frequency-domain techniques, such as lead and lag filter designs, are prevalent in industry and are often applied for use with DC servo-motors. However, classical control design techniques do not take limitations on control efforts, such as motor torques or armature voltages, into account and typically require many iterations to reach an acceptable end design. The limitations of classical control theory have, in part, led to the proliferation of state-space controller design techniques. State-space techniques also serve as the tool for developing controllers for multiple-input multiple-output (MIMO) systems. Because the aircraft motion disturbance state, process noises, and sensor noises are present, the linear plant model developed in Section 3.1.4 becomes a MIMO system. A deterministic, linear, time-invariant state-space system representation takes the form:

$$\dot{\mathbf{x}}(t) = \mathbf{A}\mathbf{x}(t) + \mathbf{B}_u\mathbf{u}(t) \quad (3.24)$$

$$\mathbf{y}(t) = \mathbf{C}_y\mathbf{x}(t) + \mathbf{D}\mathbf{u}(t) \quad (3.25)$$

Equations (3.22) and (3.23) resemble Equations (3.24) and (3.25) if the process and sensor noises in the linearized plant model are neglected. Here, \mathbf{x} is the state vector, \mathbf{u} is the control input vector, and \mathbf{y} is the system output vector.

The main precept behind state-space control techniques involves the use of state variable feedback in which combinations of the variables in the state vector, \mathbf{x} , are fed back into the system as control inputs through a gain matrix, K , in order to achieve the desired closed loop system response. Using state variable feedback, the negative feedback control law becomes:

$$\mathbf{u}(t) = -K(t)\mathbf{x}(t) \quad (3.26)$$

Assuming that the state vector is deterministic and perfectly measurable, this strategy allows the engineer to place the poles of the closed-loop system anywhere on the s -plane by adjusting the values of the gains inside the K matrix accordingly, a technique known as pole-placement [26,27]. Changing the location of the closed-loop poles in the s -plane directly impacts the speed and nature of the closed-loop system's response [23]. For the pedestal control system, it is desirable for the closed loop system poles to be in the Left Half-Plane (LHP) of the s -plane to ensure system stability. The poles must also lay far enough to the left of the origin of the s -plane so that perturbations in the system states, specifically the yaw and pitch components of pointing error, are quickly driven to zero. Moving the closed-loop system's poles farther into the LHP requires greater control effort, so a balance between speed of response and amount of control input must be determined. The pole placement technique provides the engineer with a useful tool, but pole placement alone offers no strategy as to where exactly in the LHP the poles of the closed loop system should be placed. The optimal control technique known as Linear-Quadratic Gaussian design (also called H_2 design) solves this problem by weighing the cost of control efforts against desired system response, in the presence of system and measurement uncertainties, in the design of the controller. An LQG controller will be designed for the nominal APS from Section 2.3 after the theory behind LQG controller design is briefly discussed.

3.2.1 Linear-Quadratic Regulation Theory

For linearized plant models, a quadratic cost functional may be developed that penalizes both state vector perturbations and applied control efforts. In the context of the pedestal controller system, the state perturbations of greatest concern are the pointing errors in the antenna yaw and pitch directions. The control efforts are the applied voltages to the azimuth and elevation servo-motor circuits which cause applied torques on the pedestal's gimbals. A quadratic cost functional is justified because it has the general effect of keeping a linear system model as honest as possible [27]. The

quadratic cost functional for a linear, time-invariant system may be represented as:

$$J = \frac{1}{2} \mathbf{x}^T(t) P_{t_f} \mathbf{x}(t) + \frac{1}{2} \int_{t_0}^{t_f} [\mathbf{x}^T(t) R_{xx} \mathbf{x}(t) + \mathbf{u}^T(t) R_{uu} \mathbf{u}(t)] dt \quad (3.27)$$

where R_{xx} and R_{uu} are the state and control weighting matrices that determine the degree of penalty placed upon state perturbations and exacted control efforts and P_{t_f} is the *cost-to-go matrix* evaluated at the terminal time [26–28]. Assuming deterministic, full-state feedback, a time varying value for $K(t)$ in Equation (3.26) may be found which minimizes (3.27) at every instance in time. Finding the optimal value of $K_o(t)$ which minimizes (3.27) is known as solving the Linear-Quadratic Regulation problem. For a time invariant system the value of $K_o(t)$, the optimal regulator gain, is determined by the relationship $K(t)_o = R_{uu}^{-1} B_u^T P(t)$ where $P(t)$ is the time varying cost-to-go matrix and is the solution to the Matrix Differential Riccati Equation [26–28]:

$$-\frac{dP}{dt} = P(t)A + A^T P(t) + R_{xx} - P(t)B_u R_{uu}^{-1} B_u^T P(t) \quad (3.28)$$

Equation (3.28) may be solved for $P(t)$ backwards in time with the specified boundary condition, P_{t_f} , from Equation (3.27). If the final time is assumed to be infinitely far off, an assumption valid for the pedestal controller application, then $P(t)$ reaches a steady-state value as it is solved backwards in time, and (3.28) reduces to:

$$0 = PA + A^T P + R_{xx} - PB_u R_{uu}^{-1} B_u^T P \quad (3.29)$$

Equation (3.29) is known as the Algebraic Riccati Equation [26]. The steady state value of P solved for in (3.29) may be used to find the steady state value of the gain matrix, K_o , and both values may be easily calculated when the controller is off-line [27]. Once the value of K_o is found for a deterministic, full state feedback case, the control law in (3.26) may be implemented and the performance of the resulting controller, known as the Linear-Quadratic Regulator (LQR), on the actual system may be simulated or observed.

3.2.2 Linear-Quadratic Estimation Theory

In most LQR systems, the assumptions that the state vector can be fully measured and that the system is deterministic do not hold, and the regulator must be augmented with a state estimator. For example, the linearized pedestal plant model for either the antenna pitch or yaw axis dynamics presented in Equations (3.22)–(3.23) contains an immeasurable disturbance rate input state, $D_{Q,P}$, which *must* be estimated. Modeling errors, actuator disturbances, and the effects of non-linearities on a linearized system plant constitute process noises, and any errors in the sensing of the measured states may be added to the plant model as sensor noises [27]. Process and sensor noises make the modeled dynamics of the given linear, time-invariant plant a stochastic one which may be represented as

$$\dot{\mathbf{x}}(t) = A\mathbf{x}(t) + B_u\mathbf{u}(t) + B_w\mathbf{w}(t) \quad (3.30)$$

$$\mathbf{y}(t) = C_y\mathbf{x}(t) + D\mathbf{u}(t) + \mathbf{v}(t) \quad (3.31)$$

where $\mathbf{w}(t)$ represents process noise inputs to the system and $\mathbf{v}(t)$ represents sensor noise. The system representation in Equations (3.30)–(3.31) describes the system in Equations (3.22)–(3.23) if (3.22) were multiplied through by the inverse of the inertia matrix. If information is known about the structures of the noises, then the noise dynamics may be modeled and augmented with the linear system model as shown in Section 3.1.3. If no information about the noises’ structures is known, they may be assumed to be white Gaussian noise processes. The assumption of white Gaussian noise is a worst-case scenario [27]. The white noise inputs to the stochastic system plant have covariance intensity matrices R_{ww} and R_{vv} for process and sensor noises respectively. Using white noise with specified intensities provides a means of culminating the uncertainties in the linear system into “catch-all” factors. It is desirable to develop an estimator to approximate the state variables with the minimal amount of estimation error while optimally balancing the effects of both process and sensor noises in the system. The estimated state vector is written as $\hat{\mathbf{x}}$ and the est-

imation error as $\tilde{\mathbf{x}}$ (Equations (3.32) and (3.33)). The estimation dynamics for a linear, time-invariant system may be written as

$$\dot{\hat{\mathbf{x}}}(t) = A\hat{\mathbf{x}}(t) + B_u\mathbf{u}(t) + L(t)(\mathbf{y}(t) - C_y\hat{\mathbf{x}}(t)) \quad (3.32)$$

$$\tilde{\mathbf{x}} = \mathbf{x} - \hat{\mathbf{x}} \quad (3.33)$$

where $L(t)$ is the estimator gain applied to the *innovation* or difference between measured and predicted system outputs. The estimator gain determines where in the LHP the estimator poles are located. Generally, it is desirable for the estimator poles to be faster than the regulator poles so that the estimated state vector may be used for regulator feedback without introducing large errors. The Kalman-Bucy filter provides the optimal solution to the Linear-Quadratic Estimation problem and decides where in the LHP the estimator poles should be placed based on the relative intensities of the process and sensor noises. Applying the Kalman-Bucy filter, the value of $L_o(t)$, the optimal estimator gain, is governed by the relationship $L_o(t) = Q(t)C_y^T R_{vv}^{-1}$ [26, 27]. The estimation error covariance matrix, $Q(t)$, is found from the solution of the Matrix Differential Riccati equation:

$$\frac{dQ}{dt} = AQ(t) + Q(t)A^T + B_w R_{ww} B_w^T - Q(t)C_y^T R_{vv}^{-1} C_y Q(t) \quad (3.34)$$

Equations (3.28) and (3.34) bear strong resemblance to each other and are, in fact, mathematical duals [26, 27]. The steady-state value of Q may be found by the solution of the Algebraic Riccati Equation, (3.35), if the initial time is assumed to have occurred in the distant past [27], an assumption that is generally valid for the pedestal control application.

$$0 = AQ + QA^T + B_w R_{ww} B_w^T - QC_y^T R_{vv}^{-1} C_y Q \quad (3.35)$$

3.2.3 Linear-Quadratic Gaussian Theory

The separation principle states that the optimal regulator and estimator gains can be solved for independently [29]. The resulting Linear-Quadratic Gaussian (LQG) controller dynamics may be written as

$$\dot{\hat{\mathbf{x}}}(t) = (A - B_u K_o - L_o C_y) \hat{\mathbf{x}}(t) + L_o(t) \mathbf{y}(t) \quad (3.36)$$

$$\mathbf{u} = -K_o \hat{\mathbf{x}} \quad (3.37)$$

where the estimated plant state, $\hat{\mathbf{x}}(t)$, is also the controller state variable [26, 27]. The controller dynamics may be augmented with the linear system plant dynamics to form the closed-loop system. The poles of the closed-loop, linear system, which govern the nature and speed of the system's response, are simply the union of the regulator and estimator poles. The closed loop poles of the regulator may be found by calculating the eigenvalues of the $(A - B_u K_o)$ matrix, and the estimator poles are found by solving for the eigenvalues of the $(A - L_o C_y)$ matrix. Equation (3.37) highlights the new control law for the LQG controller, $\mathbf{u}(t) = -K_o \hat{\mathbf{x}}(t)$, which is actually the optimal feedback strategy for the stochastic Linear-Quadratic control problem. For a proof of the optimality of the LQG control strategy, the reader is referred to the literature [26, 30].

3.2.4 Reference Commands

The ability for the pedestal controller to track an input reference command is needed in order to slew the antenna to various positions in the sky to track different target satellites and to intelligently dither the antenna's mainlobe in order to implement a closed-loop pointing strategy. Perhaps the best strategy for implementing a reference command in an LQG controller is to ensure that the estimation error is independent of the reference command [31]. This strategy is accomplished by changing the form of the controller dynamics in Equations (3.36)–(3.37) so that the controller explicitly has two inputs, the measurement states, \mathbf{y} , and the reference command, \mathbf{r} (3.38). The

feedback control law is also changed to incorporate the reference command (3.39).

$$\dot{\hat{\mathbf{x}}}(t) = (A - B_u K_o - L_o C_y) \hat{\mathbf{x}}(t) + L_o(t) \mathbf{y}(t) + B_u \bar{N} \mathbf{r} \quad (3.38)$$

$$\mathbf{u} = -K_o \hat{\mathbf{x}} + \bar{N} \mathbf{r} \quad (3.39)$$

Finally, the \bar{N} matrix is selected such that the gain of the closed-loop transfer function $\mathbf{Y}(s)/\mathbf{R}(s)$ equals one at DC which ensures accurate steady-state tracking of an input reference command [31].

3.2.5 Development of the LQG Pedestal Controller in MATLAB

This section develops an LQG pedestal feedback controller for the nominal APS with the aid of the MATLAB programming language. MATLAB is a scripting language used for technical computing and for developing visualizations and simulations. The MATLAB script referenced in this section uses several predefined functions found in MATLAB's Control System Toolbox. The MATLAB m-file 'controller.m', found in Appendix B.1, implements an LQG controller for the elevation motor of the nominal APS pedestal. The linearized plant model used in the controller's development is described by Equations (3.22)–(3.23), and the motor parameters used are those published in the specifications sheet for the Cleveland Motion Controls 2115 servo-motor with an F winding [20]. As an approximation to the moments of inertia for the combined antenna and elevation gimbal assembly, the calculated inertias of the 24 in. dish antenna are used in the derivation of the LQG controller. Because the same linearized plant model presented in Equations (3.22)–(3.23) is used to describe both the antenna's yaw and pitch dynamics, 'controller.m' is also used to develop the controller for the azimuth servo-motor. The nominal APS uses the same motors in both the azimuth and elevation axes, so the motor parameters do not change for the development of the azimuth motor controller. Also, because the I_{yy} and I_{zz} moments of inertia for the 24 in. dish are equal, and the inertia of the dish is used

to approximate that of the dish plus the attached elevation gimbal, the moment of inertia parameter is the same in both the elevation and azimuth controllers. Thus, ‘controller.m’ initially produces controllers for the elevation and azimuth servo-motors that are identical and collectively referred to as the *LQG controller*.

A gearing ratio of 10:1, radius of the larger output gear to the radius of the smaller motor gear, is used in the LQG controller development which leaves n_g in (3.22) equal to 0.1. This gearing ratio ensures that adequate torques are applied to the antenna to cancel the effects of the aircraft’s motion in the yaw and pitch axes of the antenna. The value of \bar{N} , the parameter introduced in Section 3.2.4, is obtained by setting the transfer function $\mathbf{Y}(s)/\mathbf{R}(s)$ equal to one at DC and comes out to be 181.185 for the pedestal controller. The state weighting matrix, R_{xx} , for the Linear-Quadratic Regulator portion of the LQG controller is determined using Bryson’s rule which simply states that the diagonals of R_{xx} be set to $1/(\text{max allowable perturbation})^2$ [28]. The maximum allowable perturbations for the velocity and position states were exaggerated to be $20 \frac{\circ}{\text{sec}}$ and 0.01° , respectively. No weighting was placed on the filter state equation in the R_{xx} matrix.

For this system, R_{uu} is a scalar, rather than a matrix, and its value is left as a design parameter to adjust the level of resulting pointing error in the LQR. Additionally, the R_{uu} value determines the placement of the regulator poles which must be placed with the location of the estimator poles in mind. The R_{ww} weighting matrix contains the variances of the process noises for each of the state equations in (3.22). The variance of the white noise input on the filter state equation, w_3 , is already determined by the modeling of aircraft disturbance motion and is set such that the power spectral density of w_3 is unity. The values of the variances for w_1 and w_2 are chosen to be the largest values possible such that the added process noises have negligible effects on the pointing performance of the LQR. All three white noise inputs are simulated in ‘controller.m’ by multiplying the variances by MATLAB’s ‘randn’ function for use in a closed-loop simulation of the controller and linear plant model.

The last design parameter in the LQG controller development process is the selection of the R_{vv} matrix. This matrix determines the weighting on the sensor noises

present in the pedestal system. The weights on the individual sensor noises should be chosen with regard to the variances present in the corresponding sensor measurements. The two states measured in the pedestal system are the antenna’s inertial angular displacement and inertial angular velocity. The antenna’s inertial displacement from the nominal pointing vector is calculated using the measurements of the resolvers, which sense local angular position in both the azimuth and elevation axis, and the C-MIGTIS IMU, which measures the Euler angles and rates of the aircraft. The inertial displacement measurement calculations are derived in Section 3.2.6.

The C-MIGTIS specifications sheet lists a $1\text{-}\sigma$ standard deviation for attitude measurements of 1 milliradian. The resolver measurements are assumed to be highly accurate when compared to the errors inherent in the IMU measurements; thus, the total variance in the antenna’s inertial angular displacement measurement is approximated as the square of the published C-MIGTIS $1\text{-}\sigma$ attitude error. The antenna’s inertial angular velocity measurement is assumed to be more accurate than the position measurement since the fiberoptic gyro sensors are purported to have small variances [21]. Also, the velocity measurements are output directly from the KVH fiberoptic gyros and do not need to be calculated like the position measurements do (See 3.2.6). For these reasons, the variance of the inertial velocity measurement is assumed to be an order of magnitude smaller than the variance of the angular displacement state. The assumed variances for the measured displacement and velocity states are used to simulate the sensor noises, v_1 and v_2 , in the closed loop simulation of the controller and linear plant model found in ‘controller.m.’

‘controller.m,’ calculates the regulator and estimator gains from Equations (3.29) and (3.35) using MATLAB’s ‘lqr’ function. The MATLAB function ‘lsim’ simulates the performance of the closed-loop, linearized system incorporating the LQG controller dynamics in (3.38)–(3.39). Several design iterations were made by adjusting the values of R_{uu} and R_{vv} before arriving at the final controller design. Initially, R_{uu} was set to 10^{-2} and the R_{vv} matrix was populated with the sensor variances. For a constant R_{uu} , if the value of R_{vv} is reduced and the estimator poles made faster, the sensor noise in the system begins to greatly affect mispointing. If R_{vv} is increased and

the estimator poles made slower, the system states are poorly estimated resulting in inaccurate feedback and poor pointing performance. The best system performance results if the R_{vv} matrix contains the sensor variances. Finally, R_{uu} is adjusted until acceptable antenna pointing performance and state estimation are achieved.

Controlled Linearized Plant Simulation Results

Figures 3-4–3-6 show the state response and estimated states for the antenna’s motion about its pitch axis for a constant reference command of 0° . Figures 3-4–3-6 are also representative of the closed-loop performance of the controlled linear plant model in the antenna’s yaw axis. The resulting open-loop pointing error components in either the pitch or yaw antenna axes, shown in Figure 3-4, have a $3\text{-}\sigma$ value of approximately 0.06° . Using the $3\text{-}\sigma$ values for component pointing errors in Equation (3.20), the linear plant controller meets the $3\text{-}\sigma$ requirement for simulated open-loop pointing accuracy of 0.1° outlined in Section 2.3. Figure 3-7 shows the motor torque required to hold the antenna stationary while subject to base motion disturbance inputs. The applied torques seen in Figure 3-7 do not exceed the maximum available motor torque for the pedestal’s CMC motors [20]. Finally, Figure 3-8 displays the frequency response Bode plot for the transfer function $\mathbf{Y}(s)/\mathbf{R}(s)$. The closed-loop bandwidth of the system may be identified from the Bode plot as the frequency at which the magnitude plot crosses the -3dB point. Figure 3-8 shows that the system bandwidth is approximately 2.5 Hz. Vibration tests conducted on the two-axis positioner used for the “EHF SATCOM on the 707” project identified the first structural resonance at a frequency greater than 30 Hz. Therefore, the 2.5 Hz bandwidth of the nominal APS should not excite any structural modes in system. The closed-loop MATLAB simulation in ‘controller.m’ simulates only the response of the linearized pedestal system and does not provide enough insight into the true closed-loop behavior of the pedestal system.

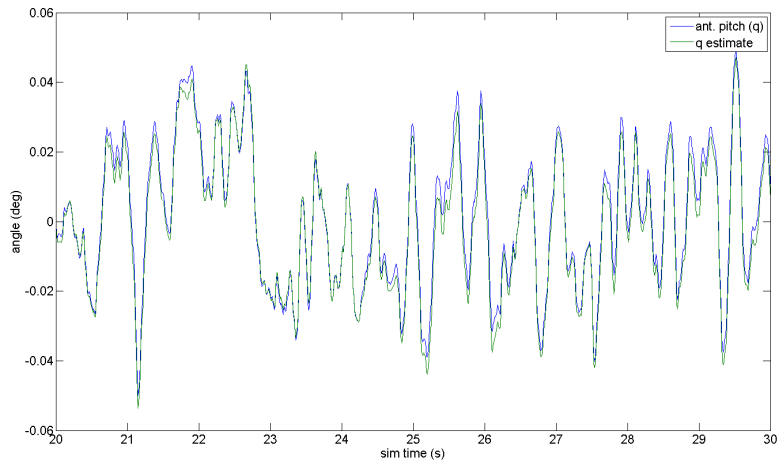


Figure 3-4: Actual and Estimated Pitch Component of Antenna Inertial Pointing Error (Linear Plant)

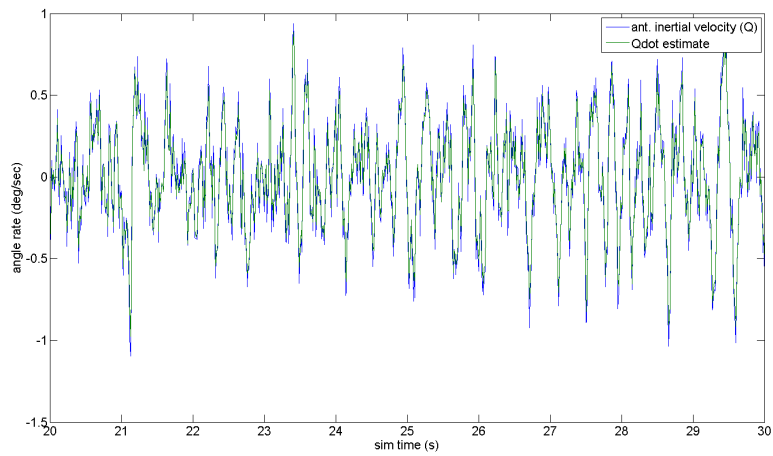


Figure 3-5: Actual and Estimated Pitch Component of Antenna Inertial Velocity (Linear Plant)

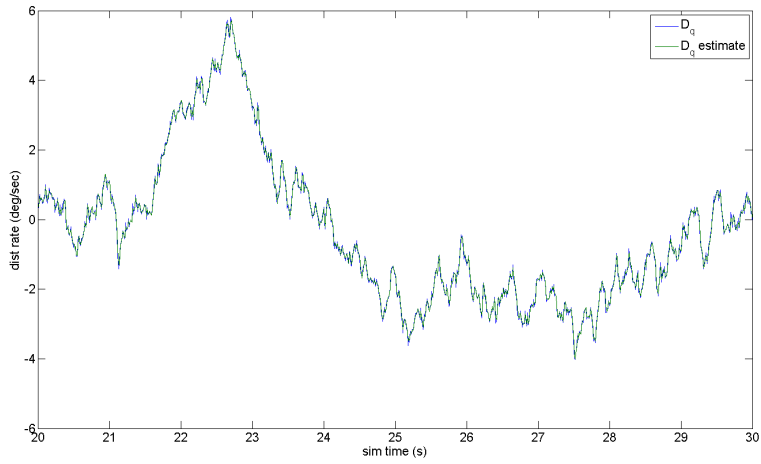


Figure 3-6: Actual and Estimated Base Motion Disturbance Input to the Antenna Pitch Axis (Linear Plant)

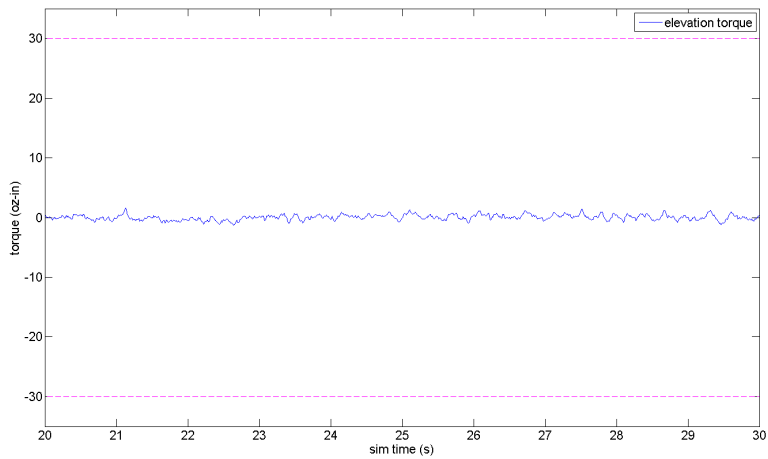


Figure 3-7: Applied Motor Torque: Elevation Motor (Linear Plant)

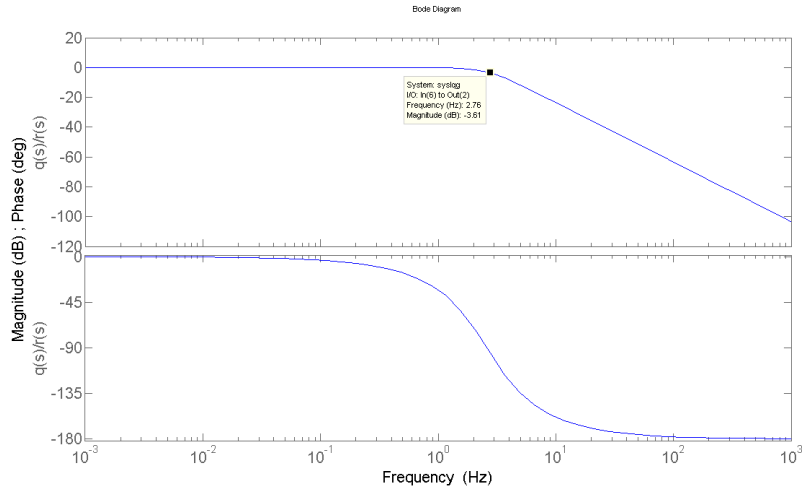


Figure 3-8: Closed-Loop Frequency Response: Elevation Motor Controller (Linear Plant)

3.2.6 Controlled Nonlinear Plant Simulation

In order to more accurately simulate the pointing performance of the LQG controller developed in Section 3.2.5, a Simulink simulation is created. Simulink is a Graphical User Interface counterpart to MATLAB used to develop simulations of dynamic systems. The Simulink simulation developed in this section incorporates the nonlinearities that are present in the pedestal's dynamics, more accurately models sensor limitations, and introduces actuator limitations such as torque-speed curves for the servo-motors. Appendix B.2 contains the Simulink model for the nominal APS. The same motor parameters and approximate moments of inertia used for the development of the LQG controller are used in the Simulink simulation. The Simulink model incorporates the non-linear pedestal system dynamics, presented in Equation (3.21), that serve to couple the antenna roll and yaw EOMs and cause the applied torque in the yaw axis to be dependent upon the cosine of the local elevation angle. The simulation also models sensor dynamics present in the measurement of inertial angular displacements and velocities including sampling rates, sensor bandwidths, error variances, and extrapolation calculations. Linear torque-speed curves are developed using the published no-load speeds and stall torques of the servo-motors and are incorporated for both the azimuth and elevation motors [20]. The torque speed curves limit

the amount of motor torque available to steer the antenna dish when the controller commands torques that are not physically achievable, i.e. the torque-speed curves allow for saturation of the pedestal's actuators. The added dynamics incorporated in the Simulink model more closely approximate the behavior of the controlled pedestal system, and the simulation allows for modifications to the feedback controller that could improve pointing performance.

The major issue that surfaces in the Simulink simulation concerns the effects of the linearization of the moment side of Equation (3.21) about a 0° local elevation operating point. The linearization has no effect on the pointing performance of the antenna in the pitch axis, but pointing in the antenna's yaw axis using the unmodified azimuth motor controller developed in 3.2.5 is decidedly worse at elevation angles greater than 60° , a condition often experienced in flight. Figure 3-9 portrays the yaw axis component of inertial pointing error under these conditions. For comparison, the pointing errors encountered at low elevation angles are also displayed in Figure 3-9. For the higher elevation angle scenario, pointing error nears 0.15° at some instances; an unacceptable amount for the nominal APS.

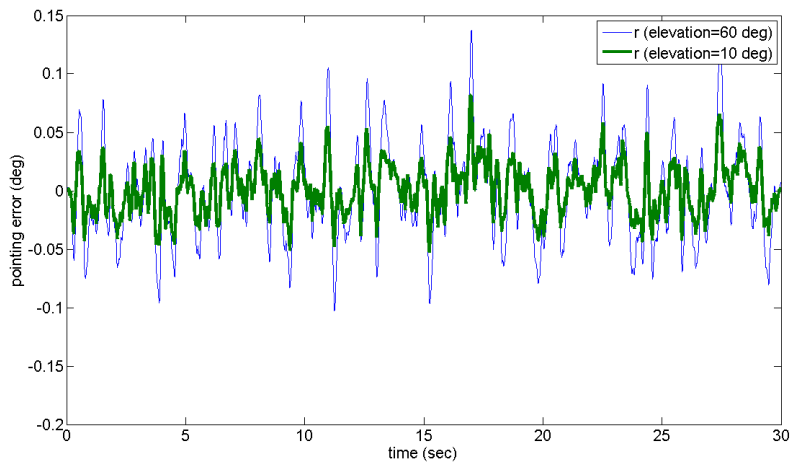


Figure 3-9: Yaw Component of Antenna Pointing Error at Different Elevations (Unmodified Controller)

In order to alleviate the problem, the azimuth motor controller output voltage is gained by the secant of the elevation angle, a technique commonly employed in

two-axis pedestal control systems [4]. Gaining the commanded output voltage by the secant of the local elevation angle eliminates the cosine term attached to the armature circuit source voltage ($e_{a_{az}}$) on the RHS of the yaw axis equation in (3.21). The added gain ensures that the pointing error component in the antenna yaw axis is minimized as elevation angles approach the keyhole region. At elevation angles nearing 90° , where the secant function approaches infinity, the azimuth motor cannot command enough torque to keep the dish pointing at the target satellite and an uncontrollable region is reached [9]. This condition is rarely reached for normal 707 flight profiles in the northern U.S. where the geostationary target satellites along the equator are at lower elevations. Figure 3-10 illustrates yaw axis pointing error for both the modified and unmodified azimuth motor controllers as the elevation angle approaches the keyhole region.

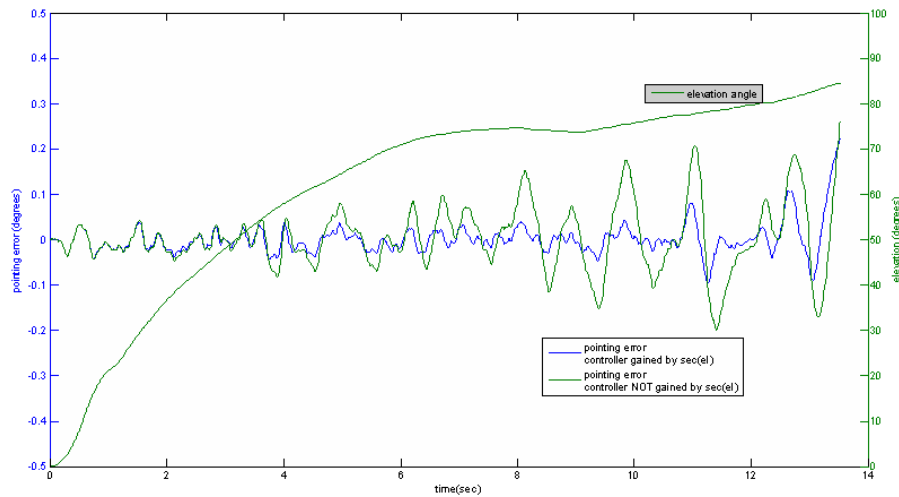


Figure 3-10: Yaw Component of Antenna Pointing Error as Elevation Changes: Modified and Unmodified Controllers

Gaining the commanded output voltage for the azimuth motor by the secant of the elevation angle does not eliminate the nonlinear and roll axis coupling terms in the remainder of the moment side of the yaw axis EOM (3.21). These terms constitute the back-emf damping torque present in the azimuth servo-motor. Because this back-emf torque is small when compared to the torque caused by the armature circuit source

voltage, the linear plant model approximation used in the development of the LQG controller becomes acceptable, and the modeling error can be accounted for to some extent by the process noise added to the velocity state equation in the linear plant model (3.22) [27].

Controlled Nonlinear Plant Simulation Results

Figures 3-11–3-16 show the Simulink simulation outputs of the antenna state variables and their estimates for the controlled pedestal operating in normal environments, or elevation angles outside the keyhole region. Of most interest to the reader is that the behavior of the pointing error components in the Simulink model (Figures 3-11 and 3-12) is nearly identical to the behavior of the pointing error components predicted by the linear system model (Figure 3-4). The $3\text{-}\sigma$ error values for the pointing error components are again found to be approximately 0.06° which meets the overall, simulated open-loop pointing requirement from Section 2.3 (3.20). The inertial velocities and base motion disturbances from the Simulink model, Figures 3-13–3-16, also exhibit behaviors very similar to their counterparts in the linear system model, Figures 3-5–3-6. Figures 3-17 and 3-18 show the step response for the antenna pitch and yaw axes, respectively. The rise time observed in these figures, which will play an important role in the antenna dithering scheme developed for the closed-loop pointing algorithms in the next chapter, is approximately 0.25 seconds. Finally, the commanded and applied motor torques for a step input in the antenna’s yaw axis occurring at 1 second are shown in Figure 3-19. The limitation on the applied torque in Figure 3-19 shows the effects of modeling the linear torque-speed curve in the simulation.

Antenna Inertial Displacement Measurements and Reference Commands

The purpose of this section is to highlight the underlying calculations involved in measuring the inertial displacement states of the antenna, and calculating and issuing reference commands, that are not obvious or explicit in the Simulink simulation. These calculations must be accomplished by the pedestal control computer in a real

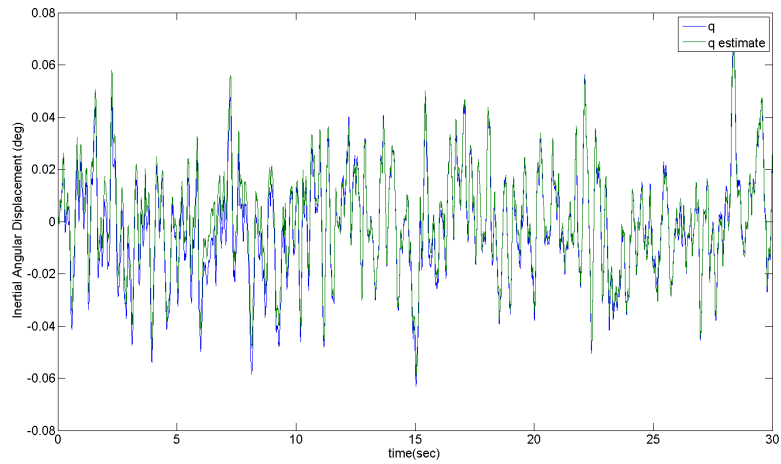


Figure 3-11: Actual and Estimated Pitch Component of Antenna Inertial Pointing Error (Simulink Simulation)

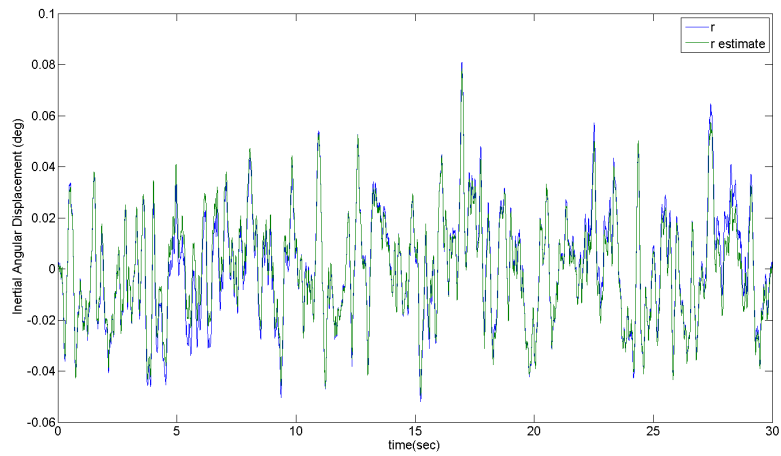


Figure 3-12: Actual and Estimated Yaw Component of Antenna Inertial Pointing Error (Simulink Simulation)

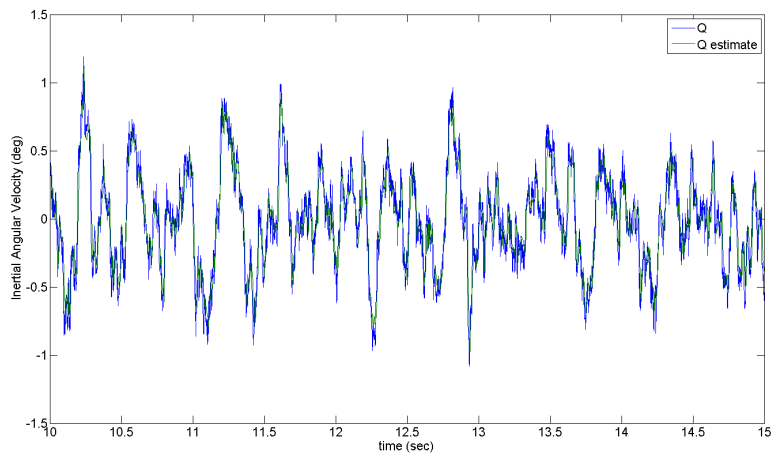


Figure 3-13: Actual and Estimated Pitch Component of Antenna Inertial Velocity (Simulink Simulation)

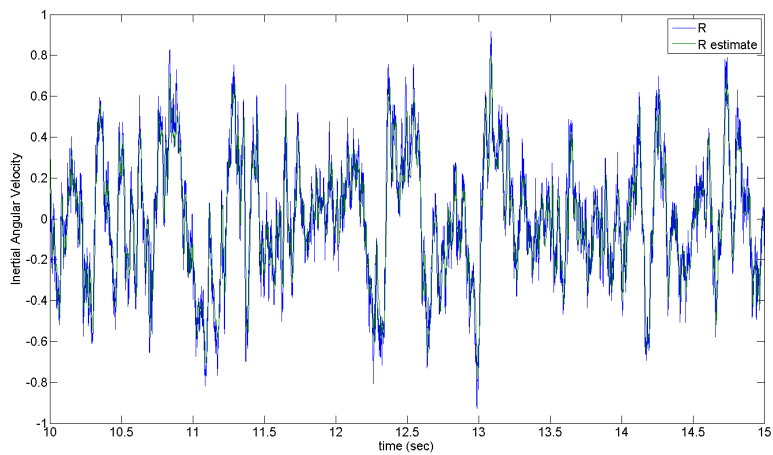


Figure 3-14: Actual and Estimated Yaw Component of Antenna Inertial Velocity (Simulink Simulation)

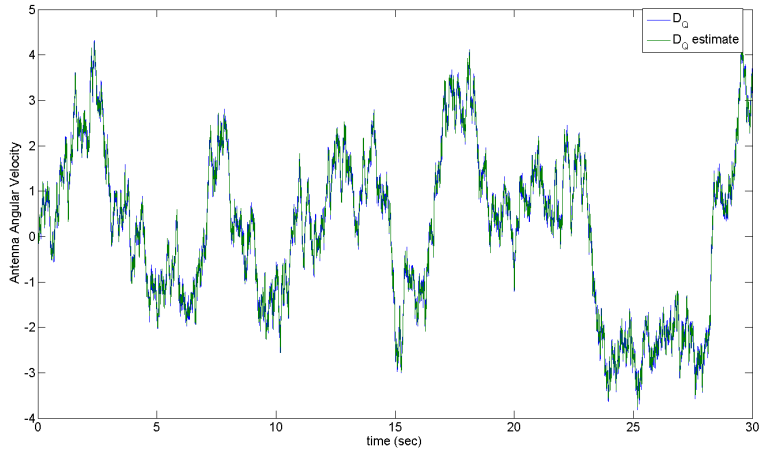


Figure 3-15: Actual and Estimated Base Motion Disturbance Input to the Antenna Pitch Axis (Simulink Simulation)

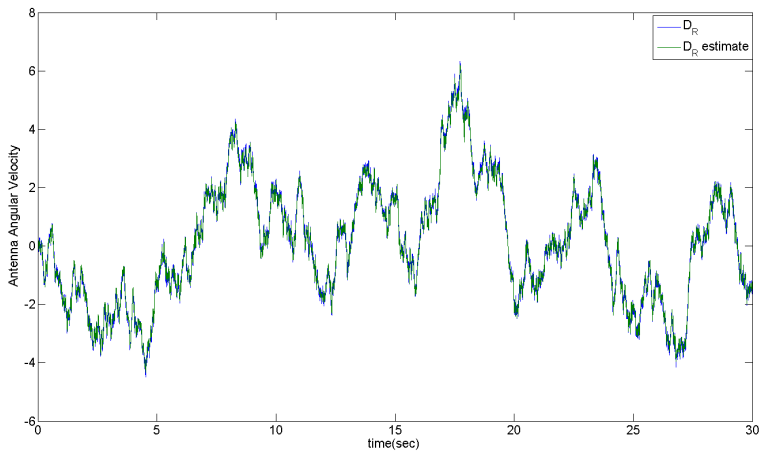


Figure 3-16: Actual and Estimated Base Motion Disturbance Input to the Antenna Yaw Axis (Simulink Simulation)

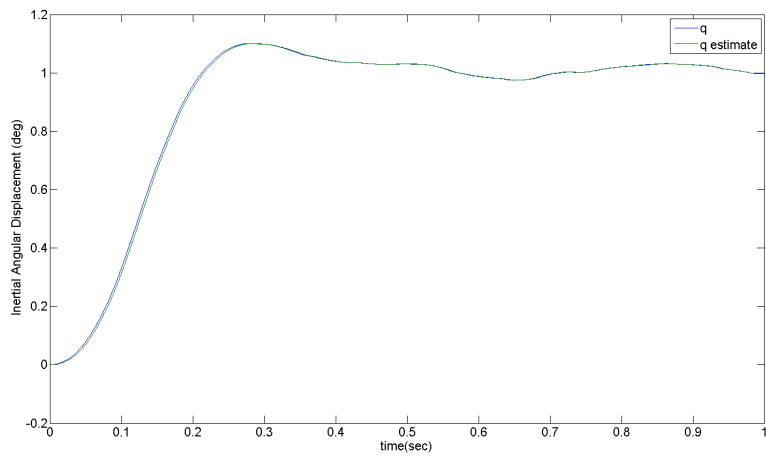


Figure 3-17: Antenna Pitch Axis Inertial Angular Displacement Step Response (Simulink Simulation)

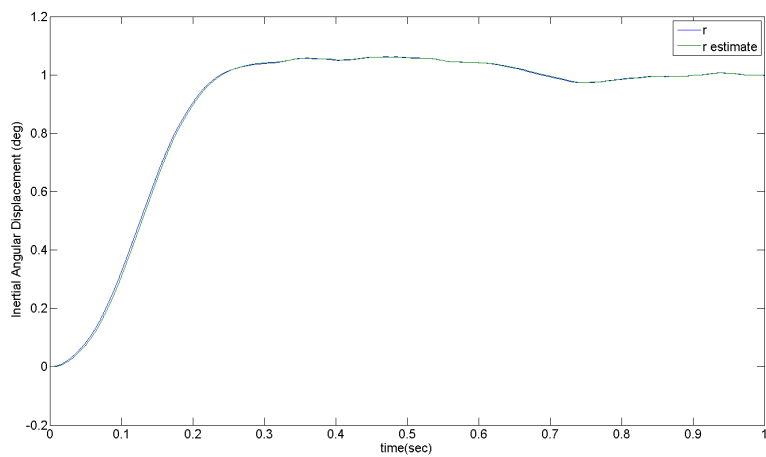


Figure 3-18: Antenna Yaw Axis Inertial Angular Displacement Step Response (Simulink Simulation)

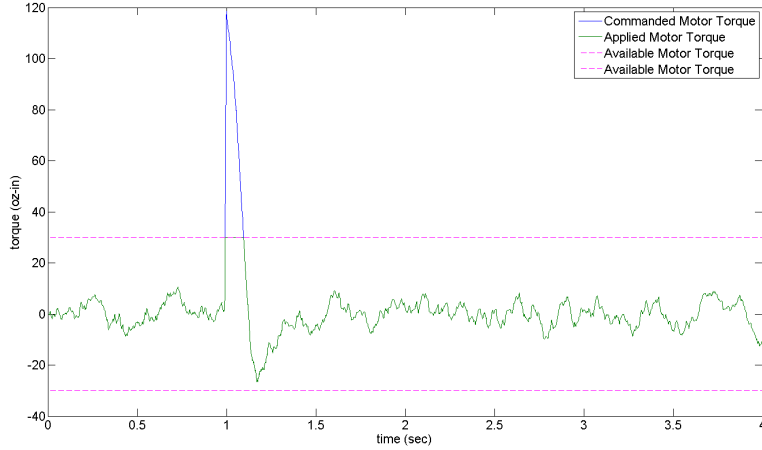


Figure 3-19: Antenna Yaw Axis Commanded and Applied Torques for a Step Response

APS. The pitch and yaw inertial displacement states of the antenna away from the desired pointing vector are calculated using a combination of local resolver measurements and IMU position measurements (aircraft Euler angles). When measuring these displacement states, q and r , the desired local azimuth and elevation look angles, az_d and el_d , from Appendix A are needed, a calculation that involves IMU measurement data. From the antenna's actual local position, as measured by the resolvers, a pointing vector in the Aircraft coordinate frame may be calculated as follows:

$$\begin{bmatrix} x \\ y \\ z \end{bmatrix}_{Aircraft} = \begin{bmatrix} \cos(el) \cos(az) \\ \cos(el) \sin(az) \\ -\sin(el) \end{bmatrix} \quad (3.40)$$

where az and el are the measured local position angles. Equation (3.41) transforms the pointing vector from Equation (3.40) through the *desired* local azimuth and elevation angles into a “Desired Antenna Body Coordinate Frame” as follows:

$$\begin{aligned}
\begin{bmatrix} x \\ y \\ z \end{bmatrix}_{Desired\ Body} &= \begin{bmatrix} \cos(el_d) & 0 & -\sin(el_d) \\ 0 & 1 & 0 \\ \sin(el_d) & 0 & \cos(el_d) \end{bmatrix} \\
&\cdot \begin{bmatrix} \cos(az_d) & \sin(az_d) & 0 \\ -\sin(az_d) & \cos(az_d) & 0 \\ 0 & 0 & 1 \end{bmatrix} \begin{bmatrix} x \\ y \\ z \end{bmatrix}_{Aircraft}
\end{aligned} \tag{3.41}$$

Finally, the angular displacement in the pitch axis, q , is found by determining the *elevation* of the pointing vector resolved in the Desired Body Coordinate Frame according to Equation (A.2). The yaw displacement, r , is found by determining the *azimuth* according to Equation (A.1). Reference commands are made simply by changing the az_d and el_d values, pursuant to changes in the inertial pointing vector from the terminal to a different spot in inertial space. The inertial pointing vector changes when the target satellite changes or when the antenna is slewed or dithered.

Because the C-MIGITS IMU used with the nominal APS only updates the aircraft Euler angles at 10 Hz, large errors in antenna inertial displacement state measurements could result because of inaccuracies in the az_d and el_d values used in Equation (3.41). To solve this problem, the values of az_d and el_d may be upsampled using velocity extrapolation according to:

$$az_d = az_{10Hz} + \dot{az}_{10Hz}\Delta t \tag{3.42}$$

$$el_d = el_{10Hz} + \dot{el}_{10Hz}\Delta t \tag{3.43}$$

where az_{10Hz} , \dot{az}_{10Hz} , el_{10Hz} , and \dot{el}_{10Hz} are calculated according to one of the methods presented in Appendix A using the 10 Hz C-MIGITS Euler angle and rate data. Δt in Equations (3.42)-(3.43) is the time difference between the last C-MIGITS data set update and the instance in time when the upsampled values of az_d and el_d are calculated. Because the C-MIGITS IMU updates at 10 Hz, Δt never exceeds 0.1 seconds.

3.3 Pointing Error Distributions

In order to facilitate simulation of the performance of closed-loop pointing control algorithms developed in the next chapter, an understanding of the statistical distributions of the pitch and yaw components of pointing error must be developed. To obtain data for modeling the distributions of q and r , the Simulink simulation from Section 3.2.6 is run for 30 seconds and the pointing error components recorded at evenly spaced time samples of 0.001 seconds (Figure 3-20). These points were then used to construct auto-correlation functions to determine the time-scale at which the pointing error distributions exhibit dependencies. The auto correlation functions are plotted in Figures 3-21 and 3-22. Figures 3-21 and 3-22 show that the initial peaks of the auto-correlation functions of the error components fall off at approximately 0.25 seconds. Thus, if the distributions of pointing error components prove to be normal, every 0.25 seconds a pointing error component may be obtained that is nearly independent of past pointing errors, assuming they occurred at 0.25 second intervals as well [32].

After the correlation time is determined, the simulation is run again for 250 seconds to record 1000 approximately independent samples of both the q and r pointing error components. In an effort to compare the resulting samples to normal distribution curves, histograms are made of the data sets and plotted together with normal distribution curves calculated from the sample means and variances. Figures 3-23 and 3-24 visually indicate the normalcy of the data; however, a statistical goodness-of-fit test is required in order to be convinced that a normal approximation to the distributions of the pointing error components accurately represents the true distributions most of the time.

The Kolmogorov-Smirnoff goodness-of-fit test for normal distributions is applied to the data sets of length 1000 where the population mean and variance are estimated by the sample mean and variance [33]. The Kolmogorov-Smirnoff test weighs the null hypothesis (H_0), that claims the sample data has a normal distribution, against the alternate hypothesis (H_a) that states the data is not from a normal distribution. α_{KS}

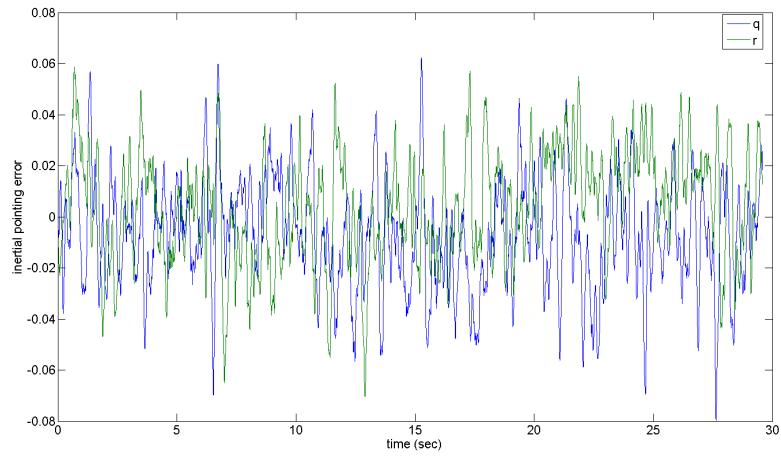


Figure 3-20: Pitch (q) and Yaw (r) Components of Antenna Pointing Error

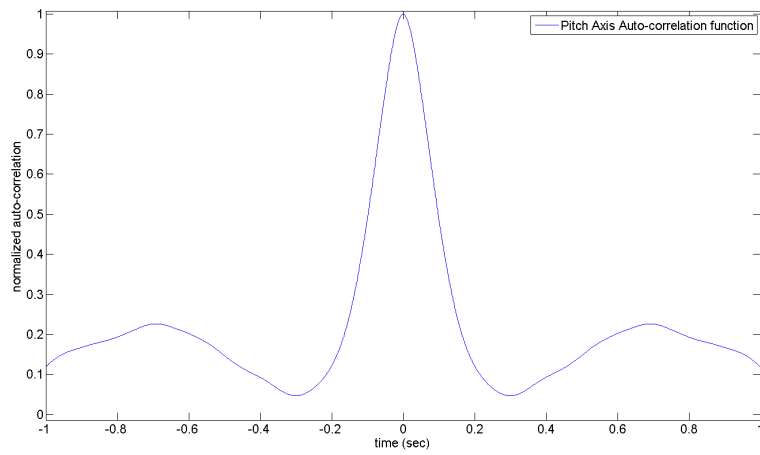


Figure 3-21: q Auto-correlation Function

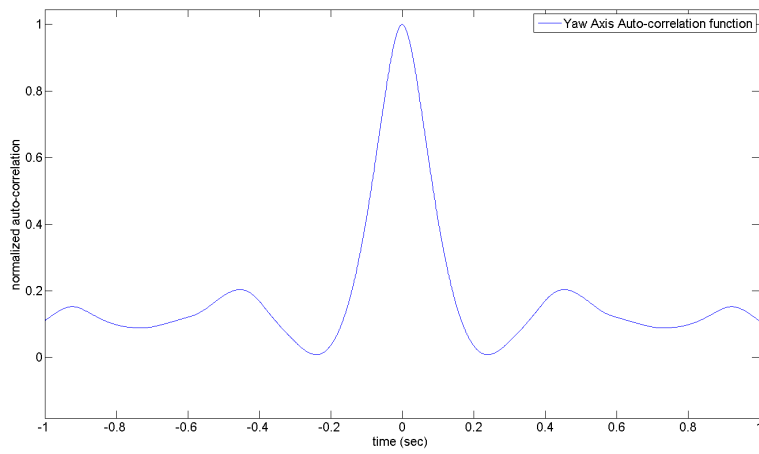


Figure 3-22: r Auto-correlation Function

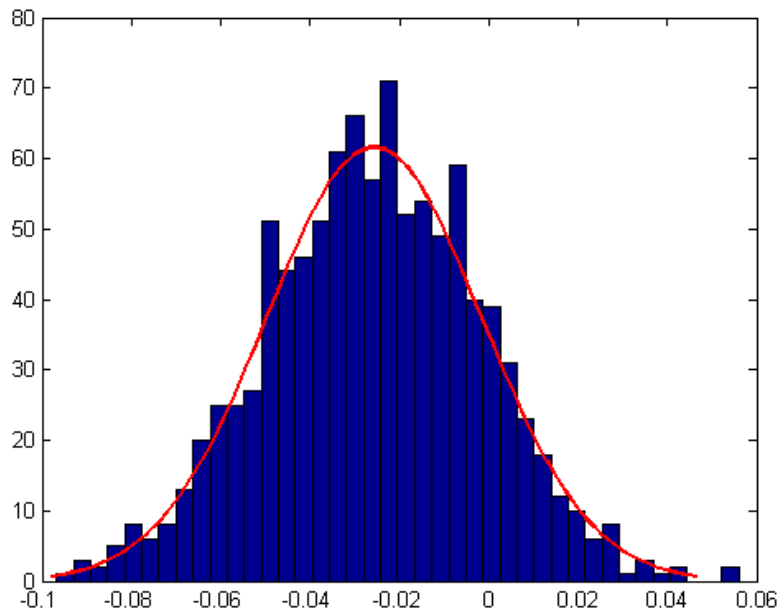


Figure 3-23: q Histogram

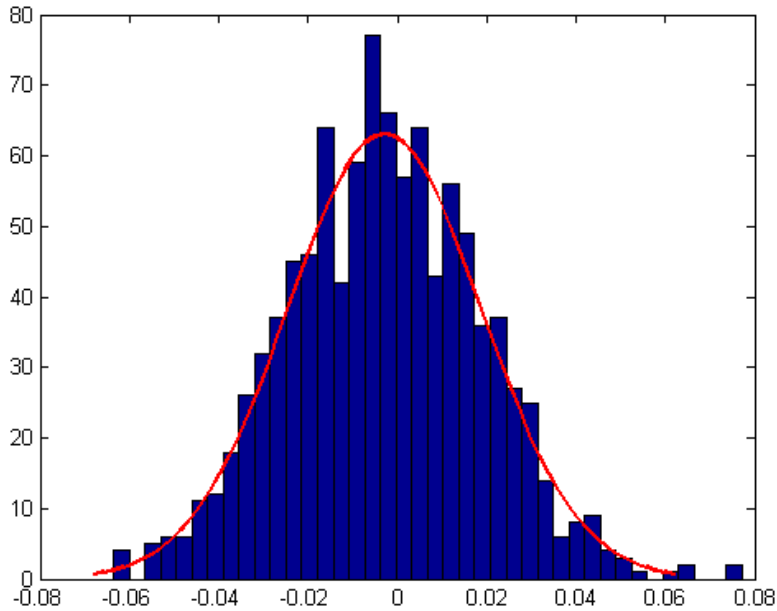


Figure 3-24: r Histogram

represents the probability of type-1 error, occurring when H_a is accepted over H_0 when H_0 is actually true. The value of α_{KS} determines the critical value for the test. If the value of the test statistic exceeds the critical value, then the null hypothesis is rejected at the α_{KS} significance level, and the data may be determined not to come from a normal population distribution. The results of the Kolmogorov-Smirnoff goodness-of-fit test for the q and r components of pointing error are summarized in Table 3.1 along with the sample statistics for mean and variance.

Table 3.1: Kolmogorov-Smirnoff Test for Pitch Error Component

	α_{KS}	Critical Value	Test Stat.	Hypothesis Accepted	\bar{x}	S^2
q	0.05	0.895	0.512	H_0	-0.006	0.0036
r	0.05	0.895	0.601	H_0	-0.003	0.0037

The results of the Kolmogorov-Smirnoff test uphold the null hypothesis claiming that the pointing error components have normal distributions; therefore, the distributions of pointing error components may be modeled as normal with means and variances equal to the sample means and variances from Table 3.1. The ability to

approximate the pointing error components as normally distributed assists in the modeling and simulation of closed-loop step-tracking algorithms developed in the next chapter.

Chapter 4

Closed-Loop Pointing Strategy

Overview

Because the nominal APS defined in Section 2.3 attempts to minimize inertial mispointing with the simplest available system, step-tracking is the closed-loop strategy that will be implemented with the nominal APS and open-loop feedback controller developed in the previous chapter. The resulting pointing strategy is classified as hybrid open/closed-loop in the sense that the closed-loop step-tracking algorithm updates the reference commands to the open-loop pedestal controller. The antenna's gain pattern will be defined as a nonlinear, scalar cost function that the step-tracking algorithms developed in this chapter must optimize. Step-tracking algorithms accomplish both spatial pull-in and closed-loop tracking by optimizing the antenna's gain pattern.

Five step-tracking algorithms will be tested through simulation in terms of how well each algorithm accomplishes spatial pull-in with various initial pointing errors. Next, selected step-tracking algorithms will be tested through simulation under conditions simulating harsher inertial open-loop pointing error and satellite motion. Finally, the best performing algorithm in the simulated spatial pull-in tests will undergo simulated closed-loop tracking tests of a target satellite. The results of each of the simulations will be used to gauge the feasibility of using step-tracking algorithms as a closed-loop pointing strategy for an airborne EHF SATCOM application.

4.1 Defining the Cost Function

The feedback metric used in a closed-loop RF SATCOM application is the received Signal to Noise Ratio (SNR) from the satellite. Because the antenna's gain determines the power of the signal measurement in the SNR metric, the antenna's gain pattern represents how signal power varies as the antenna moves off boresight. The gain pattern, measured in decibels, represents the actual SNR if an arbitrary noise floor value is subtracted from the gain values. For simulation purposes, the noise power is set to one; thus, the unmodified gain pattern models how the SNR changes as a function of pointing error.

Pointing error may be broken into two orthogonal, inertial angular components, cross-elevation (xel_i) and elevation (el_i), where the subscript i denotes inertial space. If a stationary antenna with a level base is pointed at the target satellite, cross-elevation corresponds to rotation about the dish's yaw axis, and elevation corresponds to rotations about the dish's pitch axis as in Figure 4-1. The inertial cross-elevation and elevation angles differ from r and q only by the roll angle, p , of the antenna. An equation similar to (3.20) may be defined for the total pointing error in terms of xel_i and el_i :

$$\Delta = \sqrt{el_i^2 + xel_i^2} \quad (4.1)$$

The xel_i and el_i angles provide the orthogonal coordinate system for the gain pattern which becomes a nonlinear function of the two pointing error components. For the development of step-tracking algorithms, the gain pattern serves as the cost function that the engineer must optimize. Optimization of the cost function corresponds to finding the inertial xel_i and el_i coordinates of the location of maximum antenna gain. Because cost functions are always minimized, and available optimization literature deals almost exclusively with minimization problems, the gain pattern is multiplied by -1 to form the true cost function from which the *global minimum*, corresponding to the antenna pointing on boresight, is sought. The global minimum is the unique minimum of the function, whereas *local minima* consist of other points

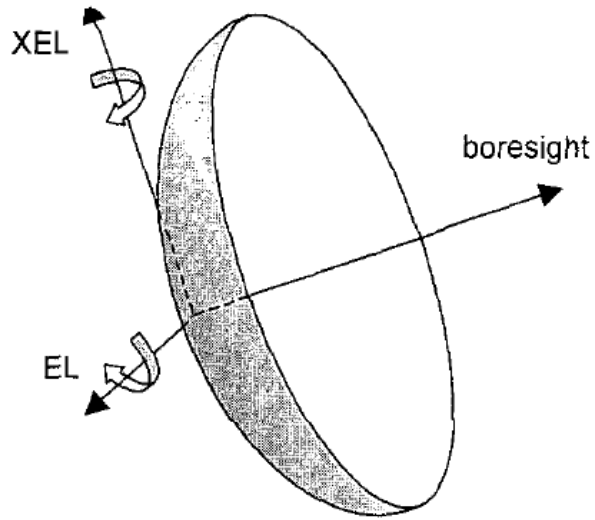


Figure 4-1: X-El, El Coordinates with respect to Dish for Stationary, Level Antenna Base. Photo Courtesy of Gawronski and Craparo [19].

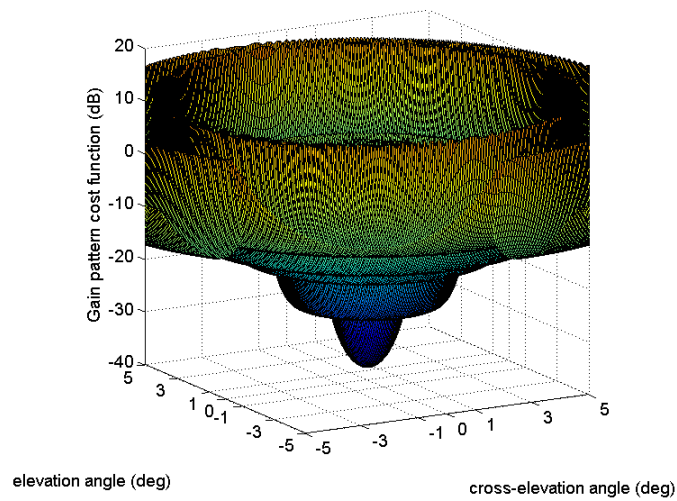


Figure 4-2: Antenna Gain Pattern Cost Function

where the cost function increases locally but then decreases again near the global minimum [34]. A *weak minimum* is defined as a local minimum where the function value remains constant in some directions but increases in others. The cost function increases in all directions near a *strong minimum*. The same terms may also be applied to any maxima in the cost function. Figure 4-2 shows the gain pattern cost function for the 24 in. dish used in the nominal APS with boresight, or the global minimum, located at the origin. Figure 4-2 is simply the negative of Figure 2-3. In Figure 4-2, one may identify several weak, local minima corresponding to the antenna's sidelobes. Weak, local maxima are also present in the cost function and correspond to the nulls in the antenna pattern.

Step-tracking algorithms move from *trial point* to *trial point* until the algorithm locates the global minimum of the cost function. A unique set of xel_i , el_i coordinates defines the location of each trial point. In order for a step-tracking algorithm to evaluate the cost function at different trial points, the desired xel_i and el_i angles must be issued to the open-loop controller as reference commands (Section 3.2.6). Although the xel_i and el_i angles differ from the r and q antenna angles only by p , no direct means of measuring the antenna roll angle exists for the nominal APS and another, somewhat more cumbersome, approach must be used. First, an initial pointing vector from the terminal to the target satellite must be calculated as in Appendix A. All subsequent inertial xel_i and el_i angles will be referenced as orthogonal angles away from the initial pointing vector. Desired xel_i and el_i angles are translated into the local desired look angles, az_d and el_d , using the following intermediate relationship:

$$\begin{bmatrix} x \\ y \\ z \end{bmatrix}_{NED} = \begin{bmatrix} \cos(az_{NED}) & -\sin(az_{NED}) & 0 \\ \sin(az_{NED}) & \cos(az_{NED}) & 0 \\ 0 & 0 & 1 \end{bmatrix} \cdot \begin{bmatrix} \cos(el_{NED}) & 0 & \sin(el_{NED}) \\ 0 & 1 & 0 \\ -\sin(el_{NED}) & 0 & \cos(el_{NED}) \end{bmatrix} \begin{bmatrix} \cos(el_i) \cos(xel_i) \\ \cos(el_i) \sin(xel_i) \\ -\sin(el_i) \end{bmatrix} \quad (4.2)$$

where az_{NED} and el_{NED} are the inertial look angles in the *North, East, Down Coordinate Frame* (Appendix A). Equation (4.2) develops a pointing vector in the topocentric North, East, Down inertial frame from which the local desired look angles, az_d and el_d , are calculated from Equations (A.1), (A.2), and (A.11). Reference commands from a closed-loop step-tracking algorithm may now be issued to the open-loop pedestal controller forming the hybrid open/closed-loop pointing strategy.

4.2 Facets of the Optimization Problem

Several issues arise when one applies step-tracking algorithms as a closed-loop antenna pointing solution for a mobile SATCOM application. First, only the *function* values of the cost function in Figure 4-2 may be obtained by measuring the SNR as the antenna points at a particular xel_i, el_i coordinate. Any gradient or second-derivative measurements of the cost function must be approximated using finite differencing. Thus, optimization methods requiring cost function derivatives at a particular trial point mandate cost function evaluations at additional surrounding trial points, and the algorithm becomes more computationally expensive. Secondly, in real SATCOM terminal systems, the SNR measurement may only be meaningfully computed to a resolution of approximately 0.1 dB. This limitation has significant implications for selecting an appropriate finite differencing interval and restricts the obtainable accuracy of cost function optimization. Thirdly, the cost function possesses multiple weak maxima and minima, corresponding to sidelobes and nulls present in the antenna gain pattern, that make the optimization difficult as these points must be distinguished from the global minimum. Fourthly, the pointing error from the open-loop pedestal controller and the noise within the terminal system make SNR measurements, and therefore the cost function, stochastic. At each trial point visited, the *stare* time must be made long enough to average the effects of both of these noise sources [11]. Stare time is the time spent averaging the SNR measurements at each inertial xel_i, el_i coordinate that the step-tracking algorithm visits. Although terminal system noise contributes to the required stare time, all closed-loop pointing strategies must in-

corporate stare times for obtaining accurate SNR measurements in the presence of system noise. Therefore, the effects of terminal system noise are not incorporated in the spatial pull-in and tracking simulations discussed in this chapter because the presence of system noise neither adds to nor detracts from the feasibility of using step-tracking algorithms for mobile SATCOM applications. Lastly, due to the motion of the aircraft and slowly time varying sources of error identified in Section 2.2.1, the satellite appears as a slowly moving target in inertial space, and the cost function develops time dependencies as well. Step-tracking algorithms must account for the apparent motion of the satellite during both the spatial pull-in stage and the tracking stage and must be robust enough to optimize a slowly time varying, stochastic cost function. Step-tracking systems must deal with all of these issues accordingly in order to successfully accomplish closed-loop antenna pointing.

Step-tracking algorithms must optimize the gain pattern cost function while minimizing the *computational expense* incurred by the algorithm. In step-tracking algorithms, excessive SNR measurements add to the computational expense metric and detract from the *convergence time*, or the time it takes the step-tracking algorithm to locate the minimum of the cost function. SNR measurements, or cost function evaluations, are much more computationally expensive than the overhead of the step-tracking algorithm, particularly when the number of independent variables that define the cost function is small [34]. Consequently, overhead times will be ignored in the performance comparisons of step-tracking algorithms developed in this chapter as the gain pattern cost function is defined by only two independent variables.

4.3 Step-tracking Using Function Comparison Methods

4.3.1 Full-field Search

A full-field function comparison search constitutes the simplest method of step-tracking. Function comparison methods work by measuring the cost function at

every location of interest in an uncertainty field and subsequently selecting the trial point that has the lowest function value as the location of the optimal solution within the field. Step-tracking algorithms employing a full-field search simply extend the uncertainty field, within the context of open-loop pointing errors, to cover an entire region where the boresight location might lie. Despite the simplicity of the approach, full-field searches provide limited usefulness in developing step-tracking algorithms for mobile SATCOM terminal systems. Because many antennas used in mobile SATCOM applications have stringent closed-loop inertial pointing requirements, a large number of trial points is needed to span the entire field of initial pointing error uncertainty during the spatial pull-in stage. For instance, with a $3^\circ \times 3^\circ$ field of uncertainty, if pointing error from boresight is limited to 0.1° , at least 900 trial points are required (Figure 4-3).

The gain pattern cost function must be evaluated at least once at every trial point within the uncertainty field in order to effectively distinguish the location of boresight from the surrounding sidelobes. Such a large number of required SNR measurements lead to a computationally expensive and inefficient approach to step-tracking. Figure 4-3 illustrates that without overlap in the search pattern the boresight location could potentially lie in-between the 0.1° search rings. Lengthy, full-field searches are also very susceptible to errors caused by the time-varying property of the cost function due to satellite motion. For this reason, full-field search approaches cannot be used for the tracking stage of a closed-loop pointing strategy. Clearly, mobile SATCOM applications requiring closed-loop pointing necessitate better step-tracking approaches than full-field searches.

4.3.2 Spiral Search

A function comparison step-tracking approach used in SATCOM applications with high gain antennas is the Spiral Search (SS) method. The SS method accomplishes spatial pull-in by obtaining SNR measurements at specified locations surrounding the initial pointing vector that form a spiral ring pattern, as shown in Figure 4-4. After all of the trial points are visited, the algorithm steps to the location coincident

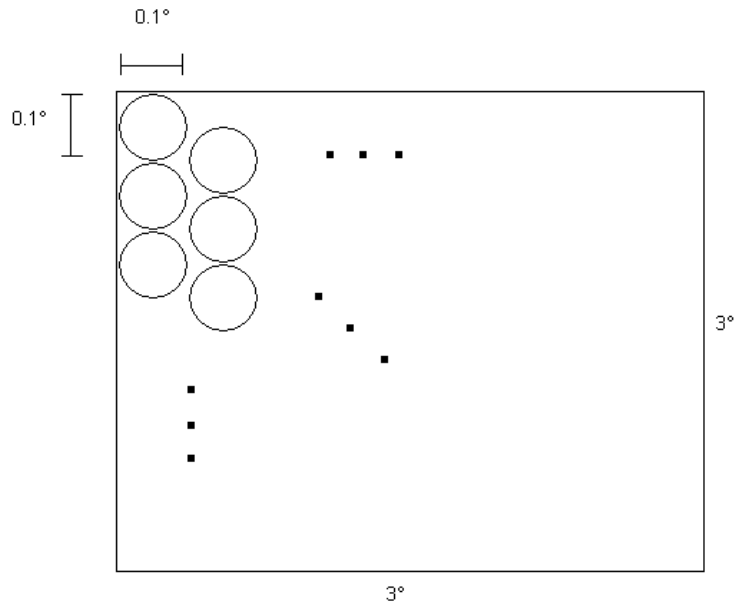


Figure 4-3: Full-Field Search Example

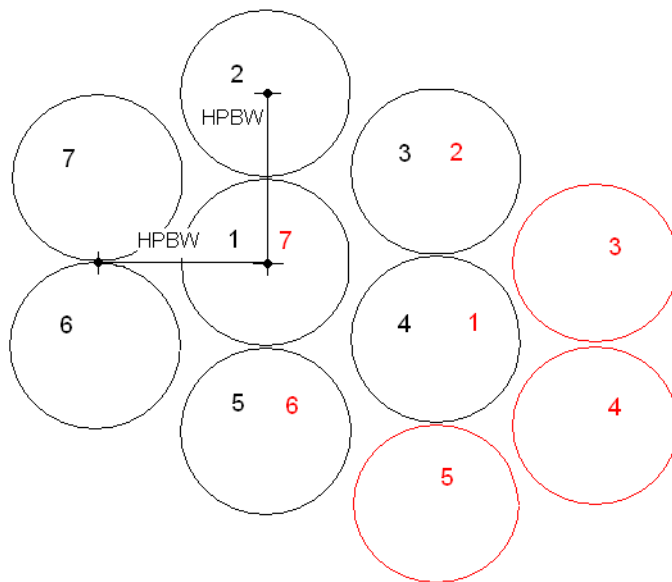


Figure 4-4: Spiral Search Pattern

with the lowest cost function value, and the test points are regenerated according to the same pattern. Old cost function measurements are not recycled because of the stochastic and time-varying properties of the gain pattern cost function even though some of the coordinates from previous iterations may coincide with the new trial point locations. Once the algorithm measures higher cost function values at each of the trial points surrounding the center point, the radius from the center point to the surrounding test points is reduced by half and the algorithm repeats. The SS algorithm terminates when the search radius is reduced to a sufficiently small value such that cost function measurements at the different trial points are not easily distinguished from one another.

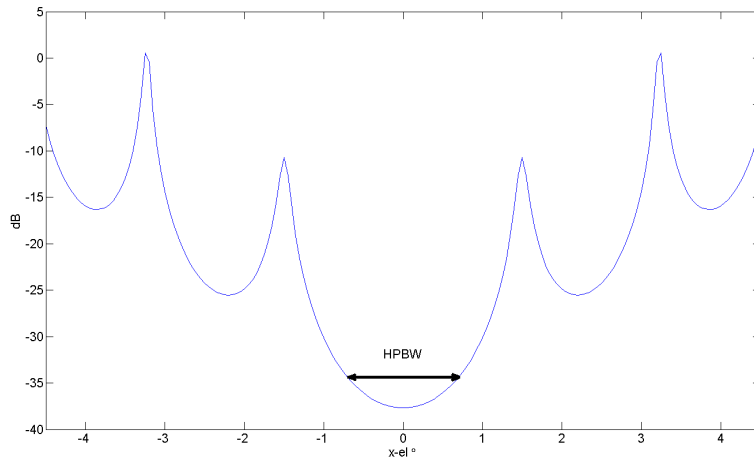


Figure 4-5: Cost Function as a Function of xel_i ($el_i = 0^\circ$)

The initial search radius equals the HPBW of the antenna. To help understand why the HPBW is used as an initial radius, a cut across one angular dimension of the gain pattern cost function is plotted in Figure 4-5. For a random initial starting distance from boresight, if the cost function is evaluated at HPBW intervals, increasing cost function values will not be observed in both directions until boresight is crossed. When this condition occurs, the HPBW scan terminates, and the trial point with the lowest cost function value lies within half of a HPBW from boresight of the cost function. The concept of scanning in HPBW intervals to eventually arrive within half the HPBW of boresight does not directly carry over to a gain pattern

cost function defined by two independent variables (xel_i and el_i); however, a spiral search method with an initial radius equal to a HPBW does locate the mainlobe of the gain pattern cost function a large percentage of the time. The SS step-tracking algorithm typically converges on boresight quickly, for cases when it does converge. The same SS algorithm used for spatial pull-in cannot be used for tracking because the first few spiral search radii are large, and the process would dither the antenna an unacceptable distance away from boresight. The non-convergence issues inherent in the SS method may also make it a less attractive option for accomplishing spatial pull-in. Because of the pitfalls inherent in the SS step-tracking algorithm, a more robust method is desired which may also be used for closed-loop tracking.

4.4 Step-tracking Using Optimization Techniques

By applying nonlinear function optimization methods to the gain pattern cost function, one may develop reliable step-tracking methods capable of accomplishing both spatial pull-in and closed-loop tracking. Optimization methods for nonlinear functions are iterative algorithms that move from trial point to trial point in the n-dimensional space spanned by the cost function until the termination conditions for the algorithm are met (if termination conditions exist). If the cost function is a function of n independent variables, then \mathbf{x} is a size-n position vector specifying the location in n-space of the trial point. For step-tracking algorithms using optimization methods, \mathbf{x} is a 2x1 vector containing the xel_i and el_i orthogonal inertial pointing angles. In general, optimization methods must satisfy

$$F_{k+1} \leq F_k \tag{4.3}$$

where F_k is the cost function evaluated at the k -th iteration of the algorithm [34]. Equation (4.3) ensures that each iteration of the optimization algorithm produces a successively smaller value of the cost function. Nonlinear cost function optimization

algorithms follow the update formula

$$\mathbf{x}_{k+1} = \mathbf{x}_k + \alpha \mathbf{p}_k \quad (4.4)$$

where \mathbf{x}_{k+1} is the next trial point location where the cost function is to be evaluated, \mathbf{x}_k is the current location, \mathbf{p}_k is a descent direction, and α is the step length taken in the descent direction [34–36]. Descent directions must follow a direction of negative curvature in the cost function, meeting the stipulation

$$\mathbf{p}_k^T G_k \mathbf{p}_k \leq 0 \quad (4.5)$$

where G_k is the second-derivative Hessian matrix of the cost function at the k -th trial point [34–36]. The specific optimization approach applied determines the descent direction in Equation (4.4). The value of α in Equation (4.4) specifies how far the algorithm should travel along the descent direction and is determined by a linear search procedure.

The terminal conditions for optimization methods must be carefully defined for the specific application. For step-tracking applications accomplishing spatial pull-in, the algorithm must locate the global minimum corresponding to the inertial angular coordinates of boresight. At boresight, or the peak of the mainlobe of the gain pattern, the gradient of the cost function vanishes; however, the gradient is also equal to zero at the weak minimums of the cost function where the sidelobes in the gain pattern occur. To effectively accomplish spatial pull-in, the algorithm must not terminate until the gradient is sufficiently close to zero *and* the minimum has been determined to be a strong one. Although the gain pattern cost function contains weak maxima, where the nulls in the gain pattern occur, the gradient values at these points cannot be precisely calculated because of the sharpness of the cost function at the nulls. As such, the weak maxima in the cost function do not have zero gradient values and do not pose potential termination points for step-tracking algorithms accomplishing spatial pull-in. Step-tracking systems may accomplish closed-loop tracking by eliminating the terminal conditions imposed in the spatial pull-in stage and running the optimization

algorithm in an infinite loop. Tracking may also be accomplished by scheduling the same algorithm used in the spatial pull-in stage to run at regular intervals or at times when the strength of the SATCOM link has been sufficiently degraded.

Optimization methods applied to nonlinear cost functions seek to achieve the highest possible asymptotic rate of convergence. An optimization algorithm asymptotically converges on the desired solution with order o , where o is the largest number such that

$$0 \leq \lim_{k \rightarrow \infty} \frac{\|\mathbf{x}_{k+1} - \mathbf{x}^*\|}{\|\mathbf{x}_k - \mathbf{x}^*\|^o} \leq \infty \quad (4.6)$$

where \mathbf{x}^* is the global minimum of the cost function. In practice, the best convergence rate that is generally attainable is quadratic convergence, where o in (4.6) equals two, so optimization literature emphasizes methods that exhibit this property [34, 36].

4.4.1 Modified Newton's Method

The first optimization method applied to the development of step-tracking algorithms is a Modified Newton's (MN) method. The precepts behind Newton's method stem from optimization techniques applied to quadratic cost functions. A generic quadratic cost function may be written as

$$F(x) = \frac{1}{2} \mathbf{x}^T A \mathbf{x} + b^T \mathbf{x} + c \quad (4.7)$$

where A must be a symmetric matrix [34]. The gradient and second-derivatives of the function in (4.7) may be calculated using Equations (4.8) and (4.9).

$$\mathbf{g}(x) = A \mathbf{x} + b \quad (4.8)$$

$$G(x) = A \quad (4.9)$$

In Equations (4.8) and (4.9), \mathbf{g} is the gradient vector and G is the second-derivative Hessian matrix. For a quadratic cost function, the exact Taylor series expansion of

the gradient at the next trial point, \mathbf{x}_{k+1} , may be written as

$$\mathbf{g}_{k+1} = \mathbf{g}_k + G\mathbf{p}_k \quad (4.10)$$

where all higher derivatives are zero for quadratic cost functions [34]. If \mathbf{x}_{k+1} is to be the minimum of the quadratic cost function, Equation (4.10) must equal zero. Newton's method algorithms subsequently determine a descent direction for use in Equation (4.4) according to

$$\mathbf{p}_k = -G^{-1}\mathbf{g}_k \quad (4.11)$$

where \mathbf{g}_k is the cost function gradient at the current trial point and G is the Hessian matrix of the assumed quadratic cost function [34–36]. Equation (4.11) exactly determines the minimum of a quadratic function in a single iteration. On non-quadratic functions, the process repeats iteratively until the minimum is found according to

$$\mathbf{p}_k = -G_k^{-1}\mathbf{g}_k \quad (4.12)$$

where G_k is now the Hessian matrix at the given trial point.

Newton's method generally exhibits quadratic convergence rates making it a viable approach for minimizing nonlinear cost functions [36]. Difficulties with the approach in (4.12) arise when G_k is not positive definite and actual descent directions are not generated; i.e. the \mathbf{p}_k vector generated by (4.12) does not satisfy (4.5). Modified Newton's Methods solve this problem by altering the Hessian matrix, G_k , to ensure that it is as close to the original G_k matrix as possible, yet sufficiently positive definite. One of the best approaches to modifying the G_k matrix employs the Cholesky Factorization described in Equations (4.13)-(4.14) [34–36].

$$G_k = L_k D_k L_k^T \quad (4.13)$$

$$d_{jj} = g_{jj} - \sum_{q=1}^{j-1} d_{qq} l_{jq}^2 \quad (4.14)$$

$$l_{ij} = (g_{ij} - \sum_{q=1}^{j-1} d_{qq} l_{iq} l_{jq}) / d_{jj} \quad i = j + 1, j + 2, \dots, n \quad (4.15)$$

where g_{ij} , l_{ij} , and d_{ij} are the elements of G_k , L_k , and D_k respectively and $j = 1, 2, \dots, n$. If G_k is positive definite, then the diagonal D_k matrix in (4.13) will have positive entries. If any of the elements of the D_k matrix are less than an arbitrarily small positive number, δ_G , then G_k is replaced by \bar{G}_k given by

$$\bar{G}_k = \bar{L}_k \bar{D}_k \bar{L}_k^T \quad (4.16)$$

$$\bar{d}_{jj} = g_{jj} + r_{jj} - \sum_{q=1}^{j-1} \bar{d}_{qq} \bar{l}_{jq}^2 = \delta_G \quad (4.17)$$

$$\bar{l}_{ij} = (g_{ij} - \sum_{q=1}^{j-1} \bar{d}_{qq} \bar{l}_{iq} \bar{l}_{jq}) / \bar{d}_{jj} \quad i = j + 1, j + 2, \dots, n \quad (4.18)$$

$$(4.19)$$

where r_{jj} is the amount added to the diagonal values of D to ensure they are greater than or equal to δ_G and j again increments column-wise from 1 to n [34]. \bar{G}_k becomes the modified approximation to the Hessian matrix at the given trial point and is related to the original approximation by $\bar{G}_k = G_k + R_k$ where R_k is a diagonal matrix containing the r_{jj} values. Because \bar{G}_k is sufficiently positive definite, a descent direction that satisfies (4.5) may now be found by solving Equation (4.20).

$$\mathbf{p}_k = -\bar{G}^{-1} \mathbf{g}_k \quad (4.20)$$

The value of δ_G places a lower limit on the “positive definiteness” requirement of \bar{G}_k . The δ_G value is rarely equal to zero to account for errors in the computation and/or approximation of the Hessian matrix. A selection of $\delta_G = 10$ is used in the modified Newton step-tracking simulations developed in this chapter with good results.

4.4.2 Quasi-Newton's Methods

Quasi-Newton methods attempt to optimize nonlinear cost functions without the use of second-derivatives while maintaining quadratic convergence rates. Quasi-Newton Methods determine the descent direction according to:

$$B_k \mathbf{p}_k = -\mathbf{g}_k \quad (4.21)$$

$$B_{k+1} = B_k + Q_k \quad (4.22)$$

where B_k in some way approximates G_k from (4.12), and Q_k is an update matrix dependent upon \mathbf{x}_k , \mathbf{x}_{k+1} , \mathbf{g}_k , and \mathbf{g}_{k+1} [34–36]. In the absence of additional knowledge about the cost function, B_0 may be initialized to the identity matrix [34, 36]. B_{k+1} must also satisfy the quasi-Newton Condition that $\rho_k B_{k+1} \Delta \mathbf{x}_k = \Delta \mathbf{g}_k$ [35]. The value of the constant, ρ_k , is normally set to unity which forces the B_{k+1} matrix to have the same curvature information as the second-derivative matrix in the \mathbf{p}_k direction for quadratic cost functions [34]. As the quasi-Newton algorithm iterates, and a cost function minima is neared, B_k becomes a successively better approximation to G_k .

Two separate methods for calculating the update matrix, Q_k , in Equation (4.22) are applied to developing step-tracking algorithms in this chapter; the method of Davidon, Fletcher, and Powell (DFP) and the method of Broyden, Fletcher, Goldfarb, and Shanno (BFGS). The formula for the DFP and BFGS update matrices are presented in Equations (4.23) and (4.24), respectively.

$$Q_k = \alpha \frac{\mathbf{g}_k \Delta \mathbf{g}_k^T}{\Delta \mathbf{g}_k^T \Delta \mathbf{x}_k} + \alpha \frac{\Delta \mathbf{g}_k \mathbf{g}_k^T}{\Delta \mathbf{g}_k^T \Delta \mathbf{x}_k} - \alpha \frac{\Delta \mathbf{g}_k \mathbf{g}_k^T \Delta \mathbf{x}_k \Delta \mathbf{g}_k^T}{(\Delta \mathbf{g}_k^T \Delta \mathbf{x}_k)^2} + \frac{\Delta \mathbf{g}_k \Delta \mathbf{g}_k^T}{\Delta \mathbf{g}_k^T \Delta \mathbf{x}_k} \quad (4.23)$$

$$Q_k = \frac{\Delta \mathbf{g}_k \Delta \mathbf{g}_k^T}{\Delta \mathbf{g}_k^T \Delta \mathbf{x}_k} + \alpha \frac{\mathbf{g}_k \mathbf{g}_k^T}{\Delta \mathbf{x}_k^T \mathbf{g}_k} \quad (4.24)$$

For derivations of the update formula in Equations (4.23)–(4.24), the reader is referred to the literature [34–36]. In general, the BFGS method is purported to have much better performance optimizing nonlinear functions than the DFP method [34], but step-tracking algorithms using both methods will be developed and applied in this chapter for comparison.

As in the modified Newton's method, quasi-Newton's methods only generate descent directions when the B_k matrix in (4.21) is positive definite. The update formula for both the DFP and BFGS methods are theoretically structured such that B_k remains positive definite at each iteration of the optimization algorithm [34, 35]. In spite of theoretical guarantees, B_k often tends to lose positive definiteness due to rounding errors, particularly when cost function gradients are approximated using finite differencing techniques (as is the case in step-tracking algorithms). To ensure B_k remains positive definite, the step-tracking algorithms developed in this chapter incorporate the same procedure outlined in Equations (4.16)-(4.18) for developing a sufficiently positive definite version of B_k when necessary. The resulting \bar{B}_k matrix, similar to \bar{G}_k in (4.16), is used to determine a descent direction according to (4.21) where B_k is replaced by \bar{B}_k .

4.4.3 Method of Steepest Descent

The simplest optimization method to develop step-tracking algorithms in this chapter is the method of Steepest Descent (SD). The SD method simply sets the descent direction equal to the negative of the cost function gradient at the current trial point according to Equation (4.25).

$$\mathbf{p}_k = -\mathbf{g}_k \quad (4.25)$$

Steepest Descent algorithms rely more heavily on accurate linear searches to determine the step length in Equation (4.4) than the Newton methods do. Accurate linear searches greatly increase the number of cost function evaluations accomplished per major algorithm iteration; an effect that is generally undesirable for applications requiring quick convergence. Steepest Descent methods exhibit only linear convergence rates but are very stable and less complex than other optimization techniques [34]. Because of the radial nature of the gain pattern cost function, SD optimization algorithms should produce descent directions which are tangent to the contours of the cost function; thus, boresight of the cost function could theoretically be found in one major algorithm iteration if the correct step length is determined. Because of the

potential for SD methods to easily optimize the gain pattern cost function without the use of second-derivative approximations, a step-tracking algorithm using an SD technique is developed in this chapter for comparison to the Newton methods.

4.4.4 Step-tracking Algorithm Architecture

The basic architecture described below produces step-tracking algorithms that accomplish closed-loop spatial pull-in of a target satellite using the methods of optimization described in Sections 4.4.1–4.4.3. This architecture changes very little as a function of optimization method. Major differences in step-tracking algorithms using optimization techniques arise only in the approach used by each method to calculate \mathbf{p}_k in Equation (4.4) (Line 24 of Algorithm 1).

Lines 1-3 initialize the terminal conditions, begin the while loop, and initialize the logical variable that determines whether or not a descent direction and step-length are calculated for this iteration (a predetermined $\alpha\mathbf{p}_k$ is calculated when the algorithm is at a local minima; Lines 8,14). Line 4 computes the value of the cost function at \mathbf{x} as well as at any nearby points required to approximate first or second-derivatives of the cost function. Lines 5-17 determine what procedures are accomplished by the algorithm when a minimum has been reached. If the algorithm determines it is currently at a local, weak minimum, Lines 6-10 instruct the algorithm to jump off of the local minimum in the direction of the global minimum. If the algorithm thinks it may have located the global minimum, lines 11-17 instruct the algorithm to repeat itself, without changing the trial point location, a number of times equal to “mincheck threshold” to make sure that the global minimum has actually been found; then the terminal conditions are set to true. The stochastic nature of the cost function makes this process necessary.

In the event that the repeated trial point is no longer close enough to the global minimum, lines 18-20 reset to zero the number of times the algorithm has repeated itself and instructs the algorithm to calculate $\alpha\mathbf{p}_k$. This event can be thought of as “falling off” of the global minimum, due to the time-varying nature of the cost function. This can occur in the amount of time it takes the algorithm to repeat

Algorithm 1 Step-Tracking Algorithm using Function Optimization Methods

```
1: set terminate = false
2: while terminate == false do
3:   set compute  $\alpha \mathbf{p}_k = \text{true}$ 
4:   perform function/gradient evaluations at  $\mathbf{x}_k$ 
5:   if criteria for minimum == true (small gradient) then
6:     check for local min
7:     if local min == true then
8:        $\alpha \mathbf{p}_k = \text{jump condition } \alpha \mathbf{p}_k$ 
9:       mincheck = 0
10:    else
11:       $\alpha \mathbf{p}_k = 0$ 
12:      mincheck = mincheck + 1
13:    end if
14:    compute  $\alpha \mathbf{p}_k = \text{false}$ 
15:    if mincheck > mincheck threshold then
16:      terminate=true
17:    end if
18:    else if mincheck > 0 && criteria for minimum ==false then
19:      mincheck = 0
20:      compute  $\alpha \mathbf{p}_k = \text{true}$ 
21:    end if
22:
23:    if compute  $\alpha \mathbf{p}_k == \text{true}$  then
24:      compute  $\mathbf{p}_k$  and initial  $\alpha$ 
25:      limit  $\alpha \mathbf{p}_k$  to a predetermined region of confidence
26:      perform linear search along  $\mathbf{p}_k$  to determine satisfactory  $\alpha$ 
27:    end if
28:     $\mathbf{x}_{k+1} = \mathbf{x}_k + \alpha \mathbf{p}_k$ 
29: end while
```

itself to check if it is on the global minimum or not. Experience has shown that the algorithm should only repeat itself once or twice at a single trial point while checking the global minimum terminal conditions in order to avoid “falling off” the global minimum during this time. Lines 23-27 determine a descent direction and a step length and are only accomplished if the algorithm is not at a minima. Line 25 limits the initial step length to within some “region of confidence.” This step is accomplished because many of the algorithms calculate very large initial step lengths away from the current trial point when smaller ones are required. Finally, Line 28 determines the next trial point according to (4.4).

The step-tracking algorithms developed to accomplish spatial pull-in may be modified for use in closed-loop tracking by simply removing the terminal conditions. Tracking algorithms also do not require the weak versus strong minimum discrimination procedure in Lines 5-21 because the strong minimum of the gain pattern cost function has already been located in the spatial pull-in stage.

Finite Difference Approximations for First and Second-Derivatives

Line 4 in Algorithm 1 instructs the step-tracking method to approximate the required first and second cost function derivatives. A standardized map of cost function evaluation locations relative to the current trial point, \mathbf{x}_k , is followed in each of the four nonlinear optimization methods when gradients or second-derivatives must be approximated. Figure 4-6 shows the cost function evaluation locations where the current trial point is labeled point 1 and δ_f is the finite differencing interval chosen. Because xel_i together with el_i and r together with q represent orthogonal components of inertial pointing error, the pointing error distributions derived for r and q in Section 3.3 are applied as distribution models for xel_i and el_i . Consequently, the $3\text{-}\sigma$ value for the open loop pointing error in the el_i and xel_i component directions is 0.06° (Sections 3.2.5 and 3.2.6). The finite differencing interval for each of the nonlinear optimization algorithms is selected to be between 2-3 times larger than the $3\text{-}\sigma$ value for the open-loop pointing error components in order to sufficiently distinguish cost function values measured at different points on the function map in Figure 4-6 [36]. The finite

differencing interval must also balance the requirement that Taylor series truncation errors be kept small; a stipulation which places an upper bound on δ_f [34–36]. A δ_f value equal to 0.16° was found to meet the above criteria and produce acceptable first and second-derivative approximations in simulation.

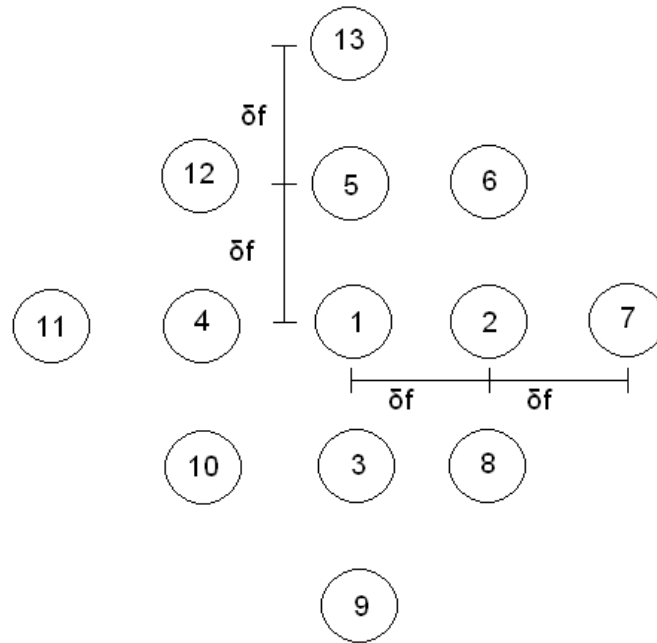


Figure 4-6: Cost Function Finite Differencing Map

The optimization algorithms utilize forward difference techniques to approximate gradient values if the algorithm is not in the vicinity of a minimum (Equation (4.26)). Forward difference techniques require less function evaluations per trial point than central difference methods but are less accurate at approximating the gradient, especially near a minimum of the cost function. For this reason, once the gradient values of the cost function fall below ten times the threshold for a cost function minimum, the algorithms switch to approximating gradient values by using central difference techniques (Equation (4.27)). The second-derivative Hessian matrix is always calculated using a forward difference approximation because the tradeoff in accuracy with a central difference Hessian calculation is not worth the computational price,

(4.28) [35]. Equation (4.29) ensures the approximation to the Hessian matrix satisfies the symmetry property of second-derivative matrices [34–36].

$$\mathbf{g}_j(\mathbf{x}) \approx \frac{F(\mathbf{x} + \delta_f \mathbf{e}_j) - F(\mathbf{x})}{\delta_f} \quad (4.26)$$

$$\mathbf{g}_j(\mathbf{x}) \approx \frac{F(\mathbf{x} + \delta_f \mathbf{e}_j) - F(\mathbf{x} - \delta_f \mathbf{e}_j)}{2\delta_f} \quad (4.27)$$

$$\tilde{\mathbf{G}}_j = \frac{\mathbf{g}(\mathbf{x} + \delta_f \mathbf{e}_j) - \mathbf{g}(\mathbf{x})}{\delta_f} \quad (4.28)$$

$$\mathbf{G} \approx \frac{1}{2}(\tilde{\mathbf{G}} + \tilde{\mathbf{G}}^T) \quad (4.29)$$

The subscript j in Equations (4.26)-(4.27) represents the j -th element of \mathbf{g} while \mathbf{e}_j represents the unit vector in the j -th direction. In Equation (4.28) the subscript j represents the j -th column of the Hessian matrix approximation, $\tilde{\mathbf{G}}$.

Minimum Discrimination

Lines 5-17 of Algorithm 1 check to see if the step-tracking algorithm has reached a cost function minima and also determine whether or not that minima is the global minimum. Each of the four nonlinear optimization algorithms use the same strategy to move away from a weak, local minimum and to travel in the direction of the global minimum. If the gradient is sufficiently small and the algorithm believes it has reached a minimum, then the algorithm carries out the function evaluations necessary to approximate the second-derivative Hessian matrix of the cost function at the current trial point according to Equation (4.28). If the algorithm is at a weak minimum, the approximation to the Hessian matrix should be nearly positive semi-definite. At the strong minimum, the approximate Hessian matrix should be strongly positive definite because the cost function has sufficient concavity in all directions. As a test for positive definiteness in the Hessian matrix, the step-tracking algorithms determine the Cholesky matrix factors of the G matrix as in Equations (4.13)-(4.15). If one or both of the elements of the diagonal D matrix are less than some small positive, δ_G , then the Hessian matrix lacks the required positive definiteness for a strong minimum [34], and the algorithm determines that the current trial point is on a sidelobe of the gain

pattern cost function. A value of $\delta_G=10$ is again used in simulation with good results for weak minimum discrimination.

If the algorithm determines that it has reached a weak minimum, a specific update, $\alpha \mathbf{p}_k$, is used in Equation (4.4) to determine the location of the next trial point. The two eigenvectors of the Hessian matrix point in the direction of maximum and minimum curvature because the cost function is a function of only two independent variables [34]. Because the gain pattern cost function is radially symmetric, and the weak minima corresponding to antenna sidelobes circle the mainlobe, one of the eigenvectors of the Hessian matrix points along the valley of the weak minimum (direction of minimum curvature), and the other points orthogonal to it; i.e. either toward boresight, or 180° away from boresight (direction of maximum curvature).

One may easily calculate a numeric value for the cost function curvature in the direction of each eigenvector by calculating $v_j^T G v_j$ where v_j is the j -th eigenvector of the Hessian matrix. Therefore, if the eigenvectors of the approximate Hessian are calculated, and the direction of maximum curvature is found, the descent direction may be taken as either v_{max} or $-v_{max}$ where v_{max} is the eigenvector corresponding to the direction of maximum curvature. Next, a step length value, α , must be calculated. The value of the step length used in Equation (4.4) when the algorithm is at a weak minimum is 1.85° , the average peak to peak distance beginning at the mainlobe and extending to the fourth sidelobe of the antenna gain pattern. Because the distance between the sidelobes in the gain pattern is a function of HPBW, the $\alpha = 1.85^\circ$ rule changes dependent upon the HPBW of the given antenna. In order to determine whether v_j or $-v_{max}$ is the appropriate descent direction, one must evaluate the cost function at $F(\mathbf{x}_k + 1.85v_{max})$ and compare the measurement to $F(\mathbf{x}_k)$. If the cost function is higher at $F(\mathbf{x}_k + 1.85v_{max})$ then the appropriate descent direction is $-v_{max}$; whereas, if the cost function is lower, then v_j should be taken as the descent direction.

Linear Search

Once the descent direction is calculated in Line 24 of Algorithm 1, its magnitude is restricted to within a specified “region of confidence” for trial points not located at a

minima in the gain pattern cost function (Line 25) [35]. The region of confidence for the step-tracking application is set to $|\mathbf{p}_k| < 1^\circ$. The 1° region of confidence prevents the nonlinear optimization algorithms from jumping over nearby local maximas as they progress into the valleys of the gain pattern cost function. Without the 1° restriction, the possibility exists for a wrong-way jump from one local maxima over the next local maxima resulting in a descent into a sidelobe valley that is even farther away from boresight. Because the distance between the nulls in the gain pattern cost function is a function of HPBW, the 1° region of confidence varies with the HPBW of the given antenna. After the conditional restriction on $|\mathbf{p}_k|$ is applied, Line 26 calculates the desired step length along the descent direction according to a linear search procedure. An appropriate step length will sufficiently reduce the *directed gradient* of the cost function along the descent direction [34–36]. The directed gradient measures the steepness of the cost function along a certain direction. If gradient values are explicitly available, the criterion for a linear search is described by

$$|\mathbf{g}(\mathbf{x}_k + \alpha\mathbf{p}_k)^T \mathbf{p}_k| \leq -\eta \mathbf{g}_k^T \mathbf{p}_k \quad (4.30)$$

where $0 \leq \eta < 1$ and is called the linear search parameter. When η equals 0, the directed gradient at $\mathbf{x}_k + \alpha\mathbf{p}_k$ must equal zero, and an exact linear search is carried out. Accurate linear searches are typically computationally wasteful; therefore, values of $\eta > 0$ are chosen for most nonlinear optimization algorithms [34,35]. If the gradient values are not available, and are instead calculated by finite differencing, the criterion in Equation (4.30) for the reduction of the directed gradient may be modified to

$$\frac{|F(\mathbf{x}_k + \alpha\mathbf{p}_k) - F(\mathbf{x}_k + \nu\mathbf{p}_k)|}{\delta_f} \leq -\eta \mathbf{g}_k^T \mathbf{p}_k \quad (4.31)$$

where ν is the multiplier that satisfies $|\mathbf{x}_k + \alpha\mathbf{p}_k| - |\mathbf{x}_k + \nu\mathbf{p}_k| = \delta_f$ [35].

The MN, BFGS, DFP, and SD algorithms implement the linear search in two steps. First, the algorithm brackets an interval containing a minimum along the descent direction, and secondly, the algorithm solves for the step length using a quadratic polynomial interpolation procedure. In order to bracket a minimum along the descent

direction, the optimization algorithms use function comparison methods [34]. $|\mathbf{p}_k|$ is taken to be the initial step size, α_0 , and a search is carried out by successively doubling the step size as in Figure 4-7 until an increase in the value of the cost function occurs. If an increase in the cost function is found on the initial step, the bracketing procedure carries out the search in the $-\mathbf{p}_k$ direction until the interval is bracketed. The step-tracking simulations developed in this chapter limit the number of times the step size is doubled when attempting to bracket a minimum along the descent direction. If a minimum has not been located within this time, the algorithm takes the initial step length, $\alpha_0 = |\mathbf{p}_k|$. This limitation eliminates wasteful computation that typically occurs near a local minima where α_0 is usually small.

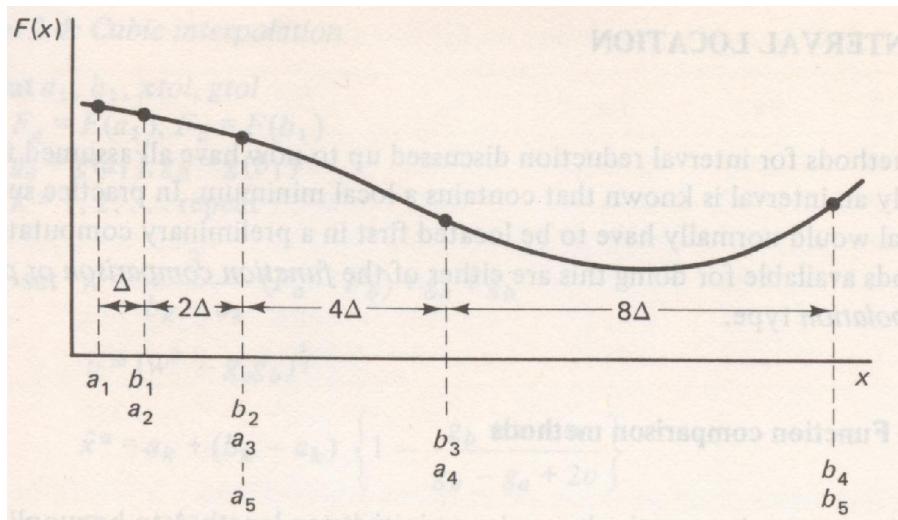


Figure 4-7: Strategy for Bracketing Minimum Along Descent Direction. Figure courtesy of Scales [34].

Once the optimization algorithm brackets a minimum along \mathbf{p}_k , a quadratic polynomial interpolation procedure is used to accomplish the linear search until the criterion in (4.31) is met. Higher order interpolation methods use function gradient values which are not explicitly available from the gain pattern cost function; therefore, the optimization algorithms use the quadratic interpolation method which does not require gradient values. For a description of both the quadratic interpolation procedure and higher order interpolation methods, the reader is referred to [34].

4.5 Spatial Pull-in Simulations

The four optimization methods described in Sections 4.4.1–4.4.3, along with the Spiral Search method from Section 4.3.2, are used to develop step-tracking algorithms that accomplish closed-loop spatial pull-in. The spatial pull-in simulations for each of the five algorithms are accomplished in MATLAB and the basic source code for each algorithm may be found in Appendix C. For simplicity in the spatial pull-in simulations, the satellite boresight always begins at 0° xel_i and 0° el_i , and the simulations limit the initial pointing error to a radius of 4.5° away from the origin. The maximum extent of this radius places the antenna’s pointing vector on the third sidelobe of the gain pattern, the assumed worst case initial pointing error for the open-loop pointing strategy. All closed-loop pointing strategies require an established communications link with the satellite in order to obtain SNR measurements. The quality of this link for the nominal APS system is severely degraded outside the 4.5° radius, and the SNR metric may not even be available for use in closed-loop pointing schemes. For this reason, the assumption that the initial pointing error falls within a 4.5° radius from boresight must be made. A random set of 1024 test points that are uniformly distributed over a circle centered at the origin with a 4.5° radius is created and shown together with the cost function contours in Figure 4-8. The spatial pull-in simulations are tested from each of the 1024 starting coordinates plotted in Figure 4-8. The average convergence time and percent convergence rates across the 1024 starting locations determine the spatial pull-in performance of each simulation.

The inertial pointing error from the open-loop feedback controller makes the SNR measurements from the gain pattern cost function stochastic, and this effect must be modeled in the MATLAB simulations. The pointing error distributions developed in Section 3.3 are applied to the MATLAB spatial pull-in simulations as distribution models for xel_i and el_i . The spatial pull-in simulations model the pointing error component distributions as normal with zero mean and variances equal to $0.0004^\circ{}^2$, an approximate worst-case scenario for the nominal APS operating in an open-loop fashion (See Table 3.1). MATLAB’s ‘randn’ function generates random pointing error

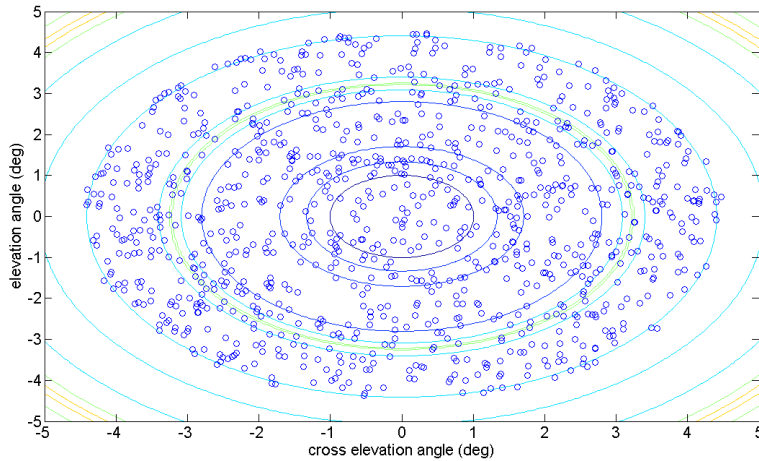


Figure 4-8: Starting Coordinates for Spatial Pull-in Simulation

component samples that meet the specified distribution parameters.

The MATLAB simulations determine the stare time by adjusting the number of cost function measurements, n , obtained at a single trial point location. For each of the n cost function measurements, an independent pointing error sample from the ‘randn’ function is added to both the desired xel_i and el_i coordinates to simulate the effects of pointing error on obtaining SNR measurements. The n cost function values for the given trial point location are next averaged, then rounded to the nearest tenth to simulate the fidelity limitation of the SNR metric. The total stare time at each trial point is determined according to

$$\text{stare time (sec)} = 0.25n \quad (4.32)$$

where the 0.25 seconds value equals the pointing error time dependency observed in Figures 3-21 and 3-22. Increasing the stare time ensures that the pointing error is, on average, closer to its population mean, which is namely zero according to the distribution models. When pointing errors average to zero, the cost function measurement at the given inertial coordinates may be more accurately determined. To get a feel for how long of a stare time is required for accurate SNR measurements, a confidence interval on pointing error may be calculated. If a confidence interval

width of 0.02° is desired for each of the inertial pointing error components, at the 95% confidence level, Equation (4.33) reveals that a sample size of 16 independent pointing error samples is required corresponding to a stare time of 4 seconds per trial point location, according to Equation (4.32). The spatial pull-in performance of each of the algorithms is examined for different stare times to see how the performance changes as a function of the stare time parameter.

$$n_{CI} = \left(\frac{2z_{\frac{\alpha}{2}}S}{w_{CI}} \right)^2 \quad (4.33)$$

In Equation (4.33) n_{CI} is the number of independent pointing error samples required corresponding to the number of cost function evaluations conducted per trial point (n). $z_{\frac{\alpha}{2}}$ is the critical value from the normal distribution corresponding to the given confidence interval, S is the standard deviation of the population, and w is the desired confidence interval width [37].

Because of the motion of the aircraft, the gain pattern cost function translates in the inertial reference frame defined by the cross-elevation and elevation axes. Figure 4-9 plots the magnitude of a geostationary target satellite's inertial angular velocity for a typical 707 flight profile. Some of the errors outlined in Section 2.2.1 also cause slowly time varying errors that can be simulated by translating the cost function at a certain velocity in the xel_i , el_i plane. The total translation of the cost function in the spatial pull-in simulations is approximated by the maximum target satellite velocity from Figure 4-9 plus an additional amount used to approximate time varying pointing errors. The spatial pull-in simulations use a value of $0.0005 \frac{\circ}{sec}$ for the total translational velocity of the cost function (v_{pat}). In the MATLAB simulation, the cost function translates equally in the negative xel_i and el_i directions for the duration of the simulation which has the largest impact on the performance of step-tracking algorithms.

Figures 3-17 and 3-18 show that the step response rise time between two inertial coordinates is 0.25 seconds, which conveniently equals the elapsed time between cost function measurements taken at a single xel_i , el_i point when stare times are

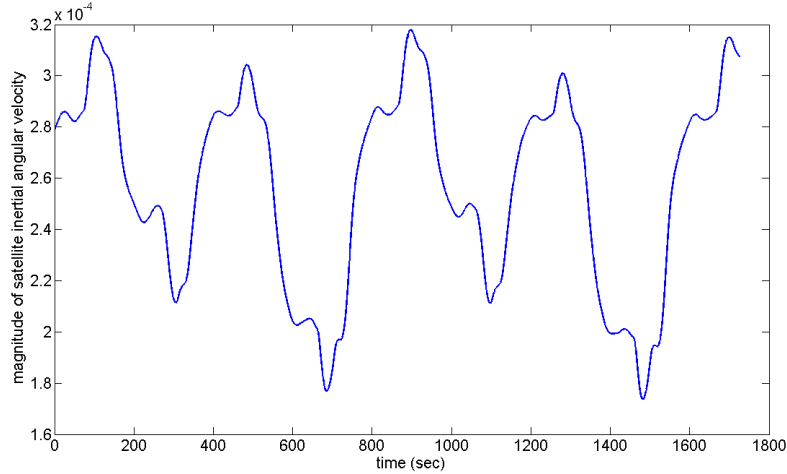


Figure 4-9: Magnitude of Satellite Inertial Angular Velocity

implemented to average the effects of pointing error. Because the elapsed time between any two cost function evaluations equals 0.25 seconds, the location of bore-sight in the xel_i , el_i plane is propagated after every cost function measurement by $0.0005 \frac{\circ}{sec} \cdot 0.25sec = 1.25 \cdot 10^{-4} \circ$. If the computational time within the step-tracking algorithm is ignored, the total convergence time to accomplish spatial pull-in may be approximated by

$$t_c = \frac{1.25 \cdot 10^{-4} \cdot nF_T}{v_{pat}} \quad (4.34)$$

In Equation (4.34), t_c equals the convergence time, $1.25 \cdot 10^{-4}$ is the angular distance the pattern travels in 0.25 seconds, F_T is the total number of cost function evaluations, n is the number of cost function evaluations performed per trial point, and v_{pat} is the translational velocity of the gain pattern cost function. Equation (4.34) directly relates the number of trial points visited in a given spatial pull-in algorithm to the convergence time for a given stare time parameter. The spatial pull-in simulations upper-bound the convergence times by limiting the number of trial points visited per simulation to 500. This restriction eliminates excessive computation for algorithms that are nonconvergent.

Spatial pull-in simulations were conducted for each of the five step-tracking algorithms in a *deterministic* state to serve as a base-line for comparing performance and determining optimal linear search parameters. The deterministic spatial pull-

in tests did not incorporate variance in cost function measurements due to inertial pointing error; therefore, the results of the deterministic simulations are completely reproduceable. The translating motion of the gain pattern cost function was also removed from the deterministic scenario. Table 4.1 contains the average number of cost function trial points visited, computed over all 1024 starting locations, for each of the step-tracking algorithms simulated in the deterministic scenario. A red subscript identifies the linear search parameter used in each simulation which ranges from 0.01 to 0.9. The simulation results for each algorithm in Table 4.1 are arranged from the fewest number of trial points visited to the greatest number of points visited for the various linear search parameters. Table 4.2 displays the spatial pull-in performance data for the best performing configuration of each algorithm from Table 4.1. The ratio listed in the first row of Table 2 is calculated by dividing the average number of trial points visited for each of the algorithms by the average number of trial points visited by the SS algorithm, the algorithm that had the lowest average number of trial points visited. The convergence times in the second row of Table 4.2 are computed according to Equation (4.34). Finally, the spatial pull-in convergence percentages in row three of Table 4.2 are given by Equation (4.35):

$$\rho = \left(1 - \frac{n_{nc}}{1024}\right) \cdot 100 \quad (4.35)$$

where ρ is the simulation's convergence percentage and n_{nc} is the number of non-converging points per simulation. For the spatial pull-in simulations, an algorithm converges from a particular starting point if the distance from boresight is reduced to within the closed-loop pointing requirement of 0.25° within 500 trial points.

After the deterministic simulations were accomplished, the pointing error and satellite motion effects were introduced into the spatial pull-in simulations. For these simulations, involving a stochastic, time-varying cost function, the stare time was varied for each algorithm as well as the linear search parameter for the optimization methods. Stare times were varied by adjusting the number of cost function evaluations conducted per trial point. Simulations were conducted with 1, 5, 10, 15, and 20 cost

function evaluations per trial point corresponding to stare times of 0.25, 1.25, 2.5, 3.75, and 5 seconds. Tables 4.3–4.12 present the results for the stochastic, time-varying cost function spatial pull-in simulations where the number of cost function evaluations conducted per trial point equals n . The simulation results for each stare time are presented in the same fashion as Tables 4.1 and 4.2. Because of the stochastic nature of the cost function, the results in Tables 4.3–4.12 are not exactly reproducible. The underlined values in Tables 4.3–4.12 represent simulation results which are not significantly different from each other according to the statistical z-test. Tables 4.3–4.12 only illustrate the statistical grouping including the best performing algorithms of each type. The z-test procedure for large samples sizes is described in [37].

Table 4.1: Average Number of Trial Points Visited for Deterministic Gain Pattern Cost Function

MN	162.8 _{0.9}	166.7 _{.05}	167.0 _{0.3}	167.3 _{0.7}	171.8 _{0.1}	172.1 _{.01}
BFGS	109.6 _{0.7}	110.0 _{0.5}	111.0 _{0.9}	114.2 _{0.3}	115.1 _{0.1}	119.2 _{.01}
DFP	125.5 _{0.1}	125.7 _{.01}	129.9 _{0.3}	133.3 _{0.5}	136.2 _{0.7}	138.3 _{0.9}
SD	223.2 _{0.1}	228.7 _{.01}	229.6 _{0.3}	278.1 _{0.5}	309.3 _{0.9}	311.7 _{0.7}
SS						68.6

Table 4.2: Algorithm Comparison for Deterministic Cost Function

	SS	BFGS _{0.7}	DFP _{0.1}	MN _{0.9}	SD _{0.1}
Ratio	1	1.60	1.83	2.37	3.25
t_c (sec)	17	27	31	40.7	56
ρ	84.8	98.3	95.4	93.8	67.9

Table 4.3: Average Number of Trial Points Visited when the Number of Cost Function Evaluations per Trial Point (n) equals 1

MN	212.5 _{0.7}	215.2 _{.01}	218.4 _{0.3}	218.4 _{0.5}	222.4 _{0.1}	223.3 _{0.9}
BFGS	162.9 _{0.7}	165.0 _{0.5}	169.0 _{0.3}	174.5 _{0.9}	177.3 _{.01}	179.3 _{0.1}
DFP	216.5 _{.01}	218.1 _{0.1}	237.6 _{0.3}	253.3 _{0.5}	287.9 _{0.7}	301.6 _{0.9}
SD	184.9 _{0.3}	189.1 _{0.1}	190.8 _{0.5}	191.7 _{.01}	200.8 _{0.7}	209.5 _{0.9}
SS						104.6

Table 4.4: Algorithm Comparison when the Number of Cost Function Evaluations per Trial Point (n) equals 1

	SS	BFGS _{0.7}	SD _{0.3}	MN _{0.7}	DFP _{.01}
Ratio	<u>1</u>	<u>1.56</u>	1.77	2.03	2.07
t_c (sec)	24	38	44	51	51
ρ	84.0	99.1	98.2	96.0	93.0

Table 4.5: Average Number of Trial Points Visited when the Number of Cost Function Evaluations per Trial Point (n) equals 5

MN	<u>127.9_{0.9}</u>	<u>131.2_{0.7}</u>	<u>131.6_{0.3}</u>	135.8 _{0.5}	137.3 _{0.1}	138.6 _{.01}
BFGS	<u>99.6_{0.7}</u>	103.9 _{0.5}	104.6 _{0.3}	104.8 _{0.9}	110.2 _{0.1}	110.3 _{.01}
DFP	<u>121.1_{0.1}</u>	<u>122.8_{.01}</u>	139.9 _{0.3}	141.2 _{0.5}	147.7 _{0.7}	151.8 _{0.9}
SD	<u>151.2_{0.1}</u>	<u>155.0_{0.3}</u>	<u>160.0_{.01}</u>	163.4 _{0.5}	179.5 _{0.7}	187.2 _{0.9}
SS						99.7

Table 4.6: Algorithm Comparison when the Number of Cost Function Evaluations per Trial Point (n) equals 5

	BFGS _{0.7}	SS	DFP _{0.1}	MN _{0.9}	SD _{0.1}
Ratio	<u>1</u>	<u>1</u>	1.22	1.28	1.52
t_c (min)	1.9	1.9	2.3	2.5	2.9
ρ	99.9	85.3	99.3	100	96.7

Table 4.7: Average Number of Trial Points Visited when the Number of Cost Function Evaluations per Trial Point (n) equals 10

MN	<u>132.5_{0.9}</u>	<u>133.0_{0.7}</u>	<u>135.6_{0.5}</u>	139.0 _{0.3}	141.6 _{0.1}	141.9 _{.01}
BFGS	<u>104.4_{0.7}</u>	<u>105.4_{0.5}</u>	<u>105.7_{0.9}</u>	111.2 _{0.3}	118.7 _{0.1}	121.6 _{.01}
DFP	<u>130.7_{0.1}</u>	<u>135.0_{.01}</u>	140.3 _{0.7}	141.7 _{0.5}	146.1 _{0.3}	146.7 _{0.9}
SD	<u>194.0_{0.1}</u>	<u>197.4_{0.3}</u>	<u>204.3_{.01}</u>	<u>204.4_{0.5}</u>	219.3 _{0.3}	226.8 _{0.9}
SS						100.1

Table 4.8: Algorithm Comparison when the Number of Cost Function Evaluations per Trial Point (n) equals 10

	SS	BFGS _{0.7}	DFP _{0.1}	MN _{0.9}	SD _{0.1}
Ratio	<u>1</u>	<u>1.04</u>	1.31	1.32	1.94
t_c (min)	3.9	3.9	5.0	5.1	7.6
ρ	84.8	100	99.0	99.9	91.4

Table 4.9: Average Number of Trial Points Visited when the Number of Cost Function Evaluations per Trial Point (n) equals 15

MN	<u>144.6_{0.7}</u>	<u>145.7_{0.9}</u>	<u>148.3_{0.5}</u>	<u>149.9_{0.3}</u>	<u>152.7_{.01}</u>	<u>154.5_{0.1}</u>
BFGS	<u>125.5_{0.7}</u>	<u>128.8_{0.9}</u>	<u>129.5_{0.5}</u>	<u>142.7_{0.3}</u>	<u>150.9_{0.1}</u>	<u>152.1_{.01}</u>
DFP	<u>182.6_{0.5}</u>	<u>183.1_{0.7}</u>	<u>185.6_{0.9}</u>	<u>194.9_{0.1}</u>	<u>195.9_{0.3}</u>	<u>203.9_{.01}</u>
SD	<u>303.3_{0.9}</u>	<u>314.3_{0.5}</u>	<u>323.0_{0.7}</u>	<u>326.3_{0.1}</u>	<u>329.9_{0.3}</u>	<u>335.1_{.01}</u>
SS						100.1

Table 4.10: Algorithm Comparison when the Number of Cost Function Evaluations per Trial Point (n) equals 15

	SS	BFGS _{0.7}	MN _{0.7}	DFP _{0.5}	SD _{0.9}
Ratio	<u>1</u>	<u>1.25</u>	1.45	1.83	3.03
t_c (min)	5.8	7.2	8.4	10.8	18.3
ρ	82.6	100	100	96.8	78.3

Table 4.11: Average Number of Trial Points Visited when the Number of Cost Function Evaluations per Trial Point (n) equals 20

MN	<u>156.4_{0.5}</u>	<u>156.6_{0.9}</u>	<u>157.8_{0.7}</u>	<u>159.0_{0.3}</u>	<u>161.2_{0.1}</u>	<u>161.8_{.01}</u>
BFGS	<u>165.4_{0.7}</u>	<u>169.2_{0.9}</u>	<u>179.2_{0.5}</u>	<u>189.6_{0.3}</u>	<u>194.8_{0.1}</u>	<u>199.7_{.01}</u>
DFP	<u>246.5_{0.9}</u>	<u>248.1_{0.7}</u>	<u>249.8_{0.5}</u>	<u>262.0_{0.3}</u>	<u>268.0_{0.1}</u>	<u>276.5_{.01}</u>
SD	<u>332.5_{0.9}</u>	<u>342.4_{0.5}</u>	<u>346.2_{0.7}</u>	<u>356.4_{0.1}</u>	<u>356.8_{0.3}</u>	<u>365.8_{.01}</u>
SS						100.8

Table 4.12: Algorithm Comparison when the Number of Cost Function Evaluations per Trial Point (n) equals 20

	SS	MN _{0.5}	BFGS _{0.7}	DFP _{0.9}	SD _{0.9}
Ratio	<u>1</u>	<u>1.54</u>	1.62	2.42	3.27
t_c (min)	7.9	12.2	12.9	19.6	26.8
ρ	76.4	100	99.9	92.8	78.2

4.5.1 Observations

Based on the spatial pull-in simulation results presented in Tables 4.3–4.12 one concludes that the SS and BFGS step-tracking algorithms consistently outperform the other algorithms. As alluded to in Section 4.3.2, the SS algorithm has convergence limitations and displays a maximum convergence percentage of only 85% for the $n=5$ scenario (Table 4.6). Most of the nonlinear optimization step-tracking algorithms display convergence percentages upwards of 90% under most circumstances. The BFGS algorithm consistently displays high convergence percentages of 98% or better. Although the BFGS algorithm typically requires a higher number of trial points to reach convergence than does the SS algorithm, the difference in convergence times between the two step-tracking methods is negligible for shorter stare times ($n < 15$).

The spatial pull-in simulation results shed light on what the optimal stare time should be for a step-tracking algorithm implemented on an airborne SATCOM terminal. Even though Equation (4.33) determined that 16 cost function measurements per trial point are necessary to reduce the pointing error confidence interval to 0.02° , such a large value of n is, in fact, undesirable. Figure 4-10 shows a scatter plot of the convergence times versus n for each of the step-tracking algorithms tested. From Figure 4-10, one sees that measuring the cost function only once at each trial point visited by the step-tracking algorithm produces convergence times much shorter than measuring the cost function 5, 10, 15, or 20 times per trial point. Tables 4.3 and 4.5 indicate that the step-tracking algorithms visit a greater number of trial points for a stare time of 0.25 seconds than for a stare time of 1.25 seconds; however, the time spent at each trial point when the stare time is 1.25 seconds increases the total convergence time substantially.

The results of the spatial pull-in simulations suggest the optimal linear search parameter that should be used in each of the different optimization algorithms for the selected stare times. The optimal linear search parameters for the algorithms in the deterministic simulations are the same, within the statistical significance groupings, as the optimal linear search parameters in the stochastic simulations for the $n=1, 5,$

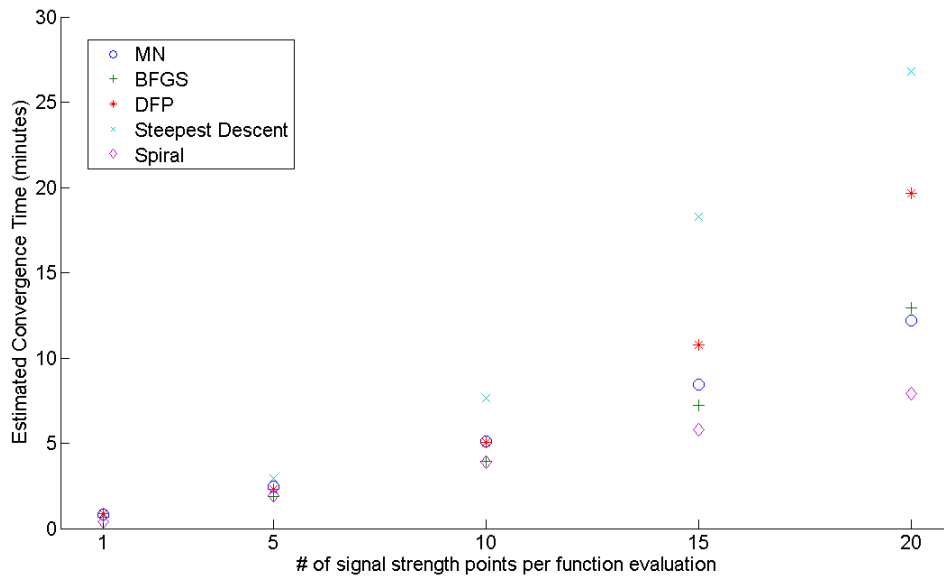


Figure 4-10: Number of Cost Function Evaluations per Trial Point vs. Spatial Pull-in Convergence Time

and 10 scenarios. Once the stare times reach 3.75 seconds or higher, cost function translational motion more strongly affects the performance of the optimization algorithms, and the linear search parameters that give the best performance change for some algorithms.

The spatial pull-in simulation results indicate that the MN, DFP, and SD algorithms do not perform as well as the BFGS and SS algorithms. Because the MN algorithm requires approximations to the second-derivative matrix at each trial point, as shown in Equation (4.12), one witnesses greater numbers of average trial point evaluations and higher convergence times when compared to the BFGS and SS algorithms. Also, because finite difference techniques approximate both the gradient and the Hessian matrix, the search direction determined by (4.12) contains errors caused by these approximations. Gill explicitly warns of the dangers of using finite difference techniques to accomplish both gradient and Hessian approximations [35]. Even so, the MN algorithm produces high convergence percentages and convergence times that may be acceptable when stare times are short.

The DFP algorithm differs from the BFGS algorithm only by the update matrix formula presented in Equation (4.23). The literature suggests that BFGS algorithms may out-perform DFP methods by as much as an order of magnitude in some instances [34]. For the spatial pull-in simulations, BFGS step-tracking algorithms consistently out-perform algorithms incorporating DFP optimization methods; therefore, BFGS methods should be favored for use in step-tracking applications.

Because of the radial nature of the gain pattern cost function, Steepest Descent methods produce search directions which provide the shortest paths to minima in the cost function when the cost function is deterministic and the errors caused by finite differencing are ignored. SD methods rely heavily on accurate linear searches which are accomplished more easily when drastic changes to the initial step length, α_0 , are not required. Equation (4.25) shows that the initial step length for the SD algorithm equals the magnitude of the gradient vector, which could be quite large. Even if the magnitude of the initial step length is restricted to a 1° region of confidence, as described in Section 4.4.4, a 1° initial step size could be too large when the trial point lies in the vicinity of a minima. In these instances, the linear search procedure must work hard both to bracket a minimum and to find a step length that meets the criterion in Equation (4.31). Newton methods typically generate initial step sizes that already meet the linear search requirement in Equation (4.31); therefore, Newton methods outperform the SD method in nearly all the spatial pull-in simulations.

4.6 Spatial Pull-in Robustness Tests

The two best-performing algorithms in Section 4.5, the SS algorithm and the BFGS algorithm with $\eta = 0.7$, were subjected to spatial pull-in tests under harsher conditions in order to test the robustness of each of the methods. The spatial pull-in robustness simulations incorporate greater open-loop pointing errors by increasing the variances on the inertial angular components of pointing error. The robustness simulations also exhibit faster translational movement (v_{pat}) of the cost function to simulate more drastic time-varying sources of open-loop pointing error or more

pronounced satellite motion. Both algorithms in the spatial pull-in robustness simulations conduct spatial pull-in from the same 1024 starting locations displayed in Figure 4-8.

During the robustness simulations, both the SS and BFGS algorithms were left in the same configurations used in the spatial pull-in tests conducted in Section 4.5. The spatial pull-in tests for increased pointing error variances and cost function velocities incorporated stare times of 0.25 and 1.25 seconds. Tables 4.13 and 4.14 present the results of the robustness simulations. The ratio value is the ratio of the average number of trial points visited for the particular velocity-variance combination listed in the given column compared to the number of trial points visited for the velocity-variance combination in the first column. The results listed in the first column of Tables 4.13 and 4.14 are the same as the results from the corresponding tests in Section 4.5. Tables 4.13 and 4.14 calculate convergence times (t_c) and percentages (ρ) according to Equations (4.34)–(4.35).

4.6.1 Observations

As expected, the performance of both algorithms degrades as the pointing error variances and pattern velocities are increased. Tables 4.13–4.14 show performance drops in terms of average number of trial points visited, convergence times, and convergence percentages. The underlined values in Tables 4.13–4.14 represent simulation results that are not statistically different from each other according to the z-test. For the $n=1$ scenario, the BFGS step-tracking algorithm feels the effects of the worsening pointing error and pattern velocity conditions much more so than the SS algorithm. The convergence percentage of the BFGS algorithm drops significantly for the last two velocity-variance combinations and average convergence times are nearly tripled. The SS algorithm demonstrates only slight drops in convergence percentages and slight increases in convergence times as conditions worsen for the $n=1$ case. For the $n=5$ case, the BFGS algorithm maintains convergence percentages greater than 95%. Table 4.14 shows that average convergence times are doubled for the BFGS approach under the harshest velocity-variance conditions of the test when $n=5$. The SS algorithm ex-

Table 4.13: Spatial Pull-in Robustness Simulation (Number of Cost Function Evaluations per Trial Point (n) equals 1)

		velocity/variance						
		5e-4/ 4e-4	1e-3/ 4e-4	5e-4/ 8e-4	1e-3/ 8e-4	2e-3/ 8e-4	1e-3/ 1.6e-3	2e-3/ 1.6e-3
BFGS	Ratio	1	1.01	<u>1.68</u>	<u>1.64</u>	<u>1.64</u>	<u>2.44</u>	<u>2.42</u>
	t_c (sec)	38	39	64	64	66	96	96
	ρ	99.1	99.5	92.6	92.5	90.4	73.2	70.9
SS	Ratio	1	1	<u>1.07</u>	<u>1.07</u>	<u>1.08</u>	<u>1.20</u>	<u>1.22</u>
	t_c (sec)	24	24	26	26	26	30	30
	ρ	84.0	85.4	84.7	85.3	85.6	83.4	83.3

Table 4.14: Spatial Pull-in Robustness Simulation (Number of Cost Function Evaluations per Trial Point (n) equals 5)

		velocity/variance						
		5e-4/ 4e-4	1e-3/ 4e-4	5e-4/ 8e-4	1e-3/ 8e-4	2e-3/ 8e-4	1e-3/ 1.6e-3	2e-3/ 1.6e-3
BFGS	Ratio	1	<u>1.09</u>	<u>1.11</u>	1.21	<u>1.61</u>	<u>1.68</u>	2.15
	t_c (min)	1.9	2.1	2.1	2.3	3.1	3.3	4.2
	ρ	99.9	100	99.9	99.8	98.8	99.6	95.1
SS	Ratio	1	1.01	1.03	<u>1.06</u>	<u>1.06</u>	<u>1.14</u>	<u>1.13</u>
	t_c (min)	1.9	2.0	2.0	2.0	2.1	2.2	2.2
	ρ	85.3	84.4	84.6	84.4	65.6	51.0	83.1

hibits significant drops in convergence percentages for the harsher velocity-variance combinations in the $n=5$ scenario, but the average convergence time is only slightly increased.

The engineer must decide how to structure the step-tracking algorithm to provide adequate spatial pull-in performance when open-loop pointing errors impose harsher conditions on the cost function. The SS algorithm may be used with a negligible stare time ($n=1$) to provide quick convergence times while achieving convergence rates of approximately 85% at best. If higher convergence percentages for spatial pull-in are desired, the engineer may opt to use the BFGS algorithm while incorporating a brief stare time, such as 1.25 seconds for the $n=5$ case. The added stare time produces longer convergence times but may be worth the trade-off for added convergence percentages.

4.7 A Look at Tracking

To demonstrate how step-tracking algorithms may be applied to accomplishing closed-loop tracking of a target satellite, the BFGS algorithm with a linear search parameter of 0.7 undergoes a series of tracking simulations. Separate tracking simulations were conducted for each of the pointing error variance and cost function velocity pairs used in Section 4.6. In a tracking configuration, the BFGS algorithm removes the terminal conditions imposed during spatial pull-in. The algorithm tracks the target satellite by continuously minimizing the gain pattern cost function until 500 trial points are evaluated in each simulation. Tracking performance of the BFGS algorithm was examined for both the $n=1$ and $n=5$ cases. According to Equation (4.34), for the $n=1$ scenario, tracking was accomplished for approximately 125 seconds per simulation, and for the $n=5$ case, tracking was accomplished for approximately 625 seconds per simulation. Each of the tracking simulations were conducted beginning from 1024 starting locations within a 0.1° radius from boresight (Figure 4-11). The close proximity of the initial starting points in the tracking simulations to boresight simulates the result of an accurate spatial pull-in procedure. During the tracking simulations,

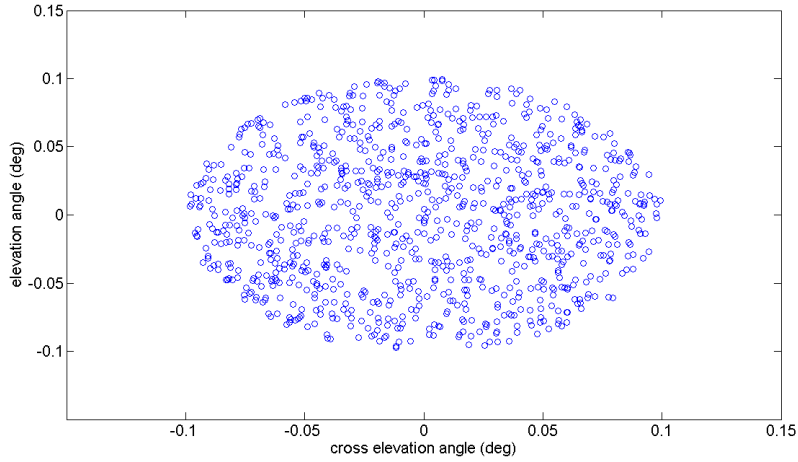


Figure 4-11: Starting Coordinates for Tracking Simulations

Table 4.15: BFGS Tracking Simulation (Number of Cost Function Evaluations per Trial Point (n) equals 1)

	velocity/variance					
	1e-3/ 4e-4	5e-4/ 8e-4	1e-3/ 8e-4	2e-3/ 8e-4	1e-3/ 1.6e-3	2e-3/ 1.6e-3
\bar{d}_{max} ($^{\circ}$)	0.073	0.082	0.080	0.081	0.101	0.107
\bar{d}_{mean} ($^{\circ}$)	0.030	0.033	0.031	0.031	0.035	0.036
\bar{d}_{σ} ($^{\circ}$)	0.026	0.026	0.026	0.025	0.028	0.030

Table 4.16: BFGS Tracking Simulation (Number of Cost Function Evaluations per Trial Point (n) equals 5)

	velocity/variance					
	1e-3/ 4e-4	5e-4/ 8e-4	1e-3/ 8e-4	2e-3/ 8e-4	1e-3/ 1.6e-3	2e-3/ 1.6e-3
\bar{d}_{max} ($^{\circ}$)	0.071	0.072	0.075	0.115	0.091	0.157
\bar{d}_{mean} ($^{\circ}$)	0.031	0.032	0.032	0.048	0.036	0.059
\bar{d}_{σ} ($^{\circ}$)	0.030	0.030	0.030	0.037	0.031	0.046

the maximum distance from boresight (d_{max}), mean distance from boresight (d_{mean}), and standard deviation of the distance from boresight (d_{σ}) were recorded for each starting location in Figure 4-11. Table 4.15 summarizes the mean of these three metrics over all 1024 initial starting points for each pointing error variance and pattern velocity combination for the $n=1$ case. Table 4.16 displays the results for the $n=5$ case. The bar above the metrics in Tables 4.15–4.16 indicates an average value.

4.7.1 Observations

Tables 4.15 and 4.16 demonstrate satisfactory tracking performance from the BFGS step-tracking algorithm. The average maximum deviations from boresight, \bar{d}_{max} , never exceed the 0.25° requirement outlined in Section 2.3, and the average mean deviations from boresight, \bar{d}_{mean} , are lower still. Even when the pointing error variances and pattern velocities are increased to values higher than those assumed for the operating environment of the nominal APS, the BFGS algorithm remains comfortably within the 0.25° requirement for closed-loop operation. Tracking for the $n=1$ case slightly outperforms the $n=5$ case for higher velocity-variance combinations.

4.8 Simulation Processing Times

Each of the individual spatial pull-in, and tracking simulations consumes a substantial amount of processing time because each simulation involves either spatial pull-in or tracking from 1024 starting locations. Figure 4-8 shows the starting locations for the spatial pull-in simulations, and Figure 4-11 depicts the initial trial points for the tracking simulations. To carry out the spatial pull-in and tracking simulations presented in this chapter, the step-tracking algorithms found in Appendix C were modified to run on a parallel processing network located at MIT Lincoln Laboratory known as the *LLGrid*. In each simulation, each of the 1024 starting locations gets assigned to one of 64 networked computers on the LLGrid; thus, a single computer becomes responsible for conducting either spatial pull-in or tracking from only 16 initial test points per simulation rather than all 1024. To compare the benefits of

using parallel processing, the total spatial pull-in simulation times, using the BFGS algorithm with a linear search parameter of 0.7, are examined as the number of cost function evaluations per trial point (n) is varied. Figure 4-12 shows these simulation times for both a single processor and for 64 networked processors on the LLGrid. One may appreciate the time-saving benefits of parallel processing when lengthy simulations involving multiple parameters are required, as was the case in the spatial pull-in and tracking simulations presented in this chapter.

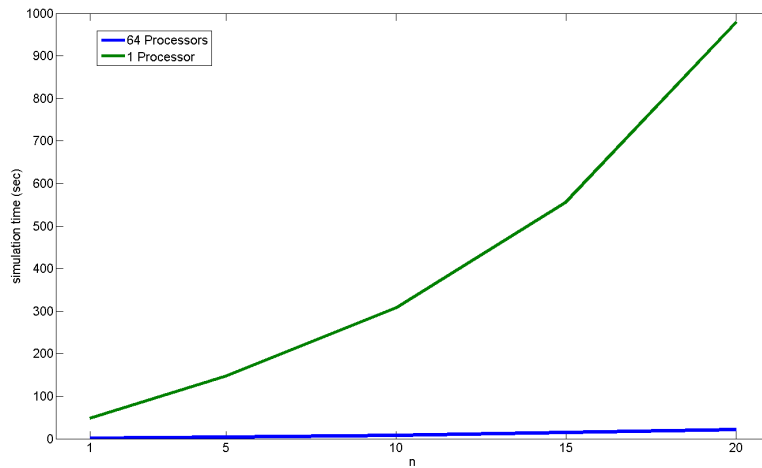


Figure 4-12: BFGS_{0.7} Spatial Pull-in Simulation Times vs. Number of Cost Function Evaluations per Trial Point (n) for Serial and Parallel Processing

Chapter 5

Conclusions

5.1 Open-loop Controller Simulation Results Summary

This thesis developed a hybrid open/closed-loop antenna pointing strategy for the nominal APS defined in Section 2.3. To accomplish open-loop pointing, a pedestal feedback controller was designed using state-space and optimal control techniques. The feedback controller mitigates the effects of base motion disturbances caused by vehicle motion and tracks reference commands issued by the closed-loop portion of the hybrid pointing scheme. The performance of the controller on both a linearized plant model and a more detailed nonlinear plant model was examined through simulation in Sections 3.2.5–3.2.6.

The controller was found to point the antenna of the nominal APS to a location in inertial space within the 0.1° requirement for open-loop pointing error before considering the effects of potential sources of error. Because the simulation results indicate that the pedestal feedback controller developed in Chapter 3 is capable of meeting the design requirement for open-loop pointing, the open-loop portion of the hybrid open/closed-loop strategy is deemed satisfactory. When sources of open-loop pointing error are introduced to the antenna pointing problem in mobile SATCOM applications, some form of closed-loop pointing is desired.

5.2 Closed-loop Step-tracking Simulation Results

Summary

Step-tracking methods were investigated for the nominal APS because they require no additional hardware components and effectively offer the simplest method of closed-loop antenna pointing. Four step-tracking algorithms were developed using methods of nonlinear cost function optimization along with a fifth algorithm developed using a spiral search function comparison technique. The closed-loop spatial pull-in performance of the five step-tracking algorithms was tested through simulation. The first set of spatial pull-in simulations assumed a particular operating environment for the nominal APS in an airborne SATCOM application. This environment includes a stochastic cost function, caused by open-loop inertial pointing errors, and a cost function that translates in inertial space due to satellite motion and an assumed amount of time-varying open-loop pointing error (See Section 4.5).

The results of the spatial pull-in simulations, presented in Tables 4.1–4.12, illustrate that the BFGS and SS algorithms outperform the remainder of the step-tracking algorithms. To meet the closed-loop pointing requirement outlined in Section 2.3, the step-tracking algorithms must converge to within 0.25° of boresight in the spatial pull-in stage. The BFGS algorithm displays very high percentages of convergence to within the 0.25° requirement (upwards of 98%) and demonstrates average convergence times on the same order as the SS algorithm for shorter stare times ($n < 15$). On average, the SS algorithm converges to within 0.25° of boresight more quickly than the BFGS algorithm but exhibits convergence percentages of only 85% or worse. The first set of spatial pull-in tests also demonstrate that stare times should typically be made as short as possible to achieve the quickest convergence times (Figure 4-10). In these tests, the average spatial pull-in convergence times for negligible stare times ($n = 1$) are less than a minute (Table 4.4).

The performance of the BFGS and SS algorithms was tested through simulation for harsher operating environments where greater open-loop pointing errors and larger effects of time-varying sources of open-loop pointing error were considered. The

results of the step-tracking algorithm robustness tests, presented in Tables 4.13 and 4.14, demonstrate that the SS algorithm continues to perform better for negligible stare times ($n = 1$); whereas, the BFGS algorithm performs better when a short stare time is incorporated, as in the $n = 5$ case. The SS algorithm in the $n = 1$ configuration shows average convergence times of 30 seconds or faster but continues to have convergence percentages of only 85% at best. The BFGS algorithm in the $n = 5$ configuration maintains convergence percentages of 95% or better but average convergence times are extended to around 4 minutes for the harshest of the velocity-variance combinations. When operating environments are worse than those assumed for the nominal APS, the engineer may select a SS step-tracking method, with quick convergence times and lower convergence percentages, or sacrifice convergence time for higher reliability with the BFGS approach. For many mobile SATCOM applications, wait times for accomplishing spatial pull-in of up to 5 minutes may be acceptable and worth the trade-off for the higher convergence percentages provided by the BFGS algorithm.

Because the SS function comparison algorithm cannot be used for tracking without major modifications to the algorithm structure, only the BFGS algorithm was implemented in closed-loop tracking simulations. To gauge the robustness of the BFGS algorithm in a tracking configuration, the tracking simulations were conducted for the same velocity-variance combinations used in the spatial pull-in robustness tests. The tracking simulations incorporated stare times of 0.25 and 1.25 seconds. The results of the tracking simulations presented in Tables 4.15 and 4.16 support the conclusion that a BFGS step-tracking algorithm could be used to maintain closed-loop inertial tracking to within the 0.25° requirement even in harsher operating environments than assumed for the nominal APS. The results of the tracking simulations also indicate that stare times should be kept as short as possible to achieve the best tracking performance.

5.3 Overall Contributions

Major contributions made by the research presented in this thesis are listed below:

1. Using optimal and state-space control techniques, this thesis developed an open-loop pedestal controller for a nominal, two-axis, azimuth-elevation APS that mitigates the effects of aircraft motion and tracks input reference commands. The techniques used to develop the pedestal controller for the nominal APS may be applied to other mobile SATCOM projects where two-axis, azimuth-elevation pedestals are employed to accomplish antenna pointing.
2. A Simulink simulation was developed to simulate the pointing performance of the open-loop pedestal controller on the nominal APS. The simulation may be easily modified and used to determine the open-loop pointing performance of similar APSs used on other SATCOM projects.
3. Closed-loop step tracking algorithms were developed and shown to offer viable solutions for accomplishing closed-loop antenna pointing on an airborne SATCOM terminal. Both the BFGS and SS algorithms offer acceptable methods for accomplishing spatial pull-in even under conditions worse than those assumed for the nominal APS. The BFGS method provides more reliable convergence guarantees at the expense of slightly longer convergence times while the SS algorithm performs in the opposite manner.
4. The BFGS step-tracking algorithm was shown to effectively accomplish closed-loop target satellite tracking. In a tracking configuration, the BFGS algorithm maintained inertial pointing to within the 0.25° of boresight requirement even when the operating conditions were harsher than those assumed for the nominal APS.
5. Because simulation results indicate that both the open-loop feedback controller and select closed-loop step-tracking methods meet the requirements for the nominal APS, the hybrid open/closed-loop approach to antenna pointing is consid-

ered feasible for an airborne SATCOM application. Both the open-loop controller development techniques, and the closed-loop step-tracking algorithms, may be applied to other SATCOM applications, either mobile or stationary. Because this thesis has shown a hybrid open/closed-loop antenna pointing strategy to be feasible, accurate antenna pointing may be accomplished with a simple, cost-effective APS without the need for more complex systems involving additional closed-loop tracking hardware.

5.4 Suggestions for Future Work

The Simulink model developed in Section 3.2.6 provides insight as to how the nominal APS, while operating in an open-loop fashion, may actually perform while operating in an airborne environment. As more complex pedestal dynamics models are developed, the new effects may easily be added to the simulation and their impact on the overall pointing error may be readily observed. In particular, models simulating the effects of the open-loop sources of error, identified in Section 2.2.1, may be added to the existing simulation. The MATLAB scripts for the step-tracking algorithms, located in Appendix C, may be converted into Simulink models and the entire open/closed-loop system could be simulated together in one location. The combined simulation could provide greater insights to using hybrid pointing strategies on mobile SATCOM terminals.

The open-loop controller developed in Chapter 3 yielded a system with a bandwidth of only approximately 2.5 Hz because the harshest disturbance inputs occurred at much lower frequencies (Figures 3-3 and 3-8). If the closed-loop pedestal controller bandwidth could be increased, the step time between trial points could be reduced. Consequently, the convergence times for the closed-loop step-tracking algorithms could be lowered as the time spent traveling between trial points would be reduced.

Both the SS and BFGS algorithms showed promising results for step-tracking approaches to accomplishing spatial pull-in. A combined SS/BFGS algorithm could

be developed that achieves shorter average convergence times than a standard BFGS approach, but higher convergence percentages than a stand-alone SS algorithm. The hybrid SS/BFGS step-tracking approach could begin the spatial pull-in process with an SS method and then switch to a BFGS method once the SS algorithm terminates. If boresight is not located when the SS algorithm terminates, the BFGS algorithm could accomplish the remainder of the spatial pull-in task. Convergence times would be reduced by allowing the SS algorithm to accomplish as much of the spatial pull-in task as possible before engaging the slower BFGS algorithm.

This thesis has shown through simulation the feasibility of using hybrid open/closed-loop pointing strategies on mobile SATCOM terminals. The suggested next step in implementing hybrid pointing strategies on actual terminal systems involves a series of hardware tests. First, the pointing strategy should be applied to a terminal system operating on the ground with no base motion disturbances. Secondly, pointing tests may be conducted with the pedestal system operating on a motion simulator table to mimic different mobile environments. Finally, the pointing strategy may be tested with a vehicle-mounted APS. The tests occur in increasing order of complexity so that issues with using a hybrid pointing strategy may be identified at the lowest level and testing costs may be kept to a minimum.

Appendix A

Satellite Look Angle Calculations

Overview

This appendix presents two ways of calculating the desired local azimuth and elevation look angles, az_d and el_d , and their rates, \dot{az}_d and \dot{el}_d , for airborne inertial pointing applications using two-axis positioners. The first method involves finding position and relative velocity vectors from a mobile terminal to a target satellite based on kinematic relationships derived from the satellite's orbital element set and the terminal's GPS location and inertial states. The second method calculates local look angles and their rates if the desired *inertial* look angles are known in addition to the terminal's inertial information.

In this thesis, the “inertial” qualifier refers to the topocentric North, East, Down (NED) reference frame. The NED frame rotates with the Earth and, therefore, is not strictly an inertial reference frame. However, engineers still regard the NED coordinate system as an inertial reference frame in many circumstances because rotations of objects in this frame are generally much faster than the rotation of the coordinate system itself [24].

The following generic formulas are used throughout this appendix to calculate look angles and look angle rates:

$$azimuth = \begin{cases} \left(\arctan \left(\frac{y}{x} \right) \right)_{\text{mod } 2\pi} & \text{if } x \geq 0 \\ \left(\arctan \left(\frac{y}{x} \right) + \pi \right)_{\text{mod } 2\pi} & \text{if } x < 0 \end{cases} \quad (\text{A.1})$$

$$elevation = \arcsin \left(\frac{-z}{\sqrt{x^2 + y^2 + z^2}} \right) \quad (\text{A.2})$$

$$\frac{d}{dt}(azimuth) = \left(\frac{\dot{y}}{x} - \frac{y\dot{x}}{x^2} \right) \sec^{-2}(azimuth) \quad (\text{A.3})$$

$$\frac{d}{dt}(elevation) = \left(\frac{-\dot{z}}{\sqrt{x^2 + y^2 + z^2}} + \frac{z(x\dot{x} + y\dot{y} + z\dot{z})}{(x^2 + y^2 + z^2)^{\frac{3}{2}}} \right) \sec^{-1}(elevation) \quad (\text{A.4})$$

where x , y , and z are the components of a pointing vector and \dot{x} , \dot{y} , and \dot{z} are the components of a relative velocity vector. In a generic reference frame, the *azimuth* look angle is a positive rotation about the z axis referenced from the x axis and ranging from 0-360°. The elevation look angle is an angle above or below the xy plane with positive elevation angles defined as angles opposite the z axis. Elevation angles range from -90° to +90°. The look angles and look angle rates expressed in Equations (A.1)-(A.4) may be calculated for any three-dimensional position/relative velocity vector combination defined in any coordinate system.

A.1 Satellite Targeting Using Classical Orbital Element Sets

If the Classical Orbital Elements (COEs) of a target satellite are known, pointing and relative velocity vectors from a mobile terminal to the satellite may be calculated at any instance in time, provided the GPS coordinates and inertial states of the terminal are known at that time. To calculate the pointing and relative velocity vectors, the position and velocity vectors of both the satellite and the terminal are calculated in Earth-Centered Inertial (ECI) coordinates. The origin of the ECI coordinate frame lies at the center of the earth and the fundamental plane is the equatorial plane. The ECI primary axis points in the direction of the Vernal Equinox (the general direction of the constellation Aries), and the z axis points toward the North Pole. Figure A-1 illustrates the ECI coordinate system [38]. The reader should note that

the ECI coordinate system does not rotate as the earth spins about its rotational axis; therefore, the ECI coordinate frame constitutes a true inertial reference frame.

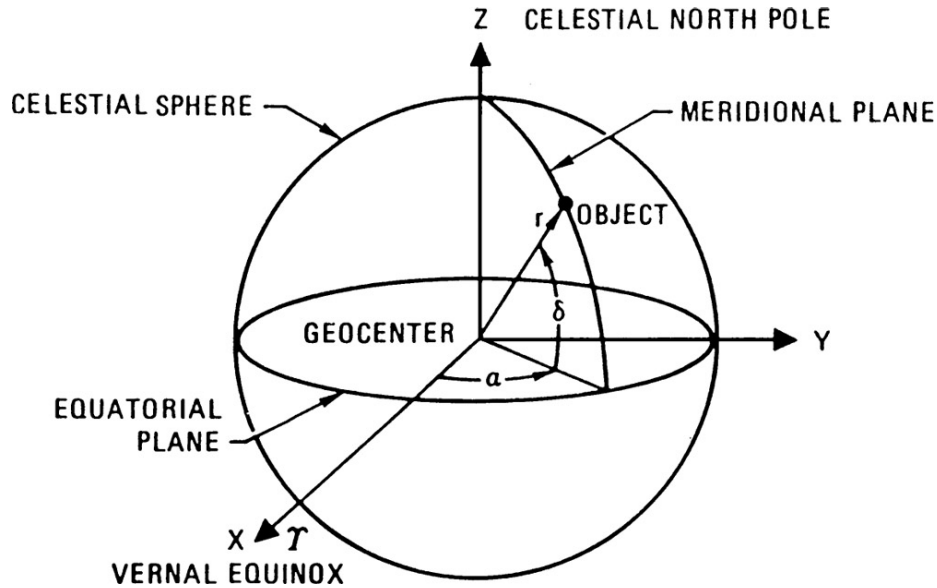


Figure A-1: Earth-Centered Inertial (ECI) Coordinate System. Photo courtesy of Chobotov [38].

To define the satellite's position and velocity vectors as continuous functions of time, the satellite's COEs need only be known at a single instance in time. The six COEs are the semimajor axis (a), eccentricity (e), inclination (i), right ascension of the ascending node (Ω), argument of perigee (ω), and true anomaly (ν). The instance in time when the COEs are defined is known as the *epoch time* [39]. The COEs are converted to an initial position and velocity vector, defined at the epoch time, according to the procedure in [39]. The initial position and velocity vectors may be propagated through time using a Sundman transformation described in [38]. The MATLAB m-file 'Keplar2RRR.m' presented in this appendix inputs a target satellite's COEs and then calculates the satellite's position and velocity vectors in ECI coordinates at a particular time since the epoch time.

After the satellite's position and velocity vectors in ECI coordinates are calculated as functions of time, one must determine the terminal's position and velocity vectors in ECI coordinates as well. The mobile terminal's position and velocity vectors are calculated as functions of time according to the procedure in [40]. The m-file

‘basemotionlatlongalt2ECINAVDATA.m’ presented in this appendix inputs a mobile terminal’s geodetic latitude, longitude, and altitude, as well as the terminal’s component velocities in the NED coordinate frame, and outputs the terminal’s position and velocity vectors in ECI coordinates at a particular time since the target satellite’s epoch time.

Once the position and velocity vectors of both the terminal and satellite are found, the pointing vector and relative velocity vectors in ECI coordinates may be calculated according to

$$\mathbf{r}_{\text{point}_{ECI}}(t) = \mathbf{r}_{\text{sat}_{ECI}}(t) - \mathbf{r}_{\text{terminal}_{ECI}}(t) \quad (\text{A.5})$$

$$\mathbf{v}_{\text{rel}_{ECI}}(t) = \mathbf{v}_{\text{sat}_{ECI}}(t) - \mathbf{v}_{\text{terminal}_{ECI}}(t) \quad (\text{A.6})$$

where $\mathbf{r}_{\text{sat}_{ECI}}$, $\mathbf{v}_{\text{sat}_{ECI}}$ and $\mathbf{r}_{\text{terminal}_{ECI}}$, $\mathbf{v}_{\text{terminal}_{ECI}}$ are the position and velocity vectors in ECI coordinates of the satellite and terminal respectively. $\mathbf{r}_{\text{point}_{ECI}}$ and $\mathbf{v}_{\text{rel}_{ECI}}$ in Equations (A.5)-(A.6) represent the resultant pointing and relative velocity vectors from the terminal to the satellite in ECI coordinates.

Next, $\mathbf{r}_{\text{point}_{ECI}}$ and $\mathbf{v}_{\text{rel}_{ECI}}$ are resolved in the NED frame through the following coordinate transformations:

$$\mathbf{r}_{\text{point}_{NED}}(t) = [R_{\text{pitch}}(-(\text{latitude}(t) + 90^\circ))] [R_{\text{yaw}}(\alpha_{ls}(t))] \mathbf{r}_{\text{point}_{ECI}}(t) \quad (\text{A.7})$$

$$\mathbf{v}_{\text{rel}_{inertial}_{NED}}(t) = [R_{\text{pitch}}(-(\text{latitude}(t) + 90^\circ))] [R_{\text{yaw}}(\alpha_{ls}(t))] \mathbf{v}_{\text{rel}_{ECI}}(t) \quad (\text{A.8})$$

where R_{yaw} and R_{pitch} are coordinate transformation matrices for rotations about the y and z axes of the given coordinate system. The $[R_{\text{yaw}}(\alpha_{ls}(t))]$ coordinate transformation in Equations (A.7)-(A.8) involves a rotation about the ECI z axis by the local sidereal time angle, $\alpha_{ls}(t)$. The local sidereal time angle is defined as the angle between the ECI primary axis and the local longitudinal meridian at a specific instance in time. $\alpha_{ls}(t)$ may be calculated according to

$$\alpha_{ls}(t) = (\text{longitude}(t) + [\alpha_{\text{g midnight}} + \omega_e t])_{\text{mod } 360^\circ} \quad (\text{A.9})$$

where *longitude* is the terminal's geodetic longitude, ω_e is the rotation rate of the earth, t is seconds since midnight of the given day, and $\alpha_{g \text{ midnight}}$ is the right ascension of the Greenwich meridian at midnight of the current day. $\alpha_{g \text{ midnight}}$ in Equation (A.9) may be calculated according to the method described in [38]. The $[R_{pitch}(-(\text{latitude}(t) + 90^\circ))]$ coordinate transformation in Equations (A.7)-(A.8) rotates the resultant vector about an intermediate pitch axis an amount equal to the negative of the geodetic latitude angle plus 90° . The resultant pointing vector, $\mathbf{r}_{\text{point}_{NED}}$ has x, y, and z components in the topocentric NED coordinate frame. The relative velocity of the target satellite, as seen in the NED frame by an observer standing at the terminal's location, is found by taking the earth's rotation into account according to

$$\mathbf{v}_{\text{rel}_{NED}}(t) = \mathbf{v}_{\text{rel inertial}_{NED}}(t) - (\omega_{e_{NED}} \times \mathbf{r}_{\text{point}_{NED}}(t)) \quad (\text{A.10})$$

where $\mathbf{r}_{\text{point}_{NED}}$ and $\mathbf{v}_{\text{rel inertial}_{NED}}$ are found from Equations (A.7)-(A.8) and $\omega_{e_{NED}}$ is the earth's rotation rate resolved in the NED frame. With the pointing and relative velocity vectors defined in the NED frame, the *inertial* look angles may be calculated using Equations (A.1) and (A.2) where x , y , and z are the components of the NED pointing vector, $\mathbf{r}_{\text{point}_{NED}}(t)$. The inertial look angle rates may be calculated using Equations (A.3) and (A.4) where \dot{x} , \dot{y} , and \dot{z} are the components of the NED relative velocity vector, $\mathbf{v}_{\text{rel}_{NED}}$. The resultant azimuth inertial look angle and its rate are given the symbols az_{NED} and \dot{az}_{NED} respectively, and the inertial elevation angle and its rate are represented as el_{NED} and \dot{el}_{NED} respectively.

To calculate the desired *local* look angles and their rates, the pointing and relative velocity vectors derived in Equations (A.7) and (A.10) must be transformed into the Aircraft coordinate frame from Section 3.1.3. This transformation is accomplished according to

$$\begin{aligned} \mathbf{r}_{\text{point}_{Aircraft}}(t) &= [R_{roll}(\Phi(t))] [R_{pitch}(\Theta(t))] \\ &\quad \cdot [R_{yaw}(\Psi(t))] \mathbf{r}_{\text{point}_{NED}}(t) \end{aligned} \quad (\text{A.11})$$

$$\begin{aligned} \mathbf{v}_{\text{rel inertial}_{Aircraft}}(t) &= [R_{roll}(\Phi(t))] [R_{pitch}(\Theta(t))] \\ &\quad \cdot [R_{yaw}(\Psi(t))] \mathbf{v}_{\text{rel inertial}_{NED}}(t) \end{aligned} \quad (\text{A.12})$$

$$\mathbf{v}_{\text{rel}_{Aircraft}}(t) = \mathbf{v}_{\text{rel inertial}_{Aircraft}}(t) - (\omega_{e_T} \times \mathbf{r}_{\text{point}_{Aircraft}}(t)) \quad (\text{A.13})$$

where $[R_{yaw}(\Psi(t))]$ is a yaw transform matrix through the Euler heading angle (Ψ), $[R_{pitch}(\Theta(t))]$ is a pitch transform matrix through the Euler pitch angle (Θ), and $[R_{roll}(\Phi(t))]$ is a roll transform matrix through the Euler roll angle (Φ) [24]. The relative velocity vector in the Aircraft coordinate frame, $\mathbf{v}_{\text{rel}_{Aircraft}}$, is the relative velocity of the target satellite as seen by an observer located on the Aircraft. Equation (A.13) calculates $\mathbf{v}_{\text{rel}_{Aircraft}}$ by accounting for the component of linear velocity contributed by the total rotational velocity, ω_{e_T} , of the Aircraft coordinate frame. ω_{e_T} is calculated according to

$$\omega_{e_T} = \omega_{e_{Aircraft}} + \omega_{A/C_{Aircraft}} \quad (\text{A.14})$$

where $\omega_{e_{Aircraft}}$ is the earth's rotation rate resolved in the Aircraft coordinate frame and $\omega_{A/C_{Aircraft}}$ is the vector of Aircraft rotational velocities calculated in Equation (3.15). Assuming that all misalignment angles between the Aircraft coordinate system and the base of the antenna positioner equal zero, the desired local look angles and local look angle rates may be calculated using Equations (A.1)-(A.4). The x , y , and z values in Equations (A.1)-(A.4) are the components of the pointing vector, $\mathbf{r}_{\text{point}_{Aircraft}}$, and the \dot{x} , \dot{y} , and \dot{z} values are the components of the relative velocity vector, $\mathbf{v}_{\text{rel}_{Aircraft}}$. Equations (A.1) and (A.3) determine az_d and \dot{az}_d , and Equations (A.2) and (A.4) determine el_d and \dot{el}_d .

A.2 Targetting Using Known Inertial Look Angles

This sections discusses the calculation of the desired *local* look angles and their rates when the *inertial* look angles are known. This situation arises when one knows the

az_{NED} and el_{NED} angles of a geostationary target satellite or when one knows a desired target location in the sky (as is the case in Section 4.1). The calculations presented in this section assume the values of \dot{az}_{NED} and \dot{el}_{NED} equal zero, implying a stationary target in the NED reference frame. In order to determine the local look angles, one first calculates a pointing vector in the NED frame using the known inertial look angles:

$$\begin{bmatrix} x \\ y \\ z \end{bmatrix}_{NED} = \begin{bmatrix} \cos(el_{NED}) \cos(az_{NED}) \\ \cos(el_{NED}) \sin(az_{NED}) \\ -\sin(el_{NED}) \end{bmatrix} \quad (\text{A.15})$$

The pointing vector from Equation (A.15) is next transformed into the Aircraft coordinate system as in Equation (A.11). Finally, the az_d and el_d look angles are calculated using Equations (A.1) and (A.2).

The desired look angle rates, \dot{az}_d and \dot{el}_d , must be chosen such that the aircraft's rotation rates resolved in the y and z components of the antenna Body reference frame are canceled out (Equation (3.16)). Thus, the desired look angle rates are calculated according to

$$\dot{el}_d = -D_Q \quad (\text{A.16})$$

$$\dot{az}_d = -\tan(el)P'_{A/C_{Base}} - R'_{A/C_{Base}} \quad (\text{A.17})$$

where $P'_{A/C_{Base}}$ and $R'_{A/C_{Base}}$ are the aircraft's rotational velocities resolved in the antenna Base x and z axes [4]. Equation (A.18) shows the calculation of $P'_{A/C_{Base}}$, $Q'_{A/C_{Base}}$, and $R'_{A/C_{Base}}$ which is an intermediate step not explicitly shown in equation (3.16)

$$\begin{bmatrix} P'_{A/C} \\ Q'_{A/C} \\ R'_{A/C} \end{bmatrix}_{Base} = \begin{bmatrix} \cos(az) & \sin(az) & 0 \\ -\sin(az) & \cos(az) & 0 \\ 0 & 0 & 1 \end{bmatrix} \begin{bmatrix} P_{a/c} \\ Q_{a/c} \\ R_{a/c} \end{bmatrix}_{Aircraft} \quad (\text{A.18})$$

A.3 Kepler2RRR.m

```
function [R, V, iter] = Kepler2RRR (sma, ecc, inc, asc, per, anom, anomType
, t)
% Misha Ivanov
% MIT LL, Grp 64
% 5 June 2006

% Given the Keplerian Elements and some time, t, this function calculates
% the Range and Velocity.
%
% use: [R, V] = Kepler2RRR (sma, ecc, inc, asc, per, anom, anomType, t)
%
% sma (m) - Semi-Major Axis, size of orbit
% ecc (ratio) - Eccentricity, shape of orbit (0<=ecc<1)
% inc (deg) - Inclination, defines orbital plane
% asc (deg) - Right Ascension of Ascending Node, defines orbital plane
% per (deg) - Argument of Perigee, defines orbit in plane
% anom (deg) - Anomaly, satellite's position in orbit
% anomType - Mean(1), True(2, default), Eccentric(3)
% t (sec) - point in time to determine output values (default = 0)

% reference - Orbital Mechanics (Chobotov), p.60-61

% edited line 66-EM

% Error Checking
if (nargin < 6)
    error('6 Input Arguments needed');
elseif (nargin == 6)
    anomType = 2;
    t = 0;
elseif (nargin == 7)
    t = 0;
end

if ((ecc>=1) || (ecc<0))
    error('ecc out of range, 0<=ecc<1');
end

format long g;

% Scientific Constants
mu = 3.986008 * 10^14;          % Earth Gravitational Constant

% Init
err = 10^-16;

% Convert Mean anomaly
if (anomType == 1)
    [E,T] = convertMeanAnomaly(anom, ecc);
    [x, y, z, x1, y1, z1] = Clas2CartT(sma, ecc, inc, asc, per, T);
elseif (anomType == 2)
    [x, y, z, x1, y1, z1] = Clas2CartT(sma, ecc, inc, asc, per, anom);
else
```

```

    [x, y, z, x1, y1, z1] = Clas2CartE(sma, ecc, inc, asc, per, anom);
end

r0 = [x y z];
dot(r0,r0);
V0 = [x1 y1 z1];

% Find X corresponding to t
r0norm = norm(r0);
V0norm = norm(V0);

deltaT = t;

a = mu/(2*mu/r0norm - V0norm^2);
if (a>0)
    P = 2*pi*sqrt(a^3/mu);
    deltaT = deltaT - fix(abs(deltaT)/P)*P;
end

X = sqrt(mu)*deltaT/abs(a);

deltaX = sqrt(a*err) + 1;
iter = 0;

while (abs(deltaX^2/a) >= err)
    Z = X^2/a;
    if (Z==0)
        C = 1/2;
        S = 1/6;
    else
        C = (1-cos(sqrt(Z)))/Z;
        S = (sqrt(Z)-sin(sqrt(Z)))/sqrt(Z^3);
    end
    % C = 1/2 - Z/24 + Z^2/720 - Z^3/40320      % approx
    % S = 1/6 - Z/120 + Z^2/5040 - Z^3/362880  % approx

    f0 = (1-r0norm/a)*S*X^3 + r0*V0'*C*X^2/sqrt(mu) + r0norm*X - t*sqrt(mu);
    f1 = C*X^2 + r0*V0'*(1-S*Z)*X/sqrt(mu) + r0norm*(1-C*Z);
    f2 = (1-r0norm/a)*(1-S*Z)*X + r0*V0'*(1-C*Z)/sqrt(mu);

    gamma = 2*sqrt(4*f1^2 - 5*f0*f2);
    gamma = abs(gamma);
    if (f1<0)
        gamma = -gamma;
    end

    deltaX = 5*f0/(f1+gamma);

    X = X - deltaX;
    iter = iter+1;
end

iter;

r = r0*V0'*(1-S*Z)*X/sqrt(mu) + r0norm*(1-C*Z) + C*X^2;

% Find r,V in terms of X,r0,V0
f = 1 - (X^2)*C/r0norm;

```

```

g = t - (X^3)*S/sqrt(mu);
f1 = sqrt(mu)*X*(S*Z-1)/(r*r0norm);
g1 = 1 - (X^2)*C/r;

R = f*r0 + g*V0;
dot(R,R);

V = f1*r0 + g1*V0;

% f
% g
% f1
% g1
% r

end

```

A.4 basemotionlatlongalt2ECINAVDATA.m

```

function [termpos,termvel,localsidereal,latdot,longdot,altdot] =
basemotionlatlongalt2ECINAVDATA(t, lat, long, alt, YR, MO, DY, Ndot, Edot,
altdot)
%Eric Marsh
%11 June 2007
%Reference Chobotov, p. 75-76, Montenbruck, p 189
%inputs:
%t (sec)= current time since midnight of the current day
%lat= geodetic lattitude in deg
%long= geodetic long. in deg (east longitude)
%alt= height above sea level (ft)
%YR= year (e.g., 1989)
%MO= month (1 for Jan., 2 for Feb. etc)
%DY= day of the month
%Ndot= North velocity (m/s)
%Edot= East velocity (m/s)
%altdot= vertical velocity (m/s) (positive is "upward" change)

%argument check to see if terminal is moving or not
if (nargin==7)
    latdot=0;
    longdot=0;
    altdot=0;
end
%error check
if (lat < -90 || lat > 90)
    error('lat must be between -90 and 90')
elseif (long < 0 || long > 360)
    error('long must be between 0 and 360 (pos in east dir)')
end

%constants
f=1/298.257223563; %see montenbruck p 189
aearth=6378137; %m

```

```

wemin=0.2506844537; %earth's rotation deg/min
werad=wemin*unitsratio('rad','deg')/60; %earth's rotation rad/sec
we=wemin/60; %earth's rotation in deg/sec

%time calculations
alphamidnight=greenwichmidnight(YR,MO,DY); %greenwich angle at midnight
%of sim day
localsidereal=mod(long+alphamidnight+we*(t),360); %local sidereal time
%angle at time 't'

%convert inputs
lat=lat*unitsratio('rad','deg');
localsidereal=localsidereal*unitsratio('rad','deg');
alt=alt*unitsratio('m','ft');
%altdot=altdot*unitsratio('m','ft'); %m/s

%calculate terminal ECI coords (position vector and velocity vector)

%%%%%%%%%%%%%%%%%%%%%%%%%%%%%%%%%%%%%%%%%%%%%%%%%%%%%%%%%%%%%%%%%%%%%%%%Method derived from Montenbruck p 188)%%%%%%%%%%%%%%%%%%%%%%%%%%%%%%%%%%%%%%%%%%%%%%%%%%%%%%%%%%%%%%%%%%%%%%%%
N=aeearth/sqrt(1-f*(2-f)*sin(lat)^2);
x=(N+alt)*cos(lat)*cos(localsidereal);
y=(N+alt)*cos(lat)*sin(localsidereal);
z=((1-f)^2*N+alt)*sin(lat);
termpos=[x y z]; %row of termpos vector gives x,y,z coord

%calculate velocity vector:
%need latdot, longdot, altdot at every time
latdot=Ndot*(1/norm(termpos)); %North velocity to latdot (rad/s) conversion
s=cos(lat)*norm(termpos);
longdot=Edot*(1/s); %East velocity to longdot (rad/s) conversion

Ndot=- (aeearth/2)*(1-2*f*(sin(lat)^2)+f^2*sin(lat)^2)^(-3/2)*(-4*f*sin(lat)
*cos(lat)*latdot+2*f^2*sin(lat)*cos(lat)*latdot);
localsiderealldot=werad+longdot;
xdot=Ndot*cos(lat)*cos(localsidereal)-N*sin(lat)*latdot*cos(localsidereal)
-N*cos(lat)*sin(localsidereal)*localsiderealldot+altdot*cos(lat)
*cos(localsidereal)-alt*sin(lat)*latdot*cos(localsidereal)-alt*cos(lat)
*sin(localsidereal)*localsiderealldot;
ydot=Ndot*cos(lat)*sin(localsidereal)-N*sin(lat)*latdot*sin(localsidereal)
+N*cos(lat)*cos(localsidereal)*localsiderealldot+altdot*cos(lat)
*sin(localsidereal)-alt*sin(lat)*latdot*sin(localsidereal)+alt
*cos(lat)*cos(localsidereal)*localsiderealldot;
zdot=((1-f)^2*Ndot*sin(lat)+(1-f)^2*N*cos(lat)*latdot+altdot*sin(lat)+alt
*cos(lat)*latdot);
termvel=[xdot ydot zdot];
%%%%%%%%%%%%%%%%%%%%%%%%%%%%%%%%%%%%%%%%%%%%%%%%%%%%%%%%%%%%%%%%%%%%%%%%

```


Appendix B

Open-Loop Controller Simulations

The following code was written using the MATLAB programming language, Version 7.4.0.287. It was run on a Dell laptop computer with a Pentium 4 processor, 2.13 GHz processor, and 2 GB of RAM using Microsoft Windows XP Professional, Version 2002 Service Pack 2.

B.1 controller.m

```
%Eric Marsh
%MIT LL, Grp 61
%February, 2008

%controller.m

%Description: This m-file develops the LQG controller for a nominal
%Antenna Positioner System and simulates the performance using lsim. The
%parameters needed for the Simulink model, 'APSSimulinkmdl.mdl' are included
%at the end of this m-file.

clear all;
close all;
load Afilt;
load Bfilt;

%plot PSD of filter
sys=ss(Afilt,Bfilt,1,0);
[mag,phase,w] = bode(sys);
mag=squeeze(mag);
db=20*log(mag);
%figure;semilogx(w,db);xlabel('freq (rad/s)'); ylabel('DB mag');
%title('Filter PSD');

%inertia in el axis:
```



```

Iyy=635;%units are in^2*lb
Iyy=Iyy*0.4535924*0.0254^2;%convert to m^2*kg
b=1/Iyy;

%motor constants:
kaz=18.7; %oz-in/amp
%kbaz=38.4; %V/10^3*RPM
kaz=kaz*0.007061552; %N-m/amp
%kbaz=kbaz*60/(2*pi)*10^-3; %Volts/(rad/sec)
kbaz=kaz;
raaz=4.84; %ohms
kel=kaz;
kbel=kbaz;
rael=raaz;

%gearing:
n=0.1; %n=r1/r2=radius of small gear/radius of large gear (m)

%reference input parameter
N=1/0.005519215703220;

%state deriv left mult matrix:
I=[Iyy 0 -Iyy; 0 1 0; 0 0 1];

A=zeros(3,3);
A(1,1)=-kel*kbel/rael*(1/n^2);
A(1,3)=kaz*kbaz/raaz*(1/n^2);
A(2,1)=1;
A(3,3)=Afilt;
A=inv(I)*A;

Bu=zeros(3,1);
Bu(1)=kel/rael*(1/n);
Bu=inv(I)*Bu;

Bw=eye(3);
Bw(3,3)=Bfilt;
Bw=inv(I)*Bw;

Cy=[1 0 0; 0 1 0]; %sensing both velocity and position
%Cy=[1 0 1]; %sensing just velocity Cy=[0 1 0]; %sensing just pos

%form controllability, observability matrices. can then check rank to see
%if system is uncontrollable or unobservable
ssol=ss(A,Bu,Cy,0);
ctol=ctrb(ssol);
obol=obsv(ssol);

%LQR for control gains:
% bryson's rule for weighting Rxx: simply 1/(xmax)^2
rxx(1)=1/(20*pi/180)^2;
rxx(2)=1/(.01*pi/180)^2;
rxx(3)=0; %zero weighting on filter state
Rxx=diag(rxx);
%Rxx=Rxx*10^9;
Ruu=10^3; %control weighting
[K,S,E]=lqr(A,Bu,Rxx,Ruu);

```

```

%LQR Sim
Ts=0.01; %sim step size
tfinal=100; %sim end time
t=0:Ts:tfinal;
x0=[0;0;0]; %begin sim with a 3 deg/sec initial condition on velocity
rho2=10^-7; %small amount of process noise (power spect. density??)
Rww=diag([rho2,rho2,1]);%white noise input with unit variance on the filter
%state
w1=sqrt(Rww(1,1))*randn(length(t),1);
w2=sqrt(Rww(2,2))*randn(length(t),1);
Dp=sqrt(Rww(3,3)/Ts)*randn(length(t),1); %white noise disturbance input
%to filter (divide by sqrt(Ts) to make pwr spectral density equal to 1)

Alqr=A-Bu*K;
Bwlqr=[0;0;Bfilt];
[y,x]=lsim(Alqr,Bw,Cy,0,[w1,w2,Dp],t,x0);
% [y,x]=lsim(Alqr,Bwlqr,Cy,0,[Dp],t,x0);
y=y*unitsratio('deg','rad');

%plots
% figure;plot(t,y(:,1)); xlabel('sim time (s)'); ylabel('inertial rate
% (deg/sec)'); legend('antpitchdot'); title('LQR with dist FF');
% figure;plot(t,y(:,2)); xlabel('sim time (s)'); ylabel('inertial angle
% (deg)'); legend('antpitch'); title('LQR with dist FF');

%LQE for estimator gains:
Rvv=eye(2);
Rvv(1,1)=10^-8; %sensor weighting on gyro
Rvv(2,2)=10^-6; %sensor weighting on position sensor
f=1;
Rvv=f*Rvv;
[L,Q,F]=lqr(A',Cy',Bw*Rww*Bw',Rvv);
L=L';

%LQG sim: (simulate plant and estimator together) see attached block
%diagram
Alqg=[A -Bu*K;L*Cy A-Bu*K-L*Cy];
Blqg=[Bw zeros(3,2) Bu*N; zeros(3,3) L Bu*N];
Clqg=[Cy zeros(2,3)]; %for measuring both velocity and position
Dlqg=zeros(2,6); % dims are rows of Clqg x cols of Blqg
syslqg=ss(Alqg,Blqg,Clqg,Dlqg);

x0lqg=[x0; zeros(3,1)];
v1=sqrt(10^-8)*randn(length(t),1); %white velocity sensor noise
v2=sqrt(10^-6)*randn(length(t),1); %white position sensor noise
%ref(:,1)=zeros(length(t),1);
ref(:,1)=[zeros(101,1);ones(9900,1)*1*pi/180]; %step response
% ref(:,1)=[zeros(101,1);ones(9900,1)*0.16*pi/180];
[ylqg,xlqg]=lsim(Alqg,Blqg,Clqg,Dlqg,[w1,w2,Dp,v1,v2,ref],t,x0lqg);
%torque calcs:
ulqgel(:,1)=-[zeros(1,3) K]*xlqg'+N*ref'; %input voltage to el motor
ilqgel=ulqgel/rael-(kbel/rael)*1/n*xlqg(:,1);
torqueel=kel*ilqgel;
%convert from N-m to oz-in:
torqueel=torqueel*1/0.007061552;

```

```

ylqg=ylqg*unitsratio('deg','rad'); %convert sim outputs to rad/sec and rad
%plots:
% figure;plot(t,ylqg(:,1));hold all; plot(t,xlqg(:,4)*180/pi);hold off;
% xlabel('sim time (s)'); ylabel('angle rate (deg/sec)');
% legend('antpitchdot','Qdot estimate'); title('LQG sim');
% figure;plot(t,ylqg(:,2));hold all; plot(t,xlqg(:,5)*180/pi);hold off;
% xlabel('sim time (s)'); ylabel('angle (deg)'); legend('antpitch','q
% estimate'); title('LQG sim'); figure;plot(t,xlqg(:,3)*180/pi);hold all;
% plot(t,xlqg(:,6)*180/pi); hold off; xlabel('sim time (s)'); ylabel('dist
% rate (deg/sec)'); legend('antpitchdist','antpitchdist estimate');
% title('dist input'); figure;plot(t,torqueel);hold all;plot([0 max(t)],[30
% 30],'m--'); plot([0 max(t)],[-30 -30],'m--');hold off; xlabel('sim time
% (s)'); ylabel('torque (oz-in)'); legend('elevation torque'); title('El
% Torque v. Time'); figure;bode(syslqg);
%
% %simulink params Ixx=1217; %units are in^2*lb
% Ixx=Ixx*0.4535924*0.0254^2;%convert to m^2*kg a=1/Ixx; Izz=Iyy; c=1/Izz;
% XEL_Gyro_BW=10000; %bandwidth in hz XEL_Gyro_Bias=0; %rad/sec
% XEL_Gyro_Noise=10^-8; %noise = avg power or variance in (rad/sec)^2
% XEL_IMU_Bias=0; %rad/sec XEL_IMU_Error=10^-6; %noise = avg power or
% variance in (rad/sec)^2 XEL_IMU_BW=10000; %bandwidth in hz
% XEL_IMU_sample_time=1/10; XEL_Veh_Pos_Command_Rate=1/1000;
% EL_Gyro_BW=10000; %bandwidth in hz EL_Gyro_Bias=0; %rad/sec
% EL_Gyro_Noise=10^-8; %noise = avg power or variance in (rad/sec)^2
% EL_IMU_Bias=0; %rad/sec EL_IMU_Error=10^-6; %noise = avg power or
% variance in (rad/sec)^2 EL_IMU_BW=10000; %bandwidth in hz
% EL_IMU_sample_time=1/10; EL_Veh_Pos_Command_Rate=1/1000;
% el_motor_noloadspeed=5500*2*pi/60; %no load speed in rad/sec
% el_motor_stall_torque=30*0.007061552; %stall torque in N-m
% az_motor_noloadspeed=5500*2*pi/60; %no load speed in rad/sec
% az_motor_stall_torque=30*0.007061552; %stall torque in N-m

```

B.2 APS Simulink Model

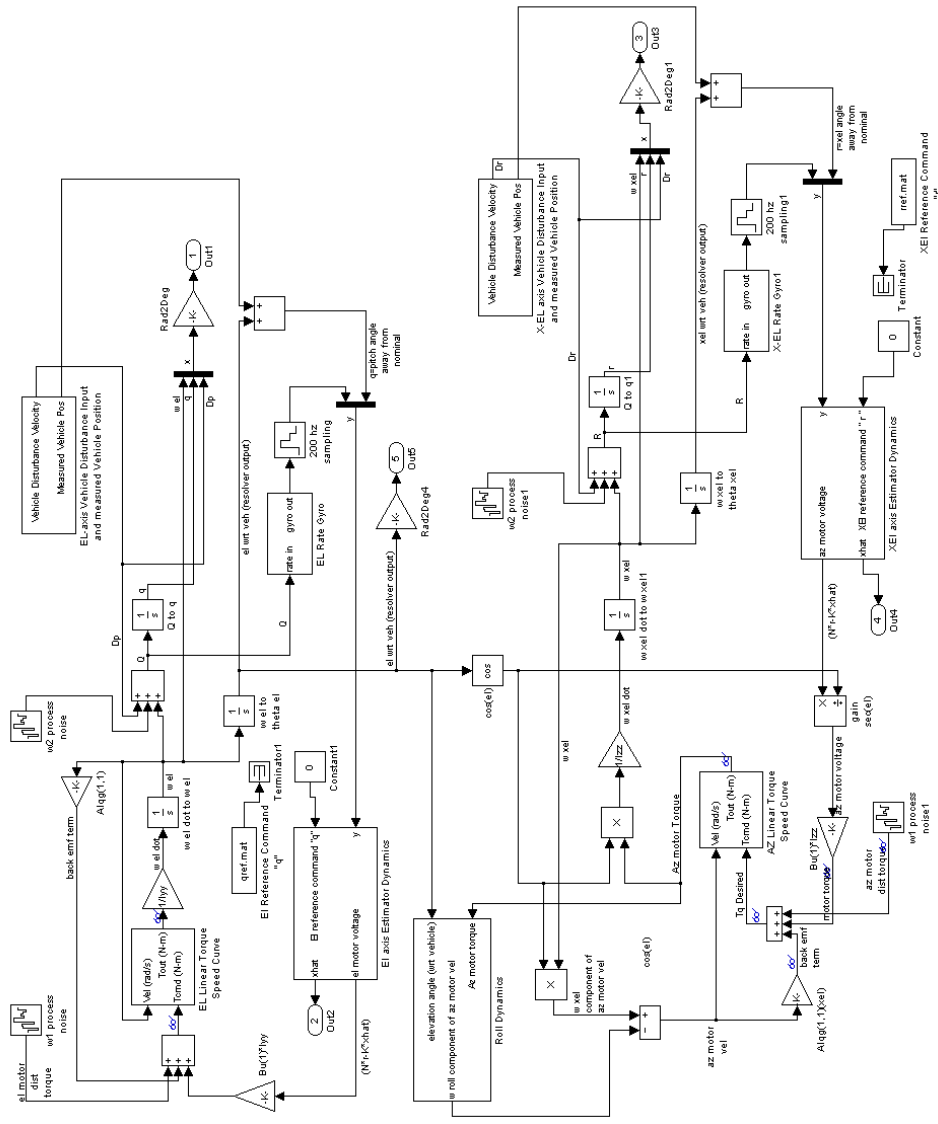


Figure B-1: Nominal APS Pedestal Feedback Controller Simulink Model (Root Level)

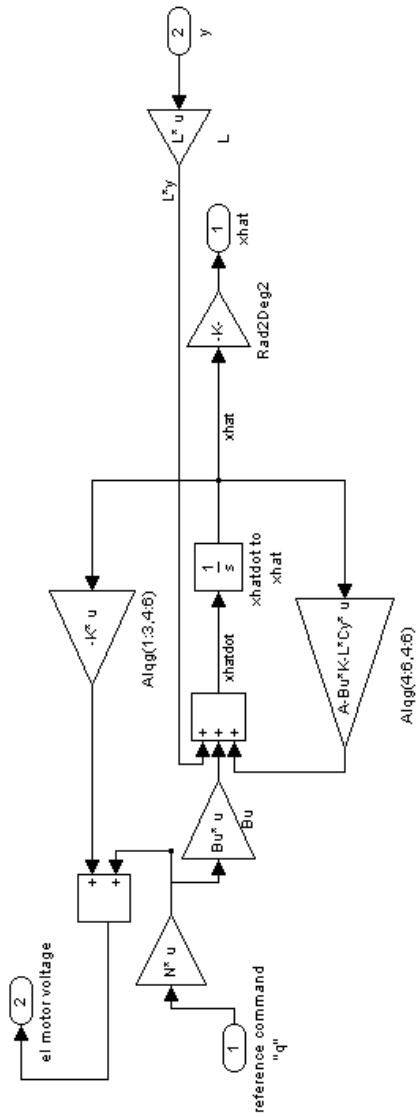


Figure B-2: Estimator Dynamics Subsystem

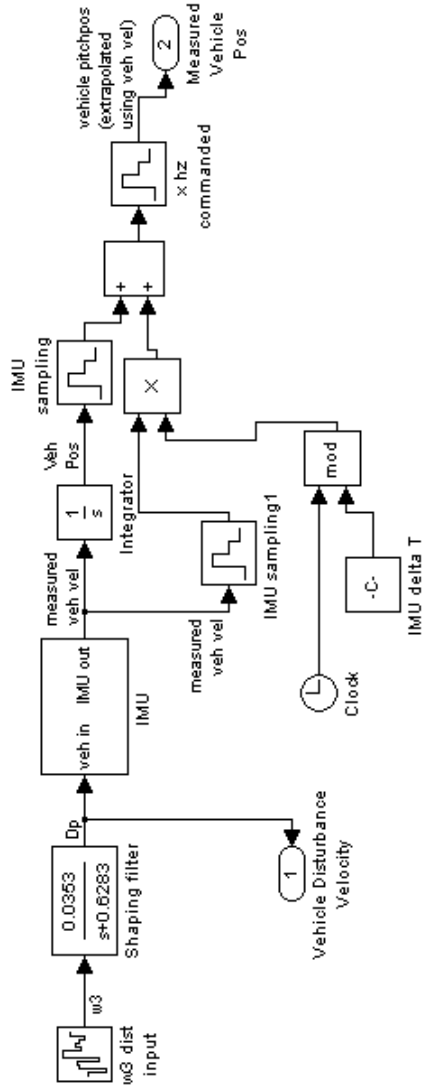


Figure B-3: Aircraft Rate Disturbance Input and Measured Aircraft Position Subsystem

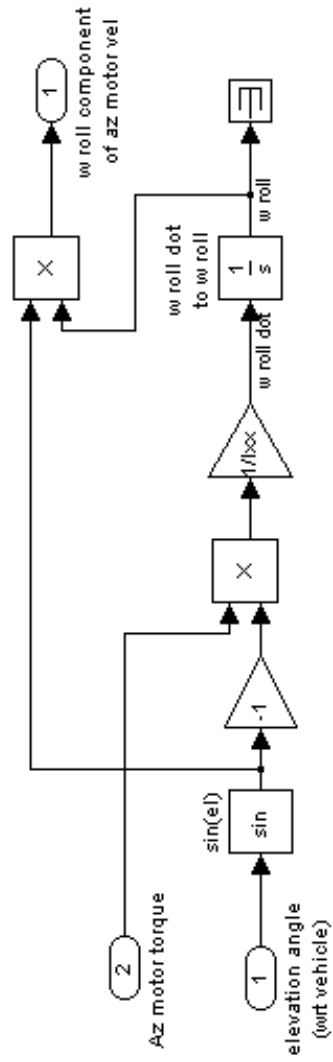


Figure B-4: Antenna Roll Dynamics Subsystem

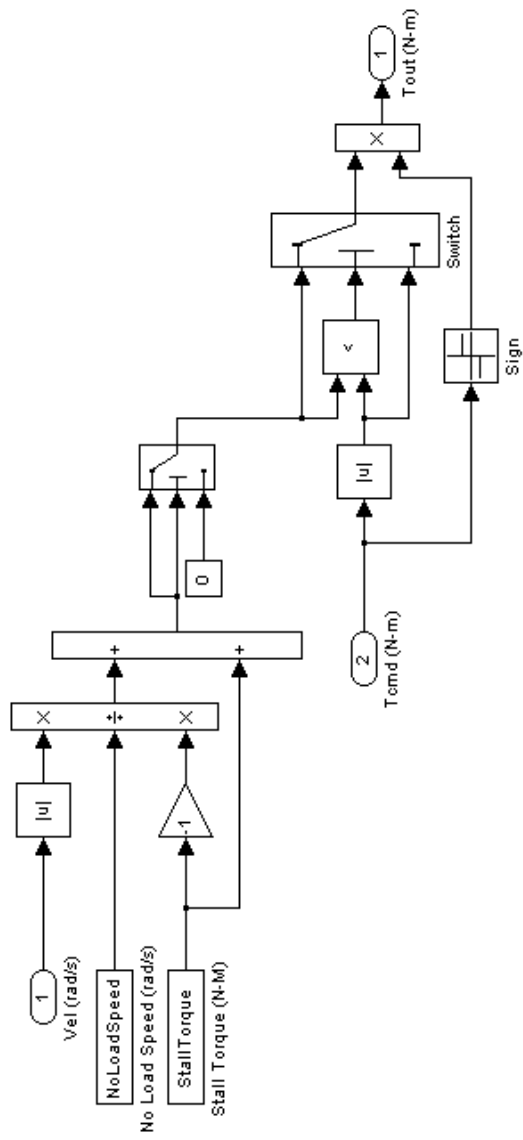


Figure B-5: Linear Torque-Speed Curve for CMC Series 2100 Servo-Motor Subsystem. Model Courtesy of M. Boulet, MIT LL, Group 76.

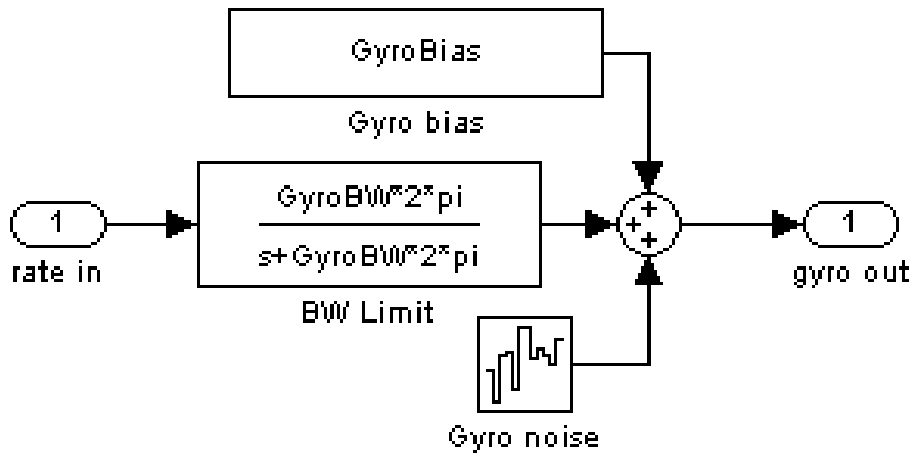


Figure B-6: KVH Gyro Sensor Subsystem. Model Courtesy of M. Boulet, MIT LL, Group 76.

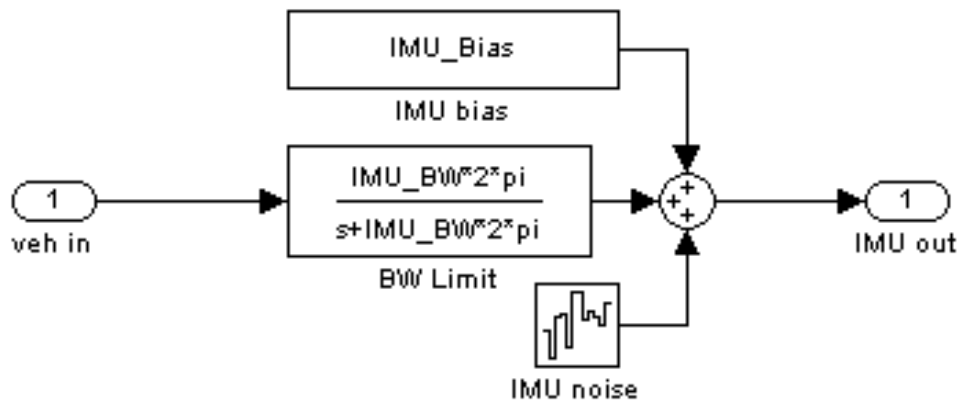


Figure B-7: IMU Sensor Subsystem. Model Courtesy of M. Boulet, MIT LL, Group 76.

Appendix C

Step-tracking Simulations

The following code was written using the MATLAB programming language, Version 7.4.0.287. It was run on a Dell laptop computer with a Pentium 4 processor, 2.13 GHz processor, and 2 GB of RAM using Microsoft Windows XP Professional, Version 2002 Service Pack 2.

C.1 spiralsearch.m

```
%Eric Marsh
%8 Jan 08
%MIT LL, GRP 61

%Spiral Search Method
%Description:
%This step-tracking simulation accomplishes spatial pull-in from the
%starting points defined in testvec.mat. The cost function is defined in
%30nov.mat.

%Spiral Search (SS) method

clear all
%close all load an antenna pattern *.mat file from genantennapattern.m
load 30nov.mat
load testvec.mat

soln=zeros(7,1000);

for mciter=1:1000
tic
xelpt=testvec(1,mciter); %initial guess
```

```

elpt=testvec(2,mciter); %initial guess
deltax=[0;0];
x=[xelpt;elpt];
xnorm=0;
deltaxnorm=0;
xelvar=.0004; %deg^2
elvar=.0004; %deg^2
ntsamps=10; %number of time samples to ensure normal distribution in xel
%and el
interp_method='linear';
radius=1.4*2;
totaliter=0;
funcevals=0;
F=zeros(7,ntsamps);
coords=zeros(2,7);
maxfuncevals=false;
satvel=0.0005; %deg/sec
satvelx=sqrt(satvel^2/2);
satvely=satvelx;
samplewaittime=0.25; %sec
sattravelx=0;
sattravely=0;
xnormfromsat=0;
satpos=0;
zerosatvel=false;

for i=1:9
    radius=radius*.5;
    iter=1;
    isctrmaxpwr=false;
    %F(1,2:7)=0;
    F(2:7,:)=0;

while isctrmaxpwr==false
    xnorm(iter+totaliter)=norm(x(:,iter+totaliter));
    satpos(iter+totaliter)=norm([sattravelx;sattravely]);
    xnormfromsat(iter+totaliter)=abs(xnorm(iter+totaliter)-
    satpos(iter+totaliter));

    if iter==1;
    coords(:,1)=[xelpt;elpt];
    end
    coords(:,2)=coords(:,1)+[0;radius];
    coords(:,3)=coords(:,1)+[radius;radius/2];
    coords(:,4)=coords(:,1)+[radius;-radius/2];
    coords(:,5)=coords(:,1)+[0;-radius];
    coords(:,6)=coords(:,1)+[-radius;-radius/2];
    coords(:,7)=coords(:,1)+[-radius;radius/2];

    if zerosatvel==false || iter==1 && i==1
    for i=1:ntsamps
        linnoisexel=randn(1,1)*sqrt(xelvar);
        linnoiseel=randn(1,1)*sqrt(elvar);
        F(1,i)=getsignalpower(coords(1,1)+linnoisexel+sattravelx,
        coords(2,1)+linnoiseel+sattravely,meshsize,xel,el,gridpow2,
        interp_method);
        sattravelx=sattravelx+satvelx*samplewaittime;
        sattravely=sattravely+satvely*samplewaittime;
    end
end
end

```

```

end
F(1,1)=mean(F(1,:));
F(1,1)=roundn(F(1,1),-1); %round to nearest tenths
funcevals=funcevals+1;

%F(1)=getsignalpower(coords(1,1),coords(2,1),meshsize,xel,el,gridpow2,i
%interp_method); funcevals=funcevals+1;
end
if zerosatvel==false || F(2,1)==0
for i=1:ntsamps
    linnoisexel=randn(1,1)*sqrt(xelvar);
    linnoiseel=randn(1,1)*sqrt(elvar);
    F(2,i)=getsignalpower(coords(1,2)+linnoisexel+sattravelx,
    coords(2,2)+linnoiseel+sattravely,meshsize,xel,el,gridpow2,
    interp_method);
    sattravelx=sattravelx+satvelx*samplewaittime;
    sattravely=sattravely+satvely*samplewaittime;
end
F(2,1)=mean(F(2,:));
F(2,1)=roundn(F(2,1),-1); %round to nearest tenths
funcevals=funcevals+1;

%F(2)=getsignalpower(coords(1,2),coords(2,2),meshsize,xel,el,gridpow2,i
%interp_method); funcevals=funcevals+1;
end
if zerosatvel==false || F(3,1)==0
for i=1:ntsamps
    linnoisexel=randn(1,1)*sqrt(xelvar);
    linnoiseel=randn(1,1)*sqrt(elvar);
    F(3,i)=getsignalpower(coords(1,3)+linnoisexel+sattravelx,
    coords(2,3)+linnoiseel+sattravely,meshsize,xel,el,gridpow2,
    interp_method);
    sattravelx=sattravelx+satvelx*samplewaittime;
    sattravely=sattravely+satvely*samplewaittime;
end
F(3,1)=mean(F(3,:));
F(3,1)=roundn(F(3,1),-1); %round to nearest tenths
funcevals=funcevals+1;

%F(3)=getsignalpower(coords(1,3),coords(2,3),meshsize,xel,el,gridpow2,i
%interp_method); funcevals=funcevals+1;
end
if zerosatvel==false || F(4,1)==0
for i=1:ntsamps
    linnoisexel=randn(1,1)*sqrt(xelvar);
    linnoiseel=randn(1,1)*sqrt(elvar);
    F(4,i)=getsignalpower(coords(1,4)+linnoisexel+sattravelx,
    coords(2,4)+linnoiseel+sattravely,meshsize,xel,el,gridpow2,
    interp_method);
    sattravelx=sattravelx+satvelx*samplewaittime;
    sattravely=sattravely+satvely*samplewaittime;
end
F(4,1)=mean(F(4,:));
F(4,1)=roundn(F(4,1),-1); %round to nearest tenths
funcevals=funcevals+1;
%F(4)=getsignalpower(coords(1,4),coords(2,4),meshsize,xel,el,gridpow2,i
%interp_method); funcevals=funcevals+1;

```

```

end
if zerosatvel==false || F(5,1)==0
for i=1:ntsamps
    linnoisexel=randn(1,1)*sqrt(xelvar);
    linnoiseel=randn(1,1)*sqrt(elvar);
    F(5,i)=getsignalpower(coords(1,5)+linnoisexel+sattravelx,
        coords(2,5)+linnoiseel+sattravely,meshsize,xel,el,gridpow2,
        interp_method);
    sattravelx=sattravelx+satvelx*samplewaittime;
    sattravely=sattravely+satvely*samplewaittime;
end
F(5,1)=mean(F(5,:));
F(5,1)=roundn(F(5,1),-1); %round to nearest tenths
funcevals=funcevals+1;
%F(5)=getsignalpower(coords(1,5),coords(2,5),meshsize,xel,el,gridpow2,i
%nterp_method); funcevals=funcevals+1;
end
if zerosatvel==false || F(6,1)==0
for i=1:ntsamps
    linnoisexel=randn(1,1)*sqrt(xelvar);
    linnoiseel=randn(1,1)*sqrt(elvar);
    F(6,i)=getsignalpower(coords(1,6)+linnoisexel+sattravelx,
        coords(2,6)+linnoiseel+sattravely,meshsize,xel,el,gridpow2,
        interp_method);
    sattravelx=sattravelx+satvelx*samplewaittime;
    sattravely=sattravely+satvely*samplewaittime;
end
F(6,1)=mean(F(6,:));
F(6,1)=roundn(F(6,1),-1); %round to nearest tenths
funcevals=funcevals+1;
%F(6)=getsignalpower(coords(1,6),coords(2,6),meshsize,xel,el,gridpow2,i
%nterp_method); funcevals=funcevals+1;
end
if zerosatvel==false || F(7,1)==0
for i=1:ntsamps
    linnoisexel=randn(1,1)*sqrt(xelvar);
    linnoiseel=randn(1,1)*sqrt(elvar);
    F(7,i)=getsignalpower(coords(1,7)+linnoisexel+sattravelx,
        coords(2,7)+linnoiseel+sattravely,meshsize,xel,el,gridpow2,
        interp_method);
    sattravelx=sattravelx+satvelx*samplewaittime;
    sattravely=sattravely+satvely*samplewaittime;
end
F(7,1)=mean(F(7,:));
F(7,1)=roundn(F(7,1),-1); %round to nearest tenths
funcevals=funcevals+1;
%F(7)=getsignalpower(coords(1,7),coords(2,7),meshsize,xel,el,gridpow2,i
%nterp_method); funcevals=funcevals+1;
end

[C,I]=min(F(:,1));

Fcent=F(I,1);

if abs(satvel) < 10000*eps %saying if satvel is zero, can save some
    %function evaluations
    zerosatvel=true;

```

```

if I==2
    F(4,1)=F(3,1);
    F(5,1)=F(1,1);
    F(6,1)=F(7,1);
    F(2,1)=0;
    F(3,1)=0;
    F(7,1)=0;
elseif I==3
    F(5,1)=F(4,1);
    F(6,1)=F(1,1);
    F(7,1)=F(2,1);
    F(2,1)=0;
    F(3,1)=0;
    F(4,1)=0;
elseif I==4
    F(6,1)=F(5,1);
    F(7,1)=F(1,1);
    F(2,1)=F(3,1);
    F(3,1)=0;
    F(4,1)=0;
    F(5,1)=0;
elseif I==5
    F(7,1)=F(6,1);
    F(2,1)=F(1,1);
    F(3,1)=F(4,1);
    F(4,1)=0;
    F(5,1)=0;
    F(6,1)=0;
elseif I==6
    F(2,1)=F(7,1);
    F(3,1)=F(1,1);
    F(4,1)=F(5,1);
    F(5,1)=0;
    F(6,1)=0;
    F(7,1)=0;
elseif I==7
    F(3,1)=F(2,1);
    F(4,1)=F(1,1);
    F(5,1)=F(6,1);
    F(2,1)=0;
    F(6,1)=0;
    F(7,1)=0;
else
    isctrmaxpwr=true;
end
elseif I ==1
    isctrmaxpwr=true;
end

coords(:,1)=coords(:,I);
F(1,1)=Fcent;

x(:,iter+1+totaliter)=coords(:,1);
deltax(:,iter+totaliter)=x(:,iter+1+totaliter)-x(:,iter+totaliter);
deltaxnorm(:,iter+totaliter)=norm(deltax(:,iter+totaliter));
iter=iter+1;
if funcevals > 500
    maxfuncevals=true;
    warning('max number of function evaluations reached')

```

```

        break
    end

end

    xelpt=coords(1,1);
    elpt=coords(2,1);
    totaliter=totaliter+iter-1;
    if maxfuncevals==true %break for loop if maxfuncevals is true
        break
    end
end

%calculate approximate time
if satvel > eps*10000 %if satvel isn't zero
    time=satpos(end)/satvel;
else
    time=0;
end
soln(1:2,mciter)=[x(1,end);x(2,end)];
soln(3,mciter)=totaliter;
simtime=toc;
soln(4,mciter)=simtime;
soln(5,mciter)=funcevals;
soln(6,mciter)=xnorm(end);
soln(7,mciter)=satpos(end);
soln(8,mciter)=xnormfromsat(end);
soln(9,mciter)=time;

end

```

C.2 modifiedNewton.m

```

%Eric Marsh 18 Dec 07

%Modified Newton's Method
%Description:
%This step-tracking simulation accomplishes spatial pull-in from the
%starting points defined in testvec.mat. The cost function is defined in
%30nov.mat.

clear all
%close all load an antenna pattern *.mat file from genantennapattern.m
load 30nov.mat
load testvec.mat

soln=zeros(7,1000);
mainlobejump=zeros(1,1000);
bracketminfalse=zeros(1,1000);
gradfalloffcount=zeros(1,1000);

for mciter=1:1000
tic
xelpt=testvec(1,mciter); %initial guess
elpt=testvec(2,mciter); %initial guess

```

```

deljstep=.16; %(deg) this is ~3* the 3sigma on the 1-d pointing error
%distributions (also good for lin interp of ant pattern and machine errors)
deltax=[0;0];
x=[xelpt;elpt];
xnorm=0;
deltaxnorm=0;
iter=1;
epsilon=0.63; %looser?
gradient=[10^2;10^2];
hessian=zeros(2,2);
interp_method='linear';
R=zeros(2,2);
funcevals=0;
xelvar=.0004; %deg^2
elvar=.0004; %deg^2
ntsamps=10; %number of time samples to ensure normal distribution in xel
%and el
Fminjump=zeros(1,ntsamps);
gradswitch=epsilon*10;
linsearchparam=0.5;
linstepcount=0;
mincheck=0;
mincheckthreshold=4;
hessianhat=zeros(2,2);
directedgrad=0;
mincheckvec=0;
gradfalloff=0;
satvel=0.0005; %deg/sec
satvelx=sqrt(satvel^2/2);
satvely=satvelx;
samplewaittime=0.25; %sec
sattravelx=0;
sattravely=0;
xnormfromsat=0;
satpos=0;

% set terminate = false
terminate=false;
% while terminate = false
while terminate==false
% set compute alpha*pk = true
computedeltax=true;
%perform function/gradient evaluations at xk: initializations
xnorm(iter)=norm(x(:,iter));
satpos(iter)=norm([sattravelx;sattravely]);
xnormfromsat(iter)=abs(xnorm(iter)-satpos(iter));
F=zeros(13,ntsamps);
g=zeros(2,5);
G=zeros(2,2);

%%%%%%%%%%%%%%%%%%%%%%%%%%%%%%%%%%%%%%%%%%%%%%%%%%%%%%%%%%%%%%%%%%%%%%%%%perform function evals:%%%%%%%%%%%%%%%%%%%%%%%%%%%%%%%%%%%%%%%%%%%%%%%%%%%%%%%%%%%%%%%%%%%%%%%%%
noisixel=randn(14,ntsamps)*sqrt(xelvar); %14th pt is for jump condition
noiseel=randn(14,ntsamps)*sqrt(elvar);

%F9,F10,F11 not needed

if Fminjump(1)==0

```



```

        computeF1=true;
else
    computeF1=false;
end
%%%F1%%%
if computeF1==true
for i=1:ntsamps
    linnoisexel=randn(1,1)*sqrt(xelvar);
    linnoiseel=randn(1,1)*sqrt(elvar);
    F(1,i)=getsignalpower(xelpt+linnoisexel+sattravelx,elpt+linnoiseel+
        sattravely,meshsize,xel,el,gridpow2,interp_method);
    sattravelx=sattravelx+satvelx*samplewaittime;
    sattravely=sattravely+satvely*samplewaittime;
end
F(1,1)=mean(F(1,:));
F(1,1)=roundn(F(1,1),-1); %round to nearest tenths
funcevals=funcevals+1;
else
    F(1,1)=Fminjump(1);
end

%%%F2%%%
for i=1:ntsamps
    linnoisexel=randn(1,1)*sqrt(xelvar);
    linnoiseel=randn(1,1)*sqrt(elvar);
    F(2,i)=getsignalpower(xelpt+linnoisexel+deljstep+sattravelx,elpt+
        linnoiseel+sattravely,meshsize,xel,el,gridpow2,interp_method);
    sattravelx=sattravelx+satvelx*samplewaittime;
    sattravely=sattravely+satvely*samplewaittime;
end
F(2,1)=mean(F(2,:));
F(2,1)=roundn(F(2,1),-1); %round to nearest tenths
funcevals=funcevals+1;

%%%F5%%%
for i=1:ntsamps
    linnoisexel=randn(1,1)*sqrt(xelvar);
    linnoiseel=randn(1,1)*sqrt(elvar);
    F(5,i)=getsignalpower(xelpt+linnoisexel+sattravelx,elpt+linnoiseel+
        deljstep+sattravely,meshsize,xel,el,gridpow2,interp_method);
    sattravelx=sattravelx+satvelx*samplewaittime;
    sattravely=sattravely+satvely*samplewaittime;
end
F(5,1)=mean(F(5,:));
F(5,1)=roundn(F(5,1),-1); %round to nearest tenths
funcevals=funcevals+1;

%%%F6%%%
for i=1:ntsamps
    linnoisexel=randn(1,1)*sqrt(xelvar);
    linnoiseel=randn(1,1)*sqrt(elvar);
    F(6,i)=getsignalpower(xelpt+linnoisexel+deljstep+sattravelx,elpt+
        linnoiseel+deljstep+sattravely,meshsize,xel,el,gridpow2,interp_method);
    sattravelx=sattravelx+satvelx*samplewaittime;
    sattravely=sattravely+satvely*samplewaittime;
end
F(6,1)=mean(F(6,:));
F(6,1)=roundn(F(6,1),-1); %round to nearest tenths

```

```

funcevals=funcevals+1;

%%%F7%%%
for i=1:ntsamps
    linnoisexel=randn(1,1)*sqrt(xelvar);
    linnoiseel=randn(1,1)*sqrt(elvar);
    F(7,i)=getsignalpower(xelpt+linnoisexel+2*deljstep+sattravelx,elpt+
        linnoiseel+sattravelx,meshsize,xel,el,gridpow2,interp_method);
    sattravelx=sattravelx+satvelx*samplewaittime;
    sattravely=sattravely+satvely*samplewaittime;
end
F(7,1)=mean(F(7,:));
F(7,1)=roundn(F(7,1),-1); %round to nearest tenths
funcevals=funcevals+1;

%%%F13%%%
for i=1:ntsamps
    linnoisexel=randn(1,1)*sqrt(xelvar);
    linnoiseel=randn(1,1)*sqrt(elvar);
    F(13,i)=getsignalpower(xelpt+linnoisexel+sattravelx,elpt+linnoiseel+
        2*deljstep+sattravelx,meshsize,xel,el,gridpow2,interp_method);
    sattravelx=sattravelx+satvelx*samplewaittime;
    sattravely=sattravely+satvely*samplewaittime;
end
F(13,1)=mean(F(13,:));
F(13,1)=roundn(F(13,1),-1); %round to nearest tenths
funcevals=funcevals+1;

if iter==1 || norm(gradient(:,iter-1)) < gradswitch
%%%F3%%%
for i=1:ntsamps
    linnoisexel=randn(1,1)*sqrt(xelvar);
    linnoiseel=randn(1,1)*sqrt(elvar);
    F(3,i)=getsignalpower(xelpt+linnoisexel+sattravelx,elpt+linnoiseel-
        deljstep+sattravelx,meshsize,xel,el,gridpow2,interp_method);
    sattravelx=sattravelx+satvelx*samplewaittime;
    sattravely=sattravely+satvely*samplewaittime;
end
F(3,1)=mean(F(3,:));
F(3,1)=roundn(F(3,1),-1); %round to nearest tenths
funcevals=funcevals+1;

%%%F4%%%
for i=1:ntsamps
    linnoisexel=randn(1,1)*sqrt(xelvar);
    linnoiseel=randn(1,1)*sqrt(elvar);
    F(4,i)=getsignalpower(xelpt+linnoisexel-deljstep+sattravelx,elpt+
        linnoiseel+sattravelx,meshsize,xel,el,gridpow2,interp_method);
    sattravelx=sattravelx+satvelx*samplewaittime;
    sattravely=sattravely+satvely*samplewaittime;
end
F(4,1)=mean(F(4,:));
F(4,1)=roundn(F(4,1),-1); %round to nearest tenths
funcevals=funcevals+1;

%%%F8%%%
for i=1:ntsamps

```

```

        linnoisexel=randn(1,1)*sqrt(xelvar);
        linnoiseel=randn(1,1)*sqrt(elvar);
        F(8,i)=getsignalpower(xelpt+linnoisexel+deljstep+sattravelx,elpt+
        linnoiseel-deljstep+sattravelx, meshsize, xel, el, gridpow2, interp_method);
        sattravelx=sattravelx+satvelx*samplewaittime;
        sattravely=sattravely+satvely*samplewaittime;
    end
    F(8,1)=mean(F(8,:));
    F(8,1)=roundn(F(8,1),-1); %round to nearest tenths
    funcevals=funcevals+1;

    %%F12%%
    for i=1:ntsamps
        linnoisexel=randn(1,1)*sqrt(xelvar);
        linnoiseel=randn(1,1)*sqrt(elvar);
        F(12,i)=getsignalpower(xelpt+linnoisexel-deljstep+sattravelx,elpt+
        linnoiseel+deljstep+sattravelx, meshsize, xel, el, gridpow2, interp_method);
        sattravelx=sattravelx+satvelx*samplewaittime;
        sattravely=sattravely+satvely*samplewaittime;
    end
    F(12,1)=mean(F(12,:));
    F(12,1)=roundn(F(12,1),-1); %round to nearest tenths
    funcevals=funcevals+1;
    end
    Fminjump=zeros(1,ntsamps);

    %%%old way%%
    % if Fminjump(1)==0
    %     computeF1=true;
    % else
    %     computeF1=false;
    % end for i=1:ntsamps if computeF1 == true
    % F(1,i)=getsignalpower(xelpt+noisexel(1,i),elpt+noiseel(1,i),meshsize,xel,
    % el,gridpow2,interp_method); else
    %     F(1,i)=Fminjump(1);
    % end
    % F(2,i)=getsignalpower(xelpt+noisexel(2,i)+deljstep,elpt+noiseel(2,i),mesh
    % size,xel,el,gridpow2,interp_method);
    % F(5,i)=getsignalpower(xelpt+noisexel(5,i),elpt+noiseel(5,i)+deljstep,mesh
    % size,xel,el,gridpow2,interp_method);
    % F(6,i)=getsignalpower(xelpt+noisexel(6,i)+deljstep,elpt+noiseel(6,i)+delj
    % step,meshsize,xel,el,gridpow2,interp_method);
    % F(7,i)=getsignalpower(xelpt+noisexel(7,i)+2*deljstep,elpt+noiseel(7,i),me
    % shsize,xel,el,gridpow2,interp_method);
    % F(13,i)=getsignalpower(xelpt+noisexel(13,i),elpt+noiseel(13,i)+2*deljstep
    % ,meshsize,xel,el,gridpow2,interp_method); if iter==1 ||
    % norm(gradient(:,iter-1)) < gradswitch
    % F(3,i)=getsignalpower(xelpt+noisexel(3,i),elpt+noiseel(3,i)-deljstep,mesh
    % size,xel,el,gridpow2,interp_method);
    % F(4,i)=getsignalpower(xelpt+noisexel(4,i)-deljstep,elpt+noiseel(4,i),mesh
    % size,xel,el,gridpow2,interp_method);
    % F(8,i)=getsignalpower(xelpt+noisexel(8,i)+deljstep,elpt+noiseel(8,i)-delj
    % step,meshsize,xel,el,gridpow2,interp_method);
    % F(12,i)=getsignalpower(xelpt+noisexel(12,i)-deljstep,elpt+noiseel(12,i)+d
    % eljstep,meshsize,xel,el,gridpow2,interp_method); end end for i=1:13
    % %average the signal to noise measurements and store in first column of F

```

```

% F(i,1)=mean(F(i,:)); end Fminjump=zeros(1,ntsamps); F=roundn(F,-1);
% %round to nearest tenths
%calculate number of points looked at (function evaluations):
% if computeF1==true
%     if iter==1 || norm(gradient(:,iter-1)) < gradswitch
%         funcevals=funcevals+10;
%     else
%         funcevals=funcevals+6;
%     end
% else
%     if iter==1 || norm(gradient(:,iter-1)) < gradswitch
%         funcevals=funcevals+9;
%     else
%         funcevals=funcevals+5;
%     end
% end
%%%%%%%%%%%%%%%%%%%%%%%%%%%%%%%%%%%%%%%%%%%%%%%%%%%%%%%%%%%%%%%%%%%%%%%%
%Form gradient vectors g3,g4 not needed
if iter==1 || norm(gradient(:,iter-1)) < gradswitch
    g(:,1)=[(F(2,1)-F(4,1))/(2*deljstep);(F(5,1)-F(3,1))/(2*deljstep)];
    gradient(:,iter)=g(:,1);
    g(:,2)=[(F(7,1)-F(1,1))/(2*deljstep);(F(6,1)-F(8,1))/(2*deljstep)];
    %g(:,3)=[(F(8,1)-F(10,1))/(2*deljstep);(F(1,1)-F(9,1))/(2*deljstep)];
    %g(:,4)=[(F(1,1)-F(11,1))/(2*deljstep);(F(12,1)-F(10,1))/(2*deljstep)];
    g(:,5)=[(F(6,1)-F(12,1))/(2*deljstep);(F(13,1)-F(1,1))/(2*deljstep)];
else
    g(:,1)=[(F(2,1)-F(1,1))/(deljstep);(F(5,1)-F(1,1))/(deljstep)];
    gradient(:,iter)=g(:,1);
    fwddifcount(iter)=1;
    g(:,2)=[(F(7,1)-F(2,1))/(deljstep);(F(6,1)-F(2,1))/(deljstep)];
    g(:,5)=[(F(6,1)-F(5,1))/(deljstep);(F(13,1)-F(5,1))/(deljstep)];
end

%form hessian (G) matrix
G(:,1)=(g(:,2)-g(:,1))/(deljstep);
G(:,2)=(g(:,5)-g(:,1))/(deljstep);
G=.5*(G+G');
hessian(:, :, iter)=G;
%modified cholesky factorization of Hessian
L=eye(2);
D=zeros(2,2);
R=zeros(2,2);
delta=10; %50; %10^-1 good? %effectively adds more damping to lin search
for j=1:2
    if j==1
        D(j,j)=G(j,j);
        if D(j,j)<delta
            R(j,j)=(delta-D(j,j));
            D(j,j)=R(j,j)+D(j,j);
        end
        L(2,j)=G(2,j)/D(j,j);
    elseif j==2
        D(j,j)=G(j,j)-D(1,1)*(L(j,1))^2;
        if D(j,j)<delta
            R(j,j)=(delta-D(j,j));
        end
    end
end

```

```

        D(j,j)=R(j,j)+D(j,j);
    end
end
end
%%%%%%
hessianhat(:, :, iter)=L*D*L';
t(:, iter)=L\ -gradient(:, iter);
rhs=inv(D)*t(:, iter);

%%%%%%%%%%%%%%%%%%%%%%%%%%%%%%%%%%%%%%%%%%%%%%%%%%%%%%%%%%%%%%%%%%%%%%%%%check for local or global min:%%%%%%%%%%%%%%%%%%%%%%%%%%%%%%%%%%%%%%%%%%%%%%%%%%%%%%%%%%%%%%%%%%%%%%%%%
% if criteria for minimum = true (small gradient)
if norm(gradient(:, iter)) < epsilon
    %check for local min
    if (norm(gradient(:, iter))<epsilon) && (R(1,1) > 0 || R(2,2) > 0) %if
        %you're at a weak min (grad small, hessian modified)
        V=zeros(2,2);
        E=zeros(2,2);
        deltaxminjump=zeros(2,1);
        jumpxel=0;
        jumpel=0;
        [V,E]=eig(hessian(:, :, iter));
        if V(:,1)'*hessian(:, :, iter)*V(:,1) > V(:,2)'*hessian(:, :, iter)*
            V(:,2)
            deltaxminjump=V(:,1);
        else
            deltaxminjump=V(:,2);
        end
        deltaxminjump=deltaxminjump*1.85; %1.85 comes from averaging
        distance between first 4 peaks on ant. pattern
        jumpxel=x(1, iter)+deltaxminjump(1);
        jumpel=x(2, iter)+deltaxminjump(2);
        for i=1:ntsamps
            linnoisexel=randn(1,1)*sqrt(xelvar);
            linnoiseel=randn(1,1)*sqrt(elvar);
            Fminjump(i)=getsignalpower(jumpxel+linnoisexel+sattravelx,
                jumpel+linnoiseel+sattravely, meshsize, xel, el, gridpow2,
                interp_method);
            sattravelx=sattravelx+satvelx*samplewaittime;
            sattravely=sattravely+satvely*samplewaittime;
        end
        Fminjump(1)=mean(Fminjump(1, :));
        Fminjump=roundn(Fminjump(1), -1); %round to nearest tenths
        funcevals=funcevals+1;
        if Fminjump(1) > F(1,1) %must check to see you are going in right
            %direction on eigenvector
            deltax(:, iter)=deltaxminjump*-1; %head the opposite way
            Fminjump(1)=0;
        else
            deltax(:, iter)=deltaxminjump; %you jumped the correct way
        end
        mincheck=0;
    else
        deltax(:, iter)=[0;0];
        mincheck=mincheck+1;
    end
end
computedeltax=false;

```

```

        if mincheck > mincheckthreshold
            %computedeltax=true; %complete one more jump (already evaluated the
            %function so might as well)
            terminate=true;
        end
    elseif mincheck > 0 && norm(gradient(:,iter)) > epsilon
        computedeltax=true;
        mincheck=0;
        gradfalloff(iter)=1;
    end
    mincheckvec(iter)=mincheck;

if computedeltax==true %%%%%%%%%%if compute alpha*pk = true%%%%%%%%%
%%%%%%%%%compute pk and initial alpha:%%%%%%%%%
deltax(:,iter)=L'\rhs;
alpha=1;
%limit alpha*pk to a predetermined region of confidence:
if norm(deltax(:,iter))>1.0 %if deltax is outside a "region of trust"
    %chosen so if you're at a max, won't go over another max (max initial
    %step routine will take)
    deltax(:,iter)=(deltax(:,iter)/norm(deltax(:,iter)))*.75;
end

%evaluate function at initial alpha=1 value:
for i=1:ntsamps
    linnoisexel=randn(1,1)*sqrt(xelvar);
    linnoiseel=randn(1,1)*sqrt(elvar);
    Falpha(i)=getsignalpower(x(1,iter)+deltax(1,iter)+linnoisexel+
    sattravelx,x(2,iter)+deltax(2,iter)+linnoiseel+sattravely,meshsize,xel,
    el,gridpow2,interp_method);
    sattravelx=sattravelx+satvelx*samplewaittime;
    sattravely=sattravely+satvely*samplewaittime;
end
Falpha(1)=mean(Falpha(1,:));
Falpha=roundn(Falpha(1),-1); %round to nearest tenths
funcevals=funcevals+1;

%evaluate point along search direction to approximate gradient at alpha=1
dx1=deltax(1,iter)/norm(deltax(:,iter));
dx2=deltax(2,iter)/norm(deltax(:,iter));
nux=dx1*deljstep;
nuy=dx2*deljstep;
if norm([alpha*deltax(1,iter);alpha*deltax(2,iter)])>=deljstep
    if alpha > 0
        nu=norm([alpha*deltax(1,iter)-nux;alpha*deltax(2,iter)-nuy])/
        norm(deltax(:,iter)); %ensure that nu value will be deljstep away
        %from alpha in 1-d
    else
        nu=-1*norm([alpha*deltax(1,iter)+nux;alpha*deltax(2,iter)+nuy])/
        norm(deltax(:,iter));
    end
else
    if alpha > 0
        nu=-1*norm([alpha*deltax(1,iter)-nux;alpha*deltax(2,iter)-nuy])/

```

```

        norm(deltax(:,iter)); %ensure that nu value will be deljstep away
        %from alpha in 1-d
    else
        nu=norm([alpha*deltax(1,iter)+nux;alpha*deltax(2,iter)+nuy])/
        norm(deltax(:,iter));
    end
end
end
for i=1:ntsamps
    linnoisexel=randn(1,1)*sqrt(xelvar);
    linnoiseel=randn(1,1)*sqrt(elvar);
    Fnu(i)=getsignalpower(x(1,iter)+nu*deltax(1,iter)+linnoisexel+
    sattravelx,x(2,iter)+nu*deltax(2,iter)+linnoiseel+sattravely,meshsize,
    xel,el,gridpow2,interp_method);
    sattravelx=sattravelx+satvelx*samplewaittime;
    sattravely=sattravely+satvely*samplewaittime;
end
Fnu(1)=mean(Fnu(1,:));
Fnu=roundn(Fnu(1),-1); %round to nearest tenths
funcevals=funcevals+1;

%%%%%%%%%%%%%%%%%%%%%%%%%%%%%%%%%%%%%%%%%%%%%%%%%%%%%%%%%%%%%%%%%%%%%%%%%perform linear search along pk to determine
%%%%%%%%%%%%%%%%%%%%%%%%%%%%%%%%%%%%%%%%%%%%%%%%%%%%%%%%%%%%%%%%%%%%%%%%%satisfactory alpha %%%%%%%%%%%%%%%%%%%%%%%%%%%%%%%%%%%%%%%%%%%%%%%%%%%%%%%%%%%%%%%%%%%%%%%%%%
linsearchconverge=false;
directedgrad(iter)=deltax(:,iter)'\*gradient(:,iter);
%if alpha=1 is not satisfactory, perform lin search:
if abs((Falpha-Fnu))/deljstep > abs(-1*linsearchparam*directedgrad(iter))
    %Criterion for lin search-(finite difference replaces gradient)- GMW
    %p. 102

    %Step 1- make sure you have an interval bracketing a minimum:
    bracketmin=true;
    if F(1,1)<Falpha %look opposite direction to find Fa and a values for
        %interval containing minimum
        alpha=-1;
        bracket_step=1;
        Fb=Falpha;
        b=1;
        Fc=F(1,1);
        c=0;
        Fa=-10^6;
        a=alpha;
        while Fa(1) <= Fc
            if bracket_step > 1
                Fb=Fc;
                b=c;
                Fc=Fa(1);
                c=a;
            end
            for i=1:ntsamps
                linnoisexel=randn(1,1)*sqrt(xelvar);
                linnoiseel=randn(1,1)*sqrt(elvar);
                Fa(i)=getsignalpower(x(1,iter)+alpha*deltax(1,iter)+
                linnoisexel+sattravelx,x(2,iter)+alpha*deltax(2,iter)+
                linnoiseel+sattravely,meshsize,xel,el,gridpow2,
                interp_method);
                sattravelx=sattravelx+satvelx*samplewaittime;
                sattravely=sattravely+satvely*samplewaittime;
            end
        end
    end
end

```

```

        end
        Fa(1)=mean(Fa(1,:));
        Fa=roundn(Fa(1),-1); %round to nearest tenths
        funcevals=funcevals+1;
        a=alpha;
        alpha=alpha*2;
        bracket_step=bracket_step+1;
    if bracket_step > 4
        bracketmin=false;
        bracketminfalse(mciter)=bracketminfalse(mciter)+1;
        warning('could not bracket minimum for lin search in less
        than 4 steps')
        break
    end
end
else %continue searching along search direction until a min is
    %bracketed- (find b)
    alpha=2;
    bracket_step=1;
    Fc=Fa*alpha;
    c=1;
    Fa=F(1,1);
    a=0;
    Fb=-10^6;
    b=alpha;
    while Fb(1) <= Fc
        if bracket_step > 1
            Fa=Fc;
            a=c;
            Fc=Fb(1);
            c=b;
        end

        for i=1:ntsamps
            linnoisexel=randn(1,1)*sqrt(xelvar);
            linnoiseel=randn(1,1)*sqrt(elvar);
            Fb(i)=getsignalpower(x(1,iter)+alpha*deltax(1,iter)+
            linnoisexel+sattravelx,x(2,iter)+alpha*deltax(2,iter)+
            linnoiseel+sattravely,meshsize,xel,el,gridpow2,
            interp_method);
            sattravelx=sattravelx+satvelx*samplewaittime;
            sattravely=sattravely+satvely*samplewaittime;
        end
        Fb(1)=mean(Fb(1,:));
        Fb=roundn(Fb(1),-1); %round to nearest tenths
        funcevals=funcevals+1;
        b=alpha;
        alpha=alpha*2-1;
        bracket_step=bracket_step+1;
    if bracket_step > 4
        bracketmin=false;
        bracketminfalse(mciter)=bracketminfalse(mciter)+1;
        warning('could not bracket minimum for lin search in less
        than 4 steps')
        break
    end
end
end
end

```



```

%Step 2- perform quadratic interpolation:
if bracketmin==true %lin search...
    linsearchconverge=true;
    linstep=1;
    while linstep==1 || abs((Falpha-Fnu))/deljstep > abs(-1*
        linsearchparam*directedgrad(iter)) %criterion for linear
        %search (finite difference replaces gradient)- GMW p. 102
        if linstep > 1
            if alpha < c && Falpha <= Fc
                b=c;
                c=alpha;
                Fb=Fc;
                Fc=Falpha;
            elseif alpha > c && Falpha > Fc
                b=alpha;
                Fb=Falpha;
            elseif alpha < c && Falpha > Fc
                a=alpha;
                Fa=Falpha;
            else
                a=c;
                c=alpha;
                Fa=Fc;
                Fc=Falpha;
            end
        end
        if Fa==Fb && Fb==Fc %can't optimize any further with quad interp
            break
        end
        if c-10000*eps<a&&a<c+10000*eps %saying if a==c
            %can't optimize any further with quad interp
            break
        end
        if -10000*eps<((b-c)*Fa+(c-a)*Fb+(a-b)*Fc)&&((b-c)*Fa+(c-a)*
            Fb+(a-b)*Fc)<10000*eps %saying if den of alpha calc == 0
            %can't optimize any further with quad interp
            break
        end
        alpha=.5*((b^2-c^2)*Fa+(c^2-a^2)*Fb+(a^2-b^2)*Fc)/((b-c)*
            Fa+(c-a)*Fb+(a-b)*Fc);
        for i=1:ntsamps
            linnoisexel=randn(1,1)*sqrt(xelvar);
            linnoiseel=randn(1,1)*sqrt(elvar);
            Falpha(i)=getsignalpower(x(1,iter)+alpha*deltax(1,iter)+
                linnoisexel+sattravelx,x(2,iter)+alpha*deltax(2,iter)+
                linnoiseel+sattravely,meshsize,xel,el,gridpow2,
                interp_method);
            sattravelx=sattravelx+satvelx*samplewaittime;
            sattravely=sattravely+satvely*samplewaittime;
        end
        Falpha(1)=mean(Falpha(1,:));
        Falpha=roundn(Falpha(1),-1); %round to nearest tenths
        funcevals=funcevals+1;
        if norm([alpha*deltax(1,iter);alpha*deltax(2,iter)])>=deljstep
            if alpha > 0
                nu=norm([alpha*deltax(1,iter)-nux;alpha*deltax(2,iter)
                    -nuy])/norm(deltax(:,iter)); %ensure that nu value
            end
        end
    end
end

```

```

        %will be deljstep away from alpha in 1-d
    else
        nu=-1*norm([alpha*deltax(1,iter)+nux;alpha*
                    deltax(2,iter)+nuy])/norm(deltax(:,iter));
    end
else
    if alpha > 0
        nu=-1*norm([alpha*deltax(1,iter)-nux;alpha*
                    deltax(2,iter)-nuy])/norm(deltax(:,iter)); %ensure
        %that nu value will be deljstep away from alpha in 1-d
    else
        nu=norm([alpha*deltax(1,iter)+nux;alpha*deltax(2,iter)+
                 nuy])/norm(deltax(:,iter));
    end
end
for i=1:ntsamps
    linnoisexel=randn(1,1)*sqrt(xelvar);
    linnoiseel=randn(1,1)*sqrt(elvar);
    Fnu(i)=getsignalpower(x(1,iter)+nu*deltax(1,iter)+
        linnoisexel+sattravelx,x(2,iter)+nu*deltax(2,iter)+
        linnoiseel+sattravely,meshsize,xel,el,gridpow2,
        interp_method);
    sattravelx=sattravelx+satvelx*samplewaittime;
    sattravely=sattravely+satvely*samplewaittime;
end
Fnu(1)=mean(Fnu(1,:));
Fnu=roundn(Fnu(1),-1); %round to nearest tenths
funcevals=funcevals+1;
linstep=linstep+1;
if linstep > 20
    linsearchconverge=false;
    break
end
end
linstepcount(iter)=linstep;
end
end
if linsearchconverge==true %if lin search produced a good alpha
    %within max number of linsteps
    deltax(:,iter)=deltax(:,iter)*alpha;
end %else, alpha remains at one (or whatever it was from the
%minimum check routine)
end
deltaxnorm(iter)=norm(deltax(:,iter));
x(:,iter+1)=x(:,iter)+deltax(:,iter);
xelpt=x(1,iter+1);
elpt=x(2,iter+1);

%jump off main lobe??
if xnormfromsat(iter) < .25 && deltaxnorm(iter) > 1.8
    mainlobejump(mciter)=mainlobejump(mciter)+1;
end
%%%%%%%%%%

iter=iter+1;
if funcevals > 500
    warning('max number of function evaluations reached')
    break

```

```

end
end

gradfalloffcount(mciter)=sum(gradfalloff);
%calculate approximate time
if satvel > eps*10000 %if satvel isn't zero
    time=satpos(end)/satvel;
else
    time=0;
end
soln(1:2,mciter)=[x(1,end);x(2,end)];
soln(3,mciter)=iter;
simtime=toc;
soln(4,mciter)=simtime;
soln(5,mciter)=funcevals;
soln(6,mciter)=xnorm(end);
soln(7,mciter)=satpos(end);
soln(8,mciter)=xnormfromsat(end);
soln(9,mciter)=time;
soln(10,mciter)=sum(linstepcount);
soln(11,mciter)=mainlobejump(mciter);
soln(12,mciter)=gradfalloffcount(mciter);

end

```

C.3 BFGS.m

```

%Eric Marsh
%MIT LL, GRP 61
%February 2008

%BFGS Quasi Newton's Method

%Description:
%This step-tracking simulation accomplishes spatial pull-in from the
%starting points defined in testvec.mat. The cost function is defined in
%30nov.mat.

clear all
%close all load an antenna pattern *.mat file from genantennapattern.m
load 30nov.mat
load testvec.mat

soln=zeros(7,1000);
mainlobejump=zeros(1,1000);
denzerocount=zeros(1,1000);
bracketminfalse=zeros(1,1000);
gradfalloffcount=zeros(1,1000);

for mciter=1:1000
tic
xelpt=testvec(1,mciter); %initial guess
elpt=testvec(2,mciter); %initial guess

deljstep=.16; %(deg) this is ~3* the 3sigma on the 1-d pointing error distributions

```

```

deltax=[0;0];
x=[xelpt;elpt];
xnorm=0;
deltaxnorm=0;
iter=1;
epsilon=0.63; %looser?
gradient=[10^2;10^2];
hessian=zeros(2,2);
interp_method='linear';
R=zeros(2,2);
funcevals=0;
xelvar=.0004; %deg^2
elvar=.0004; %deg^2
ntsamps=10; %number of time samples to ensure normal distribution in xel
%and el
Fminjump=zeros(1,ntsamps);
gradswitch=epsilon*10;
linsearchparam=0.5;
linstepcount=0;
mincheck=0;
mincheckthreshold=4;
gradientnext=[0;0];
hessianhat=zeros(2,2);
jumpcond=false;
B=eye(2);
Bunmod=eye(2);
Q=zeros(2,2);
deltag=zeros(2,1);
changeB=0;
updateB=false;
directedgrad=0;
mincheckvec=0;
gradfalloff=0;
satvel=0.0005; %deg/sec
satvelx=sqrt(satvel^2/2);
satvely=satvelx;
samplewaittime=0.25; %sec
sattravelx=0;
sattravely=0;
xnormfromsat=0;
satpos=0;

% set terminate = false
terminate=false;
% while terminate = false
while terminate==false
% set compute alpha*pk = true
computedeltax=true;
%perform function/gradient evaluations at xk: initializations
xnorm(iter)=norm(x(:,iter));
satpos(iter)=norm([sattravelx;sattravely]);
xnormfromsat(iter)=abs(xnorm(iter)-satpos(iter));
F=zeros(13,ntsamps);
g=zeros(2,5);
G=zeros(2,2);

```

```

%%%%%%%%%%%%%%%%%%%%%%%%%%%%%%%%%%%%%%%%%%%%%%%%%%%%%%%%%%%%%%%%%%%%%%%%%%perform function evals:%%%%%%%%%%%%%%%%%%%%%%%%%%%%%%%%%%%%%%%%%%%%%%%%%%%%%%%%%%%%%%%%%%%%%%%%%%
%F9,F10,F11 not needed
if iter==1
%%F1%%
for i=1:ntsamps
    linnoisexel=randn(1,1)*sqrt(xelvar);
    linnoiseel=randn(1,1)*sqrt(elvar);
    F(1,i)=getsignalpower(xelpt+linnoisexel+sattravelx,elpt+linnoiseel+
        sattravely,meshsize,xel,el,gridpow2,interp_method);
    sattravelx=sattravelx+satvelx*samplewaittime;
    sattravely=sattravely+satvely*samplewaittime;
end
F(1,1)=mean(F(1,:));
F(1,1)=roundn(F(1,1),-1); %round to nearest tenths
funcevals=funcevals+1;

%%F2%%
for i=1:ntsamps
    linnoisexel=randn(1,1)*sqrt(xelvar);
    linnoiseel=randn(1,1)*sqrt(elvar);
    F(2,i)=getsignalpower(xelpt+linnoisexel+deljstep+sattravelx,elpt+
        linnoiseel+sattravely,meshsize,xel,el,gridpow2,interp_method);
    sattravelx=sattravelx+satvelx*samplewaittime;
    sattravely=sattravely+satvely*samplewaittime;
end
F(2,1)=mean(F(2,:));
F(2,1)=roundn(F(2,1),-1); %round to nearest tenths
funcevals=funcevals+1;

%%F3%%
for i=1:ntsamps
    linnoisexel=randn(1,1)*sqrt(xelvar);
    linnoiseel=randn(1,1)*sqrt(elvar);
    F(3,i)=getsignalpower(xelpt+linnoisexel+sattravelx,elpt+linnoiseel-
        deljstep+sattravely,meshsize,xel,el,gridpow2,interp_method);
    sattravelx=sattravelx+satvelx*samplewaittime;
    sattravely=sattravely+satvely*samplewaittime;
end
F(3,1)=mean(F(3,:));
F(3,1)=roundn(F(3,1),-1); %round to nearest tenths
funcevals=funcevals+1;

%%F4%%
for i=1:ntsamps
    linnoisexel=randn(1,1)*sqrt(xelvar);
    linnoiseel=randn(1,1)*sqrt(elvar);
    F(4,i)=getsignalpower(xelpt+linnoisexel-deljstep+sattravelx,elpt+
        linnoiseel+sattravely,meshsize,xel,el,gridpow2,interp_method);
    sattravelx=sattravelx+satvelx*samplewaittime;
    sattravely=sattravely+satvely*samplewaittime;
end
F(4,1)=mean(F(4,:));
F(4,1)=roundn(F(4,1),-1); %round to nearest tenths
funcevals=funcevals+1;

%%F5%%
for i=1:ntsamps

```

```

        linnoisexel=randn(1,1)*sqrt(xelvar);
        linnoiseel=randn(1,1)*sqrt(elvar);
        F(5,i)=getsignalpower(xelpt+linnoisexel+sattravelx,elpt+linnoiseel+
        deljstep+sattravely,meshsize,xel,el,gridpow2,interp_method);
        sattravelx=sattravelx+satvelx*samplewaittime;
        sattravely=sattravely+satvely*samplewaittime;
    end
    F(5,1)=mean(F(5,:));
    F(5,1)=roundn(F(5,1),-1); %round to nearest tenths
    funcevals=funcevals+1;
    else
        F=Fnext(:,1);
    end

%Form gradient vectors g3,g4 not needed
if iter==1
    g(:,1)=[(F(2,1)-F(4,1))/(2*deljstep);(F(5,1)-F(3,1))/(2*deljstep)];
    gradient(:,iter)=g(:,1);
else
    g(:,1)=gradientnext(:,iter-1);
    gradient(:,iter)=g(:,1);
end

%%%%%%%%%%%%%%%%%%%%%%%%%%%%%%%%%%%%%%%%%%%%%%%%%%%%%%%%%%%%%%%%%%%%%%%%%check for local or global min:%%%%%%%%%%%%%%%%%%%%%%%%%%%%%%%%%%%%%%%%%%%%%%%%%%%%%%%%%%%%%%%%%%%%%%%%%
% if criteria for minimum = true (small gradient)
if norm(gradient(:,iter)) < epsilon
    %in order to check for a local v. global min, need hessian matrix (more
    %func evals):
    %%%F6%%
    for i=1:ntsamps
        linnoisexel=randn(1,1)*sqrt(xelvar);
        linnoiseel=randn(1,1)*sqrt(elvar);
        F(6,i)=getsignalpower(xelpt+linnoisexel+deljstep+sattravelx,elpt+
        linnoiseel+deljstep+sattravely,meshsize,xel,el,gridpow2,
        interp_method);
        sattravelx=sattravelx+satvelx*samplewaittime;
        sattravely=sattravely+satvely*samplewaittime;
    end
    F(6,1)=mean(F(6,:));
    F(6,1)=roundn(F(6,1),-1); %round to nearest tenths
    funcevals=funcevals+1;

    %%%F7%%
    for i=1:ntsamps
        linnoisexel=randn(1,1)*sqrt(xelvar);
        linnoiseel=randn(1,1)*sqrt(elvar);
        F(7,i)=getsignalpower(xelpt+linnoisexel+2*deljstep+sattravelx,elpt+
        linnoiseel+sattravely,meshsize,xel,el,gridpow2,interp_method);
        sattravelx=sattravelx+satvelx*samplewaittime;
        sattravely=sattravely+satvely*samplewaittime;
    end
    F(7,1)=mean(F(7,:));
    F(7,1)=roundn(F(7,1),-1); %round to nearest tenths
    funcevals=funcevals+1;

    %%%F13%%

```

```

for i=1:ntsamps
    linnoisexel=randn(1,1)*sqrt(xelvar);
    linnoiseel=randn(1,1)*sqrt(elvar);
    F(13,i)=getsignalpower(xelpt+linnoisexel+sattravelx,elpt+linnoiseel
        +2*deljstep+sattravely,meshsize,xel,el,gridpow2,interp_method);
    sattravelx=sattravelx+satvelx*samplewaittime;
    sattravely=sattravely+satvely*samplewaittime;
end
F(13,1)=mean(F(13,:));
F(13,1)=roundn(F(13,1),-1); %round to nearest tenths
funcevals=funcevals+1;

if iter==1 || norm(gradient(:,iter-1)) < gradswitch
%%%F8%%%
for i=1:ntsamps
    linnoisexel=randn(1,1)*sqrt(xelvar);
    linnoiseel=randn(1,1)*sqrt(elvar);
    F(8,i)=getsignalpower(xelpt+linnoisexel+deljstep+sattravelx,elpt+
        linnoiseel-deljstep+sattravely,meshsize,xel,el,gridpow2,
        interp_method);
    sattravelx=sattravelx+satvelx*samplewaittime;
    sattravely=sattravely+satvely*samplewaittime;
end
F(8,1)=mean(F(8,:));
F(8,1)=roundn(F(8,1),-1); %round to nearest tenths
funcevals=funcevals+1;

%%%F12%%%
for i=1:ntsamps
    linnoisexel=randn(1,1)*sqrt(xelvar);
    linnoiseel=randn(1,1)*sqrt(elvar);
    F(12,i)=getsignalpower(xelpt+linnoisexel-deljstep+sattravelx,elpt+
        linnoiseel+deljstep+sattravely,meshsize,xel,el,gridpow2,
        interp_method);
    sattravelx=sattravelx+satvelx*samplewaittime;
    sattravely=sattravely+satvely*samplewaittime;
end
F(12,1)=mean(F(12,:));
F(12,1)=roundn(F(12,1),-1); %round to nearest tenths
funcevals=funcevals+1;
end
if iter==1 || norm(gradient(:,iter-1)) < gradswitch
    g(:,2)=[(F(7,1)-F(1,1))/(2*deljstep);(F(6,1)-F(8,1))/(2*deljstep)];
    g(:,5)=[(F(6,1)-F(12,1))/(2*deljstep);(F(13,1)-F(1,1))/(2*deljstep)];
else
    g(:,2)=[(F(7,1)-F(2,1))/(deljstep);(F(6,1)-F(2,1))/(deljstep)];
    g(:,5)=[(F(6,1)-F(5,1))/(deljstep);(F(13,1)-F(5,1))/(deljstep)];
end
%form hessian (G) matrix and check to see if you are on a local minimum
G(:,1)=(g(:,2)-g(:,1))/(deljstep);
G(:,2)=(g(:,5)-g(:,1))/(deljstep);
G=.5*(G+G');
hessian(:, :, iter)=G;
%modified cholesky factorization of Hessian
L=eye(2);
D=zeros(2,2);
R=zeros(2,2);

```

```

delta=10; %effectively adds more or less damping to lin search
for j=1:2
    if j==1
        D(j,j)=G(j,j);
        if D(j,j)<delta
            R(j,j)=(delta-D(j,j));
            D(j,j)=R(j,j)+D(j,j);
        end
        L(2,j)=G(2,j)/D(j,j);
    elseif j==2
        D(j,j)=G(j,j)-D(1,1)*(L(j,1))^2;
        if D(j,j)<delta
            R(j,j)=(delta-D(j,j));
            D(j,j)=R(j,j)+D(j,j);
        end
    end
end
end
%%%%%%
hessianhat(:,:,iter)=L*D*L';
%check for local min
if (norm(gradient(:,iter))<epsilon) && (R(1,1) > 0 || R(2,2) > 0) %if
%you're at a weak min (grad small, hessian modified)
jumppcond=true;
V=zeros(2,2);
E=zeros(2,2);
deltaxminjump=zeros(2,1);
jumpxel=0;
jumpel=0;
[V,E]=eig(hessian(:,:,iter));
if V(:,1)'*hessian(:,:,iter)*V(:,1) > V(:,2)'*hessian(:,:,iter)*
V(:,2)
    deltaxminjump=V(:,1);
else
    deltaxminjump=V(:,2);
end
deltaxminjump=deltaxminjump*1.85; %1.85 comes from averaging
%distance between first 4 peaks on ant. pattern
jumpxel=x(1,iter)+deltaxminjump(1);
jumpel=x(2,iter)+deltaxminjump(2);
for i=1:ntsamps
    linnoisexel=randn(1,1)*sqrt(xelvar);
    linnoiseel=randn(1,1)*sqrt(elvar);
    Fminjump(i)=getsignalpower(jumpxel+linnoisexel+sattravelx,
jumpel+linnoiseel+sattravely, meshsize, xel, el, gridpow2,
interp_method);
    sattravelx=sattravelx+satvelx*samplewaittime;
    sattravely=sattravely+satvely*samplewaittime;
end
Fminjump(1)=mean(Fminjump(1,:));
Fminjump=roundn(Fminjump(1),-1); %round to nearest tenths
funcevals=funcevals+1;
if Fminjump(1) > F(1,1) %must check to see you are going in right
%direction on eigenvector
    deltax(:,iter)=deltaxminjump*-1; %head the opposite way
    Fminjump(1)=0;
else
    deltax(:,iter)=deltaxminjump; %you jumped the correct way

```



```

        end
        mincheck=0;
    else
        deltax(:,iter)=[0;0];
        mincheck=mincheck+1;
    end
    computedeltax=false;
    if mincheck > mincheckthreshold
        %computedeltax=true; %complete one more jump (already evaluated the
        %function so might as well)
        terminate=true;
    end
elseif mincheck > 0 && norm(gradient(:,iter)) > epsilon
    computedeltax=true;
    mincheck=0;
    gradfalloff(iter)=1;
end
mincheckvec(iter)=mincheck;

if computedeltax==true %%%%%%%%%%if compute alpha*pk = true%%%%%%%%%
%%%%%%%%%compute pk and initial alpha:%%%%%%%%%
deltax(:,iter)=inv(B(:, :, iter))*-gradient(:,iter);
alpha=1;
%limit alpha*pk to a predetermined region of confidence:
if norm(deltax(:,iter))>1.0 %if deltax is outside a "region of trust" chosen so if yo
    deltax(:,iter)=(deltax(:,iter)/norm(deltax(:,iter)))*.75;
end

%evaluate function at initial alpha=1 value:
for i=1:ntsamps
    linnoisexel=randn(1,1)*sqrt(xelvar);
    linnoiseel=randn(1,1)*sqrt(elvar);
    Falpha(i)=getsignalpower(x(1,iter)+deltax(1,iter)+linnoisexel+
    sattravelx,x(2,iter)+deltax(2,iter)+linnoiseel+sattravely,meshsize,xel,
    el,gridpow2,interp_method);
    sattravelx=sattravelx+satvelx*samplewaittime;
    sattravely=sattravely+satvely*samplewaittime;
end
Falpha(1)=mean(Falpha(1,:));
Falpha=roundn(Falpha(1),-1); %round to nearest tenths
funcevals=funcevals+1;

%evaluate point along search direction to approximate gradient at alpha=1
dx1=deltax(1,iter)/norm(deltax(:,iter));
dx2=deltax(2,iter)/norm(deltax(:,iter));
nux=dx1*deljstep;
nuy=dx2*deljstep;
if norm([alpha*deltax(1,iter);alpha*deltax(2,iter)])>=deljstep
    if alpha > 0
        nu=norm([alpha*deltax(1,iter)-nux;alpha*deltax(2,iter)-nuy])/
        norm(deltax(:,iter)); %ensure that nu value will be deljstep away
        %from alpha in 1-d
    else
        nu=-1*norm([alpha*deltax(1,iter)+nux;alpha*deltax(2,iter)+nuy])/

```

```

        norm(deltax(:,iter));
    end
else
    if alpha > 0
        nu=-1*norm([alpha*deltax(1,iter)-nux;alpha*deltax(2,iter)-nuy])/
            norm(deltax(:,iter)); %ensure that nu value will be deljstep away
            %from alpha in 1-d
    else
        nu=norm([alpha*deltax(1,iter)+nux;alpha*deltax(2,iter)+nuy])/
            norm(deltax(:,iter));
    end
end
for i=1:ntsamps
    linnoisexel=randn(1,1)*sqrt(xelvar);
    linnoiseel=randn(1,1)*sqrt(elvar);
    Fnu(i)=getsignalpower(x(1,iter)+nu*deltax(1,iter)+linnoisexel+
        sattravelx,x(2,iter)+nu*deltax(2,iter)+linnoiseel+sattravely,meshsize,
        xel,el,gridpow2,interp_method);
    sattravelx=sattravelx+satvelx*samplewaittime;
    sattravely=sattravely+satvely*samplewaittime;
end
Fnu(1)=mean(Fnu(1,:));
Fnu=roundn(Fnu(1),-1); %round to nearest tenths
funcevals=funcevals+1;

%%%%%%%%%%%%%%%%%%%%%%%%%%%%%%%%%%%%%%%%%%%%%%%%%%%%%%%%%%%%%%%%%%%%%%%%%perform linear search along pk to determine
%%%%%%%%%%%%%%%%%%%%%%%%%%%%%%%%%%%%%%%%%%%%%%%%%%%%%%%%%%%%%%%%%%%%%%%%%satisfactory alpha %%%%%%%%%%%%%%%%%%%%%%%%%%%%%%%%%%%%%%%%%%%%%%%%%%%%%%%%%%%%%%%%%%%%%%%%%%
linsearchconverge=false;
directedgrad(iter)=deltax(:,iter)'\*gradient(:,iter);
%if alpha=1 is not satisfactory, perform lin search:
if abs((Falpha-Fnu))/deljstep > abs(-1*linsearchparam*directedgrad(iter))
    %Criterion for lin search-(finite difference replaces gradient)- GMW
    %p. 102

    %Step 1- make sure you have an interval bracketing a minimum:
    bracketmin=true;
    if F(1,1)<Falpha %look opposite direction to find Fa and a values for
        %interval containing minimum
        alpha=-1;
        bracket_step=1;
        Fb=Falpha;
        b=1;
        Fc=F(1,1);
        c=0;
        Fa=-10^6;
        a=alpha;
        while Fa(1) <= Fc
            if bracket_step > 1
                Fb=Fc;
                b=c;
                Fc=Fa(1);
                c=a;
            end
            for i=1:ntsamps
                linnoisexel=randn(1,1)*sqrt(xelvar);
                linnoiseel=randn(1,1)*sqrt(elvar);
                Fa(i)=getsignalpower(x(1,iter)+alpha*deltax(1,iter)+

```

```

        linnoisexel+sattravelx,x(2,iter)+alpha*deltax(2,iter)+
        linnoiseel+sattravely,meshsize,xel,el,gridpow2,
        interp_method);
        sattravelx=sattravelx+satvelx*samplewaittime;
        sattravely=sattravely+satvely*samplewaittime;
    end
    Fa(1)=mean(Fa(1,:));
    Fa=roundn(Fa(1),-1); %round to nearest tenths
    funcevals=funcevals+1;
    a=alpha;
    alpha=alpha*2;
    bracket_step=bracket_step+1;
if bracket_step > 4
    bracketmin=false;
    bracketminfalse(mciter)=bracketminfalse(mciter)+1;
    warning('could not bracket minimum for lin search in less
    than 4 steps')
    break
end
end
else %continue searching along search direction until a min is
    %bracketed- (find b)
    alpha=2;
    bracket_step=1;
    Fc=Falpha;
    c=1;
    Fa=F(1,1);
    a=0;
    Fb=-10^6;
    b=alpha;
    while Fb(1) <= Fc
        if bracket_step > 1
            Fa=Fc;
            a=c;
            Fc=Fb(1);
            c=b;
        end
        for i=1:ntsamps
            linnoisexel=randn(1,1)*sqrt(xelvar);
            linnoiseel=randn(1,1)*sqrt(elvar);
            Fb(i)=getsignalpower(x(1,iter)+alpha*deltax(1,iter)+
            linnoisexel+sattravelx,x(2,iter)+alpha*deltax(2,iter)+
            linnoiseel+sattravely,meshsize,xel,el,gridpow2,
            interp_method);
            sattravelx=sattravelx+satvelx*samplewaittime;
            sattravely=sattravely+satvely*samplewaittime;
        end
        Fb(1)=mean(Fb(1,:));
        Fb=roundn(Fb(1),-1); %round to nearest tenths
        funcevals=funcevals+1;
        b=alpha;
        alpha=alpha*2-1;
        bracket_step=bracket_step+1;
    if bracket_step > 4
        bracketmin=false;
        bracketminfalse(mciter)=bracketminfalse(mciter)+1;
        warning('could not bracket minimum for lin search in less

```

```

        than 4 steps')
        break
    end
end
end
%Step 2- perform quadratic interpolation:
if bracketmin==true %lin search...
    linsearchconverge=true;
    linstep=1;
    while linstep==1 || abs((Falpha-Fnu))/deljstep > abs(-1*
        linsearchparam*directedgrad(iter)) %criterion for linear
        %search (finite difference replaces gradient)- GMW p. 102
        if linstep > 1
            if alpha < c && Falpha <= Fc
                b=c;
                c=alpha;
                Fb=Fc;
                Fc=Falpha;
            elseif alpha > c && Falpha > Fc
                b=alpha;
                Fb=Falpha;
            elseif alpha < c && Falpha > Fc
                a=alpha;
                Fa=Falpha;
            else
                a=c;
                c=alpha;
                Fa=Fc;
                Fc=Falpha;
            end
        end
        if Fa==Fb && Fb==Fc %can't optimize any further with quad interp
            break
        end
        if c-10000*eps<a&&a<c+10000*eps %saying if a==c
            %can't optimize any further with quad interp
            break
        end
        if -10000*eps<((b-c)*Fa+(c-a)*Fb+(a-b)*Fc)&&((b-c)*Fa+(c-a)*
            Fb+(a-b)*Fc)<10000*eps %saying if den of alpha calc == 0
            %can't optimize any further with quad interp
            break
        end
        alpha=.5*((b^2-c^2)*Fa+(c^2-a^2)*Fb+(a^2-b^2)*Fc)/((b-c)*
            Fa+(c-a)*Fb+(a-b)*Fc);
        for i=1:ntsamps
            linnoisexel=randn(1,1)*sqrt(xelvar);
            linnoiseel=randn(1,1)*sqrt(elvar);
            Falpha(i)=getsignalpower(x(1,iter)+alpha*deltax(1,iter)+
                linnoisexel+sattravelx,x(2,iter)+alpha*deltax(2,iter)+
                linnoiseel+sattravely,meshsize,xel,el,gridpow2,
                interp_method);
            sattravelx=sattravelx+satvelx*samplewaittime;
            sattravely=sattravely+satvely*samplewaittime;
        end
        Falpha(1)=mean(Falpha(1,:));
        Falpha=roundn(Falpha(1),-1); %round to nearest tenths
        funcevals=funcevals+1;
    end
end

```

```

if norm([alpha*deltax(1,iter);alpha*deltax(2,iter)])>=deljstep
    if alpha > 0
        nu=norm([alpha*deltax(1,iter)-nux;alpha*deltax(2,iter)
            -nuy])/norm(deltax(:,iter)); %ensure that nu value
            %will be deljstep away from alpha in 1-d
    else
        nu=-1*norm([alpha*deltax(1,iter)+nux;alpha*
            deltax(2,iter)+nuy])/norm(deltax(:,iter));
    end
else
    if alpha > 0
        nu=-1*norm([alpha*deltax(1,iter)-nux;alpha*
            deltax(2,iter)-nuy])/norm(deltax(:,iter)); %ensure
            %that nu value will be deljstep away from alpha in 1-d
    else
        nu=norm([alpha*deltax(1,iter)+nux;alpha*deltax(2,iter)+
            nuy])/norm(deltax(:,iter));
    end
end
for i=1:ntsamps
    linnoisexel=randn(1,1)*sqrt(xelvar);
    linnoiseel=randn(1,1)*sqrt(elvar);
    Fnu(i)=getsignalpower(x(1,iter)+nu*deltax(1,iter)+
        linnoisexel+sattravelx,x(2,iter)+nu*deltax(2,iter)+
        linnoiseel+sattravely,meshsize,xel,el,gridpow2,
        interp_method);
    sattravelx=sattravelx+satvelx*samplewaittime;
    sattravely=sattravely+satvely*samplewaittime;
end
Fnu(1)=mean(Fnu(1,:));
Fnu=roundn(Fnu(1),-1); %round to nearest tenths
funcevals=funcevals+1;
linstep=linstep+1;
if linstep > 20
    linsearchconverge=false;
    break
end
end
linstepcount(iter)=linstep;
end
end
if linsearchconverge==true %if lin search produced a good alpha
    %within max number of linsteps
    deltax(:,iter)=deltax(:,iter)*alpha;
end %else, alpha remains at one (or whatever it was from the
%minimum check routine)
end
deltaxnorm(iter)=norm(deltax(:,iter));
x(:,iter+1)=x(:,iter)+deltax(:,iter);
xelpt=x(1,iter+1);
elpt=x(2,iter+1);

%%%%%%%%%%%%%%%%%%%%%%%%%%%%%%%%%%%%%%%%%%%%%%%%%%%%%%%%%%%%%%%%%%%%%%%%calculate function values and gradient values for next
%%%%%%%%%%%%%%%%%%%%%%%%%%%%%%%%%%%%%%%%%%%%%%%%%%%%%%%%%%%%%%%%%%%%%%%%point%%%%%%%%%%%%%%%%%%%%%%%%%%%%%%%%%%%%%%%%%%%%%%%%%%%%%%%%%%%%%%%%%%%%%%%%
Fnext=zeros(13,ntsamps);
if Fminjump(1)==0
    computeF1=true;

```

```

else
    computeF1=false;
end
%%%F1%%%
if computeF1==true
for i=1:ntsamps
    linnoisexel=randn(1,1)*sqrt(xelvar);
    linnoiseel=randn(1,1)*sqrt(elvar);
    Fnext(1,i)=getsignalpower(xelpt+linnoisexel+sattravelx,elpt+linnoiseel+
sattravely,meshsize,xel,el,gridpow2,interp_method);
    sattravelx=sattravelx+satvelx*samplewaittime;
    sattravely=sattravely+satvely*samplewaittime;
end
Fnext(1,1)=mean(Fnext(1,:));
Fnext(1,1)=roundn(Fnext(1,1),-1); %round to nearest tenths
funcevals=funcevals+1;
else
    Fnext(1,1)=Fminjump(1);
end

%%%F2%%%
for i=1:ntsamps
    linnoisexel=randn(1,1)*sqrt(xelvar);
    linnoiseel=randn(1,1)*sqrt(elvar);
    Fnext(2,i)=getsignalpower(xelpt+linnoisexel+deljstep+sattravelx,elpt+
linnoiseel+sattravely,meshsize,xel,el,gridpow2,interp_method);
    sattravelx=sattravelx+satvelx*samplewaittime;
    sattravely=sattravely+satvely*samplewaittime;
end
Fnext(2,1)=mean(Fnext(2,:));
Fnext(2,1)=roundn(Fnext(2,1),-1); %round to nearest tenths
funcevals=funcevals+1;

%%%F5%%%
for i=1:ntsamps
    linnoisexel=randn(1,1)*sqrt(xelvar);
    linnoiseel=randn(1,1)*sqrt(elvar);
    Fnext(5,i)=getsignalpower(xelpt+linnoisexel+sattravelx,elpt+linnoiseel+
deljstep+sattravely,meshsize,xel,el,gridpow2,interp_method);
    sattravelx=sattravelx+satvelx*samplewaittime;
    sattravely=sattravely+satvely*samplewaittime;
end
Fnext(5,1)=mean(Fnext(5,:));
Fnext(5,1)=roundn(Fnext(5,1),-1); %round to nearest tenths
funcevals=funcevals+1;

if norm(gradient(:,iter)) < gradswitch
%%%F3%%%
for i=1:ntsamps
    linnoisexel=randn(1,1)*sqrt(xelvar);
    linnoiseel=randn(1,1)*sqrt(elvar);
    Fnext(3,i)=getsignalpower(xelpt+linnoisexel+sattravelx,elpt+linnoiseel-
deljstep+sattravely,meshsize,xel,el,gridpow2,interp_method);
    sattravelx=sattravelx+satvelx*samplewaittime;
    sattravely=sattravely+satvely*samplewaittime;
end
Fnext(3,1)=mean(Fnext(3,:));

```

```

Fnext(3,1)=roundn(Fnext(3,1),-1); %round to nearest tenths
funcevals=funcevals+1;

%%F4%%
for i=1:ntsamps
    linnoisexel=randn(1,1)*sqrt(xelvar);
    linnoiseel=randn(1,1)*sqrt(elvar);
    Fnext(4,i)=getsignalpower(xelpt+linnoisexel-deljstep+sattravelx,elpt+
    linnoiseel+sattravely,meshsize,xel,el,gridpow2,interp_method);
    sattravelx=sattravelx+satvelx*samplewaittime;
    sattravely=sattravely+satvely*samplewaittime;
end
Fnext(4,1)=mean(Fnext(4,:));
Fnext(4,1)=roundn(Fnext(4,1),-1); %round to nearest tenths
funcevals=funcevals+1;
end
Fminjump=zeros(1,ntsamps);

%Form gradient vectors gnext3,gnext4 not needed
if (norm(gradient(:,iter)) < gradswitch)
    gnext(:,1)=[(Fnext(2,1)-Fnext(4,1))/(2*deljstep);(Fnext(5,1)-
    Fnext(3,1))/(2*deljstep)];
    gradientnext(:,iter)=gnext(:,1);
else
    gnext(:,1)=[(Fnext(2,1)-Fnext(1,1))/(deljstep);(Fnext(5,1)-Fnext(1,1))
    /(deljstep)];
    gradientnext(:,iter)=gnext(:,1);
    fwddifcount(iter+1)=1;
end
deltag(:,iter)=gradientnext(:,iter)-gradient(:,iter);
%%%%%%%%%%%%%%%%%%%%%%%%%%%%%%%%%%%%%%%%%%%%%%%%%%%%%%%%%%%%%%%%%%%%%%%%%

%%%%%%%%%%%%%%%%%%%%%%%%%%%%%%%%%%%%%%%%%%%%%%%%%%%%%%%%%%%%%%%%%%%%%%%%%update B matrix%%%%%%%%%%%%%%%%%%%%%%%%%%%%%%%%%%%%%%%%%%%%%%%%%%%%%%%%%%%%%%%%%%%%%%%%%:
%conditions for update
if norm(deltag(:,iter)) > 0+10000*eps
    deltagzero=false;
else
    deltagzero=true;
end
if abs(deltag(:,iter)*deltax(:,iter)) > 0+10000*eps && abs(deltax(:,iter)'
    *gradient(:,iter)) > 0+10000*eps
    denzero=false;
else
    denzero=true;
    if norm(deltax(:,iter)) > 0+10000*eps
        denzerocount(mciter)=denzerocount(mciter)+1;
    end
end
end

if norm(deltax(:,iter)) < 0+10000*eps %if you didn't go anywhere, B is
    %what is was before
    B(:, :, iter+1)=B(:, :, iter);
elseif jumpcond==true || deltagzero==true || denzero==true %reset B to
    %identity if you just made a jump or deltag is zero or the denominator
    %of the update matrix Q is going to be zero
    B(:, :, iter+1)=eye(2);
    jumpcond=false;

```

```

    deltagzero=false;
else %update B
    Q(:, :, iter)=deltag(:, iter)*deltag(:, iter)'/(deltag(:, iter) '*
    deltax(:, iter))+alpha^2*gradient(:, iter)*gradient(:, iter)'/(alpha*
    deltax(:, iter) '*gradient(:, iter));
    B(:, :, iter+1)=B(:, :, iter)+Q(:, :, iter);
    updateB=true;
end

if updateB==true
    %modified cholesky factorization of B
    Bunmod(:, :, iter+1)=B(:, :, iter+1);
    L=eye(2);
    D=zeros(2,2);
    R=zeros(2,2);
    delta2=5;
    for j=1:2
        if j==1
            D(j,j)=B(j,j,iter+1);
            if D(j,j)<delta2
                R(j,j)=(delta2-D(j,j));
                D(j,j)=R(j,j)+D(j,j);
            end
            L(2,j)=B(2,j,iter+1)/D(j,j);
        elseif j==2
            D(j,j)=B(j,j,iter+1)-D(1,1)*(L(j,1))^2;
            if D(j,j)<delta2
                R(j,j)=(delta2-D(j,j));
                D(j,j)=R(j,j)+D(j,j);
            end
        end
    end
    end
    %%%%%%%%%%%
    B(:, :, iter+1)=L*D*L';
    if R(1,1) > 0 || R(2,2) > 0
        changeB(iter)=1;
    end
end
updateB=false;
%%%%%%%%%%%%%%%%%%%%%%%%%%%%%%%%%%%%%%%%%%%%%%%%%%%%%%%%%%%%%%%%%%%%%%%%

%jump off main lobe??
if xnormfromsat(iter) < .25 && deltaxnorm(iter) > 1.8
    mainlobejump(mciter)=mainlobejump(mciter)+1;
end
%%%%%%%%%%%%%%%%%%%%%%%%%%%%%%%%%%%%%%%%%%%%%%%%%%%%%%%%%%%%%%%%%%%%%%%%

iter=iter+1;
if funcevals > 500
    warning('max number of function evaluations reached')
    break
end
end

gradfalloffcount(mciter)=sum(gradfalloff);
%calculate approximate time
if satvel > eps*10000 %if satvel isn't zero

```



```

        time=satpos(end)/satvel;
    else
        time=0;
    end
    soln(1:2,mciter)=[x(1,end);x(2,end)];
    soln(3,mciter)=iter;
    simtime=toc;
    soln(4,mciter)=simtime;
    soln(5,mciter)=funcevals;
    soln(6,mciter)=xnorm(end);
    soln(7,mciter)=satpos(end);
    soln(8,mciter)=xnormfromsat(end);
    soln(9,mciter)=time;
    soln(10,mciter)=sum(linstepcount);
    soln(11,mciter)=mainlobejump(mciter);
    soln(12,mciter)=gradfalloffcount(mciter);
    soln(13,mciter)=denzerocount(mciter);
end

```

C.4 DFP.m

%Eric Marsh MIT LL, GRP 61 February 2008

%DFP Quasi Newton's Method

%Description: This step-tracking simulation accomplishes spatial pull-in
 %from the starting points defined in testvec.mat. The cost function is
 %defined in 30nov.mat.

clear all

%close all load an antenna pattern *.mat file from genantennapattern.m

load 30nov.mat

load testvec.mat

```

soln=zeros(13,1000);
mainlobejump=zeros(1,1000);
denzerocount=zeros(1,1000);
bracketminfalse=zeros(1,1000);
gradfalloffcount=zeros(1,1000);

```

```

for mciter=1:1000

```

```

tic

```

```

xelpt=testvec(1,mciter); %initial guess

```

```

elpt=testvec(2,mciter); %initial guess

```

```

deljstep=.16; %(deg) this is ~3* the 3sigma on the 1-d pointing error

```

```

%distributions (also good for lin interp of ant pattern and machine errors)

```

```

deltax=[0;0];

```

```

x=[xelpt;elpt];

```

```

xnorm=0;

```

```

deltaxnorm=0;

```

```

iter=1;

```

```

epsilon=0.63; %looser?

```

```

gradient=[10^2;10^2];

```

```

hessian=zeros(2,2);

```

```

interp_method='linear';

```

```

R=zeros(2,2);
funcevals=0;
xelvar=.0004; %deg^2
elvar=.0004; %deg^2
ntsamps=10; %number of time samples to ensure normal distribution in xel
%and el
Fminjump=zeros(1,ntsamps);
gradswitch=epsilon*10;
linsearchparam=0.5;
linstepcount=0;
mincheck=0;
mincheckthreshold=4;
gradientnext=[0;0];
hessianhat=zeros(2,2);
jumpcond=false;
B=eye(2);
Bunmod=eye(2);
Q=zeros(2,2);
deltag=zeros(2,1);
changeB=0;
updateB=false;
directedgrad=0;
mincheckvec=0;
gradfalloff=0;
satvel=0.0005; %deg/sec
satvelx=sqrt(satvel^2/2);
satvely=satvelx;
samplewaittime=0.25; %sec
sattravelx=0;
sattravely=0;
xnormfromsat=0;
satpos=0;

% set terminate = false
terminate=false;
% while terminate = false
while terminate==false
% set compute alpha*pk = true
computedeltax=true;
%perform function/gradient evaluations at xk: initializations
xnorm(iter)=norm(x(:,iter));
satpos(iter)=norm([sattravelx;sattravely]);
xnormfromsat(iter)=abs(xnorm(iter)-satpos(iter));
F=zeros(13,ntsamps);
g=zeros(2,5);
G=zeros(2,2);

%%%%%%%%%%%%%%%%%%%%%%%%%%%%%%%%%%%%%%%%%%%%%%%%%%%%%%%%%%%%%%%%%%%%%%%%%perform function evals:%%%%%%%%%%%%%%%%%%%%%%%%%%%%%%%%%%%%%%%%%%%%%%%%%%%%%%%%%%%%%%%%%%%%%%%%%
%F9,F10,F11 not needed
if iter==1
%%F1%%
for i=1:ntsamps
    linnoisexel=randn(1,1)*sqrt(xelvar);
    linnoiseel=randn(1,1)*sqrt(elvar);
    F(1,i)=getsignalpower(xelpt+linnoisexel+sattravelx,elpt+linnoiseel+
        sattravely,meshsize,xel,el,gridpow2,interp_method);

```

```

        sattravelx=sattravelx+satvelx*samplewaittime;
        sattravely=sattravely+satvely*samplewaittime;
    end
    F(1,1)=mean(F(1,:));
    F(1,1)=roundn(F(1,1),-1); %round to nearest tenths
    funcevals=funcevals+1;

%%F2%%
for i=1:ntsamps
    linnoisexel=randn(1,1)*sqrt(xelvar);
    linnoiseel=randn(1,1)*sqrt(elvar);
    F(2,i)=getsignalpower(xelpt+linnoisexel+deljstep+sattravelx,elpt+
        linnoiseel+sattravely,meshsize,xel,el,gridpow2,interp_method);
    sattravelx=sattravelx+satvelx*samplewaittime;
    sattravely=sattravely+satvely*samplewaittime;
end
F(2,1)=mean(F(2,:));
F(2,1)=roundn(F(2,1),-1); %round to nearest tenths
funcevals=funcevals+1;

%%F3%%
for i=1:ntsamps
    linnoisexel=randn(1,1)*sqrt(xelvar);
    linnoiseel=randn(1,1)*sqrt(elvar);
    F(3,i)=getsignalpower(xelpt+linnoisexel+sattravelx,elpt+linnoiseel-
        deljstep+sattravely,meshsize,xel,el,gridpow2,interp_method);
    sattravelx=sattravelx+satvelx*samplewaittime;
    sattravely=sattravely+satvely*samplewaittime;
end
F(3,1)=mean(F(3,:));
F(3,1)=roundn(F(3,1),-1); %round to nearest tenths
funcevals=funcevals+1;

%%F4%%
for i=1:ntsamps
    linnoisexel=randn(1,1)*sqrt(xelvar);
    linnoiseel=randn(1,1)*sqrt(elvar);
    F(4,i)=getsignalpower(xelpt+linnoisexel-deljstep+sattravelx,elpt+
        linnoiseel+sattravely,meshsize,xel,el,gridpow2,interp_method);
    sattravelx=sattravelx+satvelx*samplewaittime;
    sattravely=sattravely+satvely*samplewaittime;
end
F(4,1)=mean(F(4,:));
F(4,1)=roundn(F(4,1),-1); %round to nearest tenths
funcevals=funcevals+1;

%%F5%%
for i=1:ntsamps
    linnoisexel=randn(1,1)*sqrt(xelvar);
    linnoiseel=randn(1,1)*sqrt(elvar);
    F(5,i)=getsignalpower(xelpt+linnoisexel+sattravelx,elpt+linnoiseel+
        deljstep+sattravely,meshsize,xel,el,gridpow2,interp_method);
    sattravelx=sattravelx+satvelx*samplewaittime;
    sattravely=sattravely+satvely*samplewaittime;
end
F(5,1)=mean(F(5,:));
F(5,1)=roundn(F(5,1),-1); %round to nearest tenths
funcevals=funcevals+1;

```

```

else
    F=Fnext(:,1);
end

%Form gradient vectors g3,g4 not needed
if iter==1
    g(:,1)=[(F(2,1)-F(4,1))/(2*deljstep);(F(5,1)-F(3,1))/(2*deljstep)];
    gradient(:,iter)=g(:,1);
else
    g(:,1)=gradientnext(:,iter-1);
    gradient(:,iter)=g(:,1);
end

%%%%%%%%%%%%%%%%%%%%%%%%%%%%%%%%%%%%%%%%%%%%%%%%%%%%%%%%%%%%%%%%%%%%%%%%%check for local or global min:%%%%%%%%%%%%%%%%%%%%%%%%%%%%%%%%%%%%%%%%%%%%%%%%%%%%%%%%%%%%%%%%%%%%%%%%%
% if criteria for minimum = true (small gradient)
if norm(gradient(:,iter)) < epsilon
    %in order to check for a local v. global min, need hessian matrix (more
    %func evals):
    %%%F6%%
    for i=1:ntsamps
        linnoisexel=randn(1,1)*sqrt(xelvar);
        linnoiseel=randn(1,1)*sqrt(elvar);
        F(6,i)=getsignalpower(xelpt+linnoisexel+deljstep+sattravelx,elpt+
        linnoiseel+deljstep+sattravelx,meshsize,xel,el,gridpow2,
        interp_method);
        sattravelx=sattravelx+satvelx*samplewaittime;
        sattravely=sattravely+satvely*samplewaittime;
    end
    F(6,1)=mean(F(6,:));
    F(6,1)=roundn(F(6,1),-1); %round to nearest tenths
    funcevals=funcevals+1;

    %%%F7%%
    for i=1:ntsamps
        linnoisexel=randn(1,1)*sqrt(xelvar);
        linnoiseel=randn(1,1)*sqrt(elvar);
        F(7,i)=getsignalpower(xelpt+linnoisexel+2*deljstep+sattravelx,elpt+
        linnoiseel+sattravelx,meshsize,xel,el,gridpow2,interp_method);
        sattravelx=sattravelx+satvelx*samplewaittime;
        sattravely=sattravely+satvely*samplewaittime;
    end
    F(7,1)=mean(F(7,:));
    F(7,1)=roundn(F(7,1),-1); %round to nearest tenths
    funcevals=funcevals+1;

    %%%F13%%
    for i=1:ntsamps
        linnoisexel=randn(1,1)*sqrt(xelvar);
        linnoiseel=randn(1,1)*sqrt(elvar);
        F(13,i)=getsignalpower(xelpt+linnoisexel+sattravelx,elpt+linnoiseel
        +2*deljstep+sattravelx,meshsize,xel,el,gridpow2,interp_method);
        sattravelx=sattravelx+satvelx*samplewaittime;
        sattravely=sattravely+satvely*samplewaittime;
    end
    F(13,1)=mean(F(13,:));
    F(13,1)=roundn(F(13,1),-1); %round to nearest tenths

```

```

funcevals=funcevals+1;

if iter==1 || norm(gradient(:,iter-1)) < gradswitch
%%%F8%%%
for i=1:ntsamps
    linnoisexel=randn(1,1)*sqrt(xelvar);
    linnoiseel=randn(1,1)*sqrt(elvar);
    F(8,i)=getsignalpower(xelpt+linnoisexel+deljstep+sattravelx,elpt+
        linnoiseel-deljstep+sattravely,meshsize,xel,el,gridpow2,
        interp_method);
    sattravelx=sattravelx+satvelx*samplewaittime;
    sattravely=sattravely+satvely*samplewaittime;
end
F(8,1)=mean(F(8,:));
F(8,1)=roundn(F(8,1),-1); %round to nearest tenths
funcevals=funcevals+1;

%%%F12%%%
for i=1:ntsamps
    linnoisexel=randn(1,1)*sqrt(xelvar);
    linnoiseel=randn(1,1)*sqrt(elvar);
    F(12,i)=getsignalpower(xelpt+linnoisexel-deljstep+sattravelx,elpt+
        linnoiseel+deljstep+sattravely,meshsize,xel,el,gridpow2,
        interp_method);
    sattravelx=sattravelx+satvelx*samplewaittime;
    sattravely=sattravely+satvely*samplewaittime;
end
F(12,1)=mean(F(12,:));
F(12,1)=roundn(F(12,1),-1); %round to nearest tenths
funcevals=funcevals+1;
end
if iter==1 || norm(gradient(:,iter-1)) < gradswitch
    g(:,2)=[(F(7,1)-F(1,1))/(2*deljstep);(F(6,1)-F(8,1))/(2*deljstep)];
    g(:,5)=[(F(6,1)-F(12,1))/(2*deljstep);(F(13,1)-F(1,1))/(2*deljstep)];
else
    g(:,2)=[(F(7,1)-F(2,1))/(deljstep);(F(6,1)-F(2,1))/(deljstep)];
    g(:,5)=[(F(6,1)-F(5,1))/(deljstep);(F(13,1)-F(5,1))/(deljstep)];
end
%form hessian (G) matrix and check to see if you are on a local minimum
G(:,1)=(g(:,2)-g(:,1))/(deljstep);
G(:,2)=(g(:,5)-g(:,1))/(deljstep);
G=.5*(G+G');
hessian(:, :, iter)=G;
%modified cholesky factorization of Hessian
L=eye(2);
D=zeros(2,2);
R=zeros(2,2);
delta=10; %effectively adds more or less damping to lin search
for j=1:2
    if j==1
        D(j,j)=G(j,j);
        if D(j,j)<delta
            R(j,j)=(delta-D(j,j));
            D(j,j)=R(j,j)+D(j,j);
        end
        L(2,j)=G(2,j)/D(j,j);
    elseif j==2

```

```

        D(j,j)=G(j,j)-D(1,1)*(L(j,1))^2;
        if D(j,j)<delta
            R(j,j)=(delta-D(j,j));
            D(j,j)=R(j,j)+D(j,j);
        end
    end
end
end
%%%%%%
hessianhat(:, :, iter)=L*D*L';
%check for local min
if (norm(gradient(:, iter))<epsilon) && (R(1,1) > 0 || R(2,2) > 0) %if
    %you're at a weak min (grad small, hessian modified)
    jumpcond=true;
    V=zeros(2,2);
    E=zeros(2,2);
    deltaxminjump=zeros(2,1);
    jumpxel=0;
    jumpel=0;
    [V,E]=eig(hessian(:, :, iter));
    if V(:,1)'*hessian(:, :, iter)*V(:,1) > V(:,2)'*hessian(:, :, iter)
        *V(:,2)
        deltaxminjump=V(:,1);
    else
        deltaxminjump=V(:,2);
    end
    deltaxminjump=deltaxminjump*1.85; %1.85 comes from averaging
    %distance between first 4 peaks on ant. pattern
    jumpxel=x(1, iter)+deltaxminjump(1);
    jumpel=x(2, iter)+deltaxminjump(2);
    for i=1:ntsamps
        linnoisexel=randn(1,1)*sqrt(xelvar);
        linnoiseel=randn(1,1)*sqrt(elvar);
        Fminjump(i)=getsignalpower(jumpxel+linnoisexel+sattravelx,
            jumpel+linnoiseel+sattravely, meshsize, xel, el, gridpow2,
            interp_method);
        sattravelx=sattravelx+satvelx*samplewaittime;
        sattravely=sattravely+satvely*samplewaittime;
    end
    Fminjump(1)=mean(Fminjump(1, :));
    Fminjump=roundn(Fminjump(1), -1); %round to nearest tenths
    funcevals=funcevals+1;
    if Fminjump(1) > F(1,1) %must check to see you are going in right
        %direction on eigenvector
        deltax(:, iter)=deltaxminjump*-1; %head the opposite way
        Fminjump(1)=0;
    else
        deltax(:, iter)=deltaxminjump; %you jumped the correct way
    end
    mincheck=0;
else
    deltax(:, iter)=[0;0];
    mincheck=mincheck+1;
end
computedeltax=false;
if mincheck > mincheckthreshold
    %computedeltax=true; %complete one more jump (already evaluated the
    %function so might as well)

```

```

        terminate=true;
    end
elseif mincheck > 0 && norm(gradient(:,iter)) > epsilon
    computedeltax=true;
    mincheck=0;
    gradfalloff(iter)=1;
end
mincheckvec(iter)=mincheck;

if computedeltax==true %%%%%%%%%%if compute alpha*pk = true%%%%%%%%%%%%
%%%%%%%%%compute pk and initial alpha:%%%%%%%%%%%%%%
deltax(:,iter)=B(:, :, iter)\-gradient(:,iter);
alpha=1;
%limit alpha*pk to a predetermined region of confidence:
if norm(deltax(:,iter))>1.0 %if deltax is outside a "region of trust"
    %chosen so if you're at a max, won't go over another max (max initial
    %step routine will take)
    deltax(:,iter)=(deltax(:,iter)/norm(deltax(:,iter)))*.75;
end

%evaluate function at initial alpha=1 value:
for i=1:ntsamps
    linnoisexel=randn(1,1)*sqrt(xelvar);
    linnoiseel=randn(1,1)*sqrt(elvar);
    Falpha(i)=getsignalpower(x(1,iter)+deltax(1,iter)+linnoisexel+
    sattravelx,x(2,iter)+deltax(2,iter)+linnoiseel+sattravely,meshsize,xel,
    el,gridpow2,interp_method);
    sattravelx=sattravelx+satvelx*samplewaittime;
    sattravely=sattravely+satvely*samplewaittime;
end
Falpha(1)=mean(Falpha(1,:));
Falpha=roundn(Falpha(1),-1); %round to nearest tenths
funcevals=funcevals+1;

%evaluate point along search direction to approximate gradient at alpha=1
dx1=deltax(1,iter)/norm(deltax(:,iter));
dx2=deltax(2,iter)/norm(deltax(:,iter));
nux=dx1*deljstep;
nuy=dx2*deljstep;
if norm([alpha*deltax(1,iter);alpha*deltax(2,iter)])>=deljstep
    if alpha > 0
        nu=norm([alpha*deltax(1,iter)-nux;alpha*deltax(2,iter)-nuy])/
        norm(deltax(:,iter)); %ensure that nu value will be deljstep away
        %from alpha in 1-d
    else
        nu=-1*norm([alpha*deltax(1,iter)+nux;alpha*deltax(2,iter)+nuy])/
        norm(deltax(:,iter));
    end
else
    if alpha > 0
        nu=-1*norm([alpha*deltax(1,iter)-nux;alpha*deltax(2,iter)-nuy])/
        norm(deltax(:,iter)); %ensure that nu value will be deljstep away
        %from alpha in 1-d
    end
end

```

```

else
    nu=norm([alpha*deltax(1,iter)+nux;alpha*deltax(2,iter)+nuy])/
    norm(deltax(:,iter));
end
end
for i=1:ntsamps
    linnoisexel=randn(1,1)*sqrt(xelvar);
    linnoiseel=randn(1,1)*sqrt(elvar);
    Fnu(i)=getsignalpower(x(1,iter)+nu*deltax(1,iter)+linnoisexel+
    sattravelx,x(2,iter)+nu*deltax(2,iter)+linnoiseel+sattravely,meshsize,
    xel,el,gridpow2,interp_method);
    sattravelx=sattravelx+satvelx*samplewaittime;
    sattravely=sattravely+satvely*samplewaittime;
end
Fnu(1)=mean(Fnu(1,:));
Fnu=roundn(Fnu(1),-1); %round to nearest tenths
funcevals=funcevals+1;

%%%%%%%%%%%%%%%%%%%%%%%%%%%%%%%%%%%%%%%%%%%%%%%%%%%%%%%%%%%%%%%%%%%%%%%%%perform linear search along pk to determine
%%%%%%%%%%%%%%%%%%%%%%%%%%%%%%%%%%%%%%%%%%%%%%%%%%%%%%%%%%%%%%%%%%%%%%%%%satisfactory alpha %%%%%%%%%%%%%%%%%%%%%%%%%%%%%%%%%%%%%%%%%%%%%%%%%%%%%%%%%%%%%%%%%%%%%%%%%%
linsearchconverge=false;
directedgrad(iter)=deltax(:,iter)'\*gradient(:,iter);
%if alpha=1 is not satisfactory, perform lin search:
if abs((Falpha-Fnu))/deljstep > abs(-1*linsearchparam*directedgrad(iter))
    %Criterion for lin search-(finite difference replaces gradient)- GMW
    %p. 102

    %Step 1- make sure you have an interval bracketing a minimum:
    bracketmin=true;
    if F(1,1)<Falpha %look opposite direction to find Fa and a values for
        %interval containing minimum
        alpha=-1;
        bracket_step=1;
        Fb=Falpha;
        b=1;
        Fc=F(1,1);
        c=0;
        Fa=-10^6;
        a=alpha;
        while Fa(1) <= Fc
            if bracket_step > 1
                Fb=Fc;
                b=c;
                Fc=Fa(1);
                c=a;
            end
            for i=1:ntsamps
                linnoisexel=randn(1,1)*sqrt(xelvar);
                linnoiseel=randn(1,1)*sqrt(elvar);
                Fa(i)=getsignalpower(x(1,iter)+alpha*deltax(1,iter)+
                linnoisexel+sattravelx,x(2,iter)+alpha*deltax(2,iter)+
                linnoiseel+sattravely,meshsize,xel,el,gridpow2,
                interp_method);
                sattravelx=sattravelx+satvelx*samplewaittime;
                sattravely=sattravely+satvely*samplewaittime;
            end
            Fa(1)=mean(Fa(1,:));

```



```

        Fa=roundn(Fa(1),-1); %round to nearest tenths
        funcevals=funcevals+1;
        a=alpha;
        alpha=alpha*2;
        bracket_step=bracket_step+1;
    if bracket_step > 4
        bracketmin=false;
        bracketminfalse(mciter)=bracketminfalse(mciter)+1;
        warning('could not bracket minimum for lin search in less
        than 4 steps')
        break
    end
    end
else %continue searching along search direction until a min is
    %bracketed- (find b)
    alpha=2;
    bracket_step=1;
    Fc=Falpha;
    c=1;
    Fa=F(1,1);
    a=0;
    Fb=-10^6;
    b=alpha;
    while Fb(1) <= Fc
        if bracket_step > 1
            Fa=Fc;
            a=c;
            Fc=Fb(1);
            c=b;
        end

        for i=1:ntsamps
            linnoisexel=randn(1,1)*sqrt(xelvar);
            linnoiseel=randn(1,1)*sqrt(elvar);
            Fb(i)=getsignalpower(x(1,iter)+alpha*deltax(1,iter)+
            linnoisexel+sattravelx,x(2,iter)+alpha*deltax(2,iter)+
            linnoiseel+sattravely,meshsize,xel,el,gridpow2,
            interp_method);
            sattravelx=sattravelx+satvelx*samplewaittime;
            sattravely=sattravely+satvely*samplewaittime;
        end
        Fb(1)=mean(Fb(1,:));
        Fb=roundn(Fb(1),-1); %round to nearest tenths
        funcevals=funcevals+1;
        b=alpha;
        alpha=alpha*2-1;
        bracket_step=bracket_step+1;
    if bracket_step > 4
        bracketmin=false;
        bracketminfalse(mciter)=bracketminfalse(mciter)+1;
        warning('could not bracket minimum for lin search in less
        than 4 steps')
        break
    end
    end
end
end
%Step 2- perform quadratic interpolation:
if bracketmin==true %lin search...

```

```

linsearchconverge=true;
linstep=1;
while linstep==1 || abs((Falpha-Fnu))/deljstep > abs(-1*
    linsearchparam*directedgrad(iter)) %criterion for linear
%search (finite difference replaces gradient)- GMW p. 102
if linstep > 1
    if alpha < c && Falpha <= Fc
        b=c;
        c=alpha;
        Fb=Fc;
        Fc=Falpha;
    elseif alpha > c && Falpha > Fc
        b=alpha;
        Fb=Falpha;
    elseif alpha < c && Falpha > Fc
        a=alpha;
        Fa=Falpha;
    else
        a=c;
        c=alpha;
        Fa=Fc;
        Fc=Falpha;
    end
end
if Fa==Fb && Fb==Fc %can't optimize any further with quad interp
    break
end
if c-10000*eps<a&&a<c+10000*eps %saying if a==c
    %can't optimize any further with quad interp
    break
end
if -10000*eps<((b-c)*Fa+(c-a)*Fb+(a-b)*Fc)&&((b-c)*Fa+(c-a)*
    Fb+(a-b)*Fc)<10000*eps %saying if den of alpha calc == 0
    %can't optimize any further with quad interp
    break
end
alpha=.5*((b^2-c^2)*Fa+(c^2-a^2)*Fb+(a^2-b^2)*Fc)/((b-c)*
    Fa+(c-a)*Fb+(a-b)*Fc);
for i=1:ntsamps
    linnoisexel=randn(1,1)*sqrt(xelvar);
    linnoiseel=randn(1,1)*sqrt(elvar);
    Falpha(i)=getsignalpower(x(1,iter)+alpha*deltax(1,iter)+
        linnoisexel+sattravelx,x(2,iter)+alpha*deltax(2,iter)+
        linnoiseel+sattravely,meshsize,xel,el,gridpow2,
        interp_method);
    sattravelx=sattravelx+satvelx*samplewaittime;
    sattravely=sattravely+satvely*samplewaittime;
end
Falpha(1)=mean(Falpha(1,:));
Falpha=roundn(Falpha(1),-1); %round to nearest tenths
funcevals=funcevals+1;
if norm([alpha*deltax(1,iter);alpha*deltax(2,iter)])>=deljstep
    if alpha > 0
        nu=norm([alpha*deltax(1,iter)-nux;alpha*deltax(2,iter)
            -nuy])/norm(deltax(:,iter)); %ensure that nu value
        %will be deljstep away from alpha in 1-d
    else
        nu=-1*norm([alpha*deltax(1,iter)+nux;alpha*

```

```

                                deltax(2,iter)+nuy])/norm(deltax(:,iter));
        end
    else
        if alpha > 0
            nu=-1*norm([alpha*deltax(1,iter)-nux;alpha*
                deltax(2,iter)-nuy])/norm(deltax(:,iter)); %ensure
                %that nu value will be deljstep away from alpha in 1-d
        else
            nu=norm([alpha*deltax(1,iter)+nux;alpha*deltax(2,iter)+
                nuy])/norm(deltax(:,iter));
        end
    end
end
for i=1:ntsamps
    linnoisexel=randn(1,1)*sqrt(xelvar);
    linnoiseel=randn(1,1)*sqrt(elvar);
    Fnu(i)=getsignalpower(x(1,iter)+nu*deltax(1,iter)+
        linnoisexel+sattravelx,x(2,iter)+nu*deltax(2,iter)+
        linnoiseel+sattravely,meshsize,xel,el,gridpow2,
        interp_method);
    sattravelx=sattravelx+satvelx*samplewaittime;
    sattravely=sattravely+satvely*samplewaittime;
end
Fnu(1)=mean(Fnu(1,:));
Fnu=roundn(Fnu(1),-1); %round to nearest tenths
funcevals=funcevals+1;
linstep=linstep+1;
if linstep > 20
    linsearchconverge=false;
    break
end
end
linstepcount(iter)=linstep;
end
end
if linsearchconverge==true %if lin search produced a good alpha
    %within max number of linsteps
    deltax(:,iter)=deltax(:,iter)*alpha;
end %else, alpha remains at one (or whatever it was from the
%minimum check routine)
end
deltaxnorm(iter)=norm(deltax(:,iter));
x(:,iter+1)=x(:,iter)+deltax(:,iter);
xelpt=x(1,iter+1);
elpt=x(2,iter+1);

%%%%%%%%%%%%%%%%%%%%%%%%%%%%%%%%%%%%%%%%%%%%%%%%%%%%%%%%%%%%%%%%%%%%%%%%calculate function values and gradient values for next
%%%%%%%%%%%%%%%%%%%%%%%%%%%%%%%%%%%%%%%%%%%%%%%%%%%%%%%%%%%%%%%%%%%%%%%%point%%%%%%%%%%%%%%%%%%%%%%%%%%%%%%%%%%%%%%%%%%%%%%%%%%%%%%%%%%%%%%%%%%%%%%%%
Fnext=zeros(13,ntsamps);
if Fminjump(1)==0
    computeF1=true;
else
    computeF1=false;
end
%%%F1%%%
if computeF1==true
for i=1:ntsamps
    linnoisexel=randn(1,1)*sqrt(xelvar);

```

```

        linnoiseel=randn(1,1)*sqrt(elvar);
        Fnext(1,i)=getsignalpower(xelpt+linnoisexel+sattravelx,elpt+linnoiseel+
        sattravely,meshsize,xel,el,gridpow2,interp_method);
        sattravelx=sattravelx+satvelx*samplewaittime;
        sattravely=sattravely+satvely*samplewaittime;
    end
    Fnext(1,1)=mean(Fnext(1,:));
    Fnext(1,1)=roundn(Fnext(1,1),-1); %round to nearest tenths
    funcevals=funcevals+1;
    else
        Fnext(1,1)=Fminjump(1);
    end

%%%F2%%%
for i=1:ntsamps
    linnoisexel=randn(1,1)*sqrt(xelvar);
    linnoiseel=randn(1,1)*sqrt(elvar);
    Fnext(2,i)=getsignalpower(xelpt+linnoisexel+deljstep+sattravelx,elpt+
    linnoiseel+sattravely,meshsize,xel,el,gridpow2,interp_method);
    sattravelx=sattravelx+satvelx*samplewaittime;
    sattravely=sattravely+satvely*samplewaittime;
end
Fnext(2,1)=mean(Fnext(2,:));
Fnext(2,1)=roundn(Fnext(2,1),-1); %round to nearest tenths
funcevals=funcevals+1;

%%%F5%%%
for i=1:ntsamps
    linnoisexel=randn(1,1)*sqrt(xelvar);
    linnoiseel=randn(1,1)*sqrt(elvar);
    Fnext(5,i)=getsignalpower(xelpt+linnoisexel+sattravelx,elpt+linnoiseel+
    deljstep+sattravely,meshsize,xel,el,gridpow2,interp_method);
    sattravelx=sattravelx+satvelx*samplewaittime;
    sattravely=sattravely+satvely*samplewaittime;
end
Fnext(5,1)=mean(Fnext(5,:));
Fnext(5,1)=roundn(Fnext(5,1),-1); %round to nearest tenths
funcevals=funcevals+1;

if norm(gradient(:,iter)) < gradswitch
%%%F3%%%
for i=1:ntsamps
    linnoisexel=randn(1,1)*sqrt(xelvar);
    linnoiseel=randn(1,1)*sqrt(elvar);
    Fnext(3,i)=getsignalpower(xelpt+linnoisexel+sattravelx,elpt+linnoiseel+
    deljstep+sattravely,meshsize,xel,el,gridpow2,interp_method);
    sattravelx=sattravelx+satvelx*samplewaittime;
    sattravely=sattravely+satvely*samplewaittime;
end
Fnext(3,1)=mean(Fnext(3,:));
Fnext(3,1)=roundn(Fnext(3,1),-1); %round to nearest tenths
funcevals=funcevals+1;

%%%F4%%%
for i=1:ntsamps
    linnoisexel=randn(1,1)*sqrt(xelvar);
    linnoiseel=randn(1,1)*sqrt(elvar);

```

```

        Fnext(4,i)=getsignalpower(xelpt+linnoiseixel-deljstep+sattravelx,elpt+
        linnoiseel+sattravely,meshsize,xel,el,gridpow2,interp_method);
        sattravelx=sattravelx+satvelx*samplewaittime;
        sattravely=sattravely+satvely*samplewaittime;
    end
    Fnext(4,1)=mean(Fnext(4,:));
    Fnext(4,1)=roundn(Fnext(4,1),-1); %round to nearest tenths
    funcevals=funcevals+1;
    end
    Fminjump=zeros(1,ntsamps);

    %Form gradient vectors gnext3,gnext4 not needed
    if (norm-gradient(:,iter)) < gradswitch)
        gnext(:,1)=[(Fnext(2,1)-Fnext(4,1))/(2*deljstep);(Fnext(5,1)-Fnext(3,1))
            /(2*deljstep)];
        gradientnext(:,iter)=gnext(:,1);
    else
        gnext(:,1)=[(Fnext(2,1)-Fnext(1,1))/(deljstep);(Fnext(5,1)-Fnext(1,1))
            /(deljstep)];
        gradientnext(:,iter)=gnext(:,1);
        fwddifcount(iter+1)=1;
    end
    deltag(:,iter)=gradientnext(:,iter)-gradient(:,iter);
    %%%%%%%%%%%%%%%%%%%%%%%%%%%%%%%%%%%%%%%%%%%%%%%%%%%%%%%%%%%%%%%%%%%%%%%%%%

    %%%%%%%%%%%%%%%%%%%%%%%%%%%%%%%%%%%%%%%%%%%%%%%%%%%%%%%%%%%%%%%%%%%%%%%%%%update B matrix%%%%%%%%%%%%%%%%%%%%%%%%%%%%%%%%%%%%%%%%%%%%%%%%%%%%%%%%%%%%%%%%%%%%%%%%%:
    %conditions for update
    if norm(deltag(:,iter)) > 0+10000*eps
        deltagzero=false;
    else
        deltagzero=true;
    end
    if abs(deltag(:,iter)'*deltax(:,iter)) > 0+10000*eps
        denzero=false;
    else
        denzero=true;
        if norm(deltax(:,iter)) > 0+10000*eps
            denzerocount(mciter)=denzerocount(mciter)+1;
        end
    end
    end

    if norm(deltax(:,iter)) < 0+10000*eps %if you didn't go anywhere, B is what
        %is was before
        B(:, :, iter+1)=B(:, :, iter);
    elseif jumpcond==true || deltagzero==true || denzero==true %reset B to
        %identity if you just made a jump or deltag is zero or the denominator
        %of the update matrix Q is going to be zero
        B(:, :, iter+1)=eye(2);
        jumpcond=false;
        deltagzero=false;
    else %update B
        Q(:, :, iter)=deltag(:,iter)*deltag(:,iter)'/(deltag(:,iter)'
            *deltax(:,iter))+alpha*gradient(:,iter)*deltag(:,iter)'/
            (deltag(:,iter)'*deltax(:,iter))+alpha*deltag(:,iter)*gradient(:,iter)'/
            (deltag(:,iter)'*deltax(:,iter))-
            alpha*deltag(:,iter)*gradient(:,iter)'*deltax(:,iter)*deltag(:,iter)'/
            (deltag(:,iter)'*deltax(:,iter));
    end

```

```

        B(:,:,iter+1)=B(:,:,iter)+Q(:,:,iter);
        updateB=true;
    end

    if updateB==true
        %modified cholesky factorization of B
        Bunmod(:,:,iter+1)=B(:,:,iter+1);
        L=eye(2);
        D=zeros(2,2);
        R=zeros(2,2);
        delta2=5;
        for j=1:2
            if j==1
                D(j,j)=B(j,j,iter+1);
                if D(j,j)<delta2
                    R(j,j)=(delta2-D(j,j));
                    D(j,j)=R(j,j)+D(j,j);
                end
                L(2,j)=B(2,j,iter+1)/D(j,j);
            elseif j==2
                D(j,j)=B(j,j,iter+1)-D(1,1)*(L(j,1))^2;
                if D(j,j)<delta2
                    R(j,j)=(delta2-D(j,j));
                    D(j,j)=R(j,j)+D(j,j);
                end
            end
        end
        end
        %%%%%%%%%%%
        B(:,:,iter+1)=L*D*L';
        if R(1,1) > 0 || R(2,2) > 0
            changeB(iter)=1;
        end
    end
    updateB=false;
    %%%%%%%%%%%

    %jump off main lobe??
    if xnormfromsat(iter) < .25 && deltaxnorm(iter) > 1.8
        mainlobejump(mciter)=mainlobejump(mciter)+1;
    end
    %%%%%%%%%%%

    iter=iter+1;
    if funcevals > 500
        warning('max number of function evaluations reached')
        break
    end
    end

    gradfalloffcount(mciter)=sum(gradfalloff);
    %calculate approximate time
    if satvel > eps*10000 %if satvel isn't zero
        time=satpos(end)/satvel;
    else
        time=0;
    end
    soln(1:2,mciter)=[x(1,end);x(2,end)];
    soln(3,mciter)=iter;

```

```

simtime=toc;
soln(4,mciter)=simtime;
soln(5,mciter)=funcevals;
soln(6,mciter)=xnorm(end);
soln(7,mciter)=satpos(end);
soln(8,mciter)=xnormfromsat(end);
soln(9,mciter)=time;
soln(10,mciter)=sum(linstepcount);
soln(11,mciter)=mainlobejump(mciter);
soln(12,mciter)=gradfalloffcount(mciter);
soln(13,mciter)=denzerocount(mciter);
end

```

C.5 steepestdescent.m

```

%Eric Marsh
%2 Feb 08

```

```

%method of steepest descent algorithm

```

```

%Description: This step-tracking simulation accomplishes spatial pull-in
%from the starting points defined in testvec.mat. The cost function is
%defined in 30nov.mat.

```

```

clear all
%close all
%load an antenna pattern *.mat file from genantennapattern.m
load 30nov.mat
load testvec.mat

```

```

soln=zeros(7,1000);
mainlobejump=zeros(1,1000);
bracketminfalse=zeros(1,1000);
gradfalloffcount=zeros(1,1000);

```

```

for mciter=1:1000
tic
xelpt=testvec(1,mciter); %initial guess
elpt=testvec(2,mciter); %initial guess

```

```

deljstep=.16; %(deg) this is ~3* the 3sigma on the 1-d pointing error
%distributions (also good for lin interp of ant pattern and machine errors)
deltax=[0;0];
x=[xelpt;elpt];
xnorm=0;
deltaxnorm=0;
iter=1;
epsilon=0.63; %looser?
gradient=[10^2;10^2];
hessian=zeros(2,2);
interp_method='linear';
R=zeros(2,2);
funcevals=0;
xelvar=.0004; %deg^2
elvar=.0004; %deg^2

```

```

ntsamps=10; %number of time samples to ensure normal distribution in xel
%and el
Fminjump=zeros(1,ntsamps);
gradswitch=epsilon*10;
linsearchparam=0.5;
linstepcount=0;
mincheck=0;
mincheckthreshold=4;
hessianhat=zeros(2,2);
directedgrad=0;
mincheckvec=0;
gradfalloff=0;
satvel=0.0005; %deg/sec
satvelx=sqrt(satvel^2/2);
satvely=satvelx;
samplewaittime=0.25; %sec
sattravelx=0;
sattravely=0;
xnormfromsat=0;
satpos=0;

% set terminate = false
terminate=false;
% while terminate = false
while terminate==false
% set compute alpha*pk = true
computedeltax=true;
%perform function/gradient evaluations at xk
%initializations
xnorm(iter)=norm(x(:,iter));
satpos(iter)=norm([sattravelx;sattravely]);
xnormfromsat(iter)=abs(xnorm(iter)-satpos(iter));
F=zeros(13,ntsamps);
g=zeros(2,5);
G=zeros(2,2);

%%%%%%%%%%%%%%%%%%%%%%%%%%%%%%%%%%%%%%%%%%%%%%%%%%%%%%%%%%%%%%%%%%%%%%%%%perform function evals:%%%%%%%%%%%%%%%%%%%%%%%%%%%%%%%%%%%%%%%%%%%%%%%%%%%%%%%%%%%%%%%%%%%%%%%%%
%F9,F10,F11 not needed
if Fminjump(1)==0
    computeF1=true;
else
    computeF1=false;
end
%%%F1%%%
if computeF1==true
for i=1:ntsamps
    linnoisexel=randn(1,1)*sqrt(xelvar);
    linnoiseel=randn(1,1)*sqrt(elvar);
    F(1,i)=getsignalpower(xelpt+linnoisexel+sattravelx,elpt+linnoiseel+
    sattravely,meshsize,xel,el,gridpow2,interp_method);
    sattravelx=sattravelx+satvelx*samplewaittime;
    sattravely=sattravely+satvely*samplewaittime;
end
F(1,1)=mean(F(1,:));
F(1,1)=roundn(F(1,1),-1); %round to nearest tenths
funcevals=funcevals+1;
else

```



```

    F(1,1)=Fminjump(1);
end

%%F2%%
for i=1:ntsamps
    linnoisexel=randn(1,1)*sqrt(xelvar);
    linnoiseel=randn(1,1)*sqrt(elvar);
    F(2,i)=getsignalpower(xelpt+linnoisexel+deljstep+sattravelx,elpt+
        linnoiseel+sattravely,meshsize,xel,el,gridpow2,interp_method);
    sattravelx=sattravelx+satvelx*samplewaittime;
    sattravely=sattravely+satvely*samplewaittime;
end
F(2,1)=mean(F(2,:));
F(2,1)=roundn(F(2,1),-1); %round to nearest tenths
funcevals=funcevals+1;

%%F5%%
for i=1:ntsamps
    linnoisexel=randn(1,1)*sqrt(xelvar);
    linnoiseel=randn(1,1)*sqrt(elvar);
    F(5,i)=getsignalpower(xelpt+linnoisexel+sattravelx,elpt+linnoiseel+
        deljstep+sattravely,meshsize,xel,el,gridpow2,interp_method);
    sattravelx=sattravelx+satvelx*samplewaittime;
    sattravely=sattravely+satvely*samplewaittime;
end
F(5,1)=mean(F(5,:));
F(5,1)=roundn(F(5,1),-1); %round to nearest tenths
funcevals=funcevals+1;

if iter==1 || norm(gradient(:,iter-1)) < gradswitch
%%F3%%
for i=1:ntsamps
    linnoisexel=randn(1,1)*sqrt(xelvar);
    linnoiseel=randn(1,1)*sqrt(elvar);
    F(3,i)=getsignalpower(xelpt+linnoisexel+sattravelx,elpt+linnoiseel-
        deljstep+sattravely,meshsize,xel,el,gridpow2,interp_method);
    sattravelx=sattravelx+satvelx*samplewaittime;
    sattravely=sattravely+satvely*samplewaittime;
end
F(3,1)=mean(F(3,:));
F(3,1)=roundn(F(3,1),-1); %round to nearest tenths
funcevals=funcevals+1;

%%F4%%
for i=1:ntsamps
    linnoisexel=randn(1,1)*sqrt(xelvar);
    linnoiseel=randn(1,1)*sqrt(elvar);
    F(4,i)=getsignalpower(xelpt+linnoisexel-deljstep+sattravelx,elpt+
        linnoiseel+sattravely,meshsize,xel,el,gridpow2,interp_method);
    sattravelx=sattravelx+satvelx*samplewaittime;
    sattravely=sattravely+satvely*samplewaittime;
end
F(4,1)=mean(F(4,:));
F(4,1)=roundn(F(4,1),-1); %round to nearest tenths
funcevals=funcevals+1;
end
Fminjump=zeros(1,ntsamps);

```

```

%Form gradient vectors
%g3,g4 not needed
if iter==1 || norm(gradient(:,iter-1)) < gradswitch
    g(:,1)=[(F(2,1)-F(4,1))/(2*deljstep);(F(5,1)-F(3,1))/(2*deljstep)];
    gradient(:,iter)=g(:,1);
else
    g(:,1)=[(F(2,1)-F(1,1))/(deljstep);(F(5,1)-F(1,1))/(deljstep)];
    gradient(:,iter)=g(:,1);
    fwddifcount(iter)=1;
end

%%%%%%%%%%%%%%%%%%%%%%%%%%%%%%%%%%%%%%%%%%%%%%%%%%%%%%%%%%%%%%%%%%%%%%%%%check for local or global min:%%%%%%%%%%%%%%%%%%%%%%%%%%%%%%%%%%%%%%%%%%%%%%%%%%%%%%%%%%%%%%%%%%%%%%%%%
% if criteria for minimum = true (small gradient)
if norm(gradient(:,iter)) < epsilon
    %in order to check for a local v. global min, need hessian matrix
    %(more func evals):
    %%%F6%%
    for i=1:ntsamps
        linnoisexel=randn(1,1)*sqrt(xelvar);
        linnoiseel=randn(1,1)*sqrt(elvar);
        F(6,i)=getsignalpower(xelpt+linnoisexel+deljstep+sattravelx,elpt+
            linnoiseel+deljstep+sattravelx,meshsize,xel,el,gridpow2,
            interp_method);
        sattravelx=sattravelx+satvelx*samplewaittime;
        sattravely=sattravely+satvely*samplewaittime;
    end
    F(6,1)=mean(F(6,:));
    F(6,1)=roundn(F(6,1),-1); %round to nearest tenths
    funcevals=funcevals+1;

    %%%F7%%
    for i=1:ntsamps
        linnoisexel=randn(1,1)*sqrt(xelvar);
        linnoiseel=randn(1,1)*sqrt(elvar);
        F(7,i)=getsignalpower(xelpt+linnoisexel+2*deljstep+sattravelx,elpt+
            linnoiseel+sattravelx,meshsize,xel,el,gridpow2,interp_method);
        sattravelx=sattravelx+satvelx*samplewaittime;
        sattravely=sattravely+satvely*samplewaittime;
    end
    F(7,1)=mean(F(7,:));
    F(7,1)=roundn(F(7,1),-1); %round to nearest tenths
    funcevals=funcevals+1;

    %%%F13%%
    for i=1:ntsamps
        linnoisexel=randn(1,1)*sqrt(xelvar);
        linnoiseel=randn(1,1)*sqrt(elvar);
        F(13,i)=getsignalpower(xelpt+linnoisexel+sattravelx,elpt+linnoiseel+
            2*deljstep+sattravelx,meshsize,xel,el,gridpow2,interp_method);
        sattravelx=sattravelx+satvelx*samplewaittime;
        sattravely=sattravely+satvely*samplewaittime;
    end
    F(13,1)=mean(F(13,:));
    F(13,1)=roundn(F(13,1),-1); %round to nearest tenths
    funcevals=funcevals+1;

```

```

if iter==1 || norm(gradient(:,iter-1)) < gradswitch
%%F8%%
for i=1:ntsamps
    linnoisexel=randn(1,1)*sqrt(xelvar);
    linnoiseel=randn(1,1)*sqrt(elvar);
    F(8,i)=getsignalpower(xelpt+linnoisexel+deljstep+sattravelx,elpt+
        linnoiseel-deljstep+sattravely,meshsize,xel,el,gridpow2,
        interp_method);
    sattravelx=sattravelx+satvelx*samplewaittime;
    sattravely=sattravely+satvely*samplewaittime;
end
F(8,1)=mean(F(8,:));
F(8,1)=roundn(F(8,1),-1); %round to nearest tenths
funcevals=funcevals+1;

%%F12%%
for i=1:ntsamps
    linnoisexel=randn(1,1)*sqrt(xelvar);
    linnoiseel=randn(1,1)*sqrt(elvar);
    F(12,i)=getsignalpower(xelpt+linnoisexel-deljstep+sattravelx,elpt+
        linnoiseel+deljstep+sattravely,meshsize,xel,el,gridpow2,
        interp_method);
    sattravelx=sattravelx+satvelx*samplewaittime;
    sattravely=sattravely+satvely*samplewaittime;
end
F(12,1)=mean(F(12,:));
F(12,1)=roundn(F(12,1),-1); %round to nearest tenths
funcevals=funcevals+1;
end
if iter==1 || norm(gradient(:,iter-1)) < gradswitch
    g(:,2)=[(F(7,1)-F(1,1))/(2*deljstep);(F(6,1)-F(8,1))/(2*deljstep)];
    g(:,5)=[(F(6,1)-F(12,1))/(2*deljstep);(F(13,1)-F(1,1))/(2*deljstep)];
else
    g(:,2)=[(F(7,1)-F(2,1))/(deljstep);(F(6,1)-F(2,1))/(deljstep)];
    g(:,5)=[(F(6,1)-F(5,1))/(deljstep);(F(13,1)-F(5,1))/(deljstep)];
end
%form hessian (G) matrix and check to see if you are on a local minimum
G(:,1)=(g(:,2)-g(:,1))/(deljstep);
G(:,2)=(g(:,5)-g(:,1))/(deljstep);
G=.5*(G+G');
hessian(:, :, iter)=G;
%modified cholesky factorization of Hessian
L=eye(2);
D=zeros(2,2);
R=zeros(2,2);
delta=10; %effectively adds more or less damping to lin search
for j=1:2
    if j==1
        D(j,j)=G(j,j);
        if D(j,j)<delta
            R(j,j)=(delta-D(j,j));
            D(j,j)=R(j,j)+D(j,j);
        end
        L(2,j)=G(2,j)/D(j,j);
    elseif j==2
        D(j,j)=G(j,j)-D(1,1)*(L(j,1))^2;
        if D(j,j)<delta

```

```

                R(j,j)=(delta-D(j,j));
                D(j,j)=R(j,j)+D(j,j);
            end
        end
    end
end
%%%%%%
hessianhat(:,:,iter)=L*D*L';
%check for local min
if (norm(gradient(:,iter))<epsilon) && (R(1,1) > 0 || R(2,2) > 0) %if
    %you're at a weak min (grad small, hessian modified)
    %TOL Much looser if rounding SNR values
    V=zeros(2,2);
    E=zeros(2,2);
    deltaxminjump=zeros(2,1);
    jumpxel=0;
    jumpel=0;
    [V,E]=eig(hessian(:,:,iter));
    if V(:,1)'*hessian(:,:,iter)*V(:,1) > V(:,2)'*hessian(:,:,iter)
        *V(:,2)
        deltaxminjump=V(:,1);
    else
        deltaxminjump=V(:,2);
    end
    deltaxminjump=deltaxminjump*1.85; %1.85 comes from averaging
    %distance between first 4 peaks on ant. pattern
    jumpxel=x(1,iter)+deltaxminjump(1);
    jumpel=x(2,iter)+deltaxminjump(2);
    for i=1:ntsamps
        linnoisexel=randn(1,1)*sqrt(xelvar);
        linnoiseel=randn(1,1)*sqrt(elvar);
        Fminjump(i)=getsignalpower(jumpxel+linnoisexel+sattravelx,jumpel
            +linnoiseel+sattravely,meshsize,xel,el,gridpow2,interp_method);
        sattravelx=sattravelx+satvelx*samplewaittime;
        sattravely=sattravely+satvely*samplewaittime;
    end
    Fminjump(1)=mean(Fminjump(1,:));
    Fminjump=roundn(Fminjump(1),-1); %round to nearest tenths
    funcevals=funcevals+1;
    if Fminjump(1) > F(1,1) %must check to see you are going in right
        %direction on eigenvector
        deltax(:,iter)=deltaxminjump*-1; %head the opposite way
        Fminjump(1)=0;
    else
        deltax(:,iter)=deltaxminjump; %you jumped the correct way
    end
    mincheck=0;
else
    deltax(:,iter)=[0;0];
    mincheck=mincheck+1;
end
computedeltax=false;
if mincheck > mincheckthreshold
    %computedeltax=true; %complete one more jump (already evaluated the
    %function so might as well)
    terminate=true;
end
elseif mincheck > 0 && norm(gradient(:,iter)) > epsilon

```

```

        computedeltax=true;
        mincheck=0;
        gradfalloff(iter)=1;
    end
    mincheckvec(iter)=mincheck;

    if computedeltax==true %%%%%%%%%%if compute alpha*pk = true%%%%%%%%%
        %%%%%%%%%%compute pk and initial alpha:%%%%%%%%%
        deltax(:,iter)=-gradient(:,iter);
        alpha=1;
        %limit alpha*pk to a predetermined region of confidence:
        if norm(deltax(:,iter))>1.0 %if deltax is outside a "region of trust"
            %chosen so if you're at a max, won't go over another max (max initial
            %step routine will take)
            deltax(:,iter)=(deltax(:,iter)/norm(deltax(:,iter)))*.75;
        end

        %evaluate function at initial alpha=1 value:
        for i=1:ntsamps
            linnoisexel=randn(1,1)*sqrt(xelvar);
            linnoiseel=randn(1,1)*sqrt(elvar);
            Falpha(i)=getsignalpower(x(1,iter)+deltax(1,iter)+linnoisexel+
            sattravelx,x(2,iter)+deltax(2,iter)+linnoiseel+sattravely,meshsize,
            xel,el,gridpow2,interp_method);
            sattravelx=sattravelx+satvelx*samplewaittime;
            sattravely=sattravely+satvely*samplewaittime;
        end
        Falpha(1)=mean(Falpha(1,:));
        Falpha=roundn(Falpha(1),-1); %round to nearest tenths
        funcevals=funcevals+1;

        %evaluate point along search direction to approximate gradient at alpha=1
        dx1=deltax(1,iter)/norm(deltax(:,iter));
        dx2=deltax(2,iter)/norm(deltax(:,iter));
        nux=dx1*deljstep;
        nuy=dx2*deljstep;
        if norm([alpha*deltax(1,iter);alpha*deltax(2,iter)])>=deljstep
            if alpha > 0
                nu=norm([alpha*deltax(1,iter)-nux;alpha*deltax(2,iter)-nuy])/
                norm(deltax(:,iter)); %ensure that nu value will be deljstep away
                %from alpha in 1-d
            else
                nu=-1*norm([alpha*deltax(1,iter)+nux;alpha*deltax(2,iter)+nuy])/
                norm(deltax(:,iter));
            end
        else
            if alpha > 0
                nu=-1*norm([alpha*deltax(1,iter)-nux;alpha*deltax(2,iter)-nuy])/
                norm(deltax(:,iter)); %ensure that nu value will be deljstep away
                %from alpha in 1-d
            else
                nu=norm([alpha*deltax(1,iter)+nux;alpha*deltax(2,iter)+nuy])/
                norm(deltax(:,iter));
            end
        end
    end
end

```

```

end
end
for i=1:ntsamps
    linnoisexel=randn(1,1)*sqrt(xelvar);
    linnoiseel=randn(1,1)*sqrt(elvar);
    Fnu(i)=getsignalpower(x(1,iter)+nu*deltax(1,iter)+linnoisexel+
        sattravelx,x(2,iter)+nu*deltax(2,iter)+linnoiseel+sattravely,
        meshsize,xel,el,gridpow2,interp_method);
    sattravelx=sattravelx+satvelx*samplewaittime;
    sattravely=sattravely+satvely*samplewaittime;
end
Fnu(1)=mean(Fnu(1,:));
Fnu=roundn(Fnu(1),-1); %round to nearest tenths
funcevals=funcevals+1;

%%%%%%%%%%%%%%%%%%%%%%%%%%%%%%%%%%%%%%%%%%%%%%%%%%%%%%%%%%%%%%%%%%%%%%%%%perform linear search along pk to determine satisfactory
alpha %%%%%%%%%%%%%%%%%%%%%%%%%%%%%%%%%%%%%%%%%%%%%%%%%%%%%%%%%%%%%%%%%%%%%%%%%%
linsearchconverge=false;
directedgrad(iter)=deltax(:,iter)'\*gradient(:,iter);
%if alpha=1 is not satisfactory, perform lin search:
if abs((Falpha-Fnu)/deljstep > abs(-1*linsearchparam*directedgrad(iter)))
    %Criterion for lin search-(finite difference replaces gradient)-
    %GMW p. 102

    %Step 1- make sure you have an interval bracketing a minimum:
    bracketmin=true;
    if F(1,1)<Falpha %look opposite direction to find Fa and a values for
        %interval containing minimum
        alpha=-1;
        bracket_step=1;
        Fb=Falpha;
        b=1;
        Fc=F(1,1);
        c=0;
        Fa=-10^6;
        a=alpha;
        while Fa(1) <= Fc
            if bracket_step > 1
                Fb=Fc;
                b=c;
                Fc=Fa(1);
                c=a;
            end
            for i=1:ntsamps
                linnoisexel=randn(1,1)*sqrt(xelvar);
                linnoiseel=randn(1,1)*sqrt(elvar);
                Fa(i)=getsignalpower(x(1,iter)+alpha*deltax(1,iter)+
                    linnoisexel+sattravelx,x(2,iter)+alpha*deltax(2,iter)+
                    linnoiseel+sattravely,meshsize,xel,el,gridpow2,
                    interp_method);
                sattravelx=sattravelx+satvelx*samplewaittime;
                sattravely=sattravely+satvely*samplewaittime;
            end
            Fa(1)=mean(Fa(1,:));
            Fa=roundn(Fa(1),-1); %round to nearest tenths
            funcevals=funcevals+1;
            a=alpha;

```

```

        alpha=alpha*2;
        bracket_step=bracket_step+1;
    if bracket_step > 4
        bracketmin=false;
        bracketminfalse(1,mciter)=bracketminfalse(1,mciter)+1;
        bracketminfalse(1+bracketminfalse(1,mciter),mciter)=iter;
        warning('could not bracket minimum for lin search in less than
        4 steps')
        break
    end
    end
else %continue searching along search direction until a min is bracketed-
    %(find b)
    alpha=2;
    bracket_step=1;
    Fc=Falpha;
    c=1;
    Fa=F(1,1);
    a=0;
    Fb=-10^6;
    b=alpha;
    while Fb(1) <= Fc
        if bracket_step > 1
            Fa=Fc;
            a=c;
            Fc=Fb(1);
            c=b;
        end
        for i=1:ntsamps
            linnoisexel=randn(1,1)*sqrt(xelvar);
            linnoiseel=randn(1,1)*sqrt(elvar);
            Fb(i)=getsignalpower(x(1,iter)+alpha*deltax(1,iter)+
            linnoisexel+sattravelx,x(2,iter)+alpha*deltax(2,iter)+
            linnoiseel+sattravely,meshsize,xel,el,gridpow2,
            interp_method);
            sattravelx=sattravelx+satvelx*samplewaittime;
            sattravely=sattravely+satvely*samplewaittime;
        end
        Fb(1)=mean(Fb(1,:));
        Fb=roundn(Fb(1),-1); %round to nearest tenths
        funcevals=funcevals+1;
        b=alpha;
        alpha=alpha*2-1;
        bracket_step=bracket_step+1;
    if bracket_step > 4
        bracketmin=false;
        bracketminfalse(1,mciter)=bracketminfalse(1,mciter)+1;
        bracketminfalse(1+bracketminfalse(1,mciter),mciter)=iter;
        warning('could not bracket minimum for lin search in less
        than 4 steps')
        break
    end
    end
end
%Step 2- perform quadratic interpolation:
if bracketmin==true %lin search...
    linsearchconverge=true;
    linstep=1;

```

```

while linstep==1 || abs((Falpha-Fnu))/deljstep > abs(-1*
linsearchparam*directedgrad(iter)) %criterion for linear
%search (finite difference replaces gradient)- GMW p. 102
if linstep > 1
    if alpha < c && Falpha <= Fc
        b=c;
        c=alpha;
        Fb=Fc;
        Fc=Falpha;
    elseif alpha > c && Falpha > Fc
        b=alpha;
        Fb=Falpha;
    elseif alpha < c && Falpha > Fc
        a=alpha;
        Fa=Falpha;
    else
        a=c;
        c=alpha;
        Fa=Fc;
        Fc=Falpha;
    end
end
if Fa==Fb && Fb==Fc %can't optimize any further with quad interp
    break
end
if c-10000*eps<a&&a<c+10000*eps %saying if a==c
    %can't optimize any further with quad interp
    break
end
if -10000*eps<((b-c)*Fa+(c-a)*Fb+(a-b)*Fc)&&((b-c)*Fa+(c-a)*Fb+
(a-b)*Fc)<10000*eps %saying if den of alpha calc == 0
    %can't optimize any further with quad interp
    break
end
alpha=.5*((b^2-c^2)*Fa+(c^2-a^2)*Fb+(a^2-b^2)*Fc)/((b-c)*Fa+
(c-a)*Fb+(a-b)*Fc);
for i=1:ntsamps
    linnoisexel=randn(1,1)*sqrt(xelvar);
    linnoiseel=randn(1,1)*sqrt(elvar);
    Falpha(i)=getsignalpower(x(1,iter)+alpha*deltax(1,iter)+
linnoisexel+sattravelx,x(2,iter)+alpha*deltax(2,iter)+
linnoiseel+sattravely,meshsize,xel,el,gridpow2,
interp_method);
    sattravelx=sattravelx+satvelx*samplewaittime;
    sattravely=sattravely+satvely*samplewaittime;
end
Falpha(1)=mean(Falpha(1,:));
Falpha=roundn(Falpha(1),-1); %round to nearest tenths
funcevals=funcevals+1;
if norm([alpha*deltax(1,iter);alpha*deltax(2,iter)])>=deljstep
    if alpha > 0
        nu=norm([alpha*deltax(1,iter)-nux;alpha*deltax(2,iter)-
nuy])/norm(deltax(:,iter)); %ensure that nu value
        %will be deljstep away from alpha in 1-d
    else
        nu=-1*norm([alpha*deltax(1,iter)+nux;alpha*deltax(2,iter)+
nuy])/norm(deltax(:,iter));
    end
end

```



```

else
    if alpha > 0
        nu=-1*norm([alpha*deltax(1,iter)-nux;alpha*deltax(2,iter)
            -nuy])/norm(deltax(:,iter)); %ensure that nu value
            %will be deljstep away from alpha in 1-d
    else
        nu=norm([alpha*deltax(1,iter)+nux;alpha*deltax(2,iter)+
            nuy])/norm(deltax(:,iter));
    end
end
for i=1:ntsamps
    linnoisexel=randn(1,1)*sqrt(xelvar);
    linnoiseel=randn(1,1)*sqrt(elvar);
    Fnu(i)=getsignalpower(x(1,iter)+nu*deltax(1,iter)+linnoisexel
        +sattravelx,x(2,iter)+nu*deltax(2,iter)+linnoiseel+sattravely,
        meshsize,xel,el,gridpow2,interp_method);
    sattravelx=sattravelx+satvelx*samplewaittime;
    sattravely=sattravely+satvely*samplewaittime;
end
Fnu(1)=mean(Fnu(1,:));
Fnu=roundn(Fnu(1),-1); %round to nearest tenths
funcevals=funcevals+1;
linstep=linstep+1;
if linstep > 20
    linsearchconverge=false;
    break
end
end
linstepcount(iter)=linstep;
end
end
if linsearchconverge==true %if lin search produced a good alpha within max
    %number of linsteps
    deltax(:,iter)=deltax(:,iter)*alpha;
end %else, alpha remains at one
end
deltaxnorm(iter)=norm(deltax(:,iter));
x(:,iter+1)=x(:,iter)+deltax(:,iter);
xelpt=x(1,iter+1);
elpt=x(2,iter+1);

%jump off main lobe??
if xnormfromsat(iter) < .25 && deltaxnorm(iter) > 1.8
    mainlobejump(mciter)=mainlobejump(mciter)+1;
end
%%%%%%%%%%

iter=iter+1;
if funcevals > 500
    warning('max number of function evaluations reached')
    break
end
end

gradfalloffcount(mciter)=sum(gradfalloff);
%calculate approximate time
if satvel > eps*10000 %if satvel isn't zero

```

```

        time=satpos(end)/satvel;
else
    time=0;
end
soln(1:2,mciter)=[x(1,end);x(2,end)];
soln(3,mciter)=iter;
simtime=toc;
soln(4,mciter)=simtime;
soln(5,mciter)=funcevals;
soln(6,mciter)=xnorm(end);
soln(7,mciter)=satpos(end);
soln(8,mciter)=xnormfromsat(end);
soln(9,mciter)=time;
soln(10,mciter)=sum(linstepcount);
soln(11,mciter)=mainlobejump(mciter);
soln(12,mciter)=gradfalloffcount(mciter);
end

```

C.6 getsignalpower.m (Subroutine)

```

function [power]=getsignalpower(azpt,elpt,meshsize,az,el,powergrid,\
interp_method)
%Eric Marsh
%3 Dec 07
%interpolates signal power value from given xel,el coordinate
if mod(azpt,meshsize)==0 && mod(elpt,meshsize)==0 %is point is on mesh
    %grid (saves time rather than interpolating) change to <epsilon
    %rather than zero for being very close to mesh
    [r,c,v]=find(az<azpt+1000*eps & az>azpt-1000*eps); %accounts for
    %machine precision. like saying: [r,c,v]=find(az==azpt);
    [r1,c1,v1]=find(el<elpt+1000*eps & el>elpt-1000*eps);
    power=powergrid(c(1),r1(1));
else
    power=interp2(az,el,powergrid,azpt,elpt,interp_method);
end

```


Appendix D

List of Acronyms and Symbols

Table D.1: List of Acronyms and Abbreviations Used in This Work

Abbreviation	Description
A/C	Aircraft
APS	Antenna Positioner System
Az	Azimuth
BER	Bit Error Rates
BFGS	Broyden, Fletcher, Goldfarb, and Shano Method of Optimization
CMC	Cleveland Motion Controls
COE	Classical Orbital Elements
DFP	Davidon, Fletcher, and Powell Method of Optimization
dB	Decibels
ECI	Earth-Centered Inertial
EHF	Extremely High Frequency
EOM	Equations of Motion
EI	Elevation
GPS	Global Positioning System
HPBW	Half-Power Beamwidth
IMU	Inertial Measurement Unit

ISP	Inertially Stabilized Platform
LHP	Left Half-Plane
LHS	Left Hand Side
LOS	Line Of Sight
LQG	Linear Quadratic Gaussian
LQR	Linear Quadratic Regulator
MN	Modified Newton's Method of Optimization
NED	North, East, Down
PSD	Power Spectral Density
RF	Radio Frequency
RHS	Right Hand Side
RX	Receive
SATCOM	Satellite Communications
SD	Steepest Descent Method of Optimization
SNR	Signal to Noise Ratio
SS	Spiral Search Method of Optimization
TX	Transmit
X-EI	Cross-Elevation

Table D.2: List of Symbols Used in This Work

Symbol	Description
A	System Plant State Coefficient Matrix
A_{filt}	Filter State Equation A Matrix
az	Local Azimuth Angle ($^{\circ}$)
az_{10Hz}	Azimuth Look Angle Calculated at 10Hz Intervals ($^{\circ}$)
az_{NED}	Inertial Azimuth Look Angle (NED Frame) ($^{\circ}$)
az_d	Desired Local Azimuth Look Angle ($^{\circ}$)
B_{filt}	Filter State Equation B Matrix

B_k	Quasi-Newton Approximate to the Hessian Matrix at the k -th Trial Point
B_u	System Plant Control Coefficient Matrix
B_w	System Plant Disturbance Input Coefficient Matrix
C_y	System Plant Output Coefficient Matrix
D_P	Disturbance Rate Input about Body x Axis ($\frac{\circ}{sec}$)
D_Q	Disturbance Rate Input about Body y Axis ($\frac{\circ}{sec}$)
D_R	Disturbance Rate Input about Body z Axis ($\frac{\circ}{sec}$)
D_k	Diagonal Cholesky Factorization Matrix
d_{max}	Max Distance From Boresight (\circ)
d_{mean}	Mean Distance From Boresight (\circ)
d_σ	Standard Deviation of Distance From Boresight (\circ)
e_a	Applied Armature Source Voltage (V)
e_b	Back-EMF Voltage (V)
el	Local Elevation Angle (\circ)
el_{10Hz}	Elevation Look Angle Calculated at 10Hz Intervals (\circ)
el_{NED}	Inertial Elevation Look Angle (NED Frame) (\circ)
el_d	Desired Local Elevation Look Angle (\circ)
el_i	Inertial Elevation Look Angle (\circ)
F_T	Total Number of Cost Function Evaluations
F_k	Cost Function Value at the k -th Trial Point
G_k	Hessian Matrix at the k -th Trial Point
\mathbf{g}_k	Gradient at the k -th Trial Point
H_0	Null Hypothesis
H_a	Alternate Hypothesis
I	Moment or Product of Inertia (m^2kg)
i_a	Armature Current (A)
K_b	Back-EMF Constant ($\frac{V}{\circ/sec}$)
K_m	Motor Constant ($\frac{N-m}{A}$)
K_o	Optimal Regulator Gain Matrix

L_a	Armature Circuit Inductance (H)
L_k	Lower-Triangular Cholesky Factorization Matrix
L_o	Optimal Estimator Gain Matrix
\bar{N}	Reference Input Gain
n	Number of Cost Function Evaluations per Trial Point
n_{CI}	n Determined by the Confidence Interval Formula
n_g	Gear Ratio
n_{nc}	Number of Nonconverging Points
P	Antenna Inertial Velocity about Body x Axis ($\frac{\circ}{sec}$)
$P_{A/C}$	Aircraft Rotational Motion about Aircraft x Axis ($\frac{\circ}{sec}$)
$P'_{A/C_{Base}}$	Aircraft Rotational Motion about Base x Axis ($\frac{\circ}{sec}$)
p	Antenna Inertial Displacement about Body x Axis ($^{\circ}$)
\mathbf{p}_k	Descent Direction at the k -th Trial Point
Q	Antenna Inertial Velocity about Body y Axis ($\frac{\circ}{sec}$)
$Q_{A/C}$	Aircraft Rotational Motion about Aircraft y Axis ($\frac{\circ}{sec}$)
$Q'_{A/C_{Base}}$	Aircraft Rotational Motion about Base y Axis ($\frac{\circ}{sec}$)
Q_k	Quasi-Newton Update Matrix at the k -th Trial Point
q	Antenna Inertial Displacement about Body y Axis ($^{\circ}$)
R	Antenna Inertial Velocity about Body z Axis ($\frac{\circ}{sec}$)
$R_{A/C}$	Aircraft Rotational Motion about Aircraft z Axis ($\frac{\circ}{sec}$)
$R'_{A/C_{Base}}$	Aircraft Rotational Motion about Base z Axis ($\frac{\circ}{sec}$)
R_a	Armature Circuit Resistance (Ω)
R_{uu}	Control Weighting Matrix
R_{vv}	Sensor Noise Weighting Matrix
R_{ww}	Process Noise Weighting Matrix
R_{xx}	State Weighting Matrix
r	Antenna Inertial Displacement about Body z Axis ($^{\circ}$)
r_1	Motor Shaft Gear Radius (m)
r_2	Az/El Output Shaft Gear Radius (m)

S	Standard Deviation
T	Torque (N-m)
t_c	Convergence Time
v	Sensor Noise
v_{pat}	Cost Function Translational Velocity
v_j	j -th Eigenvector of Hessian Matrix
w	Process Noise
w_{CI}	Confidence Interval Width
\mathbf{x}^*	Location of Global Minimum
\mathbf{x}_k	x_{el_i}, el_i Coordinates of the k -th Trial Point
x_{el_i}	Inertial Cross-Elevation Look Angle ($^\circ$)
$z_{\frac{\alpha}{2}}$	z -Critical value for Confidence Interval
α	Step Length
α_{KS}	Kolmogorov-Smirnoff Significance Level
Δ	Total Inertial Pointing Error ($^\circ$)
δ_G	Positive Definiteness Requirement in Cholesky Factorization
δ_f	Finite Difference Interval
η	Linear Search Parameter
ν	Linear Search Criterion Step Length
$\dot{\theta}_1$	Motor Shaft Velocity ($\frac{^\circ}{sec}$)
$\dot{\theta}_2$	Az/El Output Shaft Velocity ($\frac{^\circ}{sec}$)
$\dot{\theta}_{roll}$	Antenna Velocity wrt the Aircraft about Body x Axis ($\frac{^\circ}{sec}$)
$\dot{\theta}_{pitch}$	Antenna Velocity wrt the Aircraft about Body y Axis ($\frac{^\circ}{sec}$)
$\dot{\theta}_{yaw}$	Antenna Velocity wrt the Aircraft about Body z Axis ($\frac{^\circ}{sec}$)
ρ	Convergence Percentage (%)
Ψ	Aircraft Heading Angle ($^\circ$)
Θ	Aircraft Pitch Angle ($^\circ$)
Φ	Aircraft Roll Angle ($^\circ$)

Bibliography

- [1] Masten, M. K., "Platforms for Optical Imaging Systems," *IEEE Control Systems Magazine*, February 2008.
- [2] Stockum, L. A. and Carroll, G. R., "Precision Stabilized Platforms for Shipboard Electro-optical Systems," *SPIE*, June 1984.
- [3] Wang, H. G. and Williams, T. C., "Strategic Inertial Navigation Systems," *IEEE Control Systems Magazine*, February 2008.
- [4] Hilkert, J. M., "Inertially Stabilized Platform Technology," *IEEE Control Systems Magazine*, February 2008.
- [5] Hwang, W. G., "Bandwidth on Demand for Deployed-IP Users," *IT Professional*, Vol. 7, No. 1, January 2005.
- [6] Hampton, P., "Naval Space Command's top functional requirements for commercial SATCOM," *Military Communications Conference Proceedings, 1999. MILCOM 1999. IEEE*, Vol. 32, November 1999.
- [7] Nicol, S., Walton, G., Westbrook, L., and Wynn, D., "Future Satellite Communications to Military Aircraft," *Electronics and Communication Engineering Journal*, Vol. 12, February 2000.
- [8] Barnes, M., "Use of Commercial Satcom in the Skynet 5 Era," *IEE Colloquium on Military Satellite Communications*, March 1995.
- [9] Debruin, J., "Control Systems for Mobile SATCOM Antennas," *IEEE Control Systems Magazine*, February 2008.

- [10] Stutzman, W. L. and Thiele, G. A., *Antenna Theory Design*, John Wiley and Sons, 2nd ed., 1998.
- [11] Johnson, M., "ARION Antenna Control and Stabilization System," *Broadcasting and Communication*, Vol. 20, 1984.
- [12] Barbour, N. and Schmidt, G., "Inertial Sensor Technology Trends," *IEEE Sensors Journal*, Vol. 1, No. 4, December 2001.
- [13] James, M. R. and Maney, J. J., "Adaptive Alignment of a Shipboard Satellite Terminal," *IEEE Military Communications Conference*, IEEE Communications Society, 1985.
- [14] Fisk, J. W., "Confidence Limits for the Pointing Error of Gimbaled Sensors," *IEEE Transactions on Aerospace and Electronic Systems*, Vol. AES-2, No. 6, November 1966.
- [15] Figucia, R. J., "Downlink Acquisition and Tracking Procedures for the ASCAMP Satellite Communications Terminal," Tech. rep., Massachusetts Institute of Technology Lincoln Laboratory, September 1993.
- [16] Claydon, B., "Earth Station Antenna Technology," *Vacation School on Satellite Communication System Planning*, IEEE, London, UK, September 1984.
- [17] Plonski, M., "Auxiliary Antenna Approach to Sidelobe Discrimination for Maximum Dynamic Range," *SPIE*, Vol. 1700, April 1992.
- [18] Reinhard, K. L. and Darlington, J. C., "Satellite Acquisition Using an Automated Technique," Tech. rep., Ford Aerospace and Communications Corporation, 1974.
- [19] Gawronski, W. and Craparo, E. M., "Antenna Scanning Techniques for Estimation of Spacecraft Position," *IEEE Antenna's and Propagation Magazine*, Vol. 44, No. 6, December 2002.

- [20] *Torquemaster Brush Servo-Motors 2100 Series*, Cleveland Motion Controls, 2002, www.cmcccontrols.com/downloads/servo_motors/platform2100.pdf.
- [21] *KVH DSP-3000 Fiber Optic Gyro Technical Manual*, KVH Industries, Inc, 2007.
- [22] *C-MIGITS III Data Sheet*, BEI Systron Donner Inertial Division, 2006.
- [23] Ogata, K., *System Dynamics*, Pearson Prentice Hall, 4th ed., 2004.
- [24] Yechout, T. R., *Introduction to Aircraft Flight Mechanics*, AIAA, 2003.
- [25] Stearns, S. D. and Hush, D. R., *Digital Signal Analysis*, Prentice Hall, 1990.
- [26] How, J. P., *Lecture Notes for 16.323: Principles of Optimal Control*, Massachusetts Institute of Technology, 2007.
- [27] Athans, M., “The Role and Use of the Stochastic Linear-Quadratic-Gaussian Problem in Control System Design,” *SPIE Milestone Series*, Vol. AC-16(6), December 1971, pp. 529–552.
- [28] Bryson, A. E. and Yu-Chi-Ho, *Applied Optimal Control*, Hemisphere Publishing Corporation, 1975.
- [29] Brown, R. G. and Hwang, P. Y., *Introduction to Random Signals and Applied Kalman Filtering*, John Wiley and Sons, 1983.
- [30] Stengel, R. F., *Stochastic Optimal Control*, John Wiley and Sons, 1986.
- [31] How, J. P., *Lecture Notes for 16.31: Feedback Control*, Massachusetts Institute of Technology, 2001.
- [32] Lancaster, H. O., “Zero Correlation and Independence,” *Australian and New Zealand Journal of Statistics*, Vol. 1, No. 2, August 1959.
- [33] Stephens, M., “EDF Statistics for Goodness of Fit and Some Comparisons,” *American Statistical Association*, Vol. 69, No. 347, September 1974.
- [34] Scales, L., *Introduction to Non-Linear Optimization*, Springer-Verlag, 1985.

- [35] Gill, P. E., Murray, W., and Wright, M. H., *Practical Optimization*, Academic Press, 1981.
- [36] Nocedal, J. and Wright, S. J., *Numerical Optimization*, Springer, 2006.
- [37] Devore, J. L., *Probability and Statistics*, Thomson, 6th ed., 2004.
- [38] Chobotov, V. A., *Orbital Mechanics*, AIAA, 3rd ed., 2002.
- [39] Sellers, J. J., *Understanding Space*, McGraw-Hill, 2nd ed., 2000.
- [40] Montenbruck, O. and Gill, E., *Satellite Orbits*, Springer, 2000.